KFA

KERNFORSCHUNGSANLAGE JÜLICH GmbH

Institut für Kernphysik

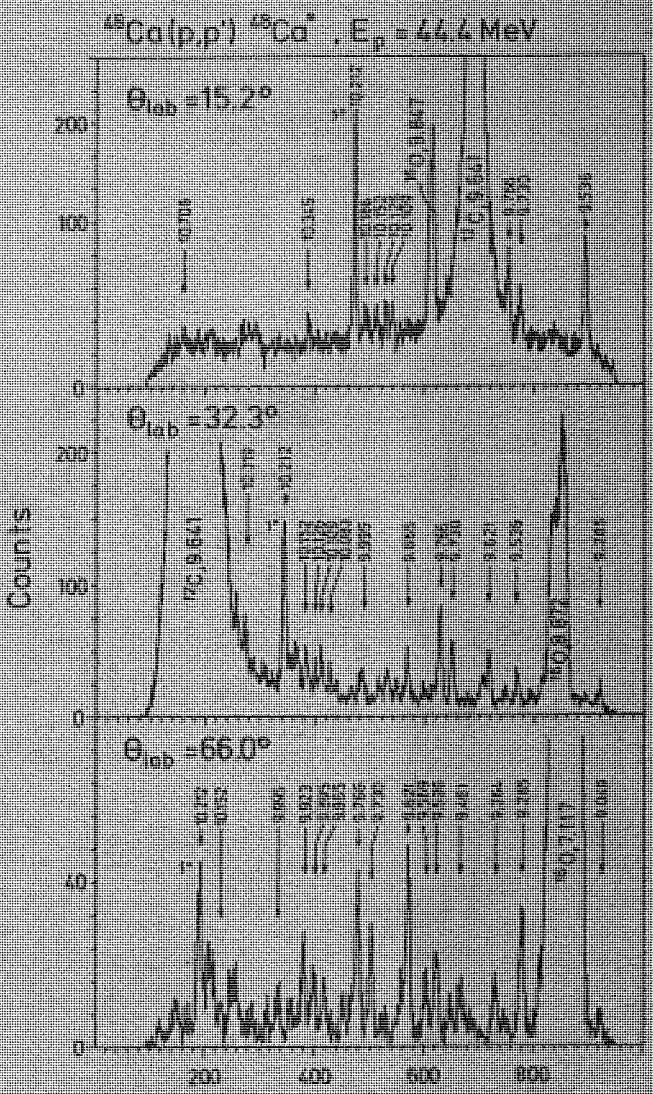

Jül - Spez 146
March 1982
ISSN 0170 - 8937

Annual Report 1981

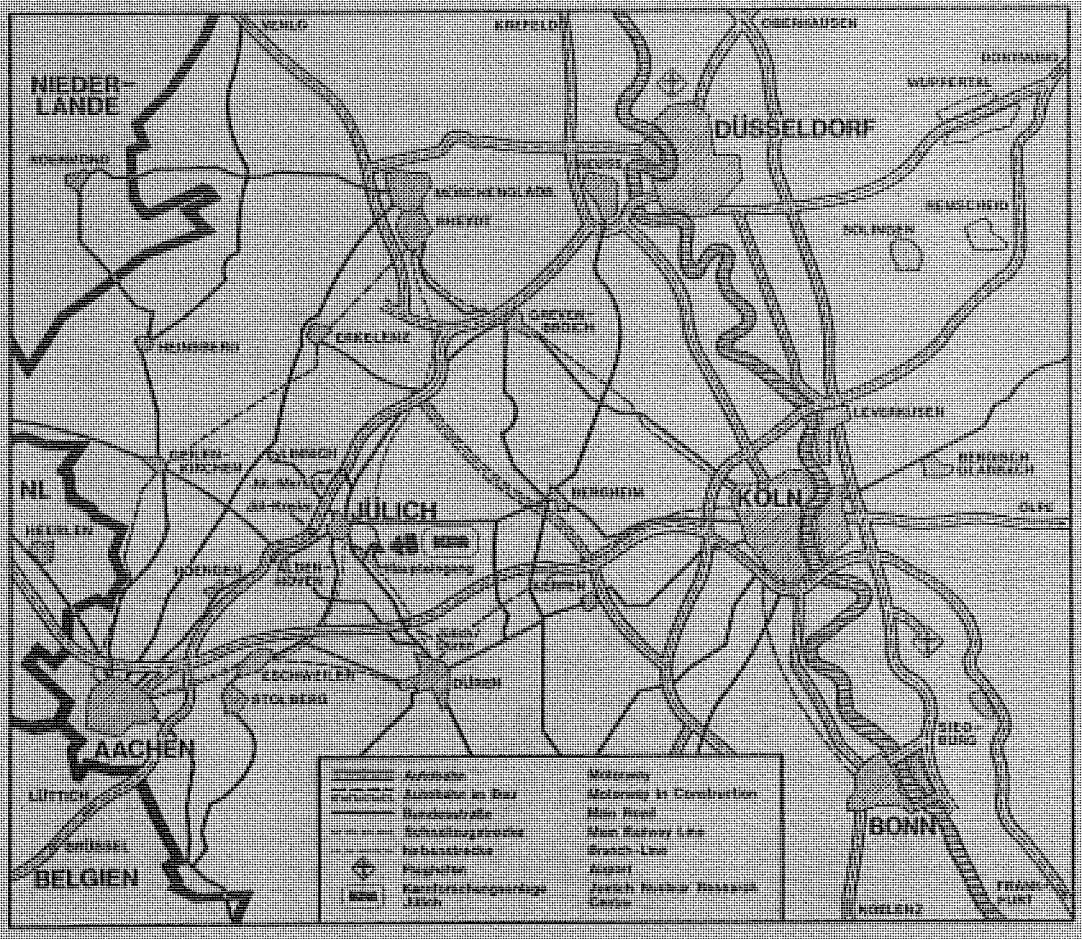

Als Manuskript gedruckt

Spezielle Berichte der Kernforschungsanlage Jülich – Nr. 146
Institut für Kernphysik Jül - Spez - 146

Zu beziehen durch: ZENTRALBIBLIOTHEK der Kernforschungsanlage Jülich GmbH
Postfach 1913 · D-5170 Jülich (Bundesrepublik Deutschland)
Telefon: 02461/610 · Telex: 833556 kfa d

Annual Report 1981

Front cover: High resolution spectra (7-10 keV) of the inelastic proton scattering on ^{48}Ca at 44.4 MeV incident energy and three different scattering angles measured with the magnet spectrometer BIG KARL. Besides the identification of 50 new levels in the measured energy range these spectra show the strong excitation of the unnatural parity 1^+ spin-flip state at 10.212 MeV excitation energy. The present interest in spin-flip states is motivated by the possibility to study the distribution of spin excitation strength in nuclei and, directly related to it, the spin and isospin dependent part of the particle hole residual interaction.

Preface

This annual report of the Institut für Kernphysik (IKP) at the Kernforschungsanlage (KFA) Jülich contains short descriptions of current research carried out by members of our institute and by guest groups frequently in cooperation with scientists of the IKP.

The majority of the experiments was performed with the use of the light charged particle beams with 22.5 - 45 MeV/amu from our cyclotron. Spin-flip states in ^{48}Ca were studied under conditions of very high resolution at our large magnetic spectrograph 'Big Karl' in collaboration with Santo's group from Münster. Schmidt-Rohr's group from the Max Planck Institut (MPI) Heidelberg has investigated the residual interaction through a ^{209}Bi(d,^{3}He) reaction study at Big Karl. This spectrograph has also been used for a test of the Born approximation for the description of the electron transfer in the $^{3}He^{++} + C \rightarrow {}^{3}He^{+} + C^{+}$ reaction. Big Karl has furthermore allowed measurements at angles as low as 1.5^{o} for detailed multipolarity assignments of giant resonances. The series of studies on giant resonances carried out in collaboration with the MPI-group from Heidelberg was supplemented by a measurement of the decay of the E2 giant resonance of ^{24}Mg. Gamma-ray spectroscopy at the cyclotron gave evidence for $h_{11/2}$ neutrons to be responsible for backbending in ^{134}Ce and for a transition from deformed shape to sphericity in ^{133}La. Through the measurement of the E3 speed of the 1.57 MeV transition in ^{147}Gd, the two-phonon octupole character of the 2.57 MeV level was confirmed in quantitative agreement with the expected strength. The $\pi h_{11/2} \rightarrow \nu h_{9/2}$ GT-decay of n-deficient Tb isotopes was investigated for obtaining spectroscopic information about the N = 82 gap in ^{146}Gd.

Neutron rich nuclei were studied also at the cyclotron, where ^{36}P was produced in the (n,2p) reaction for an investigation of levels in ^{36}S. The spectroscopy of the transitional region at A $\sim$ 100 was extended to ^{102}Zr at our fission product separator in the KFA. Work in the ^{132}Sn and Ce-regions were carried out in collaboration with various groups mainly at the ILL, CERN and BNL.

An Aachen-IKP collaboration has started a search for γ-events in connection with the question about the existence of the axion.

The theoretical studies have shown that the admixture of the Δ-resonance and thus "quenching" depends on the momentum transfer in the reaction. L_3-subshell alignments have been studied in the frame of a semi-classical theory because the alignment

should allow a sensitive test of the theory of ionization. A program has been completed which permits the calculation of 'escape widths' of giant resonances also in heavy nuclei. The adiabatic time dependent HF theory has been applied to problems in heavy ion physics.

The solar energy group has developed a universally applicable collector test stand which is now being built by a company near Jülich. Absorber pannels have been tested both in-doors and out-doors. The systematic study of our solar warm water system has led to a yield curve that allows the determination of the solar energy fraction based on the annual sunshine hours and few measurements under typical weather conditions. Round-robin tests were carried out in accordance with the IEA and CEC agreements, and additional work is going on in bilateral collaboration with various partners.

The cyclotron has been in operation for other users from the KFA for $\sim$ 11 % and for guest scientists for $\sim$ 25 %. Besides machine operation, work is carried out for the installation of an external source. In addition steps are in preparation for an improvement of the beam quality, particularly in view of high resolution work at Big Karl.

Our on-line computer system (largely PDP 15) is being replaced by a VAX 11/780. Here additional support by the board of management of our center is gratefully acknowledged.

At present, our budget is extremely tight, and a ten percent reduction of the IKP staff has been imposed on us. This reduction is planned to reduce the solar energy activities to only 20 % of the level in 1980. Our attempts to find a successor for Amand Faessler have so far been unsuccessful. We do hope though that it will be possible to fill his former position within the year 1982.

Directors of Institutes for Experimental Nuclear Physics at the neighbouring Universities in Bochum, Bonn, Köln and Münster, *Prof. Bodenstedt, Prof. Kamke, Prof. Mayer-Kuckuk, Prof. Santo, Prof. v. Brentano, Prof. v. Buttlar and their coworkers* have started to discuss *together with us* various possibilities for an optimal development and use of the regional nuclear physics facilities. Planning proceeds in a very cooperative atmosphere, and all of us hope that we can soon start work for setting up a powerful facility which is largely complementary to others.

Otto Schult

INSTITUTE FOR NUCLEAR PHYSICS

Managing director:	Prof. Dr. O. Schult
Experimental Nuclear Physics I, director:	Prof. Dr. C. Mayer-Böricke
Experimental Nuclear Physics II, director:	Prof. Dr. O. Schult
Theoretical Physics, acting director:	Prof. Dr. J. Speth

Kernforschungsanlage Jülich GmbH

Postfach 1913, 5170 Jülich, W.-Germany

CONTENTS

I EXPERIMENTAL NUCLEAR PHYSICS

1. NUCLEAR REACTIONS AND SCATTERING PROCESSES

1.1. Strong 1^+ Excitation in $^{48}Ca(p,p')$ Scattering at E_p = 44.4 MeV

G.P.A. Berg, G. Gaul[+], W. Hürlimann, I. Katayama[++], S.A. Martin, J. Meißburger, J. Römer, R. Santo[+], G. Sondermann[+], B. Styczeń[*], F. Osterfeld

Investigation of magnetic M1 transitions to unnatural parity 1^+ states provides an ideal tool to study the distribution of spin excitation strength in nuclei and, directly related to it, the spin and isospin dependent parts of the particle-hole residual interaction.

Mainly two reactions have been used so far in order to study magnetic nuclear excitations: inelastic electron scattering and the (p,n) charge exchange reaction. Also inelastic proton scattering is a good reaction to excite nuclear spin flip modes. In this experiment we measured the 1^+ state at E_x = 10.212 MeV in ^{48}Ca using (p,p') scattering at 44.4 MeV which has been seen before in $^{48}Ca(e,e')$ by the Darmstadt group[1].

Fig. 1 shows the spectra at 3 different angles with about 50 new levels in the range E_x = 9.2 - 10.7 MeV and the strong 1^+ state. The high resolution of 7 - 10 keV was obtained by using the magnetic spectrometer BIG KARL. The solid angle was 2.5 msr.

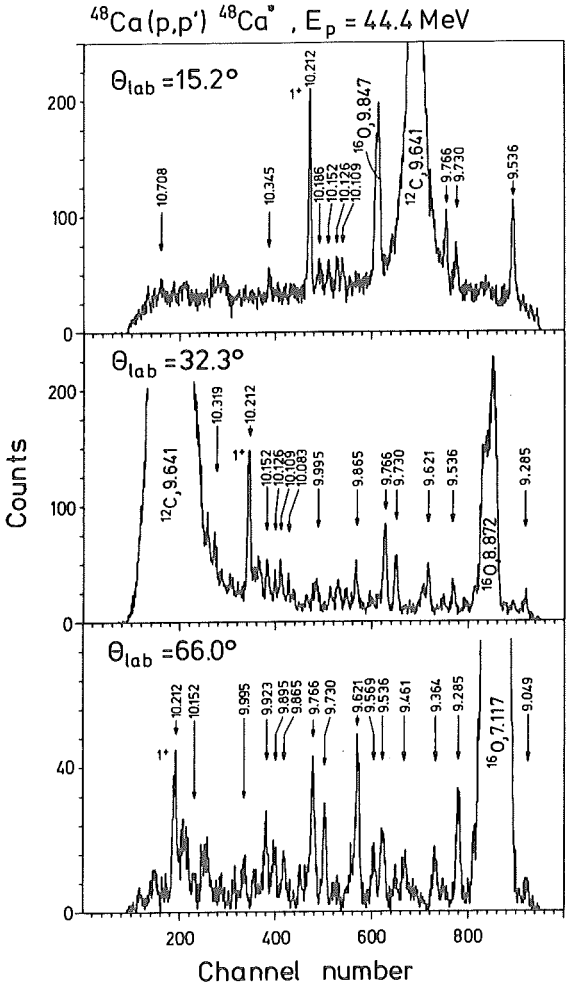

Fig. 1: Momentum spectra at 3 angles measure with magnetic spectrometer BIG KARL, energy resolution 7 - 10 keV. Strong 1^+ state at E_x = 10.212 MeV.

In Fig. 2 the angular distribution of the 1^+ states is plotted together with the results of a microscopic DWBA calculation. This calculation was performed with the code FROST-MARS[2] using the M3Y-interaction of Bertsch et al[3] and RPA-wave functions of ref. 4) for the nuclear description of the 1^+ state. The rather good agreement of the measured and calculated magnitude is surprising since the calculation does not contain the important coupling to the Δ isobar-nucleon hole excitation and also two step processes are not included in our analysis. To arrive at definite conclusions on the amount of M1 strength around E_x = 10 MeV it is therefore necessary to study the energy dependence of the 1^+ excitation. This experiment demonstrates that such investigations with protons have to be performed with extremely good energy resolution in order to isolate possibly weak 1^+ states from other levels which are present at the excitation energy relevant to 1^+ excitations.

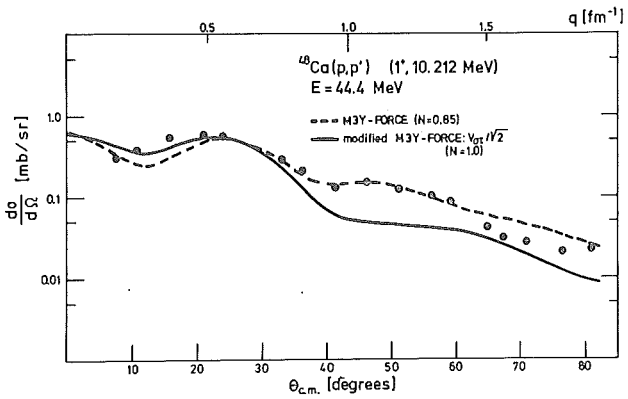

Fig. 2: Measured angular distribution of the 1^+ state (data points) and microscopic DWBA calculations (solid and dashed lines).

1) W. Steffen, H.D. Gräf, W. Gross, D. Meuer, A. Richter, E. Spamer, O. Titze and W. Knüpfer, Phys. Lett. 95B (1980) 23
2) F. Osterfeld, FROST-MARS computer code
3) G. Bertsch, J. Borysowicz, H. McManus and W.G. Love, Nucl. Phys. A (1977) 399
4) F. Osterfeld, T. Suzuki and J. Speth, Phys. Lett. Vol. 99B (1981) 75

[+] Institut für Kernphysik, Universität Münster

[++] RCNP, Osaka University, Japan

[*] Institute of Physics, Jagiellonian University, Cracow, Poland

1.2. Proton Scattering on ^{102}Pd and ^{110}Pd at E_p=45 MeV Using the Magnetic Spectrograph BIG KARL

G.P.A. Berg, E. Fretwurst, W. Hürlimann, G. Lindström*, S.A. Martin, J. Meißburger, W. Oelert, K.F. von Reden*, V. Riech , J.G.M. Römer*

The systematic investigations of the proton scattering on Palladium isotopes were continued in 1981[1]. During this period it was our main purpose to get high resolution data on the less known target nuclei ^{102}Pd and ^{110}Pd. In addition to experiments performed in Amsterdam and Hamburg [2)3)] angular distributions were measured at E_p = 45 MeV with the magnetic spectrograph BIG KARL. We used self supporting targets with isotopic enrichment of 77% for ^{102}Pd and 97% for ^{110}Pd.

An example of the proton energy spectra of ^{110}Pd is shown in fig.1.

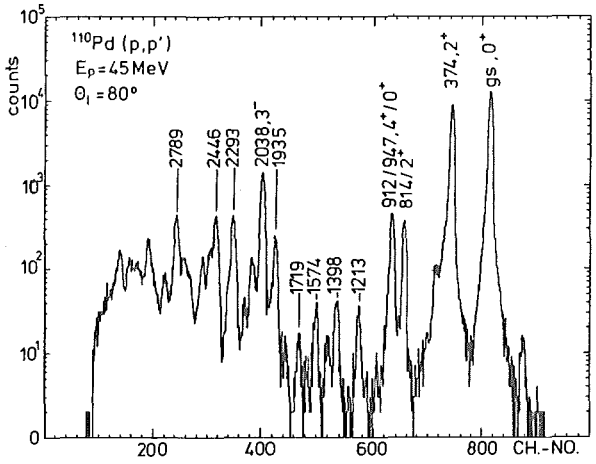

Fig.1.: ^{110}Pd (p,p') proton energy spectrum (θ = 80°)

In addition to the low lying one and two phonon vibrational levels transitions to many states with higher excitation energies are to be seen. The values are in good agreement with the level scheme given by Lederer[4].

In our measurements small distortions in the X - Y distributions of the MWPC could not be avoided. They showed up in a small overall rotation and in a bending of the single peak lines. In a normal sorting routine the x - projected data produce the energy spectrum, thus leading to a broadening of the peaks. With a projection routine that takes into account this bending in first order a clearly better resolution was obtained. The normal and improved version are shown for comparison in fig.2.

In a preliminary analysis angular distributions were extracted for the most pronounced transitions in both ^{102}Pd and ^{110}Pd (fig. 3 and 4). Good fits were obtained by coupled channels caluclations using the code ECIS. The resulting deformation parameters are in good agreement with measurements at lower energies[2,3]. In the case of ^{102}Pd a 4± level was clearly identified at 2300 keV being well fitted as a one phonon hexadecapole state.

In recent years much progress was achieved in reproducing the phenomenological optical model by microscopic nuclear

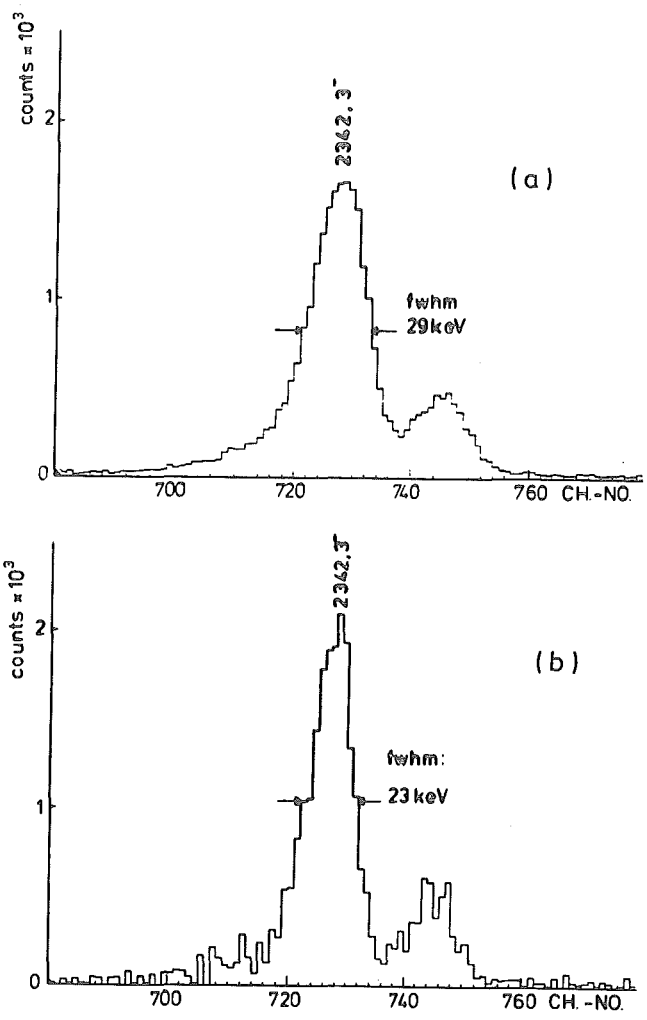

Fig.2: ^{102}Pd (p,p'), E_x = 2.342 MeV (3^-)

matter calculations (see e.g.[5)6)]). It is well known, that the accuracy of the phenomenological OM-parameters suffers from ambiguities mainly due to different possible geometries. Therefore we present instead the volume integrals for the real and imaginary part and their root mean square radii (table 1). Further discussions are outlined in[2].

Table 1

	I_V/A (MeVfm^3)	I_W/A (MeVfm^3)	$\langle R_V \rangle_{rms}$ (fm)	$\langle R_W \rangle_{rms}$ (fm)
^{102}Pd	- 359.4	- 114.1	5.082	6.060
^{110}Pd	- 363.6	- 101.7	5.287	6.267

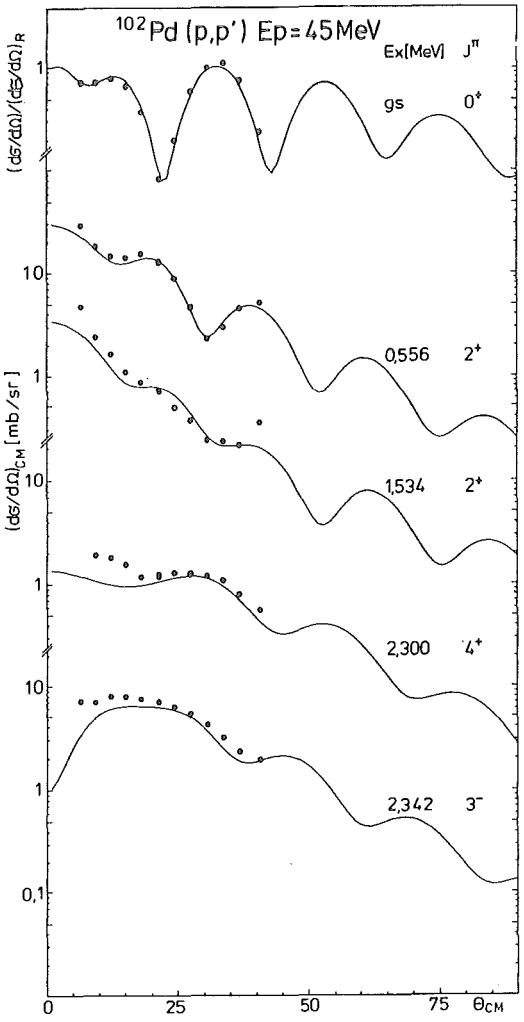

Fig. 3: ^{102}Pd (p,p') : Experimental data and CC - calculations (solid lines)

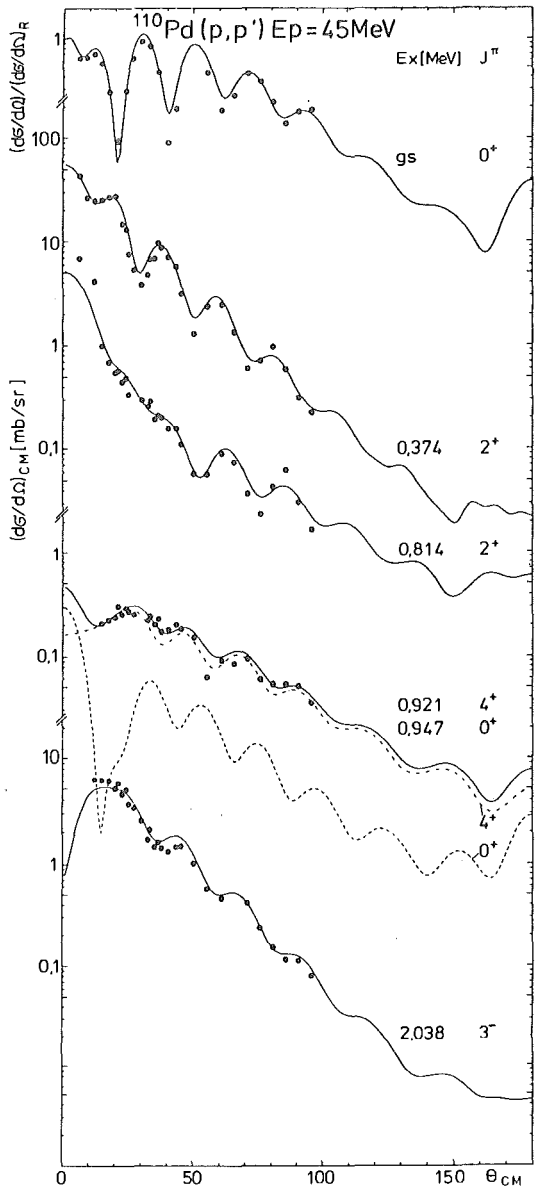

Fig. 4: ^{110}Pd (p,p') : Experimental data and CC - calculations (solid lines)

References:

1) G.P.A. Berg et al, Annual Report 1979 (p.40) and 1980, (p.36), Institut für Kernphysik, KFA Jülich

2) G. Lindström et al, Nuclear Physics Symposium, University of Leningrad 1981 and to be published

3) G. Lindström et al, Annual Report 1981, Institute for experimental Physics, University of Hamburg

4) C.M. Lederer et al, Table of Isotopes, J. Whiley & Sons, New York 1978

5) H.V. von Geramb (editor) : Microscopic Optical Potentials, Lecture Notes in Physics 89, Springer Verlag, New York 1979

6) J.P. Jeukenne et al, Phys. Rev. C 16 (1977), 80

This work was supported by Bundesminister für Forschung und Technologie.

* I. Institut für Experimentalphysik, Universität Hamburg

1.3. Seach for 1^+ States in $^{58}Ni(p,p')$ Scattering

G.P.A. Berg, G. Gaul[+], W. Hürlimann, I. Katayama[++], S.A. Martin, J. Meißburger, J. Römer, R. Santo[+], G. Sondermann[+] and B. Styczen[+++]

Encouraged by the clear observation of the 1^+ state in $^{48}Ca(p,p')$ (see contribution in this report) at E_x = 10.212 MeV we extented our search for 1^+ states to the ^{58}Ni nucleus. According to a shell model calculation by Mc Grory (private communication) several isoscalar 1^+ states are expected at excitation energies $E_x \sim 8$ MeV in this nucleus. For this purpose we measured cross section angular distributions of the $^{58}Ni(p,p')$ inelastic scattering in the angular range $\Theta_{lab} = 7^o - 75^o$ at 45 MeV incident proton energy using the high resolution magnetic spectrometer BIG KARL. Fig. 1 shows a spectrum at $\Theta_{lab} = 20^o$.

The resolution of 10 keV allows the identification of more then 30 energy level in the range from E_x = 7.1 to 8.4 MeV. The excitation energies shown are preliminary results with an error of about $\pm$ 10 keV. From the comparison of the measured angular distribution and DWBA calculations we expect the determination of the transferred angular momenta and information on possible 1^+ states in ^{58}Ni. The analysis is in progress.

+ Institut für Kernphysik, Universität Münster
++ RCNP, Osaka University, Japan
+++ Institute of Physics, Jagiellonian University, Cracow Poland

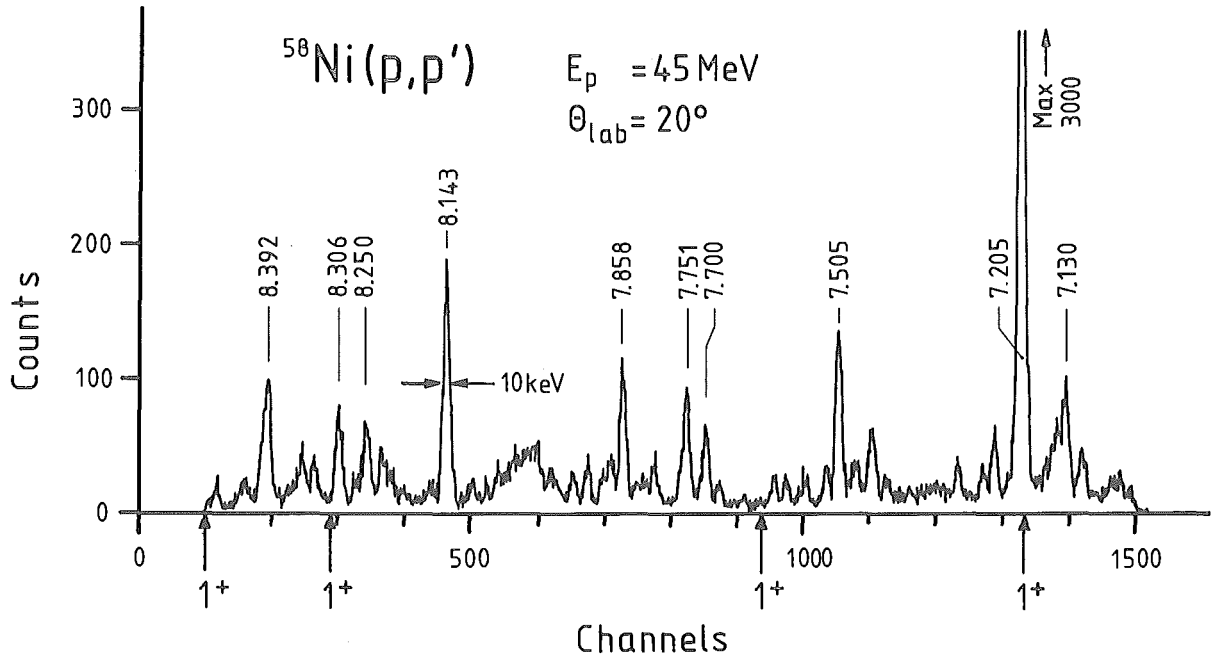

Fig. 1: Typical spectrum of $^{58}Ni(p,p')$ scattering at E_p = 45 MeV. Arrows indicate excitation energies where 1^+ states are calculated in the shell model (Mc Grory).

1.4. Nuclear spectroscopy of ^{108}Ag using the (p,d)-transfer reaction in comparison to neutron capture investigations

G.P.A. Berg, W. Hürlimann, I. Katayama[+], S.A. Martin, J. Meißburger, J. Römer, H. Seyfarth and B. Styczen[++]

The doubly-odd nuclei ^{108}Ag and ^{110}Ag are located between the vibrational nuclei of Pd and Cd and therefore are well suited to study the coupling of neutrons and protons and their coupling to the vibrational excitation modes. The splitting of the resulting multiplets - plotted as function of the angular momentum I(I+1) - is expected to follow a parabolic rule with the vertex being sensitive to the predominant particle or hole character of the quasiparticle[1]. Both nuclei ^{108}Ag and ^{110}Ag have been studied extensively by γ-ray and conversion-electron spectroscopy using thermal and resonance neutron capture. These investigations complement (d,p)- and (p,n)-measurements[2,3]. In spite of the great amount of data high resolution charged particle reaction studies are necessary to resolve remaining ambiguities in spin and parity assignments. Further the knowledge of experimental spectroscopic factors helps to verify the model wave functions.

In a first measurement of the deuteron spectrum for the reaction $^{109}Ag(p,d)^{108}Ag$ (Fig. 1) the resolution of ΔE = 4.0 keV ($\Delta E/E = 2.2 \cdot 10^{-4}$) was achieved in the spectra using the high resolution, variable dispersion spectrometer BIG KARL[4]. Because of the limited energy range four different magnet settings were necessary to cover excita-

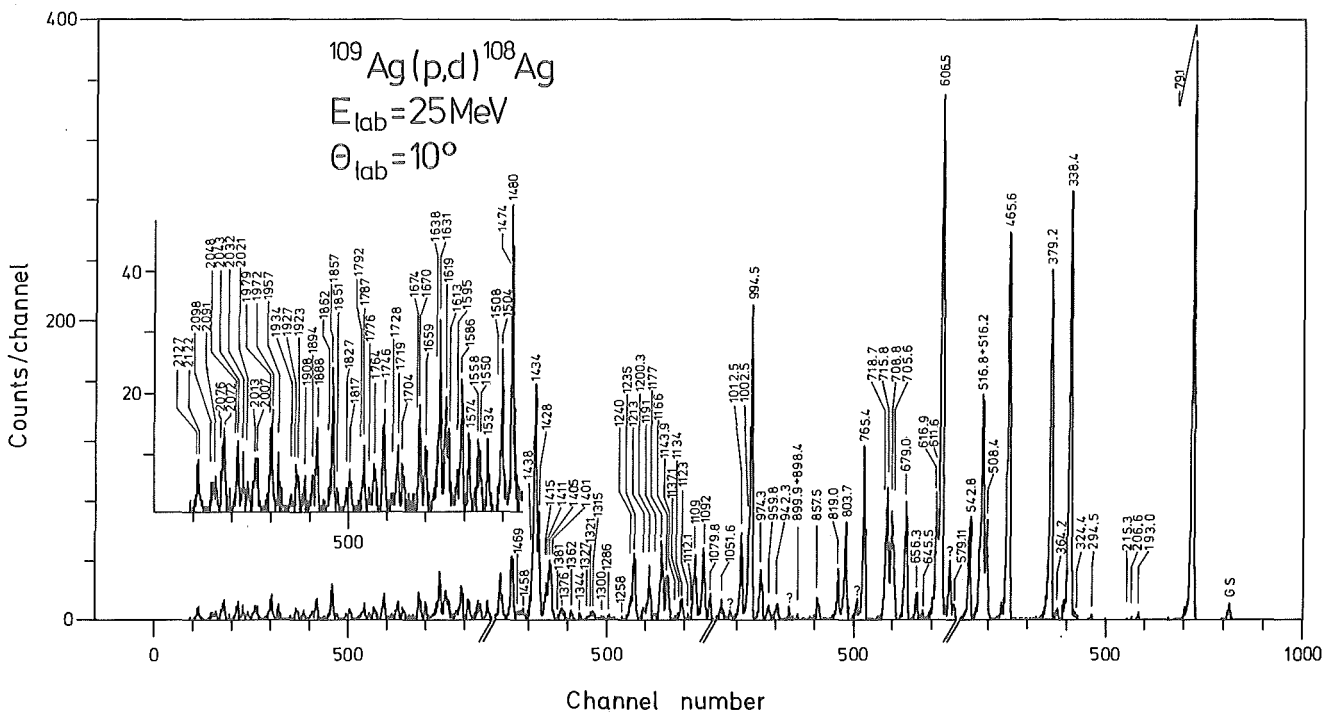

Fig. 1: Spectrum of the ^{109}Ag(p,d)^{108}Ag reaction (E_d = 18 MeV for GS excitation). Four spectra have been measured with integrated beam current of 1.6 mCoul (each two channels summed up in contrast to Fig. 2). Peak components of known states are labelled with accuracy of 0.1 keV, new energies are given to 1 keV. The lines at 79.1, 379.2, 679.9 and 1012.5 keV have been used for energy and line-shape calibration.

tion energies from E_x = 0 to 2.1 MeV. The dispersion of the double analyzing magnet system of the beam line was matched to the dispersion of the spectrometer set to 16.1 cm/% momentum. The solid angle was dΩ = 1.2 msr. A 30 cm long multi-wire proportional chamber in the detector plane (spatial resolution x < 0.4 mm) was used to measure the momentum spectra. The target consisted of a 100 µg/cm^2 thick selfsupported ^{109}Ag foil (isotopic enrichment: 99.4 %).

The spectra were analyzed with use of the program SAMPO which fits peaks of Gaussian shape with exponential low-energy tails. The quality of the obtained fits is demonstrated in Fig. 2. From the 41 components resolved for E_x < 1 MeV 35 can be assigned uniquely to states known from the neutron capture studies. The fitted energies agree with the known states within 0.5 keV except for the very weak states. Up to $E_x \sim$ 2.1 MeV the systematic errors of the given energies are estimated to increase to 6 keV due to the lack of calibration lines above ∿ 1 MeV in the present preliminary measurement. An additional measurement with a target of well suited Q value can yield these necessary lines. The planned measurement of angular distributions will give additional spectroscopic information, and will help to sort out possible impurity lines above $E_x \sim$ 1 MeV.

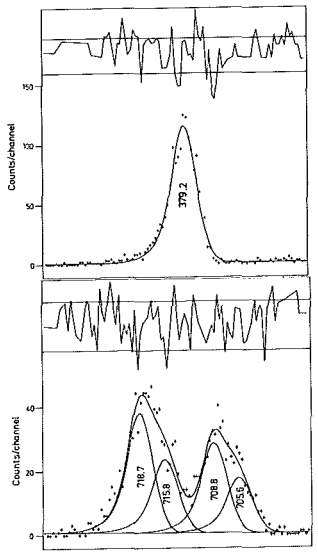

Fig. 2: Experimental data and the fitting results together with the residuals and the 2σ band.

References

1) V. Paar, Nucl. Phys. A331 (1979) 16
2) C.E. Brient, P.J. Riley, H. Seitz and S. Sen, Phys. Rev. C6 (1972) 1837
3) T. Hattori, M. Adachi, H. Taketani, J. Phys. Soc. Japan 41 (1976) 1830
4) S. Martin, G. Berg, A. Hardt, W. Hürlimann, M. Köhler, J. Meißburger, T. Sagefka and O.W.B. Schult, 1979 Proc. Daresbury Study Weekend, Ed. SRC Daresbury Lab. p. 38

+ RCNP Osaka University, Japan

++ Inst. of Physics, Jagiellonian University, Cracow, Poland

1.5. Investigation of Core-Coupled Multiplets in ^{143}Nd by ^{145}Nd(p,t) Reaction

J. Wrzesinski[+], C. Wesselborg[+], K.O. Zell[+], D. Bazzacco[+], P. von Brentano[+], C.F. Moore[++], G.P.A. Berg, W. Hürlimann, I. Katayama[*], S.A. Martin, J. Meißburger, W. Oelert, J. Römer and B. Styczen[**]

The investigation of the particle vibration coupling is important in view of the shell model and the collective model theories. Complete multiplets are usually investigated using direct reactions such as (p,t) or (p,p') on odd target nuclei. With in-beam gamma-ray spectroscopy only few states of a multiplet can be observed due to the large cross section of the Yrast levels.

Searching for core-coupled multiplets in the ^{146}Gd region we performed the ^{145}Nd(p,t)^{143}Nd two-nucleon transfer reaction at an incident energy of E_p = 25 MeV.

High resolution spectra (E/ΔE = 2000 - 3000) of the reaction products were measured using the BIG KARL magnetic spectrometer and a position sensitive multi-wire-proportional chamber in the focal plane. Because of the limited energy range excitation energies from 0 to 3.5 MeV were measured using 6 different magnet settings for the scattering angle of $\theta_{lab} = 5^0$. The six spectra were combined and the resulting triton spectrum is shown in fig. 1. The resolution is 7 - 10 keV depending on the position along the detector plane due to higher order aberrations. Angular distributions of the tritons have been measured for the excitation energy range from 2.8 to 3.5 MeV. In Fig. 2 some of the angular distributions are presented showing a clear dependence on angular momentaL. L-values have been assigned by comparison with the shape of the angular distributions in the ^{144,146}Nd (p,t)^{142,144}Nd reactions[1-2].

An extension of our measurements to the remaining excitation energy range (E_x < 2.8 MeV) and to the ^{143}Nd(p,p')^{143}Nd reaction is in preparation.

Due to the short usable length of the detector system (around 30 cm) a lot of beam time was spent in this high resolution experiment. Therefore it was decided to build in collaboration with the Los Alamos Laboratories a new detector system covering the full focal plane of 100 cm.

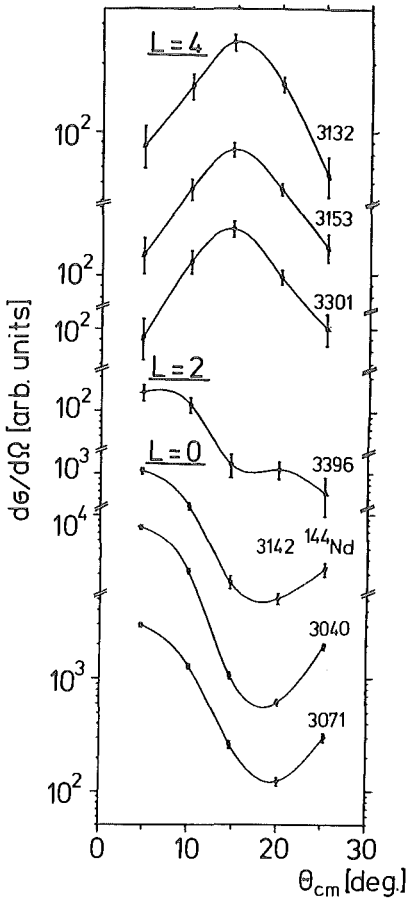

Fig. 2: Sample angular distributions from the ^{145}Nd(p,t)^{143}Nd reaction. The solid lines are drawn to guide the eye.

References

1) S. Raman, R.I. Auble, J.B. Ball, E. Newman, J.C. Wells, Jr., and J. Jin, Phys. Rev. C14, 1381 (1976)

2) K. Yasi, Y. Aoki, J. Kawa and K. Sato, Phys. Lett. 29B, 647 (1969)

+ Institut für Kernphysik, Universität Köln, F.R. Germany

++ Dept. of Physics, The University of Texas, Austin, USA

* RCNP, Osaka University, Japan

** Institute of Physics, Jagiellonian University, Cracow, Poland

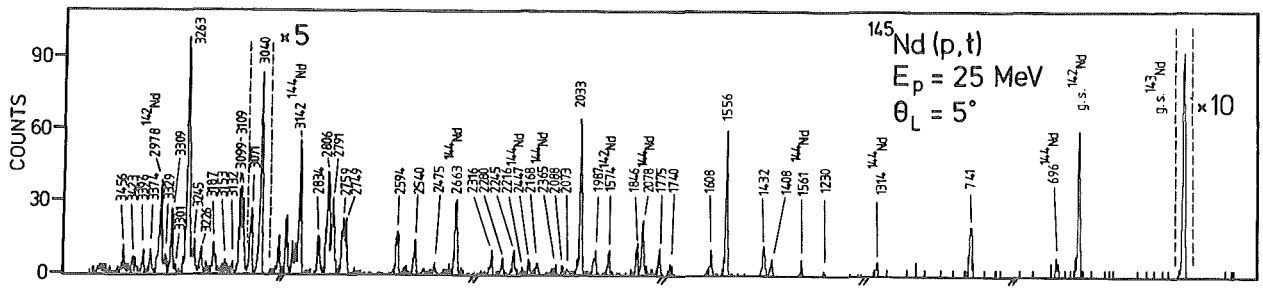

Fig. 1: High resolution spectrum of the ^{145}Nd(p,t)^{143}Nd reaction using the magnetic spectrometer BIG KARL. The excitation energies of some of the states are indicated.

1.6. High Energy Proton Stripping by ^{27}Al and ^{28}Si Nuclei: Ground State Transitions

A. Djaloeis, S. Gopal, J. Bojowald, C. Mayer-Böricke, W. Oelert, N.G. Puttaswamy and P. Turek

Proton stripping experiments on ^{27}Al and ^{28}Si targets through the (τ,d) reaction, have been performed at E_τ = 130 MeV. Experimental details and some preliminary results have been reported[1] earlier.

In this report we present experimental results and their analysis for the ground-state transitions which involve two different single (ℓj)-transfers, namely $(1d_{5/2})$ and $(2s_{1/2})$ for the $^{27}Al(\tau,d_0)^{28}Si$ and $^{28}Si(\tau,d_0)^{29}P$ reactions, respectively. For these two experimental angular distributions, we have studied systematically the dynamical aspects of the reactions in order to obtain a consistent set of best-fit DWBA parameters. Using these parameters the spectroscopic information has been extracted and compared with that available in the literature.

The theoretical cross section is calculated in the DWBA formalism, employing the DWUCK4[2] programme. The relation between the experimental $(d\sigma/d\Omega)_{exp}$ and the theoretical $(d\sigma/d\Omega)_{DW}$ cross section for a (τ,d) reaction is given by[2]:

$$(d\sigma/d\Omega)_{exp} = 4.42 \left[\sum_{\ell j} \frac{G(n\ell j)}{2j+1} (d\sigma/d\Omega)_{DW} \right]$$

where $$G(n\ell j) = \frac{2J_f+1}{2J_i+1} C^2 S(n\ell j).$$

The quantity C^2 is the isospin coupling coefficient, $S(n\ell j)$ is the spectroscopic factor and $G(n\ell j)$ is the spectroscopic strength for the proton stripped into the orbit specified by the principal quantum number n and by the orbital and total angular momentum ℓ and j, respectively. The initial (target) and the final (residual nucleus) spins are denoted by J_i and J_f, respectively.

A list of the optical model potential (OMP) and DWBA parameters used in the present work is given in table 1.

Extensive calculations show that the use of the OMP combination DSSH(τ)-BSSD3(d) including non-locality (NL) and finite-range corrections (AFR) gives the best description of the experimental data. The results are shown in fig. 1. Consequently, the DSSH-BSSD3 OMP combination was used to extract the spectroscopic strengths.

The spectroscopic strengths for the proton stripped to the ground state of the final nuclei ^{28}Si and ^{29}P extracted in this work as well as those available in the litterature are summarized in table 2. It can be seen that for the ^{29}P case, previous experimental $G(2s_{1/2})$ values show large discrepancies up to a factor of 3, the lowest and the highest values being 0.42 and 1.36, respectively. Similarly for ^{27}Al, experimental $G(1d_{5/2})$ values are found to vary from 0.25 to 1.0. At lower incident energies these discrepancies might reflect the inadequacy of the DWBA to describe the reaction mechanism since at these energies indirect processes and even fluctuation in the cross sections may play a significant role. Further uncertainties are introduced because of the subjectivity in normalizing the DWBA to the experimental angular distribution, in particular when the fit is not good.

In this work the $G(2s_{1/2})$ for the $^{28}Si(\tau,d_0)^{29}P$ reaction is found to be 0.89±0.18. This value agrees well with that obtained (0.90) by a shell model calculation[20] performed in a full $1d_{5/2}$-$2s_{1/2}$-$1d_{3/2}$ basis space. For the $^{27}Al(\tau,d_0)^{28}Si$ reaction, on the other hand, the presently

Set	$V^{(a)}$ (MeV)	r_V (fm)	a_V (fm)	$W_s^{b)}$ (MeV)	$W_V^{a)}$ (MeV)	r_W (fm)	a_W (fm)	V_{so} (MeV)	r_{so} (fm)	a_{so} (fm)	Ref.
τ^+: JVSH	110.0	1.128	0.856		21.6	1.613	0.643				present
JSSH	110.0	1.113	0.860	20.2		1.105	0.833				"
DVSH	110.0	1.084	0.973		28.4	1.466	0.707				"
DSSH	110.0	1.081	0.988	19.9		1.050	0.886				"
d*: DMSD1	55.0	1.170	0.873	3.0	13.1	1.262	0.730	3.0	1.070	0.660	3)
DMSD2	55.0	1.170	0.873	3.0	13.1	1.262	0.730	6.0	1.070	0.660	present
BSSD1	47.0	1.180	0.720	10.0		1.15	0.900	12.5	1.100	1.000	4)
BSSD2	47.0	1.180	0.720	10.0		1.150	0.900	6.0	1.100	1.000	present
BSSD3	47.0	1.180	0.720	10.0		1.150	0.900	6.0	1.180	0.720	"
BMSD4	58.9	1.180	0.754	5.5	7.6	1.270	0.814	6.0	0.900	0.900	5)

In all sets r_c = 1.3 fm.

Proton bound-state parameter: λ = 25.0 (Thomas spin-orbit form),
r_0 = 1.25 fm,
a = 0.65 fm.

Non-locality parameter: $\beta(p)$ = 0.85 fm^{-1}
$\beta(\tau)$ = 0.25 fm^{-1}
$\beta(d)$ = 0.54 fm^{-1}
Finite-range parameter: R = 0.77 fm
} ref. 6)

\+ The analytical form of the potential shapes is given in ref. 7).

* " " " " " " " " " " ref. 3).

a) Woods-Saxon.

b) Woods-Saxon derivative.

Table 1: Optical-model and DWBA parameters

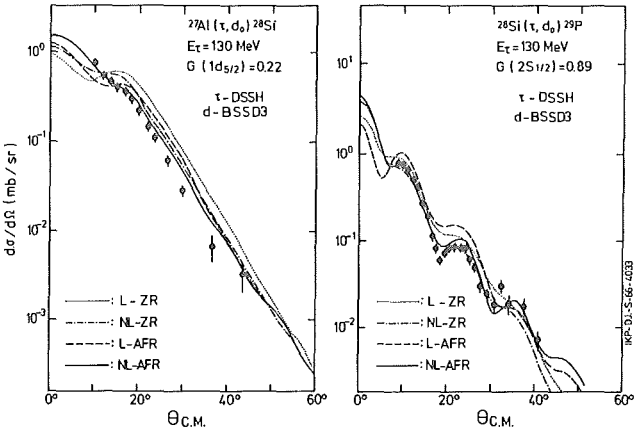

Figure 1: see text.

	Reaction	E_{inc} (MeV)	G(nℓj)	Ref.
Target: ^{27}Al	(τ,d_0)	37.7	0.44	11)
$J_i^\pi = 5/2^+$	(d,n_0)	6	0.26	12)
$J_f^\pi = 0^+$	(τ,d_0)	8	0.49	8)
nℓj = $1d_{5/2}$	(α,t_0)	104	1.0	13)
	(α,t_0)	27.2	0.44	14)
	(α,t_0)	25.2	0.58 0.86 0.90	15)
	(τ,d_0)	130	0.22±0.04*	pres.work
	theory		0.53 0.61	19) 20)
Target: ^{28}Si	(d,n_0)	7.9	1.36	17)
$J_i^\pi = 0^+$	(τ,d_0)	35.3	0.42	16)
$J_f^\pi = 1/2^+$	(τ,d_0)	38.5	1.02	9)
nℓj = $2s_{1/2}$	(τ,d_0)	25	1.30	10)
	(τ,d_0)	29	1.08	18)
	(τ,d_0)	130	0.89±0.18*	pres.work
	theory		1.0 0.90	19) 20)

*The quoted error reflects only the experimental error and the uncertainty in matching the theoretical curve to the experimental angular distribution.

Table 2: Spectroscopic strengths $G(n\ell j) = (2J_f+1)(2J_i+1)^{-1}C^2S(n\ell j)$ for proton stripping to the ground-states of ^{28}Si and ^{29}P.

extracted $G(1d_{5/2}) = 0.22\pm0.04$ differs largely from $G(1d_{5/2}) = 0.61$ predicted by the same shell model calculation[20]. The reason for this discrepancy is not understood at present, in particular if one compares the ratio $G(2s_{1/2})/G(1d_{5/2})$ of the presently extracted spectroscopic strengths for the two transitions studied and the one predicted by the shell model. However, considering the deformation of the ^{27}Al and ^{28}Si nuclei, the neglect of 1f-2p shell in the above shell model calculation might not be justified. How far the inclusion of the 1f-2p shell will affect the present shell model predictions remains to be seen.

References

1) A. Djaloeis et al., Annual Report 1980, KFA-IKP, Jül-Spez-99, p. 19

2) P.D. Kunz, Computer Code DWUCK 4, Univ. of Colorado, Boulder, USA

3) W.W. Daehnick, J.D. Childs, and Z. Vrcelj, Phys. Rev. C21 (1980) 2253 and references therein; L.D. Knutson and W. Haeberli, Phys. Rev. Lett. 30 (1973) 986, and Phys. Rev. C12 (1975) 1469

4) J. Bojowald, C. Mayer-Böricke, M. Rogge, and P. Turek, Annual Report 1979, KFA-IKP, Jül-Spez-72, p. 1, and Annual Report 1980, KFA-IKP, Jül-Spez-99, p. 1

5) P.W. Keaton and D.D. Armstrong, Phys. Rev. C8 (1973) 1692

6) J.R. Shepard, W.R. Zimmermann, and J.J. Kraushaar, Nucl. Phys. A275 (1977) 189

7) A. Djaloeis, J.P. Didelez, A. Galonsky, and W. Oelert, Nucl. Phys. A306 (1978) 221

8) J. Kalifa, G. Rotbard, M. Vergnes, and G. Ronsin, J. de Phys. 34 (1973) 139

9) R.J. Peterson and R.A. Ristinen, Nucl. Phys. A246 (1975) 402

10) W.W. Dykoski and D. Dehnhard, Phys. Rev. C13 (1976) 80

11) R.W. Barnard and G.D. Jones, Nucl. Phys. A108 (1968) 641

12) W. Bohne et al., Nucl. Phys. A131 (1969) 273

13) G. Hauser et al., Nucl. Phys. A182 (1972) 1

14) O.F. Nemets et al., UFZH 22 (1977) 246

15) V.M. Lebedev et al., Nucl. Phys. A298 (1978) 206

16) P. Leleux, P.C. Macq, J.P. Meulders, and C. Pirart, Z. Physik 271 (1974) 139

17) Buccino et al., Nucl. Phys. 86 (1966) 353

18) Koyama et al., J. Phys. Soc. Japan 43 (1977) 755

19) B.H. Wildenthal and J.B. McGrory, Phys. Rev. C7 (1973) 714

20) W. Chung and B.H. Wildenthal, Michigan State University, East Lansing, USA, private communication

1.7. The (d,^{3}He) Reaction on Iron Isotopes

N.G. Puttaswamy, A. Djaloeis, P.W.M. Glaudemans, K. Heyde**, P. van Isacker**, V. Lopac***, C. Mayer-Böricke, B.C. Metsch*, W. Oelert, V. Paar***, P. Turek, M. Waroquier**, G. Wenes***

The structure of the energy levels of nuclei near the doubly-magic ^{56}Ni has received considerable attention in recent years[1]. Therefore we started a systematic investigation on one-nucleon-transfer reactions in the middle of the fp-shell. Spectroscopic factors extracted this way should provide a test of the wave functions and hence should supply arguments for the model space and residual interactions used for the theoretical calculations. With this aim we studied the (d,^{3}He) reaction on the even iron isotopes at E_d=80 MeV and have obtained spectroscopic information on the energy levels in ^{53,55,57}Mn.

Typical ^{3}He spectra, which have been detected by three ΔE-E silicon surface-barrier counter telescopes mounted inside the scattering chamber, are shown in Fig. 1. An

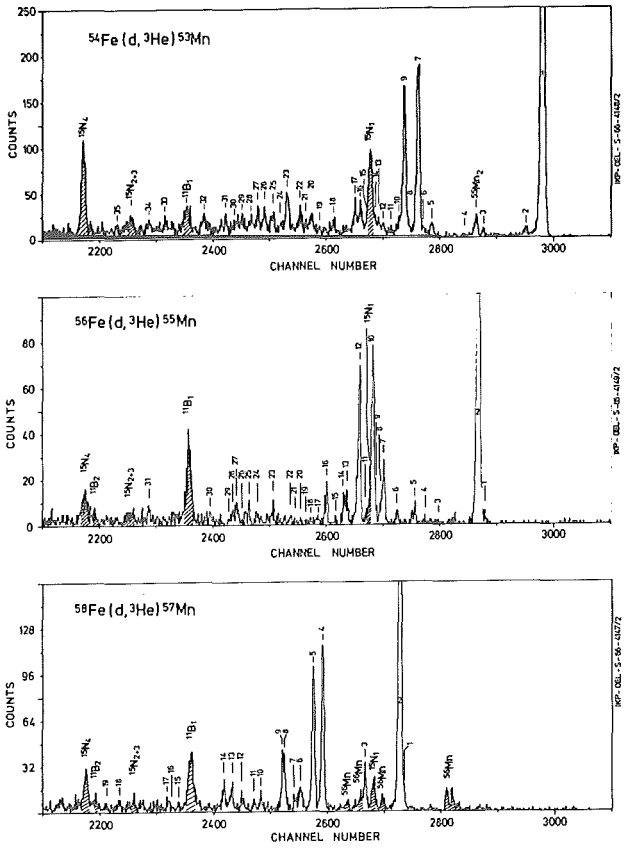

Figure 1: Energy spectra of ^{3}He particles at 9.9° lab. from the (d,^{3}He) reaction on iron isotopes. The peaks are numbered in the order of increasing excitation energy. A straight-line background is assumed only for the ^{53}Mn spectrum.

energy resolution of about 70 keV FWHM has been obtained. Distorted-Wave-Born-Approximation (DWBA) calculations have been performed employing the zero-range code DWUCK4[2] using a finite-range correction factor of 0.77 fm and non-locality parameters of 0.54, 0.25 and 0.85 fm for the particles d, ^{3}He and p, respectively.

The extracted spectroscopic factors are compared to three different theoretical predictions: i) shell-model calculations performed in truncated model spaces A and B using Kuo-Brown (KBI) and surface delta interactions (SDI), ii) quasi-particle-core-coupling calculations (QPCC), where up to three quadrupole phonons, up to two octupole phonons or up to mixed two quadrupole and one octupole phonon states are considered, iii) cluster-vibration-model (CVM) calculations, where odd Mn and even Fe isotopes are described by coupling three- and two-proton holes, respectively, to the quanta of quadrupole vibration. For more details on the experimental and theoretical evaluation of the spectroscopic information we refer to Ref. 3 and references therein. The results indicate in general fair agreement between the experimental and the theoretical values of the spectroscopic strengths. A comparison of the distribution of the experimental and the shell-model $f_{7/2}$ ℓ=3 strengths is presented in Fig. 2 by adding up the strengths

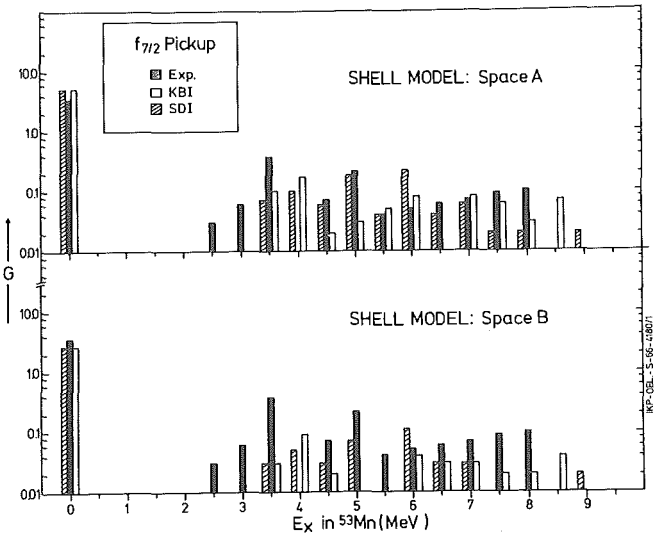

Figure 2: Comparison of the distribution of experimental $f_{7/2}$ strength with shell-model predictions for ^{53}Mn. Both the experimental and the theoretical strengths have been added up in 0.5 MeV bins.

in 0.5 MeV energy bins. For the model space A, the theoretical strength for the g.s. is larger than the experimental value whereas the agreement for the excited states is satisfactory. In the case of model space B, the strength to all states is reduced by about 50 %. An extension of the model space for ^{53}Mn by the inclusion of an additional particle-hole configuration is expected to enhance the predicted strengths. Such a calculation seems desirable but is impeded by the enormous dimensions of the corresponding model space.

The QPCC calculations yield agreement to the experimental data with regard to the positive-parity levels. The ground states of all the Mn isotopes are predicted to be $7/2^-$, whereas experimentally both ^{55}Mn and ^{57}Mn have spin and parity $5/2^-$. This difficiency is removed by the CVM calculations and the correct spin-parity is predicted for the ground states of all the Mn isotopes.

A comparison of the distribution of the experimental and the theoretical ℓ=2 strengths for $d_{3/2}$ and $d_{5/2}$ pick-up is presented in Fig. 3. The agreement for the case of the $d_{3/2}$ strength is satisfactory. The $d_{5/2}$ strength predicted around E_x = 9 MeV by the QPCC calculation is not seen in the present experiment indicating (i) that the strength may actually be expected to be present at higher excitation

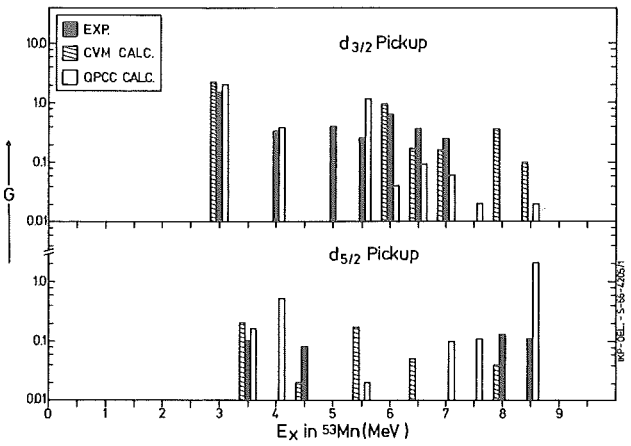

Figure 3: Comparison of the distribution of the experimental $d_{3/2}$ and $d_{5/2}$ strengths with the predictions from QPCC and CVM calculations for ^{53}Mn.

energy, and/or (ii) that there is a large spreading of the strengths. The CVM calculation indeed predicts a low value for the $d_{5/2}$ strengths. The present experimental study of the (d,^{3}He) reaction on iron isotopes has led to the identification of many new levels in the odd Mn isotopes; most of these levels with $E_x \geq 4$ MeV are found to have ℓ=2 pickup strength. The experimentally deduced excitation energies and spectroscopic strengths for the $1/2^+$ and $3/2^+$ levels in the Mn isotopes are rather well predicted by the QPCC and CVM calculations; in particular, the agreement for the lowest $1/2^+$ and $3/2^+$ levels is very good.

References

1) J.P. Elliott, in Structure of Medium-Heavy Nuclei 1979, edited by the 'Demokritos' Tandem Accelerator Group, Athens (The Institute of Physics, Bristol, 1979), p. 1;
P.W.M. Glaudemans, ibid, p. 11

2) P.D. Kunz, computer code DWUCK, University of Colorado, Boulder, Bolorado, 1974, unpublished

3) N.G. Puttaswamy et al., to be published

* Rijksuniversiteit Utrecht, The Netherlands

** Laboratorium voor Kernfysica, Gent, Belgium

*** University of Zagreb, Yugoslavia

1.8. Study of the ^{62}Ni(d,^{3}He)^{61}Co Reaction

A. Marinov, G. Berg, W. Hürlimann, I. Katayama**, S. Martin, C. Mayer-Böricke, J. Meißburger, W. Oelert, J. Roemer, M. Rogge, J. Tain, P. Turek, L. Zemło****

A study of the ^{62}Ni(d,^{3}He)^{61}Co reaction has been started using 78 MeV deuteron beam from the isochronous cyclotron JULIC and the QQDDQ magnetic spectrometer BIG KARL. The aim of the experiment is to study proton hole states in ^{61}Co up to an excitation energy of about 7 MeV at high bombarding energy and with as good resolution as possible. About 100 µg/cm^2 nickel target enriched to 99.3 % with ^{62}Ni has been bombarded with a well-focused momentum-analysed deuteron beam of 78 MeV. ^{3}He particles were measured using the multi-wire proportional counter situated in the focal plane of the BIG KARL magnetic spectrometer. Additionally a ΔE gas proportional and a plastic scintillation counter were used for particle identification; they are situated behind the focal plane. Meanwhile a region of excitation energy up to about 2.6 MeV in ^{61}Co has been studied. Total energy resolution of about 25 keV (FWHM) has been obtained. Figure 1 shows a typical spectrum which was obtained at 7.5°. Energy spectra were measured in the angular range of 3° to 33.6° to the incident beam in steps of 1.5° to 3°. The ground state and eleven excited states in ^{61}Co are clearly seen in these spectra. In addition few states which are very weakly populated in the (d,^{3}He) reaction were also seen. The analysis of the data in terms of the DWBA calculations is in progress.

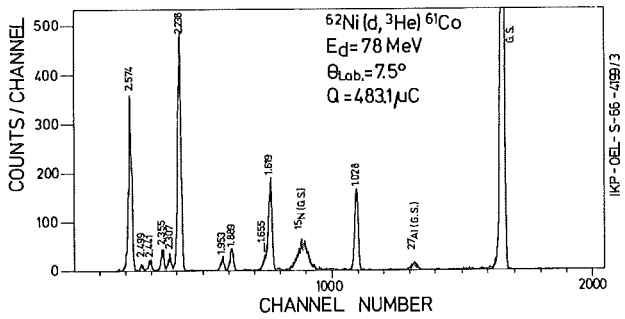

Figure 1: ^{3}He-particle spectrum of the ^{62}Ni(d,^{3}He)^{61}Co reaction measured at a deuteron energy of 78 MeV and at a scattering angle of 7.5° to the incident beam.

* On leave of absence from the Racah Institute of Physics, The Hebrew University of Jerusalem

** On leave of absence from Research Center for Nuclear Physics, Osaka University, Japan

*** On leave of absence from Institute of Nuclear Research, Warsawa, Poland

1.9. Investigation of proton-particle proton-hole multiplets in ^{208}Pb

G.P.A. Berg, W. Hürlimann, I. Katayama[*] *G. Mairle*[+], *S. Martin, J. Meißburger, J. Römer, K. Schindler*[+], *U. Schmidt-Rohr*[+], *B. Styczen*[++]

Angular distributions of ^{3}He particles from the $^{208}Pb(d,^{3}He)^{207}Tl$ and $^{209}Bi(d,^{3}He)^{208}Pb$ reactions have been measured at 45 MeV using the magnetic spectrometer BIG KARL. A DWBA analysis shows that the four lowest states of ^{207}Tl can be regarded as pure single proton hole states in the $3s_{1/2}$, $2d_{3/2}$, $1h_{11/2}$ and $2d_{5/2}$ shells of ^{208}Pb. The $^{209}Bi(d,^{3}He)^{208}Pb$ spectra can be interpreted, therefore, as consisting of proton-particle ($1h_{9/2}$) proton-hole multiplets with respect to ^{208}Pb. The related effective residual interactions can be deduced from the distribution of the spectroscopic strengths if all final spins and the detailed j-mixing are known. A first inspection of the spectra yielded the monopoles of these effective interactions: -0.29 MeV, -0.32 MeV, -0.37 MeV and -0.30 MeV for a proton in the $1h_{9/2}$ shell and proton holes in the $3s_{1/2}$, $2d_{3/2}$, $1h_{11/2}$ and $2d_{5/2}$ shells, respectively. A more refined analysis will provide higher multipoles and diagonal matrix elements of the effective residual interactions. The data contain new information on high spin states and complete results from recent (e,e') and (p,p') experiments; they can be used as a test of available shell model calculations and can be treated as a basis for new ones.

+ MPI für Kernphysik, Heidelberg
* RCNP Osaka University, Japan
++ Institute of Physics, Jagiellonian University, Cracow, Poland

1.10. Alpha-Transfer-Reaction Study in the Middle of the sd-Shell

W. Oelert, G.P.A. Berg, A. Djaloeis, C. Mayer-Böricke, and P. Turek

The alpha-transfer reaction study on ^{32}S and ^{34}S leading to final states in ^{28}Si and ^{30}Si measured via the $(d,^{6}Li)$ reaction at E_d = 80 MeV has been completed. This investigation should be of interest to observe: i) the behaviour of the ground state to ground state transition spectroscopic factors in the middle of the sd-shell, where strong deviations have been observed between theoretical shell model predictions and experimental results which themselves do not give a consistent picture, and ii) the alpha spectroscopic strengths for excited states, which e.g. for the first 2^+ states are predicted[1] to increase with increasing mass number throughout the sd-shell for pickup reactions.

A typical energy spectrum is shown in Fig. 1. A gas cell filled with $H_2{}^{A}S$ was used as target. Unfortunately all

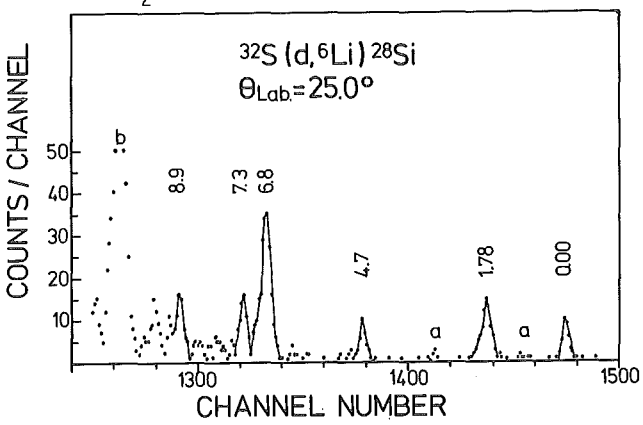

Figure 1: ^{6}Li spectrum of the $^{32}S(d,^{6}Li)^{28}Si$ reaction
a and b denote impurity yield.

materials ordered (by three different producers) had either ^{14}N or ^{16}O impurities, which was identified by the kinematic shift of the ^{6}Li reaction products and by measuring the $(d,^{6}Li)$ reaction on air as gas target. After identifying the yield resulting from the impurities their peak positions were used for the energy calibration of the spectra. Even though the pressure in the cell remained constant during a run, the H_2S gas deteriorated under the influence of the beam. The number of sulfur atoms of the H_2S gas in the cell decreased by a factor of two after the bombardment with 17 m Coulomb (rather independently of the beam intensity). Therefore a monitor detector, which counted the elastically scattered deuterons, was essential to determine the relative cross sections. Because of the rather low cross sections a high intensity achromatic beam was used. An overall energy resolution of 350 keV FWHM was typical for the ^{6}Li spectra.

The experimental angular distributions were compared to FR-DWBA calculations using parameters as described earlier[2] to extract alpha spectroscopic factors S_α. The quality of the fits obtained between experimental angular distributions and theoretical DWBA curves can be seen in Fig. 2 and Fig. 3. Details of the comparison between experimental and shell model theoretical spectroscopic fac-

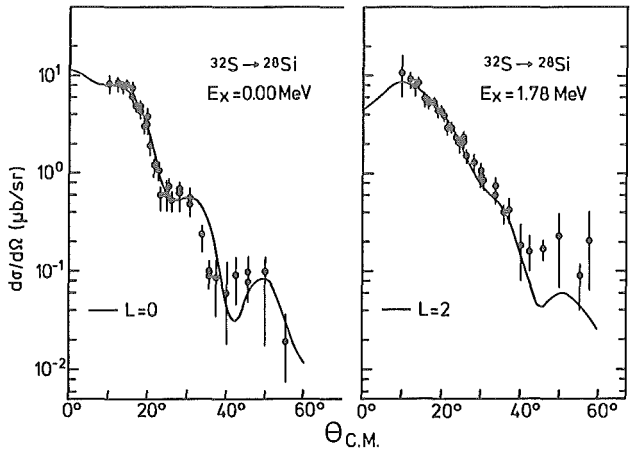

Figure 2: Experimental angular distribution for transitions observed in the $^{32}S(d,^{6}Li)^{28}Si$ reaction, compared to DWBA predictions.

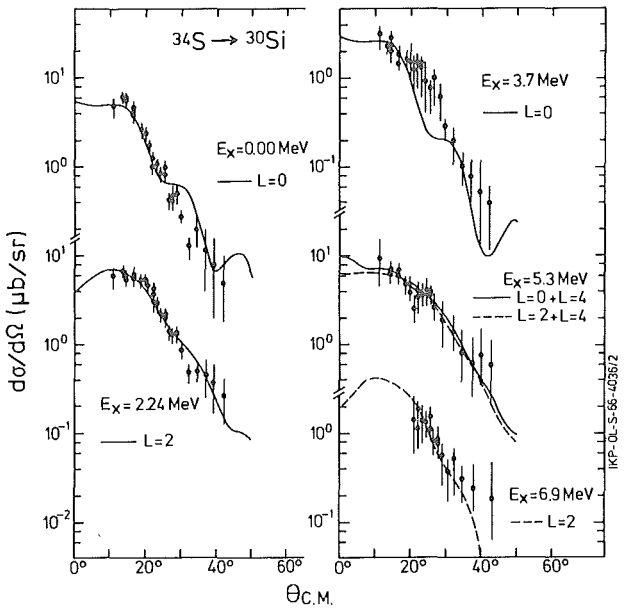

Figure 3: Same as Fig. 2 for the $^{34}S(d,^{6}Li)^{30}Si$ reaction.

tors are given elsewhere[3]. With respect to the analysis of excited states, the following results may be summarized: The experimental and theoretical relative spectroscopic factors for the first excited 2^+ states are in rather good agreement. In ^{28}Si the first 4^+ state is predicted to be weakly excited (S_α = 0.02), whereas the experimental value is a factor of twenty larger. Experimental and theoretical spectroscopic factors for the second 4^+ state are in reasonable agreement, both being relatively large. It seems that at least phenomenologically the situation here is similar to that as described[4] in the case of the $^{26}Mg(d,^{6}Li)^{22}Ne$ reaction.

As summarized by Fulbright[5] and Chung et al.[6] the experimental ground state to ground state transition alpha spectroscopic factors do in general follow the theoretically predicted decrease with increasing mass up to the middle of the sd-shell, independently of the reaction type. For larger masses, however, significant deviations from the predicted values of the shell model calculations are observed and, furthermore, the experimental values themselves do not give a consistent picture. Since the experimental spectroscopic factors are extracted by the ratios of experimental to DWBA cross sections the question arises whether the source of inconsistencies is due to experimental deviations between different investigations or due to insufficient description of the reaction mechanism by the DWBA. Fig. 4 shows that the slope of the

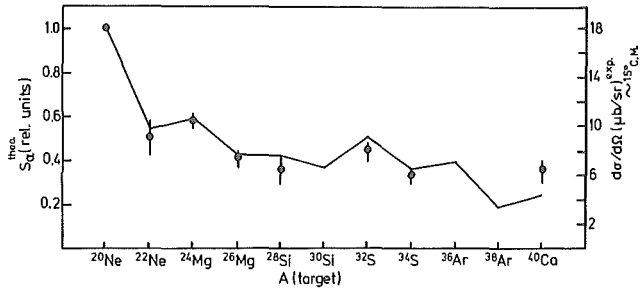

Figure 4: Solid line and scale at the left hand side: Theoretical ground state alpha spectroscopic factors for sd-shell nuclei. Points and scale at the right hand side: Experimental cross sections at the maximum of the angulare distribution at ∿ 15° c.m..

experimental cross sections agrees very well with that of the predicted spectroscopic factors throughout the sd-shell. Consequently the figure provides strong indications that the commonly extracted experimental spectroscopic factors are extremely dependent on the DWBA parameters employed. As described by Fulbright[5] it seems that employing a radius dependence as $R = r_0 \cdot (A^{1/3} + 6^{1/3})$ for the ^{6}Li optical potential in the DWBA calculations diminishes the discrepancies between theoretically predicted and experimentally evaluated spectroscopic factors. However, this ad hoc prescription probably indicates the necessity of selecting the correct optical potential family and the necessity to stay within this family in a systematic investigation with a decreasing value of the volume integral for increasing masses as described recently by a systematic ^{6}Li optical potential consideration[7]. Preliminary results of the analysis for ground state to ground state alpha transfer transitions seem to resolve the strong discrepancies between experimental and theoretical relative spectroscopic factors observed in the upper half of the sd shell.

References

1) W. Chung et al., to be published
2) W. Oelert et al., Phys. Rev. C20 (1979) 459
3) W. Oelert et al., to be published
4) W. Oelert et al., Phys. Rev. C22 (1980) 408
5) H.W. Fulbright, Ann. Rev. Nucl. Part. Sci. 29 (1979) 161
6) W. Chung et al., Phys. Lett. 79B (1978) 381
7) P. Lezoch et al., Phys. Rev. C23 (1981) 2763

1.11. Breakup of ^{3}He-projectile at E_{in} = 130 MeV

J. Bojowald, A. Djaloeis, S. Gopal, C. Mayer-Böricke, W. Oelert, N.G. Puttaswamy and P. Turek

Deuteron spectra from the bombardment of ^{27}Al, ^{59}Co, ^{93}Nb and ^{197}Au targets by 130 MeV ^{3}He-projectiles have been measured at the Jülich cyclotron. The experimental details have been reported previously[1].

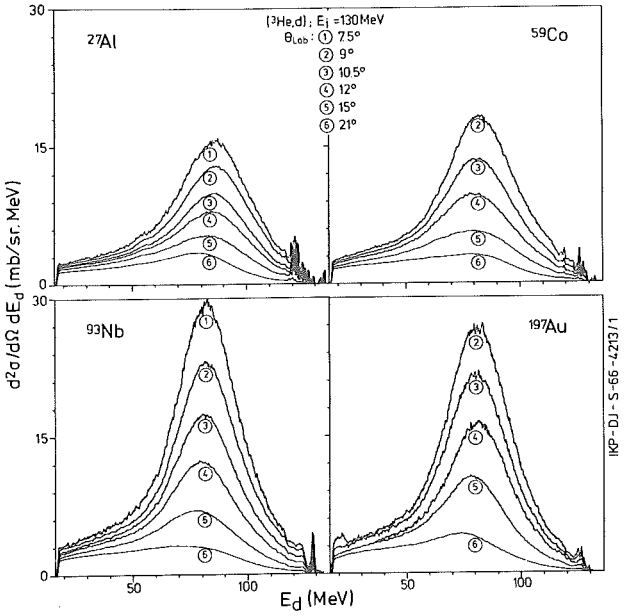

Figure 1: Examples of d-spectra from the (^{3}He,d) reaction at E_{in} = 130 MeV.

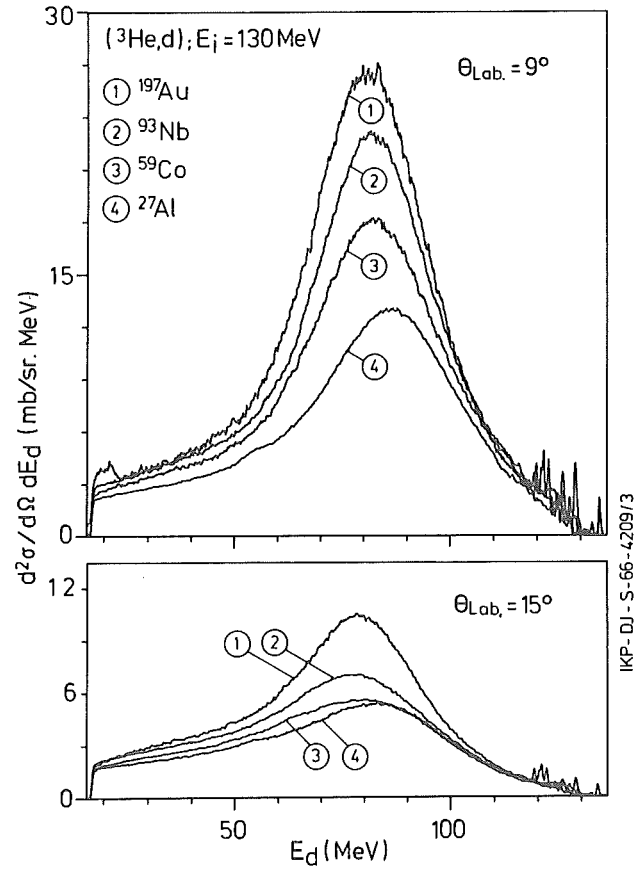

Figure 2: Dependence of d-spectra on the target mass for the (^{3}He,d) reaction at E_{in} = 130 MeV.

Examples of the measured spectra are shown in fig. 1, which clearly exhibits the ^{3}He-breakup peak located at about 2/3 E_{in}. Apart from the forward peaking of the ^{3}He-breakup cross section, one sees that the peak position tends to move towards lower energies as the angle increases (see also fig. 4). Fig. 2 shows the dependence of the breakup peak on the target mass A for θ_L = 9° and 15°.

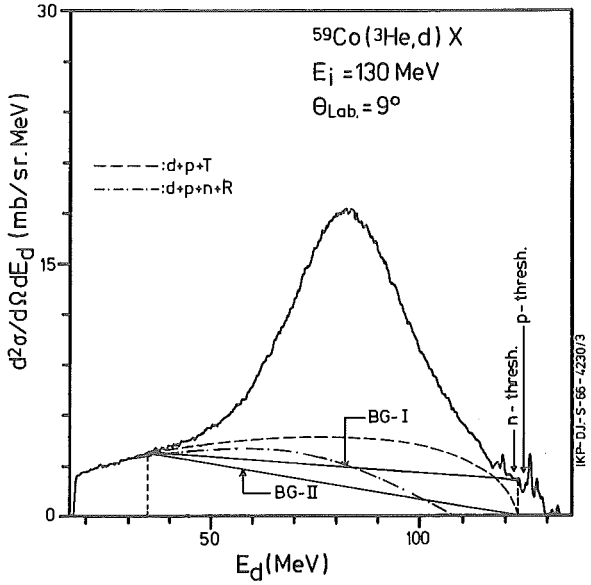

Figure 3: Illustration of two types of background used in extracting the breakup bump.

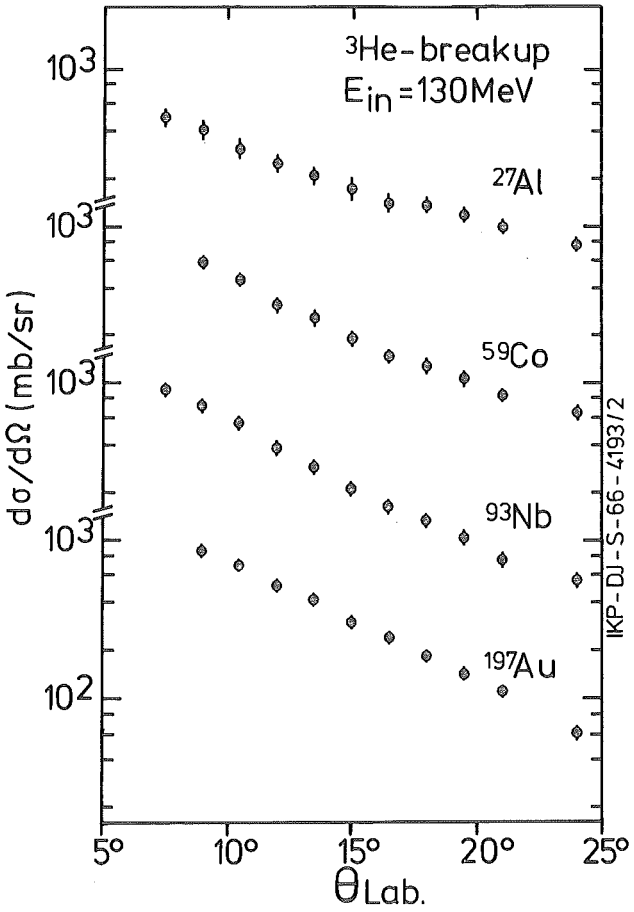

Figure 4a: Angular distribution of dσ/dΩ of the ^{3}He-break up bump at E_{in} = 130 MeV.

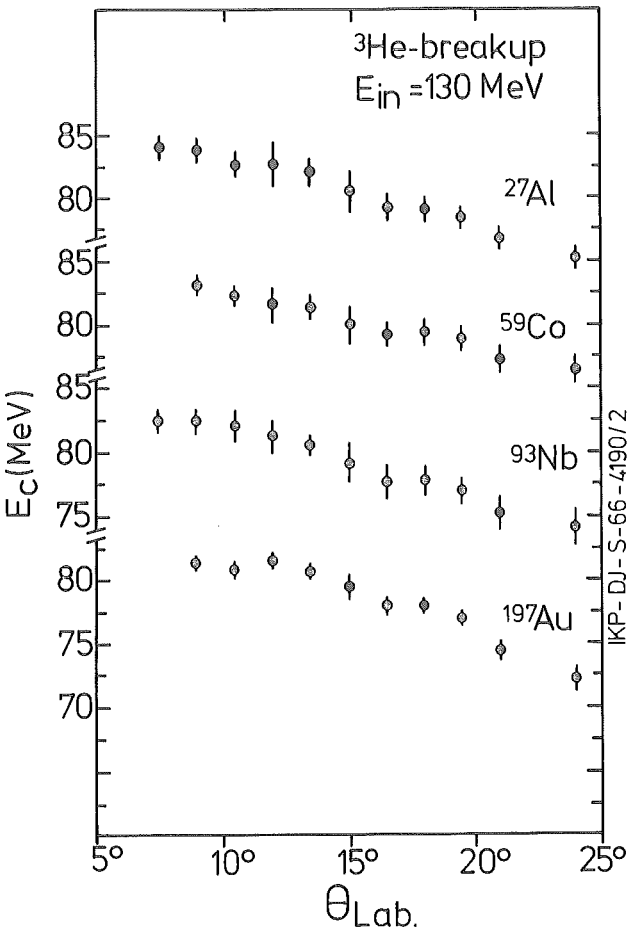

Figure 4b: As Figure 4a but for E_c.

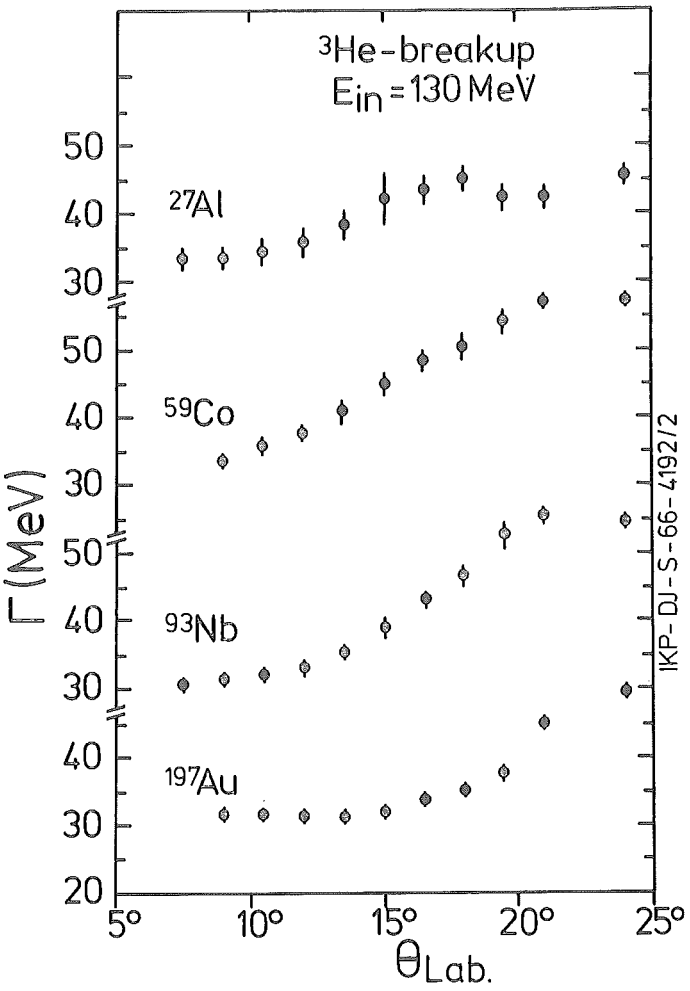

Figure 4c: As Figure 4a but for Γ.

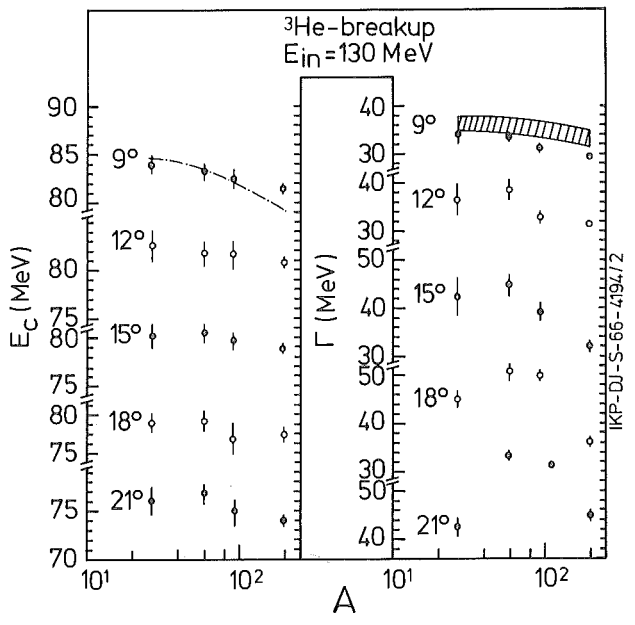

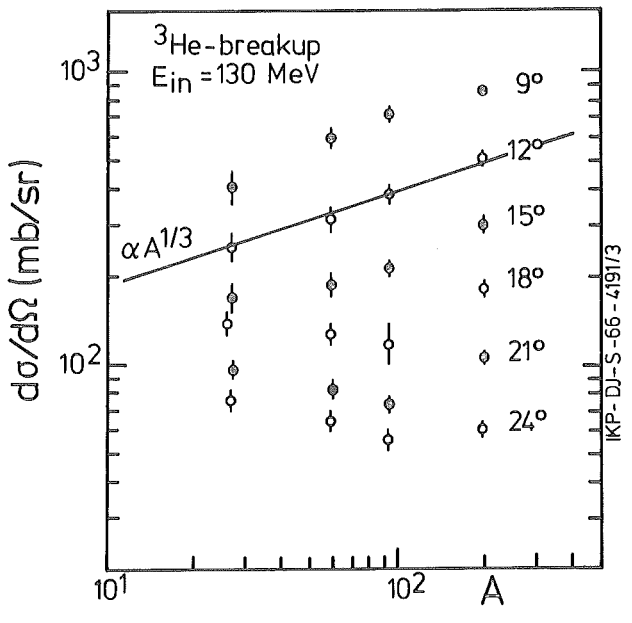

Figure 5: Target mass dependence of $d\sigma/d\Omega$, E_c, Γ and σ_{bn} of the ^{3}He-brekup bump at E_{in} = 130 MeV.

The quantities $d\sigma/d\Omega$ (breakup differential cross section), E_c (centroid position of the breakup peak) and Γ (FWHM of the breakup peak) have been extracted from the spectra after subtracting the backgrounds shown in fig. 3. The quoted uncertainties of the extracted quantities reflect the difference between the two chosen background shapes. The "true background" is expected to lie somewhere in between.

Fig. 4 shows the angular dependence of $d\sigma/d\Omega$, E_c and Γ. For all the four targets, $d\sigma/d\Omega$ and E_c fall down almost exponentially (with a slope $a \approx -0.18$/deg.) and linearly, respectively, as the angle θ increases. On the other hand, Γ increases with θ, with a trend, different from one target to the other.

The A-dependence of $d\sigma/d\Omega$, E_c and Γ at different angles is shown in fig. 5. The trend $d\sigma/d\Omega \sim A^{1/3}$ [see ref. 2)] is observed only at very forward angles ($\theta_L \lesssim 15^o$). At $\theta_L = 9^o$ the E_c-values seem to follow[2] $E_c \approx \frac{1}{3}[2E_{in} - V_c(Z)]$ where $V_c(Z)$ denotes the Coulomb barrier suffered by ^{3}He due to the target charge Z; large deviations are seen at larger angles. Similar comments can be made on the values of Γ, which was previously reported[2] to follow $\Gamma = 1.41(1-V_c/E_{in})\sqrt{E_{in}\varepsilon}$, ε being the proton binding energy in ^{3}He.

To understand quantitatively the features of the data, a theoretical analysis similar to that reported in ref. 3) is necessary.

References

1) A. Djaloeis, S. Gopal, J. Bojowald, C. Mayer-Böricke, W. Oelert, N.G. Puttaswamy and P. Turek, Annual Report 1980, IKP-KFA Jülich, West Germany, JÜl-Spez-99, p. 19

2) N. Matsuoka, A. Shimizu, K. Hosono, T. Saito, M. Kondo, H. Sakaguchi, Y. Toba, A. Gato, F. Ohtani and N. Nakanishi, Nucl. Phys. A311 (1978) 173

3) A. Budzanowski, G. Baur, C. Alderliesten, J. Bojowald, C. Mayer-Böricke, W. Oelert, P. Turek, F. Rösel and D. Trautmann, Phys. Rev. Lett. 41 (1978) 635;

R. Shyam, G. Baur, F. Rösel and D. Trautmann, Phys. Rev. c22 (1980) 1401

1.12. Small angle α scattering experiments

H.P. Morsch, M. Rogge, P. Turek, P. Decowski, L. Zemło, S.A. Martin, G.P.A. Berg, I. Katayama, J. Meißburger, J. Römer, J. Reich, P. Wucherer, W. Bräutigam

We continued our efferts[1] to investigate small angle α scattering (at E_x = 172 MeV) using the magnetic spectrograph BIG KARL. The motivation for these experiments is a detailed study of the new giant resonances[2] (isoscalar octupole and dipole resonances) as well as the investigation of the giant quadrupole and monopole resonances at low momentum transfer. In the small angle region there are large differences in the excitation of L=1 and 3 resonances (fig. 1), in the angular range 3-5° the giant

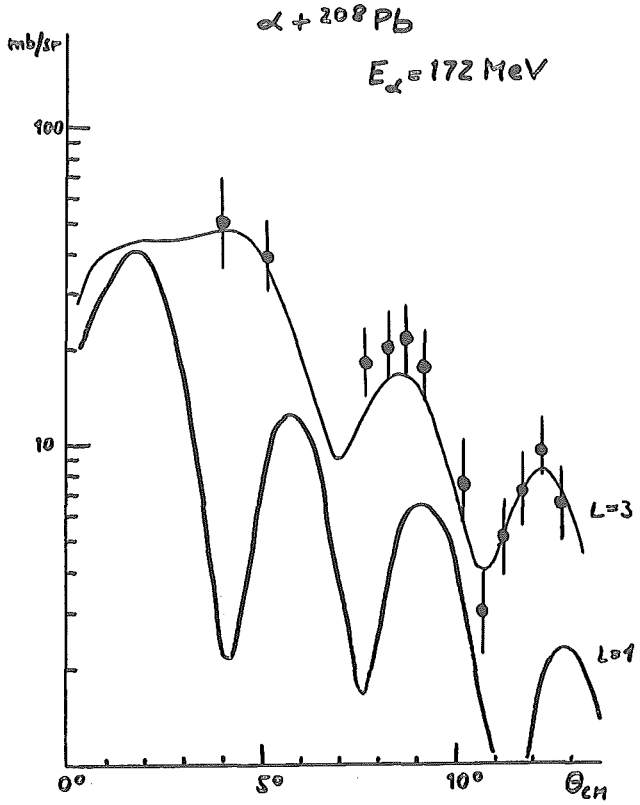

Figure 1: Small angle behaviour of L=1 and 3 differential cross sections. The data points indicate the giant octupole yields.

octupole resonance is strongly excited whereas the L=1 excitation is weak. At smaller angles of about 2° we expect also strong excitation of the L=1 resonance. Thus, from a careful measurement of small angle scattering these two resonances can be studied separately, this was not possible at larger angles (see ref. 2).

A problem in these forward angle experiments was to confine the emittance of the beam to a few mm mrad without creating too much halo. This was done already in the cyclotron by using special slit heads at the S- and SW-target in addition to the axial phase slits in the cyclotron center. The other slits in the beam line were used to clean up the beam. Another quite severe problem encountered is related to scattering from the walls of BIG KARL. It gives rise to increased background but can also cause a broad structure in the region of giant resonances due to scattering of the elastic line at very small angles. To eliminate these contributions a single wire counter was set up[3] which was placed about 60 cm behind the multiwire proportional chamber. By this means it was so far possible to measure the broad giant resonances at high excitation energies down to angles of 2.5° whereas results from the giant quadrupole and monopole region were obtained for angles θ>1.5°. In spectra taken for seven nuclei between Sn and U the giant octupole resonance was clearly observed. Fig. 2 shows a spectrum from ^{208}Pb in which the high lying

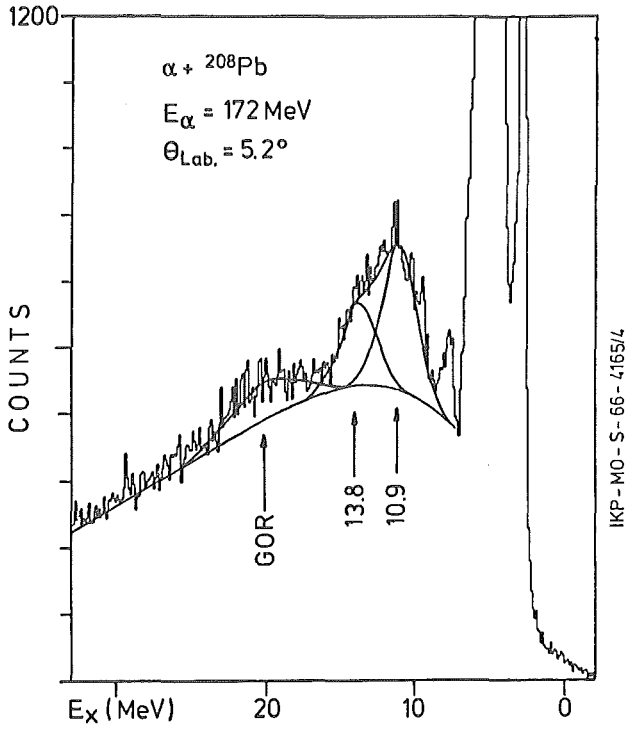

Figure 2: Spectrum of α scattering from ^{208}Pb at a scattering angle of 5.2°.

resonance bump is clearly seen. In the region of the giant quadrupole resonance (E_x = 10.9 ± 0.2 MeV) there is evidence for the fine structure seen in proton[4] and electron scattering[5]. Two structures at E_x = 10.2 and 11.2 are consistent with those from (e,e'). However, the isoscalar sum rule strength extracted from hadron scattering[6] is significantly larger than that extracted from electron scattering[7].

References

1) H.P. Morsch, S.A. Martin, G.P.A. Berg, J. Meißburger, M. Rogge, P. Turek, C. Sükösd, J. Reich, Annual Report 1980, IKP, KFA Jülich, Jül-Spez-99 (1981) 10

2) H.P. Morsch, M. Rogge, P. Turek and C. Mayer-Böricke, Phys. Rev. Lett. 45 (1980) 337

3) P. Decowski, M. Rogge, L. Zemło, H.P. Morsch, contribution to this annual report, p. 126

4) H.P. Morsch, P. Decowski and W. Benenson, Phys. Rev. Lett. 37 (1976) 263 and Nucl. Phys. A297 (1978) 317

5) F.R. Buskirk, H.-D. Gräf, R. Pitthan, H. Theissen, O. Titze and Th. Walcher, Phys. Lett. 42B (1972) 194; A. Schwierczinski, R. Frey, A. Richter, E. Spamer, H. Theissen, and O. Titze, Phys. Rev. Lett. 35 (1975) 1244

6) H.P. Morsch, C. Sükösd, M. Rogge, P. Turek, C. Mayer-Böricke, Phys. Rev. C22 (1980) 489

7) G. Kühner, D. Meuer, S. Müller, A. Richter, E. Spamer, O. Titze and W. Knüpfer, Phys. Lett. 104B (1981) 189

1.13. Fission decay of isoscalar giant resonances excited in 172 MeV α scattering from ^{238}U

H.P. Morsch, M. Rogge, C. Sükösd, H. Machner, P. David, J. Debrus*, H. Janßen* and J. Schulze**

The $^{238}U(\alpha,\alpha'f)$ experiment discussed in ref. 1 was completed. Fig. 1 shows α spectra coincident with fission in different direction. Pronounced threshold peaks are

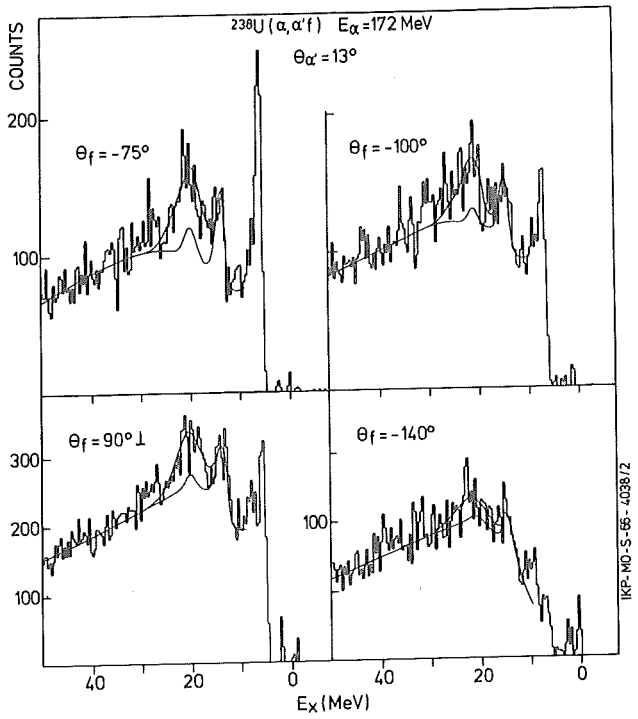

Figure 1: α spectra of the reaction $^{238}U(\alpha,\alpha'f)$ in coincidence with fission fragments at θ_f = -75°, -100°, -140° in plane and 90° out of plane (⊥).

observed at $E_x \geq B_f$ and $> B_{nf}$, these are most pronounced in the U recoil direction. In the excitation region of the new giant resonances seen in (α,α')[2] a broad bump is observed which is interpreted as decay of these giant resonances. In fig. 2 a comparison is made between singles (α,α') and coincidence $(\alpha,\alpha'f)$ spectrum in the U recoil direction (for $E_x \sim 11$ MeV). The coincidence data were analysed by assuming a smooth background which extends from the high energy region to the foot of the first chance fission peak (above B_f). Threshold peaks above B_{nf} and B_{2nf} due to second and third chance fission threshold effects were added. The remaining structure was fitted by two resonances at 17 and 21 MeV taken from the fits to the (α,α') spectra[3]. To reduce uncertainties in the extraction of resonance yields and threshold parameters data at lower incident energy[4] were included in our analysis. At this energy of 120 MeV high lying giant resonances are weakly excited, so the spectrum is dominated by threshold effects. The background shape shown in fig. 1 and 2 is consistent with the lower energy data in position and relative size of all three threshold peaks. Correlation functions are given in fig. 3. The yields due to threshold peaks show a strong unisotropy, the in plane data are well fitted by the model in ref. 5 assuming only K=0 decay in the region of the barrier.

In the region of the giant quadrupole resonance (GQR, E_x = 10.8 ± 0.3 MeV) which is excited strongly in the

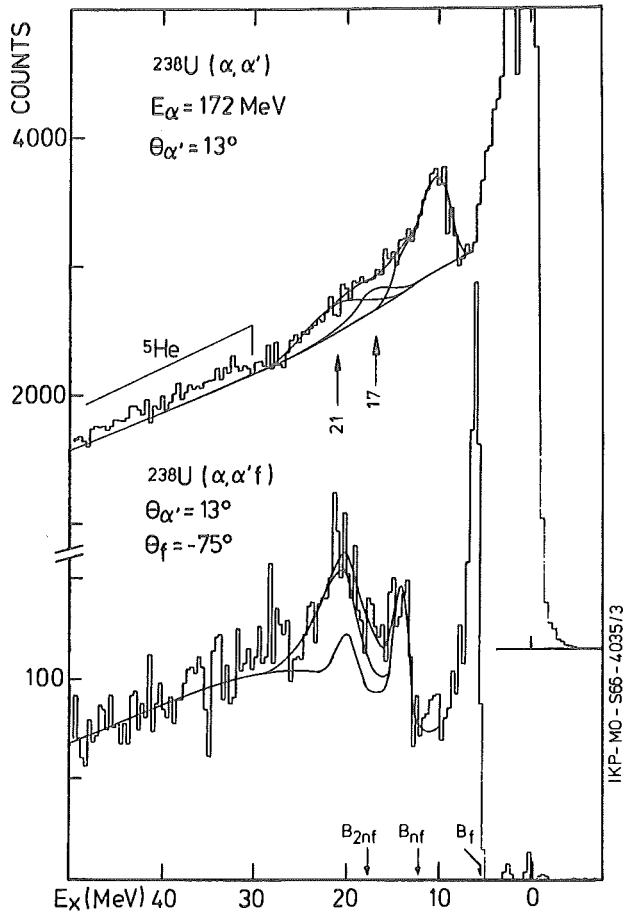

Figure 2: Comparison of (α,α') spectrum with the coincidence $(\alpha,\alpha'f)$ spectrum at θ_f = -75°. Background and fits to the giant resonances are indicated.

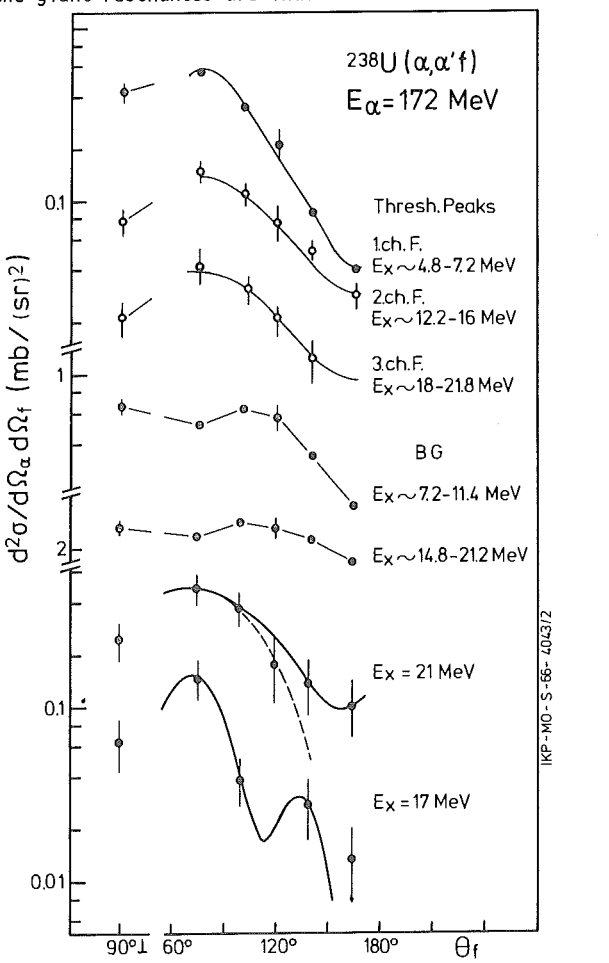

Figure 3: Double differential cross sections as a function of the fission angle.

(α,α') reaction only a small peak is seen in the $(\alpha,\alpha'f)$ reaction in recoil direction. This peak is identical to the one interpreted by ref. 6 as GQR decay. Assuming a correlation function $W_{2+} \sim |P_2|^2$ a GQR fission probability P_f of 3 % is obtained. In ref. 6 a much larger fission probability was extracted by assuming isotropy of this peak or K=1 and 2 decay at other fission angles; this is not confirmed by our results in which this peak is seen only in the U recoil direction. Correcting the results of ref. 6 using W_{2+} as discussed above yields $P_f \sim 0.07$ which is in agreement with our results if the background line in our spectra is drawn somewhat lower. Our results are consistent with other results[7-9] indicating a fission probability of the GQR smaller than that of the background.

Different from the GQR the fission decay of the high lying resonances is quite large. Quite surprisingly, the correlation functions for these yields show also an unisotropic behaviour which is well described by pure $|P_1|^2$ and $|P_3|^2$ distributions. The fact, that a good description of the data is obtained assuming pure L=1 and 3 decay supports the L assignments for these resonances from the (α,α') experiment[2].

In fig. 4 the fission probability is given for background and giant resonance peaks. The hatched area is obtained

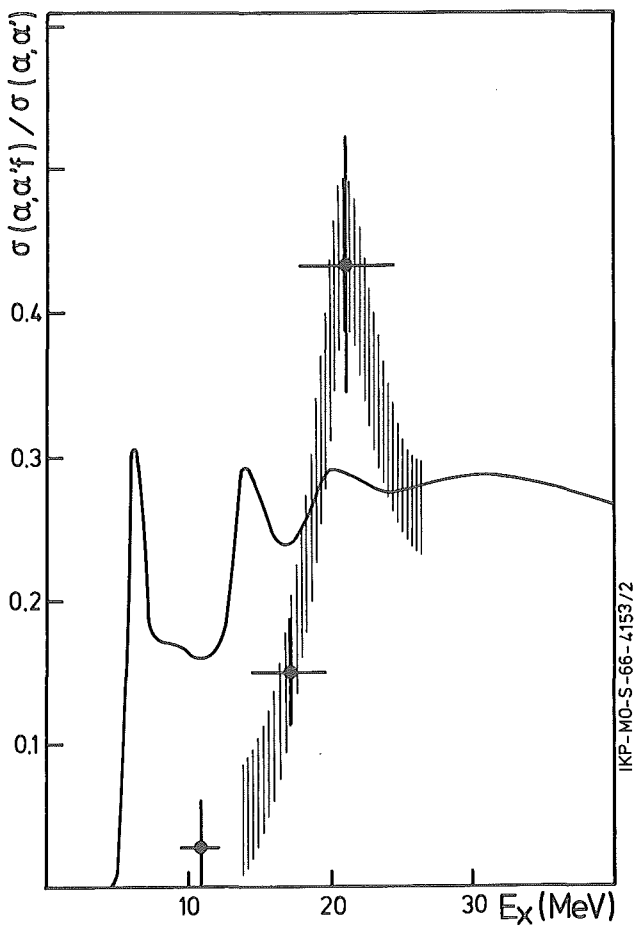

Figure 4: Fission probability of the background (solid line), giant resonance (points) and the whole giant resonance region (hatched area). The horizontal bars indicate the widths (FWHM) of the assumed giant resonances.

by evaluating the yield above background. An increase of giant resonance decay yield with increasing excitation energy is obtained which is stronger than that of the underlying background. The behaviour at higher excitation energy confirms the assumption of a strong resonance at $E_x \sim 21$ MeV (isoscalar giant dipole resonance). The fact that a very different fission probability is found for the giant resonances and the background is in disagreement with the usual statistical decay model.

Resonances

1. H.P. Morsch, M. Rogge, C. Sükösd, H. Machner, P. David, J. Debrus, H. Janßen, J. Schulze, Annual Report 1980, IKP, KFA Jülich, Jül-Spez-99 (1981) 12
2. H.P. Morsch, M. Rogge, P. Turek, C. Mayer-Böricke, Phys. Rev. Lett. 45 (1980) 337
3. H.P. Morsch, M. Rogge, P. Turek, C. Mayer-Böricke, Annual Report 1980, IKP, KFA Jülich, Jül-Spez-99 (1981) 8 and submitted to Phys. Rev.
4. B.B. Back, A.C. Shotter, T.J.M. Symons, A. Bice, C.K. Gelbke, T.C. Awes, and D.K. Scott, Phys. Rec. C23 (1981) 1105
5. R. Vandenbosch and R. Huizenga, Nucl. Fission, Acad. Press, N.Y., London (1973) 183
6. F.E. Bertrand, J.R. Beene, C.E. Bemis Jr., E.E. Gross, D.J. Horen, J.R. Wu, W.P. Jones, Phys. Lett. 99B (1981) 213
7. J. van der Plicht, M.N. Harakeh, A. van der Woude, P. David, J. Debrus, H. Janszen and J. Schulze, Nucl. Phys. A346 (1980) 349
8. J. Aschenbach, R. Haag, H. Krieger, Z. Phys. A292 (1979) 285
9. H. Ströher, R.D. Fischer, J. Drexler, K. Huber, U. Kneissel, R. Ratzek, H. Ries, W. Wilke, and H.J. Maier, Phys. Rev. Lett. 47 (1981) 318

*Institut für Strahlen- und Kernphysik, Universität Bonn

1.14. Experimental Evidence for Asymmetric Excitation of Nuclei

U. Bechstedt, H. Machner, A. Budzanowski, P. Jahn and C. Mayer-Böricke*

Last year we reported on an coincidence experiment we performed to study the decay of continuum states via particle emission[1]. In that experiment we measured the ^{58}Ni(α,α'c) reaction (c = charged particle A ≤ 4) at an incident energy of E_α = 140 MeV. We have now completed the analysis of the data. Spectra of protons were deduced in coincidence with α'-particles from three energy bins each 20 MeV wide with mean α'-particle energies $\bar{E}_{\alpha'}$ = 65 MeV, 84 MeV and 103 MeV in the lab. system. The proton spectra were taken at angles -150°, -120°, -75°, -60°, +30°, +60°, +105°, +120° in lab. system. (For the notation of angles see Fig. 2). Proton spectra in coincidence with $\bar{E}_{\alpha'}$ = 65 MeV are shown in Fig. 1. The spectra

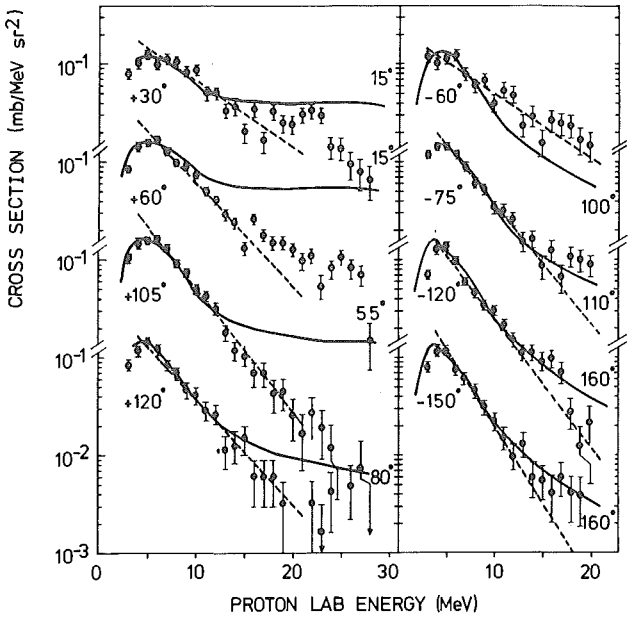

Figure 1: Proton spectra in lab. system detected at angles -150°, -120°, -75°, -60°, +30°, +60°, +105° and +120° in coincidence with inelastically scattered α-particles at -30° with $\bar{E}_{\alpha'}$ = 65 MeV. The dashed lines are the exp[-E/T] functions fitted in the energy interval 6-12 MeV. The solid lines are the experimental (p,p') spectra[4] at the angles indicated on the right hand side (see text).

for the other α' energy intervals look similar. As can be seen proton spectra show a maximum of the cross-section at the Coulomb energy and towards higher energies an exponential decrease of cross section with energy that can be resonably well approximated by a simple $e^{-E/T}$ dependence in the range from 6 MeV to 12 MeV. This enabled us to ascribe a nuclear temperature T to each spectrum by means of a least square fit. The results of these temperature fits are shown as dashed lines in Fig. 1 and for each α'-particle energy interval in Fig. 2 a-c as function of the angle of proton emission.

We notice that for each angle the temperature falls down with decreasing energy transfer. Its angular distribution, however, shows a striking feature namely that it is not symmetric about the direction of the transferred momentum q. The highest values of the temperature are found on the right hand side of the q direction in the forward

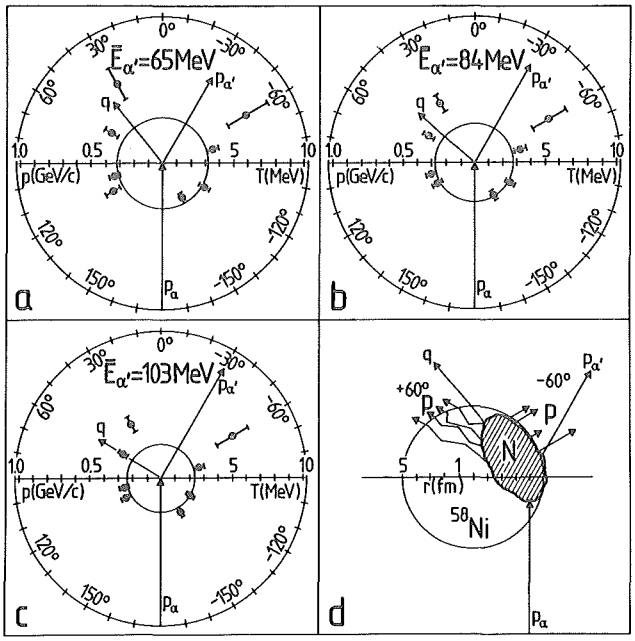

Figure 2 a-c: Angular dependence of the extracted nuclear temperatures for $\bar{E}_{\alpha'}$ = 65 MeV (part a), $\bar{E}_{\alpha'}$ = 84 MeV (part b) and $\bar{E}_{\alpha'}$ = 103 MeV (part c). The linear momenta of the incoming and outgoing α-particles (p_α and $p_{\alpha'}$ resp.) as well as the momentum transfer q are indicated by arrows. The small circle indicates the temperature of the fully equilibrated system at corresponding energy transfers. Part d: Schematic picture of underlying reactions mechanism (see text). The shaded area indicates the early stage of the equilibration process.

hemisphere (with respect to the beam direction). This indicates that a coincidence experiment selects events in which the nucleus is asymmetrically excited. As reported before[2] different models like exciton model, fireball or firestreak model, hot spot model or quasi free scattering model QFSM which are orthogonal in their physical assumptions can equally well reproduce the continuous spectra of secondary particles from inclusive measurements. It is the hope that a coincidence experiment can discriminate between some of these models. According to QFSM we expect each α'-particle being accompanied by a fast nucleon moving into q-direction and starting an equilibration process. The observed proton spectra should then show some similarity to the spectra of inelastically scattered protons as pointed out by Cowley et al.[3]. The solid lines in Fig. 1 show spectra of protons from the ^{54}Fe(p,p') reaction measured by Bertrand and Peelle[4] at E_p = 62 MeV suitably normalized to our data. The angles of the inelastically scattered protons are chosen as close as possible to the angles between the q direction and the direaction of proton emission measured in our experiment. The shapes of both spectra follow each other to a great extend on the right hand side of the beam direction, whereas on the left hand side the coincidence spectra show less high energetic protons. This is another indication for an asymmetrical excitation of the emitting nucleus. This can be explained when considering that the mean free path of the α-particle (1.8 fm according to an optical model estimation) is short compared to the nuclear dimensions. From this one expects that the region emitting the fast α-particle is localized on the α'-emission side of the nucleus. So protons detected on the right hand side of the q-direction have to pass a shorter way through nuclear

matter than those detected on the left hand side. A schematic picture of that effect is shown in Fig. 2d. As a consequence the spectra from the right hand side of the q-direction are dominated by the early stage of the equilibration process and show higher temperatures whereas proton emission from the left hand side occures when the dissipation process is spread over a larger volume of the nucleus thus showing lower temperatures.

From a simple calculation using energy and momentum conservation one can estimate the number N of nucleons sharing the excitation energy U corresponding to the measured temperatures T: $U+E_{kin}=\Delta E_\alpha, q^2=2NmE_{kin}, T^{-1}=\sqrt{aU^{-1}}-5\cdot(4U)^{-1}$ where ΔE_α and q are transferred energy and momentum, m nucleon mass, a level density parameter and E_{kin} the kinetic energy of the group of N nucleons. With an a-value of 9.33 MeV^{-1} given by Töke and Swiatecki[5] for a nucleus of mass A=64 we get from the temperature at -60^o: $N=12^{+8}_{-5}$, $N=11^{+8}_{-4}$ and $N=7^{+6}_{-2}$ for $\bar{E}_{\alpha'}$ = 64, 88 and 103 MeV respectively. From the temperature at $+120^o$ we correspondingly get $N=34^{+11}_{-8}$, $N=46^{+12}_{-8}$ and $N=35^{+8}_{-6}$.

Results of this investigation rule out definitely the model of a static hot spot[6] since temperatures of the emission in q-direction are always higher than in the opposite direction where temperatures near to that of the fully equilibrated system show up.

However, we claim that we have found experimental evidence for a locally excited nucleus with a hot zone around the q-direction.

References

1) U. Bechstedt, et al., Annual Report 1980, IKP, KFA Jülich, JÜl-Spez.-99, Febr. 1981, p. 29

2) U. Bechstedt, et al., Annual Report 1979, IKP, KFA Jülich, JÜl-Spez.-72, März 1980, p. 30

3) A.A. Cowley et al., Phys. Rev. Lett. 45 (1980) 1930

4) F.E. Bertrand and R.W. Peelle, Phys. Rev. C8 (1973) 1045

5) J. Töke and W.J. Swiatecki, GSI-24-81 (unpublished, 1981)

6) R. Weiner and M. Weström, Nucl. Phys. A286 (1977) 282

1.15. Fireball analysis of $^{54}Fe(\alpha,\alpha'x)$ reactions at 120 MeV

H. Machner, U. Bechstedt, A. Djaloeis, and P. Jahn

The quantity $d^3\sigma/dv^3$ is invariant under Galilei transformations. Thus, a countour diagram of $d^3\sigma/dv^3$ versus linear momentum perpendicular to the beam axis $p_\perp$ and versus the rapidity $y = \text{arctanh}\,(v_{||}/c)$ should show up features of the emitting system. If a system emitts particles isotropic in its rest frame - as do compound nuclei - the contour diagramm shows concentric semicircles around the system rapidity. At non relativistic energies the rapidity reduces to $p_{||}$ the linear momentum parallel to the beam axis.

We have deduced $d^3\sigma/dv^3$ for α-emission from 120 MeV α particles on ^{54}Fe. Not all data points are on semicircles. But large cross sections at backward angles and small ones at forward angles tend to be semiconcentric about an origin v_s. In fig. 1 data (dots) are shown together with semicircles around $v_S = 3\sqrt{\text{MeV/u}}$ with u being the nucleon mass.

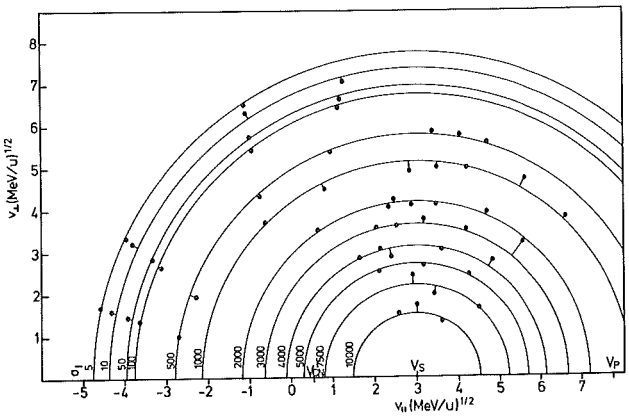

Figure 1: Contour diagramm of Galilei-invariant cross sections σ_I (given by dots, in units of $10^5 \frac{mb}{MeV\,sr\sqrt{MeV\,u}}$, u = nucleon mass) as function of the velocity parallel to the beam axis $p_{||}$ and the velocity perpendicular to the beam axis $p_\perp$. Also shown are semicircles centered around $v_s=3\sqrt{MeV/u}$ and the beam velocity v_p and the compound nucleus velocity v_{CN} obtained from linear momentum conservation.

These points are nearly on the semicircles indicated in the figure and may therefore origin from a source moving with v_s in the beam direction. Indicated are also the beam velocity v_p and compound nucleus velocity v_{CM}. From linear momentum conservation we get (neglecting the binding energy of α-particles):

$$\sqrt{2m_\alpha E_\alpha} = m_s v_s \qquad (1)$$

This leads to $m_s \approx 10$ nucleons.

The α-emission is assumed to have a Maxwellian distribution within the rest frame of the source.

$$\frac{d^2\sigma'}{d\epsilon' d\Omega'} = c\sqrt{\epsilon_{\alpha'}}\, e^{-\epsilon_{\alpha'}/T} \qquad (2)$$

with T the temperature of the source.
A fit of (2) to the data results in T=28 MeV. This seems to be a very high temperature when compared to the total excitation energy of 148 MeV. In a simple fermi gas model the total excitation energy is

$$E = U + E_{kin} \quad \text{with}$$
$$U \approx a \cdot T^2 \text{ and } a = A/C$$
$$\text{and } E_{kin} = 1/2\, m_s v_s^2$$

Using the values obtained from the rapidity analysis we get U=980 MeV and E_{kin} = 45 MeV. This contradicts to energy conservation. Therefore the assumption of a moving source is questionable. Comparison with data is made in figure 2.

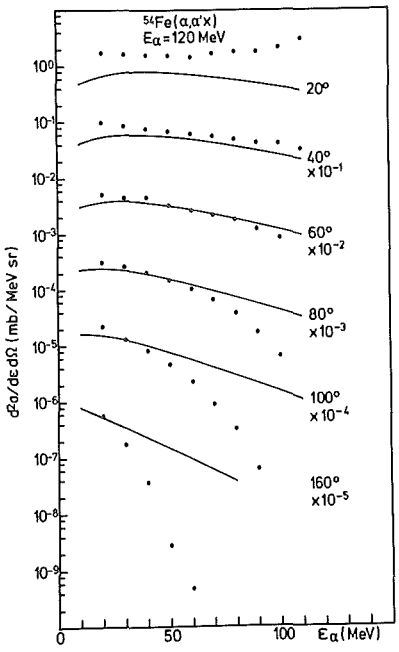

Figure 2: Data (dots) are compared with calculated spectra. The calculations assume a moving source with velocity $v_s = 3\sqrt{MeV/u}$ in beam direction and a temperature of 28 MeV.

1.16. Time Scales in Pre-Equilibrium Model Formulations*

H. Machner

A number of different pre-equilibrium models has been formulated. Some of these treat the nuclear excitations in terms of particles (p) and holes (h) (= excitons n=p+h) with respect to the Fermi surface[1]. Besides this feature they have some common assumptions, namely:

- the transitions between two different states can increase (or decrease) the number of excitons at most by two;
- the contributions to the cross sections from different particle-hole states can be incoherently summed up. The last assumption leads to the criterion

$$t_{resp} < \tau \qquad (1)$$

with t_{resp} the response time (i.e. the time an interaction needs to take place) and τ the time between two interactions. In the hybrid model[2] τ^H is simply estimated from the transition rate λ_+ going from a state n to a state n+2:

$$\tau^H = \frac{1}{\lambda_+(\varepsilon)} = \frac{\Lambda(\varepsilon)\cdot K}{v} \qquad (2)$$

with $\Lambda(\varepsilon)$ the mean free path of nucleons in nuclear matter and v the particle velocity. The quantity K is a scaling factor for the mean free path. Λ is calculated from free nucleon-nucleon cross sections corrected for the Pauli-Principle.

The response time t_{resp} has been calculated in the spirit of the hybrid model as for free nucleons. The response or interaction time is derived from the range b and the depth V_0 of the nucleon-nucleon potential

$$t^H_{resp} = \frac{2b + \lambda\!\!\!^{-}}{\sqrt{v^2 + \frac{V_0}{2m}}} \qquad (3)$$

m being the nucleon mass. The de Broglie wave length $\lambda\!\!\!^{-}$ is only a very small correction to the potential range. The range is given in two limiting cases: with a repulsive core at high energies and without at low energies. We have chosen b = 1.7 fm and 2.7 fm for these cases[3], respectively. From the ground state of the deuteron we learn

$$V_0 b^2 = 102 \text{ MeV fm}^2 \quad . \qquad (4)$$

This relation defines now V_0 and therefore t^H_{resp}. The resulting two curves are shown in fig.1. They are compared with lifetimes $\tau_H(E)$ calculated for K-values of 1, 2 and 4. Obviously only $\tau_H(E)$ with K=4 satisfies condition (1) in the range of some tens of MeV where this model has been applied. This seems to contradict recent comments on mean free pathes in nuclear reactions[4].

For the exciton model[5] $\tau_E(n,E)$ has been derived from the transition rate $\lambda(n\to n+2)$ areraged over all possible configurations:

$$\tau_E(n,E)=\lambda^{-1}(n\to n+2,E)=(\varrho(p,h,E))^{-1}$$
$$\Big[\int_0^E \lambda^p_+(u)\varrho(p-1,h,E-u)\cdot\varrho(1,0,u)+$$
$$\lambda^h_+(u)\varrho(p,h-1,E-u)\varrho(0,1,u)du\Big]^{-1} \qquad (5)$$

with $\varrho(p,h,E)$ the Ericson-level density. Again values for K=1,2,4 are shown for a two particle-one hole state in fig. 2. The response time t^E_{resp} has been calculated in

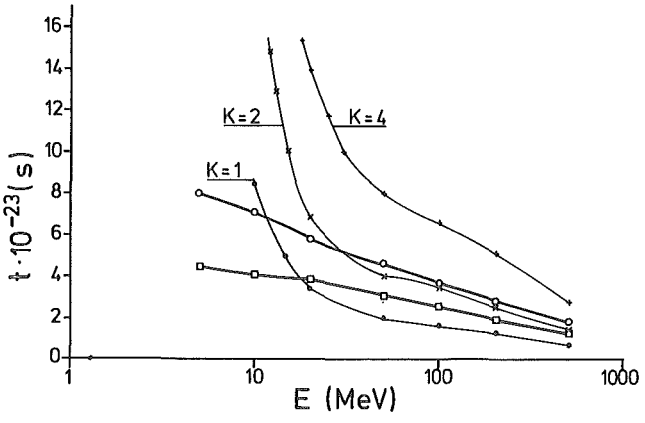

Figure 1: Response times t_{resp} for free nucleon-nucleon interaction in the approximation for low (thick solid curve with open circles) and high (thick solid curve with open squares) energies. The time τ between two succeeding interactions is calculated in the hybrid model approach for mean free paths multiplied by the factor K indicated in the figure.

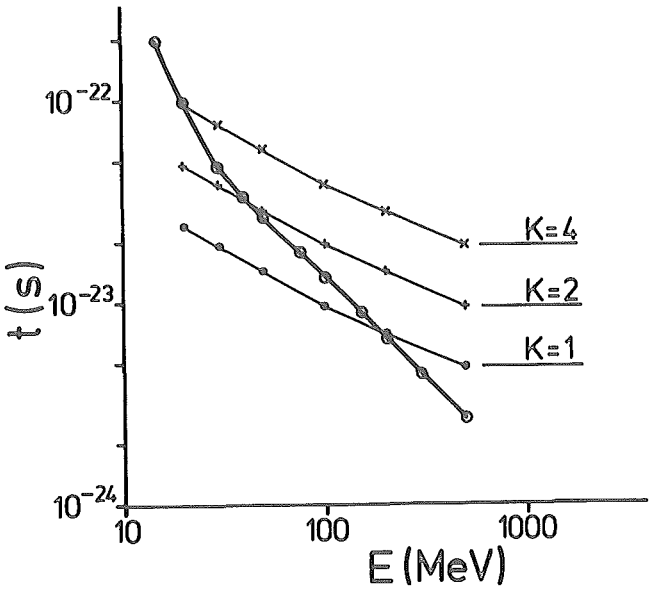

Figure 2: The response time t_{resp} (n) (thick solid line) from equ. (6) is compared with times τ_n between two interactions. Again a mean free path multiplier is indicated. All calculations for this figure have been performed in the framework of the exciton model for the exciton number n=p+h=3(2p,1h).

the framework of the exciton model following a conjecture of Agassi et al.[6] as

$$t^E_{resp}(n) = \hbar \max \left\{ \frac{d\varsigma(n,E)}{dE} \frac{1}{\varsigma(n,E)}, \frac{d\lambda_c(n,E)}{dE} \cdot \frac{1}{\lambda_c(n,E)}, \right.$$

$$\left. \frac{d[\lambda_+(n,E)+\lambda_-(n,E)]}{dE} \cdot \frac{1}{\lambda_+(n,E)+\lambda_-(n,E)} \right\} . \qquad (6)$$

For n=3 (2p+1h) this function is shown in fig. 2. Again K=4 satisfies the condition (1). For energies above 100 MeV shorter mean free path values (K=2) seem already to satisfy condition (1). This is in agreement with the practice to use K=3-5 to adjust calculated cross sections to experimental values[2,7].

*Condensed from Z. Physik A - Atoms and Nuclei, 302 (1981) 125

References

1) M. Blann, Annu. Rev. Nucl. Sci. 25 (1975) 123

2) M. Blann, Phys. Rev. Lett. 27 (1971) 337

3) A. Bohr and B. Mottelson, Nuclear Structure, Vol. I, New York: Benjamin Publ. 1959

4) M. Blann, Phys. Lett. 67B (1977) 145
M. Blann, Phys. Rev. C17 (1978) 1871

5) E. Gadioli, E. Gadioli-Erba, L. Sajo-Bohus, G. Tagliaferri, Riv. Nuovo Cimento 6 (1976) 1

6) D. Agassi, H.A. Weidenmüller, G. Mantzouranis, Phys. Rep. 22C (1975) 145

7) H. Machner, Phys. Rev. C21 (1980) 2695

1.17. Investigation of the (p,^{3}He) Reaction on ^{13}C, ^{15}N and ^{16}O at E_p = 45 MeV

V. Rapp, G. Staudt**

Our last measurement of (p,^{3}He) reactions completed the investigation in the p-shell at an incident energy of 45 MeV, mainly. The experimental set up was a conventional triple telescope with a veto as third detector. The particle discrimination has been obtained off-line at Tübingen[1]. From the spectra one could reduce angular distributions (10^o-150^o) for various transitions leading to states up to 15 MeV excitation energy of the residual nuclei ^{13}C and ^{14}N.

In the reaction ^{16}O(p,^{3}He)^{14}N the transitions leading to states with negative parity, which cannot be populated through a one-stage two nucleon pick-up are turning out with a comparable strength. This is obvious since the sd-shell will play its part most strongly in this reaction rather than in any other one using p-shell nuclei as target. In fig. 1 the angular distributions of transitions

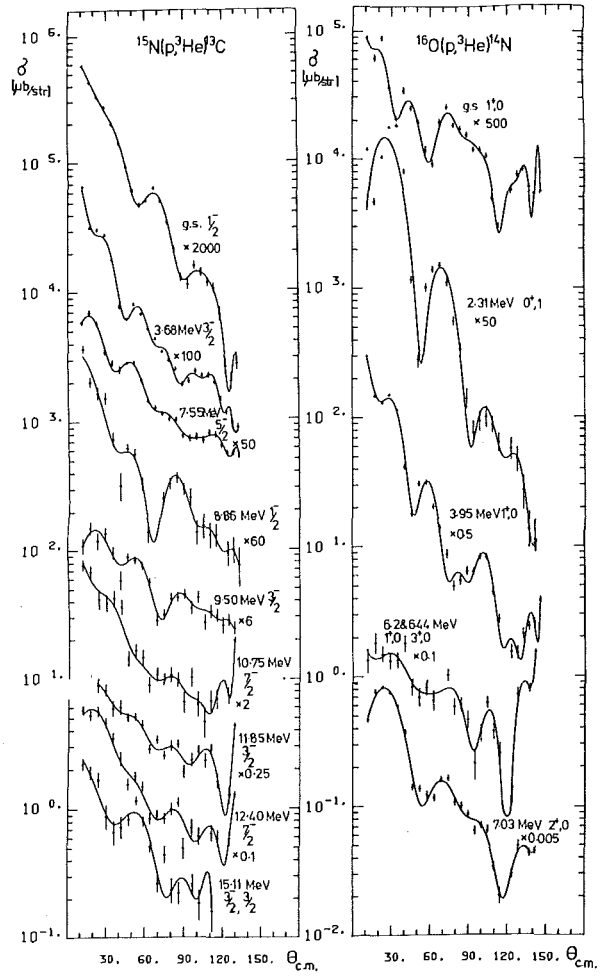

Figure 1: Angular distributions for the reaction (p, ^{3}He) on ^{16}O and ^{15}N leading to various states in ^{14}N and ^{13}C, respectively.

leading to states having the same parity as the ground state. They can be explained in a direct reaction model. A series of DWBA calculations for direct two-nucleon-pick-up reactions for target nuclei ranging from ^{10}B to ^{16}O has been undertaken[1]. The most satisfactory set of entrance potentials[2] found is one which varies smoothly with energy and mass number of the target nucleus. Similar a consistent one nucleon potential[3,4] was used to describe the various two-particle states of the bound state of the target nucleus. The real part of the He potentials for the various exit channels were adjusted to fit the respective ground state transitions, whereas the imaginary part was left unchanged[5]. The fitted values are V = 118.61 MeV, r = 1.15 fm, and a = 0.5739 fm.

The deuteron transfered can be either in its ground state (s=1, and t=0) or in its first excited state (s=0, and t=1). This mixing of configurations in one reaction requires a careful consideration of the relative strengths of both. One has to take into account the isospin Clebsch-Gordons for the target and the ejectile and both spectroscopic factors[6,7]. With these weights the DWBA calculations for the reaction ^{13}C(p,^{3}He)^{11}B are being shown in fig. 2. The spin for the state at 8.56 MeV in the residual

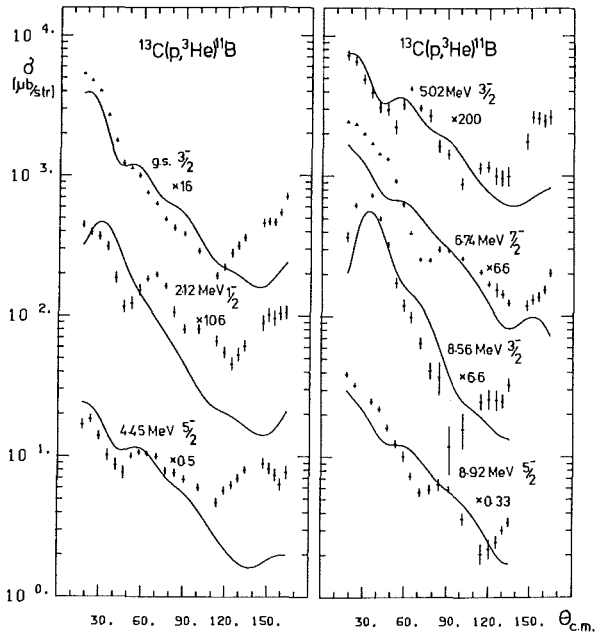

Figure 2: Comparison between experiment and microscopic DWBA calculations.

nucleus has been taken to be 3/2 in accordance with the assignment for the corresponding state in ^{11}C [8]. The experimental result is well described by the calculation.

In fig. 3 there is a comparison between the experimental transition strength, which is considered to be the inte-

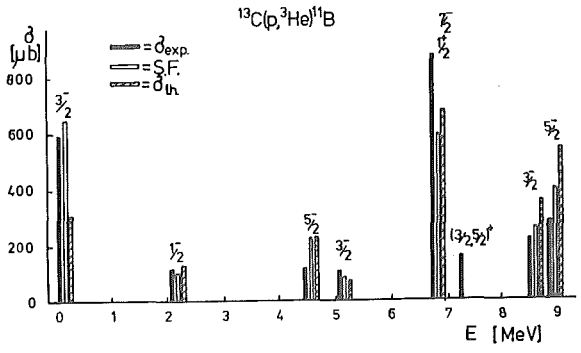

Figure 3: Comparison between $\sigma_{exp}(0^o\text{-}90^o)$, and bare spectroscopic factors and σ_{th}.

grated cross-section (0^o-90^o) and the spectroscopic factors for the target nucleus and the theoretical transition strength. It is amazing that the bare spectroscopic

factor for the target nucleus coincides with experimental data, so well. On the other hand this effect is neither specific for ^{13}C nor $(p,^3He)$ [9,10].

References

1) V. Rapp, to be published
2) H. Leeb and G. Eder, Lecture Note in Physics 89, 181
3) K. Bear and P.E. Hodgson, J. Phys. G, Vol. 4 No. 12 (1978) L287
4) G. Eder and H. Oberhummer, Lett. al Nuo. Cim. 15 (1976) 609
5) H.-J. Trost et al., Nucl. Phys. A337 (1980) 377
6) S. Cohen and D. Kurath, Nucl. Phys. A141 (1970) 145
7) Kunz, unpublished
8) H.T. Fortune et al., Phys. Rev. C2 (1970) 425
9) F. Hoyler et al., Annual report, Heidelberg, 1980, p108
10) F. Weng, Ph.D. thesis, Tübingen 1979

*Phys. Inst. Universität Tübingen

1.18. Analysis of the Reaction $^{20}Ne(p,\alpha)^{17}F$

T. Rohwer, W. Oelert*

We have analysed the reaction $^{20}Ne(p,\ )^{17}F$ to the first four states in ^{17}F. Differential cross sections were measured at 22.5, 27.0, 35.0 and 45.0 MeV incident energy (using the cyclotron JULIC) in order to get information about the reaction mechanism.

The angular distributions are shown in fig. 1 together with the results of Falk et al.[1] at 42.6 MeV. For the higher incident energies the distributions of a transition to the same level in ^{17}F are much alike and characteristic of the transfered angular momentum[2].

We therefore tried to describe the distributions with zero-range DWBA using cluster form-factors. The optical potential for the protons was taken from the literature[3]. For the outgoing channels the optical potential was fitted[4] to give best agreement of the transition to the $1/2^-$ state at 3.1 MeV. The potential is given in table 1. The

	V	r	a	W'	r'	a'
$^{17}F+\alpha$	176.9	1.754	0.677	10.0	1.754	0.677
$^{17}F+t$	*	1.866	0.55			

Table 1: Optical potential parameters used in the DWBA calculations, * varied to yield binding energy.

parameter of the radius in the bound state potential of rb=1. 886 fm is necessary to describe the slope of the distributions.

The result of the DWBA calculation is shown in fig. 1 as solid line. Each DWBA cross section is normalized to the experiment according to the formula:

$\sigma_{exp} = \varepsilon \times S(\alpha) \times S(^{20}Ne) \times Do^2 \times \sigma_{DWBA}$.

$S(^{20}Ne)$ is the spectroscopic factor for the three nucleon transfer given by Chung[5] and $Do^2 = 23 \times 10^4$ fm^3 MeV^2 is given by Kunz[6].

The normalization factor as a function of incident energy is shown in fig. 2 for the ground state and the first excited state in ^{17}F. In the case of the $1/2^-$ state at 3.1 MeV and the $5/2^-$ state at 3.86 MeV the product $\varepsilon \times S(^{20}Ne)$ is shown. The normalization factor lies in the range between 100 and 10 and decreases with increasing energy. This may be due to the fact that the antisymmetrization is not properly taken into account. According to Fliessbach[7] this effect should decrease with increasing energy.

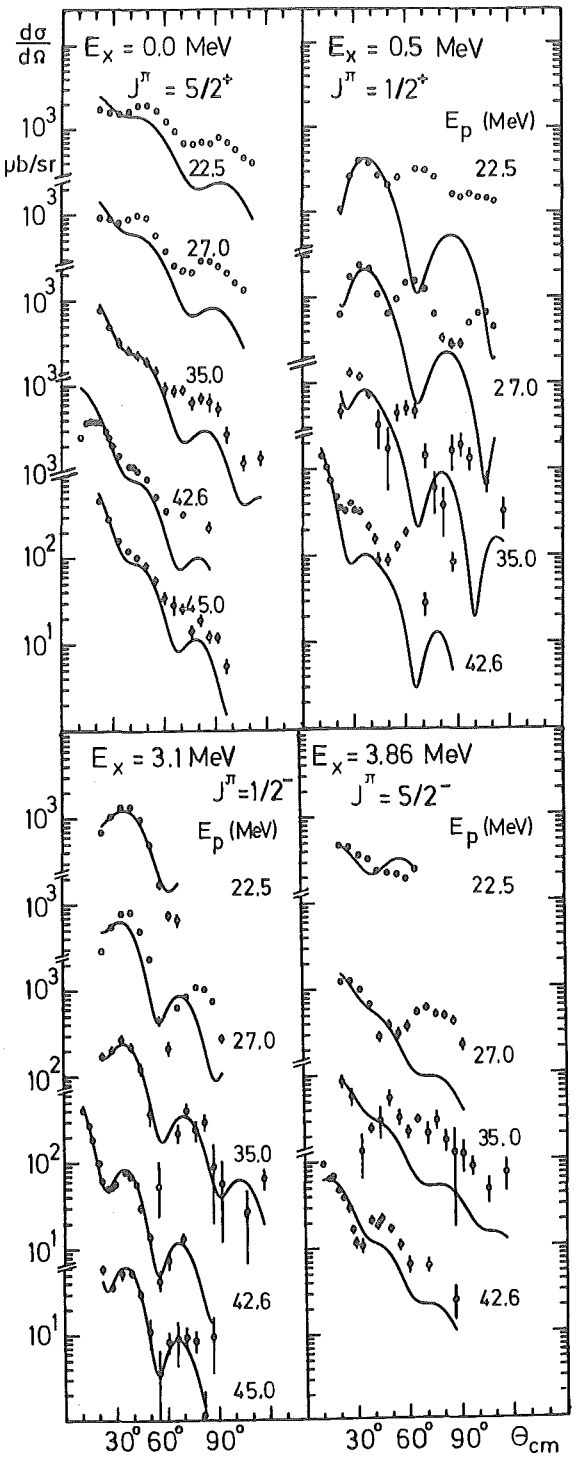

Figure 1: Angular distributions of the reaction $^{20}Ne(p,\alpha)^{17}F$ between 22.5 and 45 MeV. The solid lines represent DWBA calculations.

Fig. 2 shows that the normalization factor for the transfer to the $1/2^+$ state at 0.5 MeV in ^{17}F is about a factor of 2 lower than the value for the ground state. Besides the possibility that the spectroscopic factors are wrong

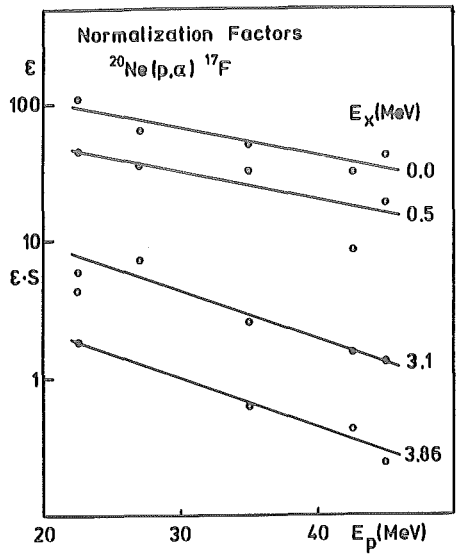

Figure 2: Normalization factors as a function of energy obtained from the DWBA analysis of the four transitions.

one has to notice that the fit to the angular distribution is very poor. A much better agreement between theory and experiment is obtained if one includes couplings between the first two states in ^{17}F due to rotation (solid line) or vibration (dashed line) in the residual nucleus, as shown in fig. 3.

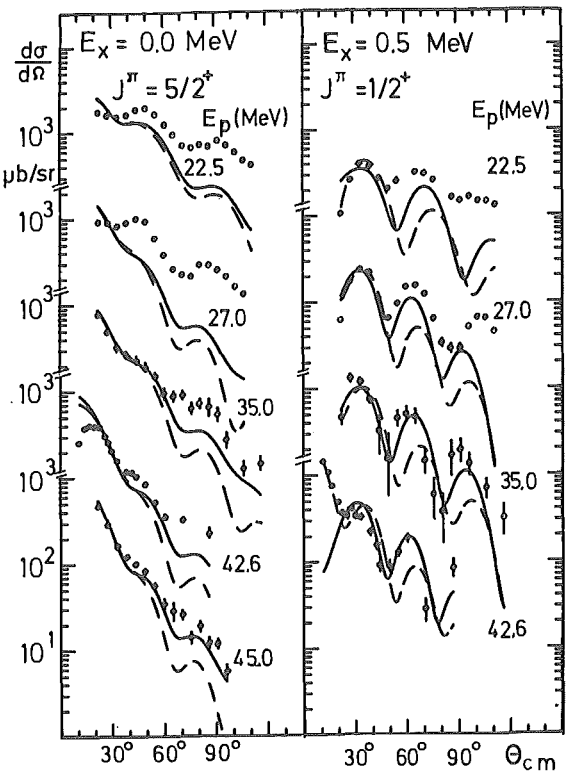

Figure 3: Results of the coupled channel analysis. Solid lines show results of the channel couplings due to rotations dashed lines due to vibrations in the residual nucleus.

This interpretation is supported by the description of the positive-parity states in ^{17}F using the intermediate coupling unified model by Chung and Shin[8]. We took the deformation parameter of β = 0.32 from this work. The optical potentials are the same as for fig. 1 except that the imaginary part of the α-potential is reduced to 7 MeV.

Before coming to final conclusions one has to take into account other two-step processes as for example inelastic excitations in ^{20}Ne or E1-transitions in ^{17}F [9]. This analysis has to be postponed, however, until the spectroscopic amplitudes which enter the calculation are known.

References

1) W.R. Falk, private communication
2) H.J. Hauser et al., contribution to this report
3) F.D. Becchetti, Jr. and G.W. Greenless, Phys. Rev. 182 (1969) 1190
4) H. Leeb, Program GOMFIL, unpublished
5) W. Chung, unpublished
6) P.D. Kunz, Program CHUCK, unpublished
7) T. Fliessbach, Z. Physik A288 (1978) 219
8) W.H. Chung and Y.M. Shin, Nuov. Cim. 60A (1980) 27
9) H.T. Fortune et al., Phys. Rev. C12 (1975) 1723

*Physik. Inst., Universität Tübingen

1.19. DWBA analysis of the (p,α) reactions on ^{26}Mg and ^{27}Al

F. Hoyler, G. Staudt*, S.A. Martin, W. Oelert*

The (p,α) reactions on ^{26}Mg and ^{27}Al have been measured using the 45 MeV proton beam of the JULIC cyclotron. In a first experiment the outgoing α particles were detected with silicon surface detectors. In order to resolve more excited states in ^{23}Na the ^{26}Mg(p,α)^{23}Na experiment was also performed using the magnetic spectrometer BIG KARL[1].

In fig. 1 the angular distributions of some transitions to states in ^{23}Na measured in the scattering chamber are shown. The 0.44 MeV level was used to normalize the spectrometer data. The solid lines represent DWBA calculations in zero range cluster form factor approximation. The optical potential parameters are summarized in table 1. Since no elastic α-scattering data in this region of energy for ^{23}Na are known, the α optical potential has been fitted to the reaction data shown in fig. 1. For this procedure the fitting code GOMFIL written by Leeb[2] has been used.

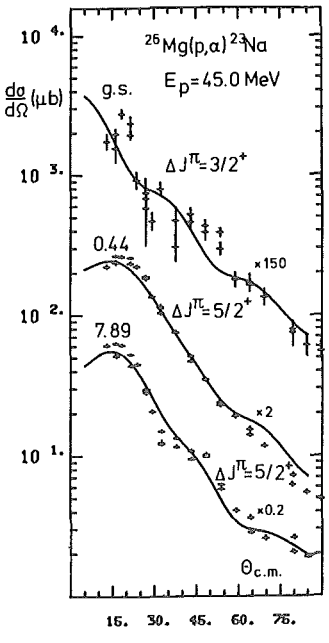

Figure 1: Angular distributions of the reaction ^{26}Mg(p,α)^{23}Na solid lines represent DWBA calculations.

Fig. 2 shows some results of the BIG KARL experiment. The solid lines represent DWBA calculations done with the same set of parameters as used in fig. 1.

	V	r	a	W_I	W_{Surf}	r	a	V_{LS}	r_{LS}	a_{LS}	r_C
^{26}Mg+p	43.07	1.17	0.75	7.2	12.57	1.32	0.624	24.16	1.01	0.75	1.2
^{27}Al+p*	40.69	1.17	0.75	11.27		1.32	0.51	26.52	1.01	0.75	1.2
^{23}Na+a	202.6	1.279	0.676	8.09		1.279	0.624				1.3
^{24}Mg+a*	202.7	1.32	0.565	36.49		1.41	0.58				1.3
^{23}Na+t	**	1.3	0.65								1.2
^{24}Mg+t	**	1.3	0.65								1.2
^{24}Mg+p	54.0	1.236	0.62					7.0	1.236	0.65	1.2
^{24}Mg+n	54.0	1.236	0.62					7.0	1.236	0.65	

Table 1: Optical potentials as used in DWUCK4, * as used in DWUCK5, ** varied to yield binding energy.

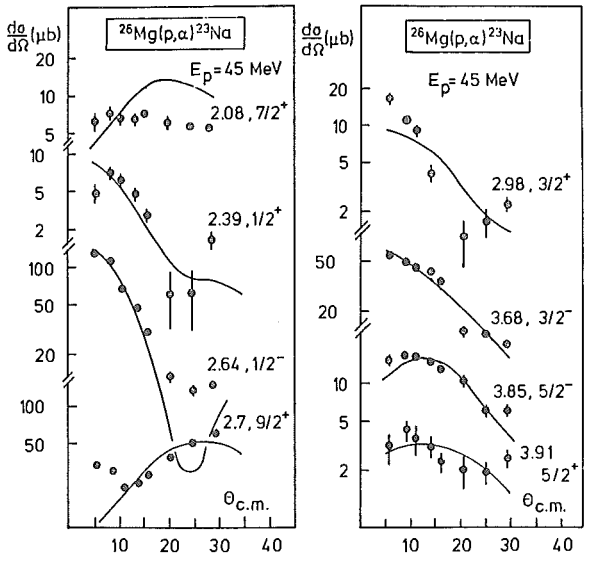

Figure 2: Angular distributions of the reaction ^{26}Mg(p,α)^{23}Na BIG KARL experiment. Solid lines represent DWBA calculations.

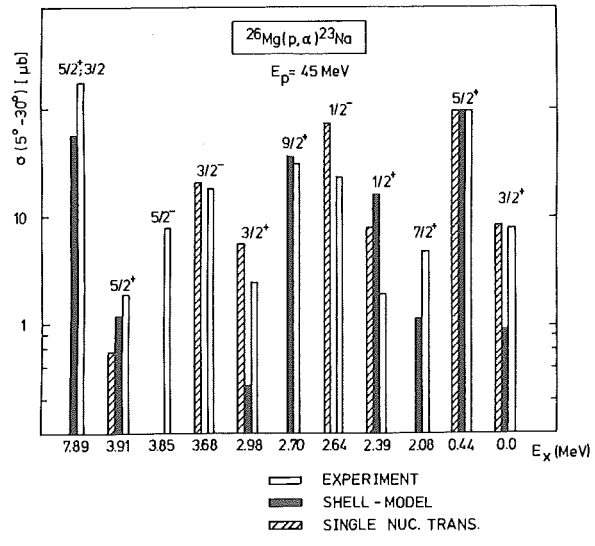

Figure 3: Transition strength for ^{26}Mg(p,α)^{23}Na at E_p=45 MeV experimental data (white bars), shell model prediction (black bars) and single nucleon transfer (hatched bars) normalized to 0.44 MeV level.

In fig. 3 the experimental (p,α) transition strengths to states in ^{23}Na (white bars) are compared with shell model predictions (black bars) given by the DWBA - cross sections multiplied by the spectroscopic factors of Chung and Wildenthal[3] and with the corresponding experimental single particle transfer spectroscopic factors (hatched bars) taken from the compilation of Endt[4]. The data are normalized to the first $5/2^+$ level in ^{23}Na and are plotted on a logarithmic scale. The shell model predictions agree reasonably well with the experimental data, but there are some severe deviations especially for the $3/2^+$ states. An even better agreement is observed in the comparison to the single particle transfer. This supports the spectator model which predicts the two neutrons being coupled to seniority zero and hence acting as a spectator. But in this model the $7/2^+$ or the $9/2^+$ states cannot be excited via triton transfer. The rather strong transitions to the $7/2^+$ and $9/2^+$ states imply the importance of seniority three transfer for the (p,α) reaction.

In order to investigate the influence of the different configurations of the three transfered nucleons, microscopic calculations are in progress. These calculations are based on microscopic form factors calculated in the formalism of Oberhummer[5]. In this formulation exact finite range DWBA calculations are possible. In fig. 4 results of this type of calculations are presented for the ^{27}Al(p,α)^{24}Mg g.s. reaction at 45 MeV. The solid line represents the cluster form factor calculations in finite range using the code DWUCK5. The optical potentials (table 1) have been found by fitting the elastic scattering data for both, the proton and alpha channel at appropriate energies. The dashed line represents a finite range microscopic form factor calculation. The spectroscopic amplitudes of the nine configurations taken into account have been calculated by Pfeifer[6] and are collected in table 2, the parameters for the single particel bound states are given by Hodgson[7]. It should be noted that in this calculation no free parameters have been used apart from a normalization constant N ≙ 2000 in order to give the correct absolute cross section. As can be seen from fig. 4, in both cases the shape of the calculated angular distributions is nearly the same. Beyond it further calculations have shown, that the shape is nearly insensitive to the spe-

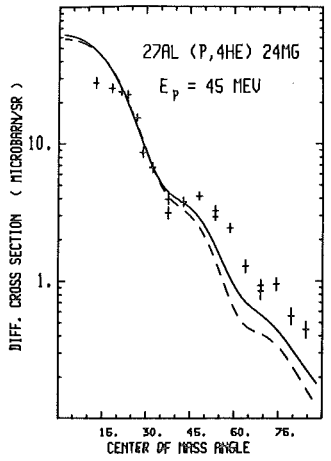

Figure 4: Finite-range DWBA calculation for ^{27}Al(p,α)^{24}Mg g.s. at E_p=45 MeV.
Optical potentials of tab. 1.
Solid line: cluster form factor, dashed line: microscopic form factor.

n l j 1 1 1	n l j 2 2 2	L 12	n l j 3 3 3	$S^{1/2}(\gamma,LSJ)$	Δν
1 $d_{5/2}$	1 $d_{5/2}$	0	1 $d_{5/2}$	0.107	1
1 $d_{5/2}$	1 $d_{5/2}$	2	1 $d_{5/2}$	0.0683	3
1 $d_{5/2}$	1 $d_{5/2}$	4	1 $d_{5/2}$	0.0917	3
1 $d_{5/2}$	1 $d_{5/2}$	2	2 $s_{1/2}$	0.0101	3
1 $d_{5/2}$	1 $d_{5/2}$	0	1 $d_{3/2}$	-.0027	3
1 $d_{5/2}$	1 $d_{5/2}$	2	1 $d_{3/2}$	-.0011	3
1 $d_{5/2}$	1 $d_{5/2}$	4	1 $d_{3/2}$	-.0021	3
1 $d_{3/2}$	1 $d_{3/2}$	0	1 $d_{5/2}$	0.0313	1
2 $s_{1/2}$	2 $s_{1/2}$	0	1 $d_{5/2}$	0.0824	1

Table 2: Spectroscopic amplitudes for the reaction $^{27}Al(p,\alpha)^{24}Mg$ g.s.. Angular momentum transfer L=2, J=5/2.

cial three - nucleon configuration: the cluster approximation is a good approximation to a microscopic calculation. An open problem is the discrepancy in the absolute cross sections, which is well known from other investigations of (p,α) reactions[5].

References

1) F. Hoyler, G. Staudt, G.P.A. Berg, W. Hürlimann, I. Katayama, S.A. Martin, J. Meißburger, B. Styczen, IKP Annual Report 1980, Jül-Spez-99 (1981) 39

2) H. Leeb, private communication

3) W. Chung, private communication

4) P.M. Endt, ADNDT 19 (1977) 23

5) H. Oberhummer, Nuov. Cim. 55A (1980) 253

6) F. Brunner, H.H. Müller, W. Reichart, P. Schober, H. Jasicek, H. Oberhummer and W. Pfeifer, subm. to Helv. Phys. Acta

7) K. Bear and P.E. Hodgson, J. Phys. G4 (1978) L287

*Physik. Inst., Universität Tübingen

1.20. Microscopic model calculation for (p,α) reactions on light nuclei

H.-J. Hauser, F. Hoyler*, H. Oberhummer**, G. Staudt**

In continuation of our systematic study of (p,α) reactions on light nuclei, we have measured (p,α) reaction cross sections for different transitions in the target nuclei ^{15}N, ^{16}O, ^{17}O and ^{18}O. The measurements with a projectile energy of 45 MeV have been performed at the cyclotron JULIC. Some angular distributions of differential cross sections together with results of former experiments are given in fig. 1. Obviously the shape of the angular distributions is mainly determined by the total angular momentum transfer ΔJ. That signifies, that the shape is insensitive to the specific configuration of the transfered nucleons in the target nucleus.

Up to now we have analysed some of these experimental results in zero range DWBA using the code DWUCK4. The three-nucleon form factors required for the DWBA were calculated with the microscopic formalism of Oberhummer[1]. The calculations have shown, that for 1p-shell target nuclei the form factors for given orbital angular momentum transfer ΔL are nearly insensitive to the specific three-nucleon configurations. In fig. 2 a comparison between the experimental angular distributions of four transitions to highly excited states in ^{12}C and the results of DWBA calculations is shown. The parameters of the optical potential for the α-particle are fitted to experimental data[2] of elastic α-scattering at 42 MeV projectile energy, those for the proton are similar to a set used by Pignanelli[3]; (see table). The single particle potentials used in the calculations of the microscopic form factors are drawn from the work of Bear and Hodgson[4].

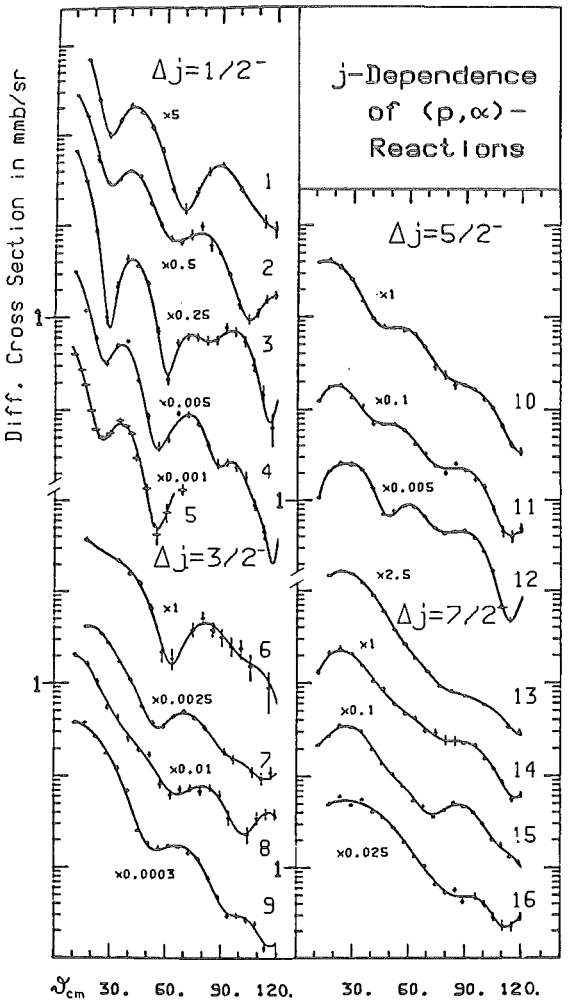

Figure 1: J-dependence of angular distributions;
1: 13C(p,α)10B(1.7); 2: 14N(p,α)11C(2.0); 3: 15N(p,α)12C(0.0);
4: 16O(p,α)13N(0.0); 5: 20Ne(p,α)17F(3.1): 6:11B(p,α)8Be(0.0);
7: 12C(p,α)9B(0.0); 8: 15N(p,α)12C(15.1); 9: 16O(p,α)13N(3.51);
10: 14N(p,α)11C(0.0); 11: 15N(p,α)12C(16.1); 12: 16O(p,α)13N(7.38);
13: 13C(p,α)10B(0.0); 14: 14N(p,α)11C(6.48); 15: 15N(p,α)12C(14.1);
16: 15N(p,α)12C(20.5).

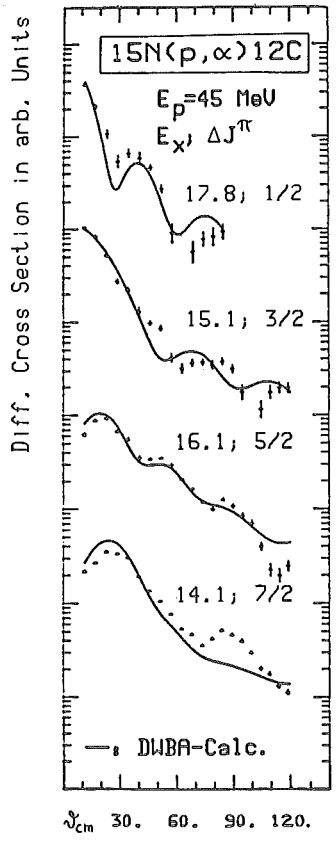

Figure 2: DWBA-calculations (DWUCK4) with microscopic form factors and measured optical potentials for entrance- and exit-channel.

	V	V_{LS}	r_V	a_V	W_V	W_D	r_W	a_W	r_0
$^{15}N+p$	42	32.0	1.13	0.66	5.7	10.3	1.42	0.48	1.25
$^{12}C+\alpha$	215		1.25	0.61	7.9		2.14	0.21	1.25

Table 1: Optical potentials as used in DWUCK4.

The insensitivity of the microscopic form factors to the underlying nucleon configuration only seems to be valid for such transitions, where the transfered nucleons originate from the same major shell. Referring to this it should be noted, that the transition $^{20}Ne(p,\alpha)^{17}F$ (3.10 MeV; $1/2^-$) fits well in the $J=1/2^-$ systematics of the 1p-shell nuclei whereas the transition $^{20}Ne(p,\alpha)^{17}F$ (3.86 MeV; $5/2^-$) does not fit in the $J=5/2^-$ systematics (see ref.5). In order to study the angular distributions and the transition strengths for (p,α) reactions, where the three transfered nucleons do not descend from the same major shell, we started (p,α)-experiments on ^{17}O and ^{18}O.

References

1) H. Oberhummer, Nuov. Cim. 55A (1980) 253
2) N. Baron et al., Phys. Rev. C4 (1971) 1159
3) M. Pignanelli et al., Phys. Rev. C10 (1974) 445
4) K. Bear and P.E. Hodgson, J. Phys. G4 (1978) L287
5) T. Rohwer and W. Oelert, contribution to this report

* Physik. Inst., Universität Tübingen

**Alexander von Humboldt followship

1.21. Light Particle Coincidences in α-induced Reactions+

B. Ludewigt, G. Gaul*, R. Glasow*, H. Löhner**, R. Santo**

In order to study the various processes contributing to the continuous spectra of α-induced reactions at 172.5 MeV a coincidence experiment has been performed on a ^{58}Ni target. For the detection of the reaction products (A≤4) 4 telescopes have been used in the scattering chamber placing the telescopes T1, T2, T4 in one plane (Fig. 1).

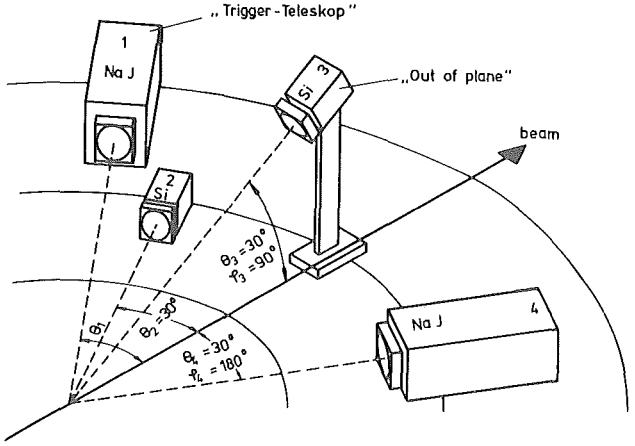

Figure 1: Experimental set-up for the coincidence measurements.

Telescope T3 was mounted out of the reaction plane defined by telescopy 1 and the beam axis.

	ΔE-detector	E-detector
T1	SB, 1000 μm	NaJ, 8 cm
T2	SB, 500 μm	SB, 4x2000 μm
T3	SB, 500 μm	SB, 4x2000 μm
T4	SB, 1000 μm	NaJ, 8 cm

Table 1: Detectors used in telescopes T1-T4.

Two particle coincidences have been measured by detecting one reaction product T1 at angles $\theta_1=20^0$, 40^0, 50^0 and 65^0 and the other in one of the three telescopes T2, 3, 4 at $\theta_3=\theta_4=\theta_2=30^0$. The ΔE- and E-signals and the time differences between the ΔE-signals have been written event-by-event on magnetic tape.

The largest fraction of the observed yield turned out to be p-p-coincidences.

In table 2 some typical coincidences ratios C are listed for a specified energy window in the telescopes involved.

T1	T2, 3, 4	θ_1	$C = {}^{(1-3)}/_{(1-4)}$
energy interval (MeV)			
20-80	22-40	20^0	0.79 (7 %)
20-80	22-40	50^0	0.59 (6 %)
20-80	22-40	65^0	0.56 (11 %)

Table 2: Proton-proton coincidence ratios.

As one of the most significant features we observe an appreciable reduction of the "out of plane" to "in plane" correlation pointing to a direct reaction contribution. The corresponding coincidence spectra displaying this difference are shown in Fig. 2.

For further analysis of the reaction mechanism we make the most simple assumption that the cross section decom-

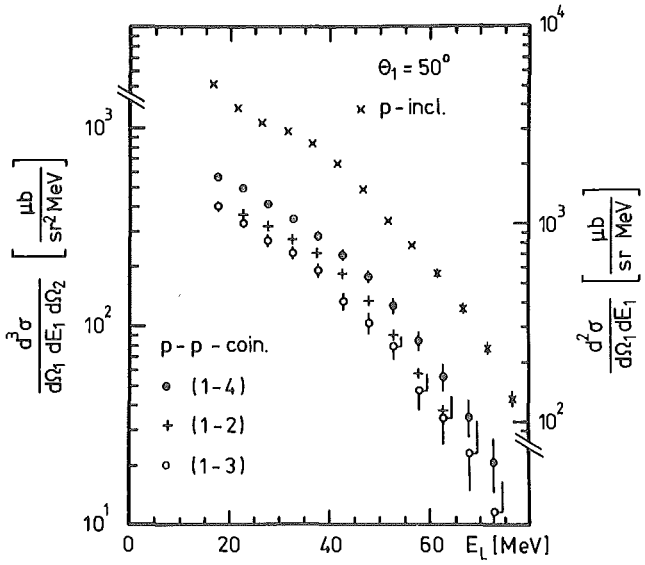

Figure 2: Proton-proton coincidence spectra.

poses into a quasifree nucleon-nucleon scattering part (QFS) and a remaining (possibly thermal) component leading to uncorrelated p-p-coincidences. With this simple separation the difference (1-4)- (1-3) is identified with the QFS contribution. The QFS cross section has been calculated folding the free p-p-cross section with the momentum distribution of the involved projectile and target

protons. As shown in Fig. 3 the calculated curve normalized to the experimental data, agrees well with the measured difference spectrum. The QFS-part of the inclusive p-spectrum may be calculated by integrating over the second proton. An estimation based on the above outlined calculations yields a fraction of QFS of roughly 50 % of the cross section in the energy region 20 MeV $\leq E_p \leq$ 50 MeV at $\theta_p = 50^o$. This result depends, however, strongly on the assumptions made above, in particular the momentum distributions of the nucleons in the target and projectile. Another interesting feature has been observed in the α-p-coincidences. Fig. 4 shows the spectrum of the summed energies of the α-particle and the proton detected at opposite sides of the beam axis at $\theta_\alpha = 20^o$ and $\theta_p = 30^o$, respectively. The peak at an energy of about 170 MeV is an indication for a direct knock-out process, where the α-projectile removes directly a proton from the target nucleus leaving the residual nucleus in a low lying state.

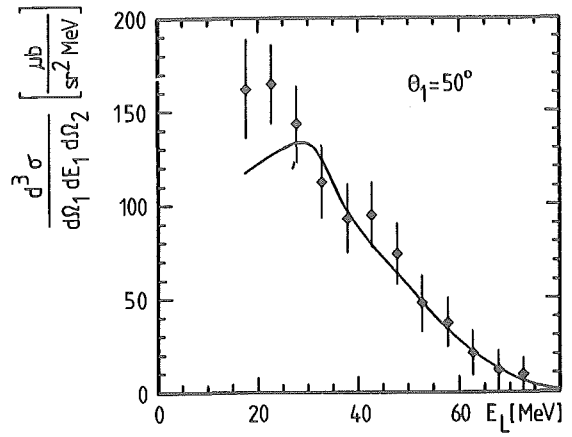

Figure 3: Experimental "in plane" - "out of plane" proton-difference spectrum at $\theta_p = 50^o$ and preliminary QFS calculation (line).

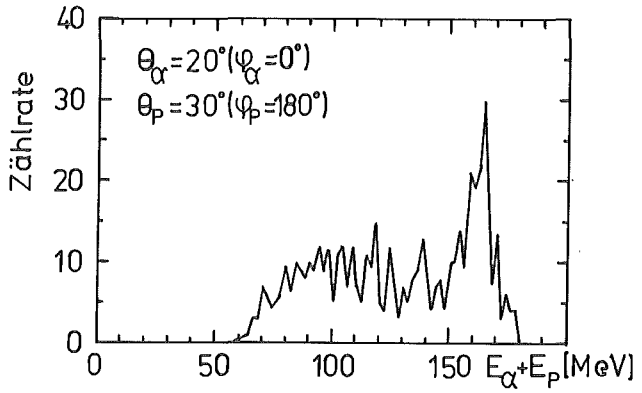

Figure 4: Summed Proton-α-coincidence energy spectrum.

+ Supported in part by the Bundesminister for Forschung und Technologie

* Institut für Kernphysik der Universität Münster

**Present address: Lawrence Berkeley Laboratory, University of California, USA

1.22. α-Emitter Yields from α-Induced Reactions on ^{206,208}Pb and ^{209}Bi

*G.P.A. Berg, J. Ernst**, W. Friedland**, W. Hürlimann, I. Katayama, D. Kolev*,**, S.A. Martin, J. Meißburger, J.G.M. Römer, W. Scholz**, S. Suhr**, J. Tain*

The previous study of α-emitter yields from ^{232}Th + α reactions[1,2] was extended to Pb and Bi targets. Alpha-emitting recoil nuclei from ^{206,208}Pb, ^{209}Bi(α,xnyp) reactions were investigated with the moving tape system BANDIT[3] at 130, 135, 150 and 170 MeV bombarding energy. The tape velocities were adjusted to decay-times of 100 ms to 10 min. The very complex spectra were analyzed by the code ALFUN[4]. Preliminary results for ^{209}Bi + α indicate that e.g. at 170 MeV bombarding energy the residual nuclei ^{200m,g}At and ^{195m,g}Po are produced with cross sections of the order of mb. The yields and isomeric ratios shall be compared to predictions of the code EXCLUSIVE INDEX allowing for the emission of two pre-equilibrium nucleons before the compound nucleus evaporation cascade[5].

Due to the high neutron flux at the position of the Si detector in about 5 cm distance from the target the energy resolution is limited to about 60 keV making it difficult to unambiguously separate nearby α-lines. In order to improve the resolution, and in addition to enable the direct (fast) α-spectroscopy of the target without destroying a Si detector by fission products the facilities of the Big Karl magnetic spectrograph are presently being adapted for α-detection[6]. By using multi-line α-sources the setting of the Big Karl magnets was optimized for rather low main fields of about 1.7 kG. In a first test run α-particles at energies of 5.5 ± 0.4 MeV were detected from the ^{209}Bi + α reaction at 130 MeV bombarding targets of 70 and 300 μg/cm^2 and taking spectra during the 50 s "on" and 50 s "off" periods of the slow beam pulsing system of JULIC. As a focal plane α-detector the multi-wire-proportional-chamber of Big Karl was used being run at a reduced gas pressure of 400 mbar.

References

1) R. Ibowski, W. Scholz, J. Bisplinghoff, J. Ernst, H. Keuser and T. Mayer-Kuckuk, Proc. of the International Conference on "Nuclear Reaction Mechanisms", Varenna, Italy, June 18 - 21, 1979, p. 103

2) J. Ernst, W. Friedland, T. Mayer-Kuckuk and W. Scholz, Proc. of the International Conference on Nuclear Physics, Berkeley, California, August 24 - 30, 1980, p. 449

3) W. Friedland, J. Ernst, T. Mayer-Kuckuk and W. Scholz, Annual Report 1979, Institut für Kernphysik, KFA Jülich, Jül-Spez-72, p. 34

4) W. Wätzig and W. Westmeier, Nucl. Instr. and Meth. 153 (1978) 517

5) J. Ernst, W. Friedland and H. Stockhorst, Annual Report 1979 - 1980, Institut für Strahlen- und Kernphysik der Universität Bonn, p. 26, to be published

6) S. Suhr, Diplomarbeit in progress, University of Bonn

* Now at University of Sofia, Sofia, Bulgary

**Institut für Strahlen- und Kernphysik der Universität Bonn, 5300 Bonn 1

1.23. Measurement and Theoretical Predictions of Integral Excitation Functions for α-Induced Reactions on Ti, V and Mn

*R. Michel**, *G. Brinkmann**, *M. Galas**, *R. Stück**

Completing a systematic investigation of α-induced reactions on target elements $22 \leqq Z \leqq 28$ fifty excitation functions were measured for the production of radionuclides $42 \leqq A \leqq 58$ from natural titanium, vanadium and manganese for 15 MeV $\leqq E_\alpha \leqq$ 172.5 MeV.

Because of the rather high (up to ∼ 5 %) abundance of titanium in the lunar surface, this element deserves particular interest as target element with regard to certain cosmochemical applications. So the new measurements on Ti - together with earlier ones on Fe and Ni - now permit a quantitative description of the interaction of solar α-particles with extraterrestrial matter. Analogous model calculations were already performed for the interaction of solar protons with the lunar surface[1], as well as with meteorites and cosmic dust[2].

Moreover, these experimental excitation functions are useful for testing actual theories of nuclear reactions. So the experimental data were compared with theoretical predictions on the basis of the hybrid model of preequilibrium reactions[3]. The faculty of this model for "a priori" calculations is of high value in the field of applications of cross sections.

There are discrepancies, however, between the newly measured excitation functions and the theoretical ones which are similar to those described earlier[4] for cobalt. These deviations give evidence for a greater complexity of the initial reaction phase of α-induced reactions than accounted for by "OVERLAID ALICE"[5]. In particular, incomplete break-up of the incoming α-particle will result in a lower excitation energy of the compound system, thus rising the cross sections for exit channels with small mass differences between target and product nuclide. An example of this type is given in fig. 1. At 170 MeV

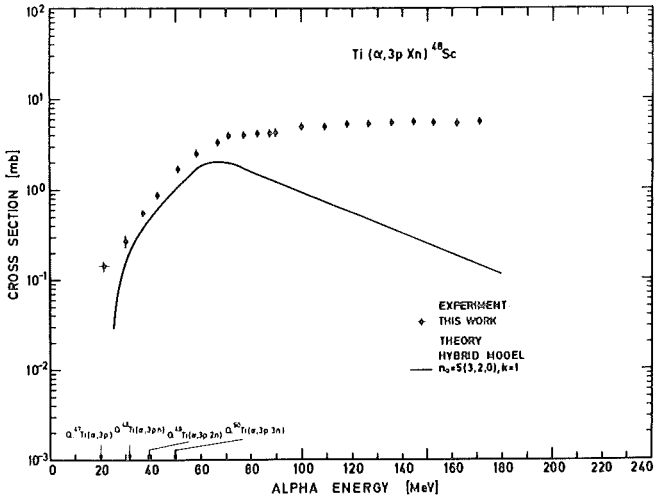

Figure 1: Experimental cross sections and hybrid model calculations for Ti(α,3pxn)^{48}Sc.

the experimental data for Ti(α,3pxn)^{48}Sc are underestimated by theory by more than a factor of 10. But since Ti has 5 stable isotopes, here it is difficult to attribute the discrepancy to a particular reaction channel.

In the case of V and Mn which are - or at least can be regarded as - single isotope targets, the experimental cross sections permit a more detailed theoretical analysis. Exemplarily in fig. 2 a comparison of experimental

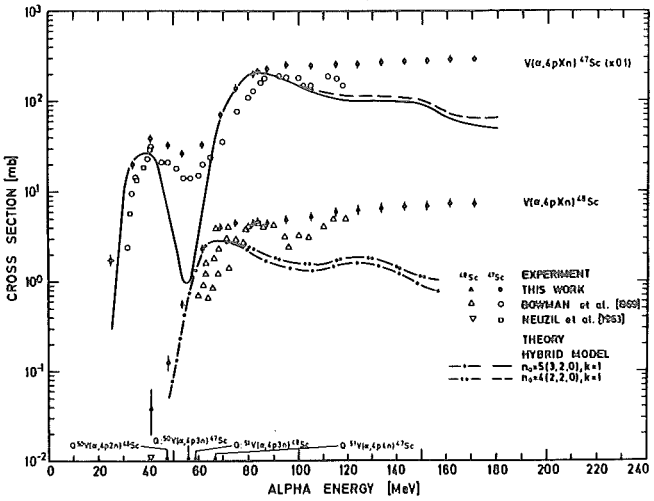

Figure 2: Experimental and theoretical excitation functions for the production of ^{47}Sc and ^{48}Sc from V.

and hybrid model data for V(α,4pxn) reactions leading to ^{47}Sc and ^{48}Sc is made. For ^{47}Sc in the energy region between 50 and 60 MeV preequilibrium α-emission in the reaction ^{51}V(α,2α)^{47}Sc is to be observed which is not described by the theory. At higher energies, the evaporation peak of the ^{51}V(α,α2p2n)^{47}Sc reaction is adequately reproduced. Above 100 MeV, however, the experimental cross sections show a strong levelling-off which is not to be seen in the calculations.

Also for the ^{51}V(α,4p3n)^{48}Sc reaction the calculated cross sections at 170 MeV deviate from the experimental ones by an order of magnitude. Here, possibly break-up effects may be important, so that the actual reaction to be attributed would be ^{51}V(n,α)^{48}Sc rather than ^{51}V(α,4p3n)^{48}Sc. A more detailed analysis of excitation functions measured is in progress. Together with recently started studies of excitation functions for ^{2}H- and ^{3}He-induced reactions on cobalt it will permit a comprehensive survey on reactions of light particles with elements $22 \leqq Z \leqq 28$.

References

1) R. Michel and G. Brinkmann, J. Radioanal. Chem. 59 (1980) 467

2) R. Michel, G. Brinkmann and R. Stück, submitted to Earth and Planetary Science Letters

3) M. Blann, Phys. Rev. Lett. 27 (1971) 337

4) R. Michel and G. Brinkmann, Nucl. Phys. A 338 (1980) 167

5) M. Blann (1978) UR-NSRL-181

*Institut für Kernchemie der Universität zu Köln

1.24. Continuous charged particle spectra from $^{40}Ca+^{6}Li$ reactions at an incident energy of 26 MeV/nucleon

H. Rebel, H.J. Gils*, R. Planeta*, J. Buschmann*, B. Neumann**, H. Klewe-Nebenius**, S. Zagromski**, R. Shyam***, and H. Machner*

The investigation of break-up reactions is of great interest, because by this way the internal motion of constituents in nuclei can be studied. This has been done within simple models based on quasi free scattering mechanism[1-4]. However, these models account only for the elastic break-up mode. But at reasonable energies inelastic break-up modes come into play. Such processes like incomplete fusion, absorptive break-up or massive transfer have been found to be the dominant contribution. For a review see reference 5. We have used the ^{6}Li beam of the Karlsruhe Isochronous Cyclotron as a tool to study break-up processes. This particle seems favourable for such studies because it first is intermediate between light and really heavy ions and second it is weakly bound (E_B = 1.47 MeV).

In a series of experiments targets of ^{40}Ca have been bombarded with 156 MeV ^{6}Li-ions. Charged particle spectra of outgoing nuclei with A≤4, Z≤2 have been detected using solid state telescopes. Spectra were recorded over an angular range from 9° to 50° and in some cases up to 90°. A complete compilation of the data is given in ref. 6.

In all spectra at forward angle a bell shape structure is to be seen centered around beam velocity. This structure is superimposed on a flat continuum from pre-equilibrium reactions. We have analyzed the data in a way similar to that of ref. 7.

The inclusive break-up spectra have been calculated in terms of the DWBA approach of Baur et al.[8]. Within this approach the cross sections for elastic as well as inelastic break-up are calculated from the T-matrix. Excitations of the ^{6}Li projectile prior to break-up has not been taken into account. To simplify the computation of the T-matrix the zero range approximation has been applied. For the break-up of ^{6}Li into deuteron and α-particle a zero range constant D_0 has been obtained from the Fourier transform $\phi(p)$ of the s-wave part of the wave function

$$D_0 = \lim_{p\to 0} \phi(p) \qquad (1)$$

to be -69.6 MeV $fm^{3/2}$.

The pre-equilibrium contribution has been calculated with the help of the exciton coalescence model[9]. At the high excitation energy under discussion here the emission of more than one particle during the pre-equilibrium phase is possible. This has been taken into account by calculating the equilibration process with the help of master equations for residual nuclei after neutron and proton emission[10]. This leads to

$$\frac{d^2\sigma_x(E,\theta)}{dE d\Omega} = \sigma_0 \sum_{\substack{n=n_0 \\ \Delta n=2}} W_x(p,h,E,\theta)\tau_n \qquad (2)$$

for the cross section of the first emitted particle of type x. The quantity W_x is the emission rate into the direction θ from a state with p particles and h holes (n=p+h)[9]. The average n-exciton state life time τ_n is derived from the system of master equations and σ_0 denotes the reaction cross section. Taking energy and particle conservation into account the second particle cross section for a particle of type y following an already emitted particle of type x is

$$\frac{d^2\sigma_{xy}(E_y,\theta)}{dE_y d\Omega} = \sigma_0 \sum_{\substack{n=n_0 \\ \Delta n=2}} \int W_x(p,h,E_x)\tau_n \cdot \left[\sum_{\substack{m=m_0 \\ \Delta m=2}} W_y(p-p_x,h,E_y,\theta)\cdot\tau_m\right] dE_x \qquad (3)$$

with $m_0 = n-p_x$.

The absolute height of complex particle spectra has been obtained by adjusting the free model parameter i.e. P_0 the radius of the coalescence sphere in momentum space[9]. This adjustment has been done at an angle of θ = 45° where the contribution from the break up is negligible. The obtained values for P_0 are given in the table and agree with earlier results from light ion induced reactions[11]. In the figure data are compared with calculations including both break-up and pre-equilibrium. It is to be seen that at lower energies still a large part of the cross section is unexplained. However, with respect to the linear scale, in the break-up region the incoherently summed calculations give reasonable agreement.

particle	t	^{3}He	α
P_0(MeV/c)	271	248	354

Table 1: Used values of the coalescence radius

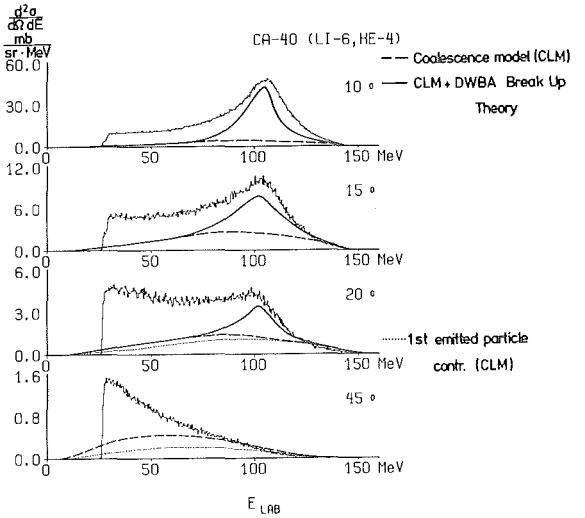

Figure 1: $^{40}Ca(^{6}Li,\alpha x)$ at E_{Li} = 156 MeV. Pre-equilibrium emission background as predicted by the coalescence model and total break-up calculation compared with data.

References:

1) R. Serber, Phys. Rev. 72 (1947) 1008

2) L. Landau and F. Lifshitz, JETP 18 (1948) 750

3) E.H.L. Aarts et al. Phys. Lett. 105B (1981) 130

4) M.S. Hussein and K.W. McVoy, in Continuum Spectra of Heavy Ion Reactions, Harwood Academic Publishers, 1980

5) A. Budzanowski, in Proc. of the Adriatic Europhysics Study Conference, 1981, N. Cindro, W. Greiner, A. Ricci (Edts.), North Holland Publ., Amsterdam (in press)

6) K. Feißt, B. Neumann, J. Buschmann, H.J. Gils, and H. Rebel, Int. Report, Kernforschungszentrum Karlsruhe (unpublished)

7) U. Bechstedt et al., Nucl. Phys. A343 (1980) 221

8) G. Baur and D. Trautmann, Phys. Rep. 25C (1976) 293; R. Shyam, G. Baur, F. Rösel, and D. Trautmann, Phys. Rev. C19 (1979) 370

9) H. Machner, Phys. Lett. 86B (1979) 129

10) H. Machner, to be published

11) H. Machner, Phys. Rev. C21 (1980) 2695

* Institut für Angewandte Kernphysik, Kernforschungszentrum Karlsruhe

** Institut für Radiochemie, Kernforschungszentrum Karlsruhe

*** Daresbury Laboratory, Daresbury, Warrington, United Kingdom

1.25. Light Charged Particle Emission from $^{197}Au + ^{20}Ne$

H. Machner, G. Riepe, D. Protić, H.J. Bohlen, and G. Fuchs**

The study to light particle emission from heavy-ion induced reactions is a tool to investigate the underlying reaction mechanisms. At energies above the binding energy per nucleon spectra of secondary particles are dominated by pre-equilibrium emission and projectile break-up. The latter has been studied extensively from a few MeV up to relativistic energies. For a recent review see ref. 1. Pre-equilibrium reactions have been successfully reproduced in light-ion induced reactions in terms of time dependent approaches[2]. However, the situation in heavy-ion induced reactions is not so clear. Thus, we have measured spectra of light charged particles ($Z \leq 3$, $A \leq 10$) over a large energy range. The reaction chosen was $^{197}Au + ^{20}Ne$ at 392 MeV bombarding energy using the coupled accelerator system VICKSI of the HMI Berlin. Inclusive spectra were taken at 11 different angles from 5^{o} to 140^{o} in the laboratory system. The particles were spectroscopied with a stack of solid state counters. This arrangement consists of one 400 µm Si-surface barrier and seven high-purity Ge-diodes[3] with total thickness of ~ 80 mm. This set up allows the spectroscopy of protons up to 200 MeV. Energy calibration was accomplished with recoiling protons and deuterons from a deuterized polyethylen target.

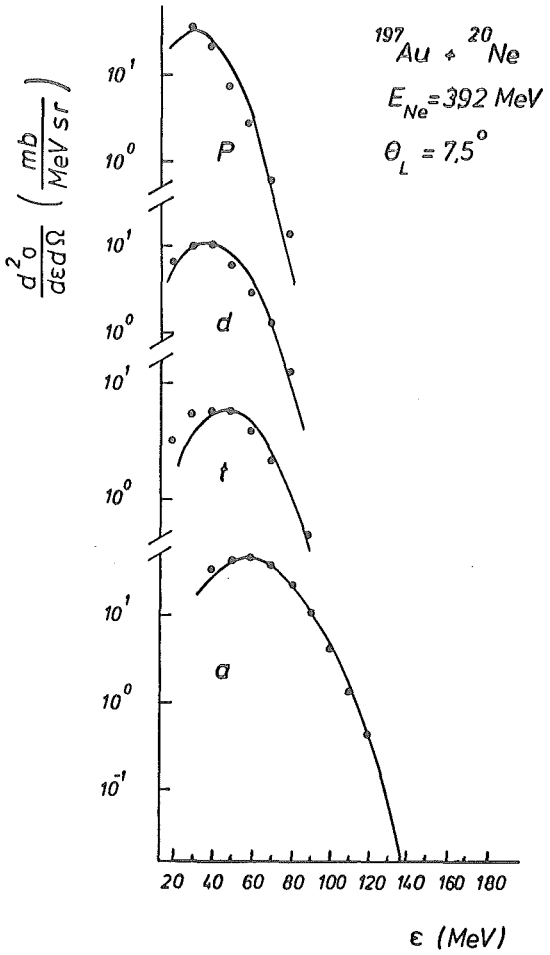

Figure 1: Cross sections for particle types indicates in the figure from $^{197}Au + ^{20}Ne$ reactions are shown as dots. They are well reproduced by Gaussians (solid line).

In fig. 1 an example for the emission angle 7.5^{o} is given. The cross sections can be very well approximated by Gaussians. From the analysis of spectra with good statistics ($A \leq 4$) a linear dependence of the centroid (ε_m) as well as the width σ with mass number (A) of the outgoing particle was obtained.

$$\varepsilon_m(A) = 21.1 \text{ MeV} + 9.59 \text{ MeV} \cdot A \quad (1)$$

$$\sigma_m(A) = 11.1 \text{ MeV} + 2.20 \text{ MeV} \cdot A \quad (2)$$

Eq. 1 clearly shows that the origin of the Gaussians is not projectile breakup which should result into centroids around the beam velocity and correspondingly to $\approx 20 \cdot \text{MeV} \cdot A$.

At present data analysis is in progress.

References

1) A. Budzanowski in Proc. Adriatic Europhysics Study Conf. 1981, North Holland Publ. (in press)

2) H. Machner, Phys. Lett. 86B (1979) 129; H. Machner, Z. Physik A302 (1981) 126 and references therein

3) G. Riepe et al., Nucl. Instr. Meth. 177 (1980) 361

*HMI für Kernphysik, Postfach, 1000 Berlin

1.26. Study of pre-equilibrium emission following the bombardment of nuclei with 200 MeV protons

H. Machner, D. Protić, G. Riepe, J.P. Didelez, N. Frascaria*, E. Gerlic*, E. Hourani*, H. Morlet**

The measurements of continuous particle spectra following the bombardment of nuclei with 200 MeV protons[1] have been continued. We have extended previous measurements by now spectroscopying secondary helium isotopes from an ^{197}Au target. Details of the experimental technique can be found elsewhere[1]. Data analysis is under way. The hydrogen isotopes show some features previously observed at lower proton energies (90 MeV)[2]: Spectra of the different hydrogen isotopes at the same laboratory angle have the same spectral shape when corrected for different Q-values. The cross sections scale $\sigma(p):\sigma(d):\sigma(t)\approx 100:10:1$.

These spectra have been analyzed in terms of ECM[3]. At the high bombarding energy we here have to deal with the emission of more than on particle during the pre-equilibrium phase has to be taken into account. We have restricted ourselves to only second chance emission following neutron and proton emission. To make the calculations feaseable in finite computer time we have limited the calculations to only 15 interactions. The contributions from more complex states are negligible. The calculations have been performed in a grid of 10 MeV excitation energies. The time evolution of the system is followed by a set of master equations

$$\frac{dP(n,t)}{dt} = \lambda_+(n-2,E)P(n-2,t)+\lambda_-(n+2,E)P(n+2,t) - [\lambda_+(n,E)+\lambda_-(n,E)+\sum_x \lambda_c^x(n,E)]P(n,t)$$

with the initial condition (1a)

$$P(n,t=0)=\delta(n,n_0), \quad (1b)$$

for the occupation probability P(n,t) of a state with n excitons (n = particles + holes) at the time t. The quantities $\lambda_\pm$ denote averaged transition rates[4] between neighbouring states with $n' = n \pm 2$ while λ_c^x denotes the continuum emission rate for a particle of type x. After emission the system may be far from equilibrium. We take this into account by a second system of master equations:

$$\frac{dQ(m,t)}{dt} = \lambda_+(n-2,U)Q(m-2,t)+\lambda_-(m+2,U)Q(m+2,t) - [\lambda_+(m,U)+\lambda_-(m,U)+\sum_x \lambda_c^x(m,U)]Q(m,t) \quad (2)$$

with $U=E-B_x-\varepsilon_x$ (B_x and ε_x are binding and channel energy of the particle of type x) and $m_0=n-p_x$. The initial condition is

$$Q(m,t=0)=\delta(m,m_0)\,\frac{1}{\sigma_0}\,\frac{d\sigma}{d\varepsilon}(n,\varepsilon) \quad (2a)$$

with $\frac{d\sigma}{d\varepsilon}(n,\varepsilon)$ the cross section for the first particle emission with energy ε from a state with exciton number n and σ_0 the reaction cross section. In fig. 1 angle integrated cross sections for proton emission are compared with calculations using a mean free path multiplication factor of two. Such a small factor is reasonable at the high excitation energy[4].

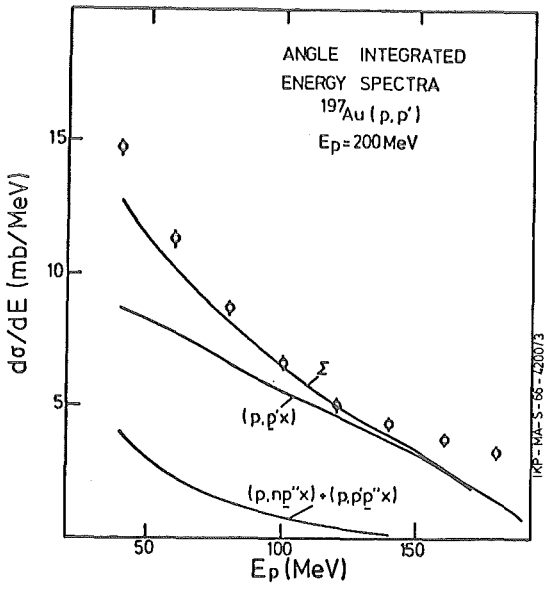

Figure 1: Angle integrated energy spectra of protons from 200 MeV protons on ^{197}Au. Data are shown with statistical error bars. Calculations as described in the text are shown. First chance and second chance emission are separately shown as well as the sum of both.

Contributions from first and second chance emission are separately shown as well as the sum of both. In the fig.2

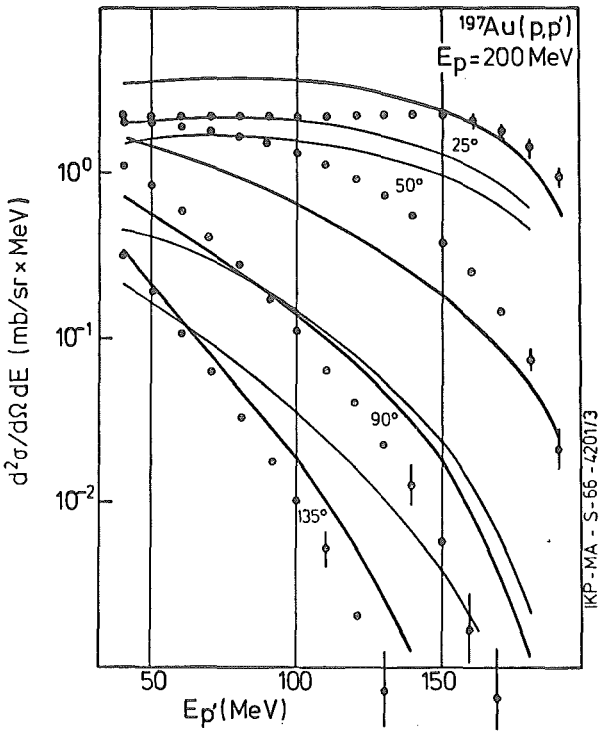

Figure 2: Cross sections of protons from 200 MeV protons on ^{197}Au are shown for different angles. Calculations assuming an exponential angular distribution after one intraction and including secondary chance emission are shown as thick solid curves. Thin solid curves assume a cosinus-dependence of the angular distribution.

spectra at different angles are compared with the calculations. The initial angular distribution has been approximated as an exponential[5]. For comparison calculations using a cosinus-dependence[3] and only one particle emission with mean free path multiplier of four is also shown. Within the rigorous model assumptions - for instance

equidistant spacing single particle levels - the agreement between data and model prediction is good. From figures 3 and 4 it can be seen that the angular distri-

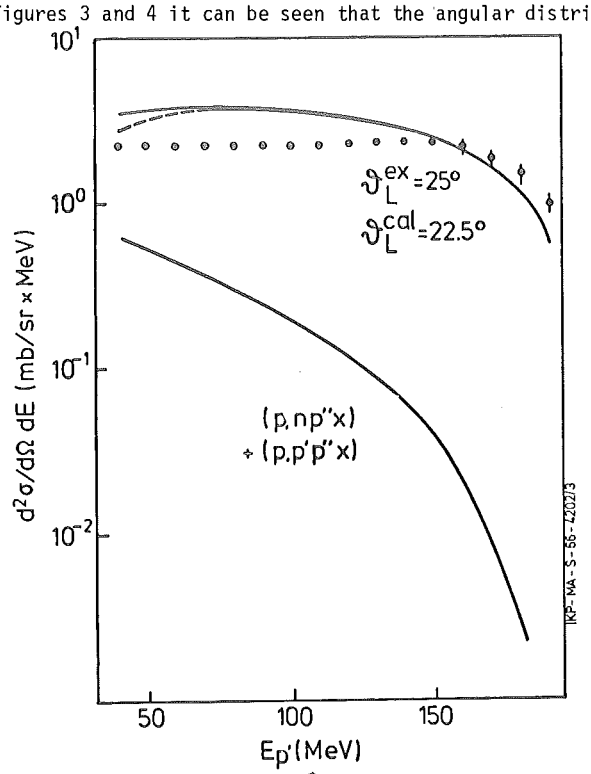

Figure 3: Cross sections for ϑ_L=25° are compared with calculations (calculations for 22.5°). First chance emission - shown as dashed line - is at high energies nearly identical with the sum (solid line) including second chance emission, which is separately shown.

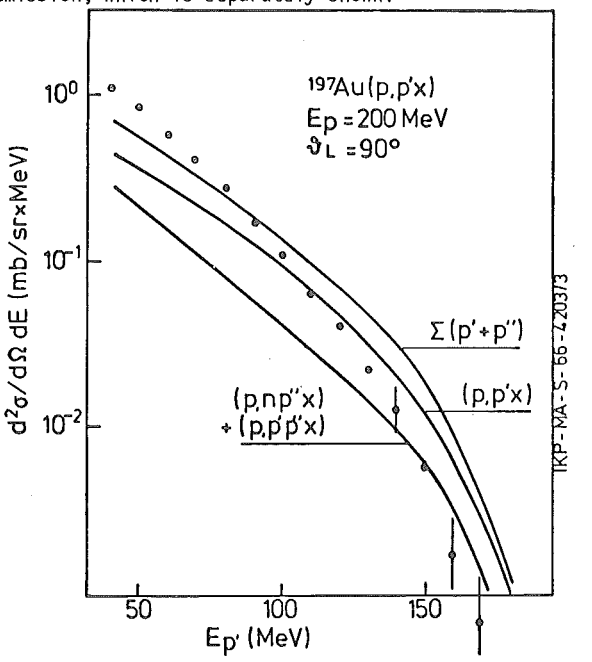

Figure 4: Similar to fig. 3 for ϑ_L=90°. First chance emission is also drawn as a solid line.

butions of first and second chance emission are very different. While the first chance emission is strongly forward peaked, secondary chance emission is more flat due to its origin from states near the compound nucleus. A similar conclusion may be drawn from fig. 1 for the energy dependence. Protons with high energies are mainly emitted in the early stages. Thus, they stem mainly from first chance emission.

References

1) J.P. Didelez, et al., Annual Report 1980, IKP der KFA Jülich, Jül-Spez-99 (1981) 35
2) J.R. Wu, et al., Phys. Rev. C19 (1979) 698
3) H. Machner, Phys. Lett. 86B (1979) 129
4) H. Machner, Z. Physik A - Atoms and Nuclei 302 (1981) 125
5) H. Machner, et al., to be published

*Institut de Physique Nucléaire, F-91406 Orsay, France

1.27. Interpretation of proton spectra measured in the ^{209}Bi(α,pxn) reaction by the exciton model

R.M. Lieder, B. Bochev, J.P. Didelez, T. Kutsarova, H. Machner, M. Müller-Veggian, A. Neskakis and C. Mayer-Böricke*

Proton spectra have been measured for the ^{209}Bi(α,pxnγ) reaction at a beam energy of 75 MeV (ref. 1). The particle-γ coincidence technique was used in this investigation. In the analysis proton spectra corresponding to the individual reaction channels were produced by setting gates on characteristic γ lines of the respective final nuclei[1]. The particle telescope has been placed at angles of 45°, 90° and 135° with respect to the beam direction.

In order to interprete the proton spectra and angular distributions as observed in the (α,pxn) reactions, calculations in the framework of the exciton model have been carried out. This model is based on the assumption that the incoming projectile by interacting with the target nucleus gives rise to a simple initial configuration characterized by a small number n_0 of particles and holes (excitons). Successive two-body interactions between excitons and further particles or holes cause an intra-nuclear cascade which eventually leads to a compound-nucleus state. The intermediate states are characterized by an increasing exciton number n. At each stage of this equilibration process a competition exists between two decay modes of the composite system, viz. the decay by particle emission and the decay by exciton-exciton interaction. In the calculations for each stage the probability for particle emission and the intranuclear transition rate have to be evaluated and to be compared with each other.

Inclusive proton spectra for the $^{209}Bi(\alpha,pxn)$ reaction at E_α = 75 MeV have been calculated in the framework of the exciton model[2]. A comparision of the experimental and calculated p spectra for an angle of 45° are shown in fig. 1. The experimental proton spectrum is the sum

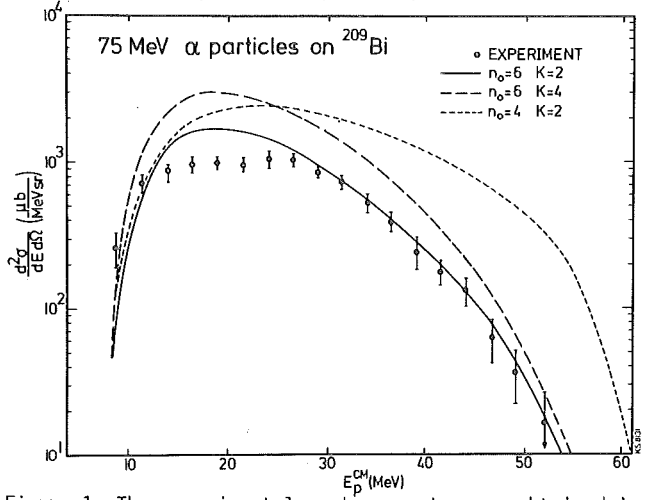

Figure 1: The experimental proton spectrum as obtained in the $^{209}Bi(\alpha,pxn)$ reaction for a beam energy of 75 MeV and an angle of 45° is compared with predictions of the exciton model.

of the proton spectra of the individual reaction channels. It is assumed that this corresponds almost to an inclusive proton spectrum. An inclusive spectrum can strictly speaking only be a singles spectrum since in a coincidence experiment only those reaction channels are observed which lead to an excitation of the target nucleus. In an elastic break-up reaction, e.g., the target nucleus is not excited. At an angle of 45° it is on one hand, expected that the elastic break-up reaction contributes only little to the cross section. On the other hand such a mechanism is not included in the exciton model calculations since a fusion of the projectile and the target nucleus is assumed. Therefore, the comparision of experimental and calculated proton spectra, as presented in fig. 1, is meaningful.

The parameters used in the exciton model calculations are the mean free path multiplication factor K = 2, 4 and the initial number of exciton n_0 = 4, 6. It can be seen in fig. 1 that the calculation with K=2 and n_0 = 6 reproduces the data best. In a previous calculation[3] of excitation functions for the $^{209}Bi(\alpha,n)$, $^{209}Bi(\alpha,p)$ and $^{209}Bi(\alpha,pn)$ reactions in the framework of the hybrid model it was found that the experimental data are reproduced best for n_0 = 4. The difference to the present results is noteworthy. It may be due to the fact that the hybrid model was used in the latter case but the exciton model in the former one. On the other hand this result may indicate an open problem since Gadioli et al.[4] were able to reproduce excitation functions of (α,n) reactions in the framework at the exciton model using n_0 = 4 as well. This problem needs a further investigation.

The mechanism to produce high energy protons in the exciton model can be explained in the following way: The first interaction of the projectile and target nucleus cannot be treated in the framework of the exciton model. It is assumed that all energy is used to excite the fused system and that a configuration comprising a certain initial exciton number is formed. This highly excited state may decay into a level lying close to the yrast line by emission of one proton of high energy. Such a process is similar to a direct reaction.

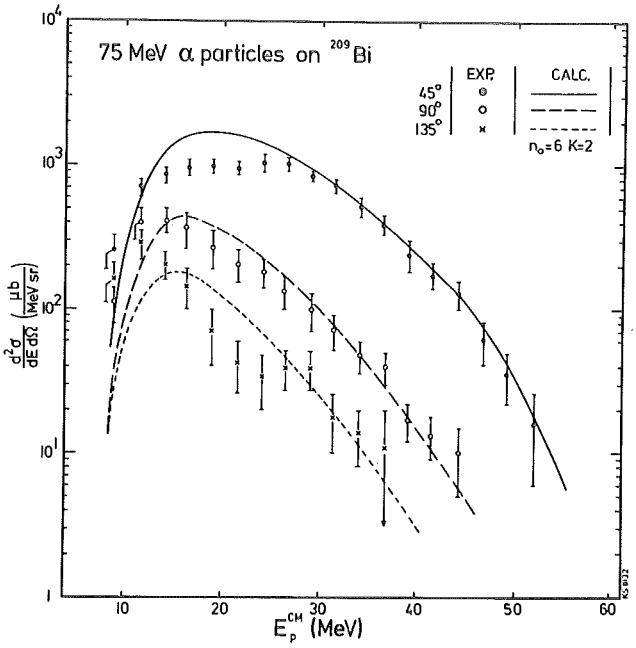

Figure 2: Experimental proton spectra as obtained in the $^{209}Bi(\alpha,pxn)$ reaction for a beam energy of 75 MeV and angles of 45°, 90° and 135° are compared with predictions of the exciton model.

Calculations of inclusive proton spectra for the $^{209}Bi(\alpha,pxn)$ reaction at a beam energy of 75 MeV have been carried out in the framework of the exciton model not only for an angle of 45° but also for angles of 90° and 135°. The parameters were n_0 = 6 and K = 2. The results are compared in fig. 2 with the experimental proton spectra taken at the same angles. It can be seen that the calculations reproduce the data very well. It may be concluded, therefore, that the inclusive proton spectra and angular distributions as measured in the $^{209}Bi(\alpha,pxn)$ reaction can be understood in the framework of the exciton model.

References

1) R.M. Lieder, B. Bochev, T. Kutsarova, H. Beuscher, D.R. Haenni, T. Morek, M. Müller-Veggian, A. Neskakis, C. Mayer-Böricke and J.P. Didelez, Physica Scripta 24 (1981) 123

2) H. Machner, Phys. Lett. 86B (1979) 129

3) J.P. Didelez, R.M. Lieder, H. Beuscher, D.R. Haenni, H. Machner, M. Müller-Veggian and C. Mayer-Böricke, Nucl. Phys. A341 (1980) 421

4) E. Gadioli, E. Gadioli Erba, L. Sajo-Bohus and G. Tagliaferri, Riv. Nuovo Cimento 6 (1976) 1

*Institut de Physique Nucléaire, F-91406 Orsay, France

1.28. Non-Equilibrium Particle Emission in 45 MeV α Particle Bombardment of ^{159}Tb

*J.-P. Didelez**, B. Bochev, R.M. Lieder, T. Kutsarova, T. Morek***, A. Neskakis, M. Müller-Veggian, and C. Mayer-Böricke*

From previous studies[1,2,3] of ^{209}Bi(α, charged particle xnγ) reactions leading to Po nuclei at 45 MeV and 75 MeV by means of particle-γ coincidence techniques important conclusions could be drawn about the depopulation mechanism and the reaction mechanism for nonequilibrium reactions. It has been shown in particular that the observed decomposition of the particle spectra can be understood in the framework of the yrast picture describing the depopulation mechanism. We have extended the study of the nonequilibrium reaction mechanism by investigating the ^{159}Tb(α,charged particle xnγ) reaction. A Tb target has been chosen for the following reasons: i) No long living isomers exist in the resulting Dy nuclei. The presence of such isomers in the Po nuclei hindered to draw clear-cut conclusions about the depopulation mechanism. ii) The even-mass Dy nuclei show yrast bands of rotational character which enables to measure side-feeding distributions and γ-ray multiplicities.

In the present contribution the energy spectra and angular distributions of p, d and t as measured in the bombardment of ^{159}Tb with 45 MeV α particles shall be described. In fig. 1 the double differentiated cross sections of the

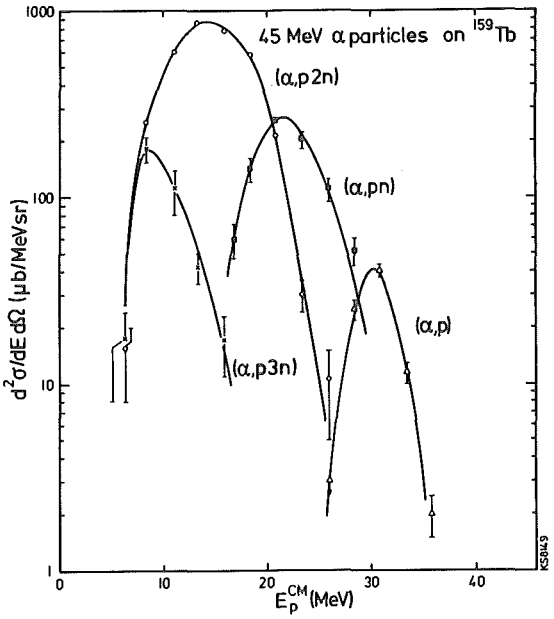

Figure 1: Doubly differential cross sections for the ^{159}Tb(α,pxnγ) reaction at 45°. The error bars include only the statistical uncertainties. The curves are eye-guiding lines.

pxn channels for an angle of 45° of the particle telescope with respect to the beam direction is shown. As in the case of ^{209}Bi(α,pxnγ) reactions at E_α = 45 MeV each channel is characterized by a pronounced peak. Similar results are obtained for the dxn and txn channels. They are shown in fig. 2 and fig. 3, respectively. These results allow to confirm our previous conclusions that the peaks in the particle spectra are produced by the depopulation mechanism.

Angular distribution experiments show that the energies and widths of the peaks corresponding to the (α,p), (α,pxn), (α,d), (α,d2n) and (α,t2n) reaction channels are within the experimental uncertainties independant of the particle emission angle. The comparison of the differential cross sections of the (α,p2n), (α,dn), (α,t) and (α,tn) channels at 45° with those at 90° and 135° indicates, however, that the energies and widths of the peaks decrease with increasing angle. This can be understood assuming that each peak is a superposition of at least two components with different energies and angular distributions. This is analogous to the results obtained for the ^{209}Bi(α,t)^{210}Po and ^{209}Bi(α,dn)^{210}Po reactions. Energy integrated angular distributions for the various reaction channels are shown in fig. 4. It was possible to separate the peak of the (α,t) channel into two components which are both represented in fig. 4. The high-energy component shows a larger anisotropy than the low-energy component. The latter has an angular distribution similar to those of the (α,p) and (α,d) channels.

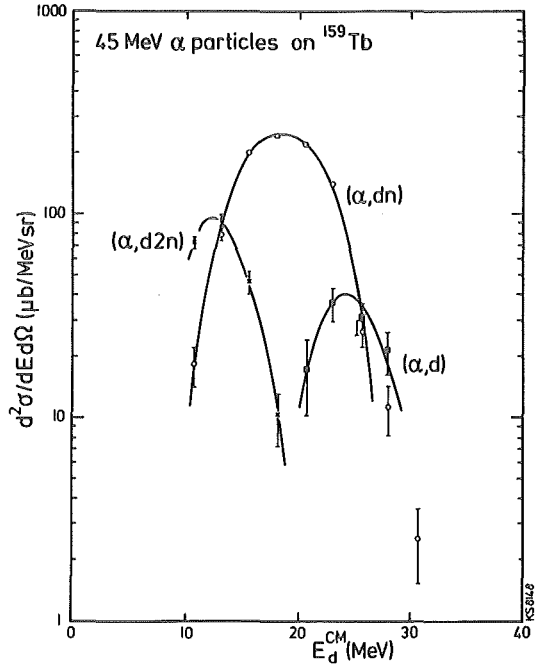

Figure 2: As in fig. 1 but for the ^{159}Tb(α,dxnγ) reaction.

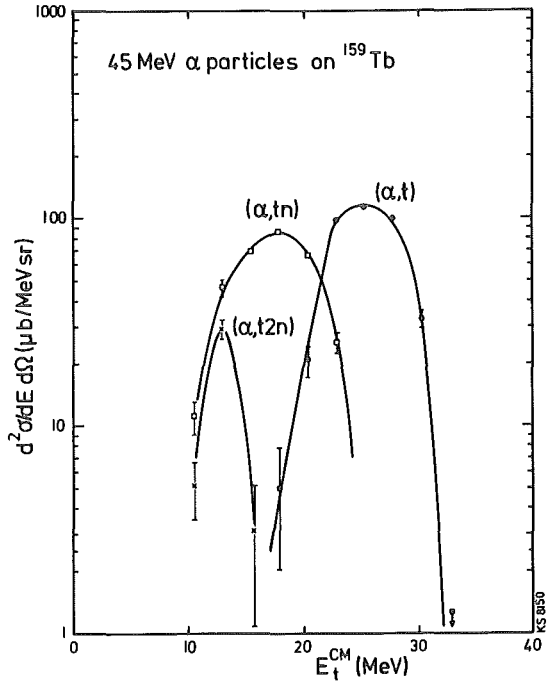

Figure 3: As in fig. 1 but for the ^{159}Tb(α,txnγ) reaction.

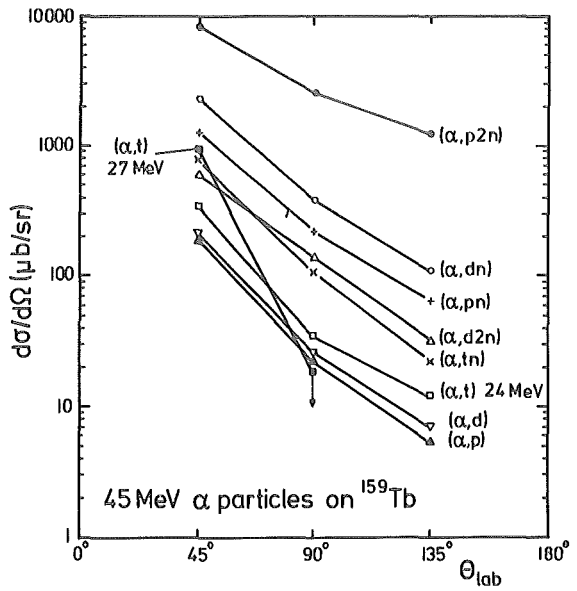

Figure 4: Energy-integrated cross sections as a function of the laboratory angle for the ^{159}Tb(α,charged particle xnγ) reaction.

The energies and widths of the charged particle peaks are in good agreement with the expectations deduced from the yrast picture. This means that charged particles of large energy are emitted as first particle after the complete fusion. The neutrons are evaporated subsequently. Furthermore conclusions about the reaction mechanism can be drawn considering that the (α,t), (α,dn) and (α,d2n) channels have each at least two components with different angular distributions. The steep angular distribution of the high-energy component of the (α,t) reaction may indicate that it is caused by a break-up fusion mechanism.

References

1) B. Bochev, R.M. Lieder, J.-P. Didelez, T. Kutsarova, H. Beuscher, D. Haenni, H. Machner, T. Morek, M. Müller-Veggian, A. Neskakis and C. Mayer-Böricke, Annual Report 1979, IKP, KFA Jülich, Jül-Spez-72 (1980) 33

2) R.M. Lieder, B. Bochev, T. Kutsarova, H. Beuscher, D.R. Haenni, T. Morek, M. Müller-Veggian, A. Neskakis, C. Mayer-Böricke, and J.P. Didelez, Physica Scripta 24 (1981) 123

3) T. Kutsarova, B. Bochev, J.P. Didelez, R.M. Lieder, T. Morek, M. Müller-Veggian and C. Mayer-Böricke, Annual Report 1980, IKP, KFA Jülich, Jül-Spez-99 (1981) 58

* Institut de Physique Nucléaire, F-91406 Orsay, France

** Warsaw University, Warsaw, Poland

1.29. Study of Non Equilibrium Particle Emission from the ^{159}Tb(α,charged particle xnγ) reaction at E_α = 75 MeV

T. Kutsarova, B. Bochev, R.M. Lieder, J.P. Didelez, A. Neskakis, T. Morek**, M. Müller-Veggian, and C. Mayer-Böricke*

In the present work we continue our investigations of non equilibrium processes for the reaction ^{159}Tb(α, charged particle xnγ), which was studied at 45 MeV incident energy[1]. Measurements of energy spectra and angular distributions of p, d and t have been carried out at E_α = 75 MeV. We used the particle-gamma coincidence technique in order to obtain the double differential cross section for each reaction channel. The spectra of the charged particles were measured at 45°, 90° and 135° with respect to the beam direction. The double differential cross sections for the pxn, dxn and txn channels taken at an angle of 45° are shown in figs. 1-3. Each

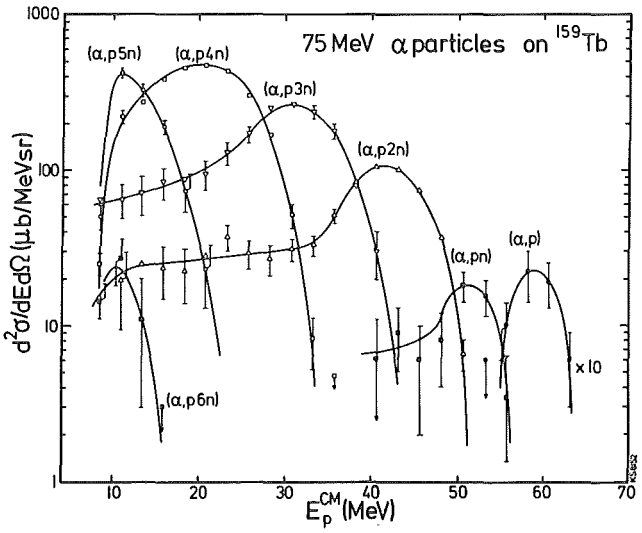

Figure 1: Double differential cross sections of the ^{159}Tb(α,pxnγ)$^{162-x}$Dy reaction at 45° for a beam energy of 75 MeV. The error bars include only the statistical uncertainties. The curves are eye-guiding lines.

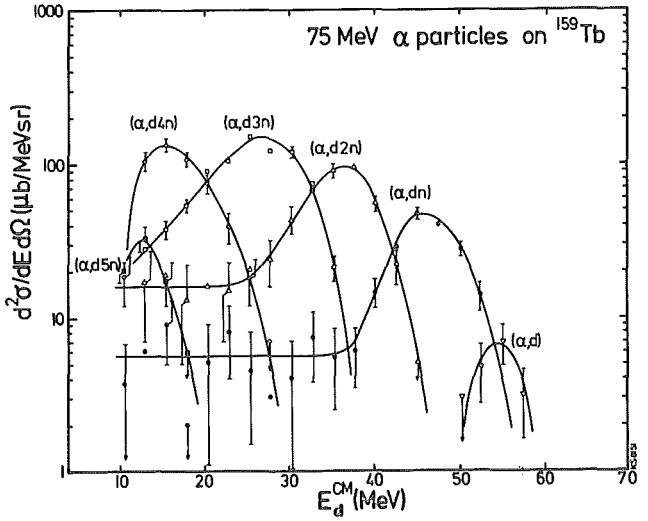

Figure 2: As in fig. 1 but for the ^{159}Tb(α,dxnγ)$^{161-x}$Dy reaction.

reaction channel is characterized by a pronounced peak. The reaction channels with two and more emitted particles show low energy tails, which extend approximately to the Coulomb barrier for particle emission. This result is

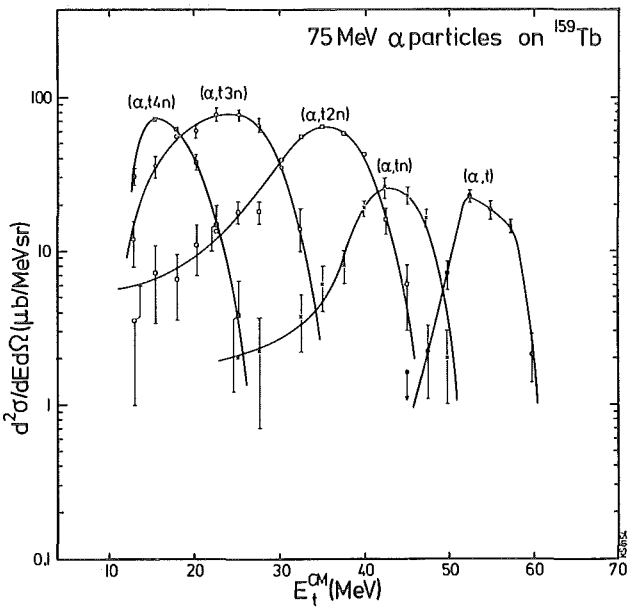

Figure 3: As in fig. 1 but for the $^{159}Tb(\alpha,tx n\gamma)^{160-x}Dy$ reaction.

similar to that obtained for the $^{209}Bi(\alpha,$charged particle $xn\gamma)$ reaction at the same beam energy[2]. For the peak regions the charged particles take away most of the available kinetic energy as can be concluded from the energy balance. The remaining excitation energy corresponds approximately to the sum of the binding energies of the x neutrons emitted in each channel. These features of the deexcitation mechanism suggest that the charged particles are emitted at first and that the neutrons are evaporated subsequently. This result is in good agreement with the expectation of the deexcitation model[2]. For the tail regions in addition to the charged particle at least one neutron is emitted with a large kinetic energy, i.e. in the non-equilibrium phase. The remaining neutrons are evaporated. It is necessary to notice that the tail regions show no structure within the statistical uncertainties. Therefore, it seems that for the tail regions, the fast neutron and the charged particle are emitted with the same probability. For a given reaction channel the charged particles emitted in the tail region have angular distributions with a smaller anisotropy than those emitted in the peak region.

For the yrast bands of the final even-mass Dy nuclei side feeding distributions have been determined. They represent the intensity of the side feeding of yrast states as a function of spin. The examination of these side feeding distributions shows that they have maxima at angular momenta of $(6\pm2)\hbar$ for both the peak and tail regions of the particle spectra. From this result it may be concluded that the location of the entry point does not depend on the very first stage of the deexcitation of the fused nucleus. Previously evidence was obtained that the location of the entry point is independent of the excitation energy of the fused nucleus[2]. The present result supports further our conclusion, that the location of the entry point depends mainly on the properties of the final nucleus[2].

References

1) J.P. Didelez, B. Bochev, R.M. Lieder, T. Kutsarova, T. Morek, A. Neskakis, M. Müller-Veggian, and C. Mayer-Böricke, separate contribution to this report

2) R.M. Lieder, B. Bochev, T. Kutsarova, H. Beuscher, D.R. Haenni, T. Morek, M. Müller-Veggian, A. Neskakis, C. Mayer-Böricke, and J.P. Didelez, Physica Scripta 24 (1981) 123

* Institut de Physique Nucléaire, F-91406 Orsay, France

** Warsaw University, Warsaw, Poland

1.30. Emission of nonequilibrium Particles in the Bombardment of ^{159}Tb with 110 MeV α Particles and the Validity of the PEP Model

B. Bochev, R.M. Lieder, J.-P. Didelez, T. Kutsarova, T. Morek**, A. Neskakis, M. Müller-Veggian, D. Protić, G. Riepe and C. Mayer-Böricke*

The promptly emitted particle (PEP) model[1] can explain the production of protons and neutrons with energies much larger than the projectile energy per nucleon. The main idea of this model is the coupling of the relative motion of the nucleons in the colliding nuclei to the Fermi motion. In the simplest case of a rectangular distribution of the internal velocities v_f the maximum energy of the forward PEP protons can be calculated as

$$E_{PEP}^{c.m.}(\text{forward}) = \{[E_F + E_R + 2\cos_\alpha \sqrt{E_F E_R} - (U + V_c^\alpha)]^{1/2} - \frac{m_{proj}}{m_{proj} + m_{tar}} \sqrt{E_R}\}^2 + V_c^p \qquad (1)$$

where $E_R = (E_{c.m.} - V_c^\alpha)$ is the relative energy, E_F is the Fermi energy, V_c^α and V_c^p are the Coulomb barriers for the the α particle and the proton respectively, U is the nuclear potential and α is the angle between the relative velocity and the Fermi velocity. m_{proj} and m_{tar} are the masses of the projectile and the target, respectively.

It is interesting to compare the predictions of the PEP model and those of the deexcitation model (Yrast picture)[2] with the experimental values of the maximum proton energy obtained in (α,pxn) reactions at different beam energies. According to the deexcitation model (DM) the entry point is independant of the excitation energy. Therefore, for a given reaction channel the particle energy is a linear function of the excitation energy. For the (α,p) reaction, which takes place at the largest proton energies, the p energy is

$$E_{DM}^{c.m.} = E_{exc.} - E_\gamma^{entry}, \qquad (2)$$

where $E_{exc.}$ is the excitation energy of the reaction and E_γ^{entry} is the energy of the entry point.

We studied the $^{209}Bi(\alpha,pxn)$ reaction at beam energies of 45 and 75 MeV (ref. 2). The maximum proton energy corresponding to the (α,p) channel was found to be E_p=26.5 MeV and E_p=54 MeV for the beam energies of 45 and 75 MeV, respectively. These values are in good agreement with expectations of the deexcitation model. In the PEP model the

maximum proton energy for forward angles was calculated, assuming E_F = 37 MeV, to be E_{PEP} = 31 MeV and E_{PEP} = 54 MeV for E_α = 45 MeV and E_α = 75 MeV, respectively. These values agree with the experimental results. For backward angles, however, the calculated proton energies were approximately 15 MeV lower than the experimental values. This results from the fact that in eq. 1 the term correcting for the velocity of the nucleus from which the proton is emitted has to be changed. It becomes

$$-\frac{m_{tar}}{m_{tar} + m_{proj}}$$ for protons emitted in backward direction.

Similar results were obtained for the ^{159}Tb(α,pxn) reaction at beam energies of 45 MeV (ref. 3) and 75 MeV (ref. 4). The experimental proton energies for the (α,p) channel were well reproduced by the deexcitation model for both beam energies, whereas PEP model calculations agree with the experimental data only for forward angles.

From eq. 1 and eq. 2 one can deduce that for beam energies $\gtrsim$ 75 MeV a deviation of the maximum proton energy predicted by the PEP and deexcitation models exists. For E_α = 110 MeV, e.g., the maximum proton energy for the ^{159}Tb(α,p) channel is E_{DM} = 95 MeV in the deexcitation model whereas the PEP model predicts for protons emitted in forward direction a maximum energy of only E_{PEP} = 75 MeV. This means that the channels with x=0 and x=1 of the ^{159}Tb(α,pxnγ)$^{162-x}$nDy reaction should not be observable. We studied this reaction at a beam energy of 110 MeV to check the above predictions. As in our previous experiments we used the p-γ coincidence technique[2]. The particle telescope which consisted of a 700 μ Si detector as ΔE-counter and two HPGe detectors with a total thickness of 27 mm as E-counter was able to stop protons with energies up to $\gtrsim$ 120 MeV. The double differential cross sections of the (α,pxnγ) channels are shown in fig. 1. The (α,p) channel has a pronounced peak at 93 MeV.

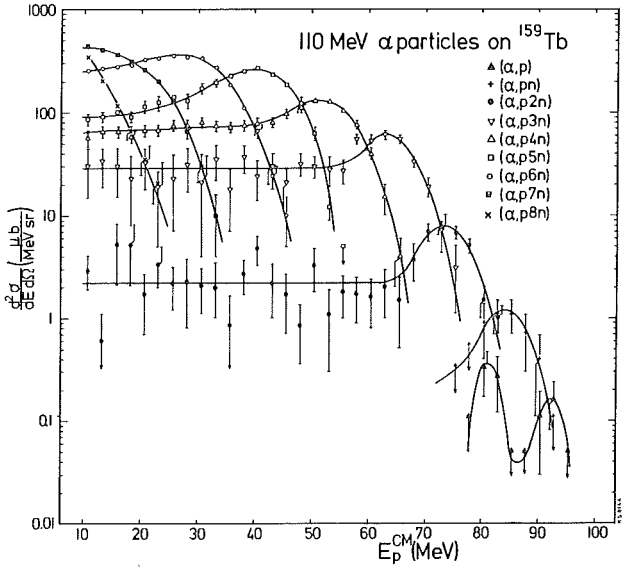

Figure 1: Double differential cross sections of the ^{159}Tb(α,pxnγ)$^{162-x}$Dy reaction for E_α = 110 MeV. The position of the particle telescope is 45° with respect to the beam direction. The error bars include only the statistical uncertainties. The curves are eye-guiding lines.

The energy of this peak is in a good agreement with the prediction of the deexcitation model but is ≈ 18 MeV larger than that of the PEP model. Also the (α,pn) channel can be seen in fig. 1. It can be summarized that the maximum proton energies observed at beam energies of 45 MeV and 75 MeV and at an angle of 45° can be reproduced by PEP model calculations. However, the high-energy protons observed in forward direction at a beam energy of 110 MeV and those observed in backward direction for beam energies of 45 MeV and 75 MeV cannot be explained in the framework of the PEP model.

In the (α,p) channel two peaks seem to appear. The peak at 80 MeV may be caused by a giant resonance. This suggestion is suported by the energy difference between both proton peaks being 13 MeV. It would be of great interest to search for γ rays of this energy emitted in coincidence with protons.

References

1) J.P. Bondorf, J.N. De, G. Fai, A.O.T. Karvinen, B. Jakobsson, and J. Randrup, Nucl. Phys. A333 (1980) 285

2) R.M. Lieder, B. Bochev, T. Kutsarova, H. Beuscher, D.R. Haenni, T. Morek, M. Müller-Veggian, A. Neskakis, C. Mayer-Böricke and J.P. Didelez, Physica Scripta 24 (1981) 123

3) J.P. Didelez, B. Bochev, R.M. Lieder, T. Kutsarova, T. Morek, A. Neskakis, M. Müller-Veggian and C. Mayer-Böricke, separate contribution to this annual report.

4) T. Kutsarova, B. Bochev, R.M. Lieder, J.P. Didelez, A. Neskakis, T. Morek, M. Müller-Veggian and C. Mayer-Böricke, separate contribution to this annual report

* Institut de Physique Nucléaire, F-91406 Orsay, France

** Warsaw University, Warsaw, Poland

1.31. Elastic Scattering of 50 MeV π^- on $^{32,36}S$ for the Determination of Radii Differences of the Neutron Distribution

B. Barnett, E.W. Blackmore**, K.L. Erdmann**, D.R. Gill**, N. Grion***, B. Gyles*, R.R. Johnson*, J. Kraushaar****, G. Lolos*, S. Martin, T. Masterson****, C. Wiedner******

In the (3,3) resonance the $\pi^-n(\pi^+p)$ scattering amplitude is three times larger than the π^-p (π^+n) amplitude. In spite of the small impact parameter of λ = 0.5 fm of the resonance pions differences in the rms radii of the neutron distributions could be deduced from different positions of the diffraction minima of isotopical pairs like $^{18,16}O$ [1]. For low energy pions the mean free path is λ = 8 fm and the amplitude ratio $\pi^-n/\pi^-p \approx$ 2-3 because of the interference of s and p partial waves and the Coulomb waves. This property is described in all models and was used to determine the difference $\Delta\langle r^2\rangle^{1/2}$ of neutron radii of isotopical pairs from Li to Mg targets[2]. It was found that the numerical results are rather independent of the choice of the theoretical description and the involved potential parameters - except $\langle r_n^2\rangle^{1/2}$ - as long as they reproduce correctly the elastic scattering angular distribution. A decisive test of the method of the comparison of charge radii from π^+ and electron scattering has been performed for ^{11}B and ^{12}C only [3]. Further experiments on $^{40,48}Ca$ and $^{32,36}S$ targets are planned[4]. The sensitivity on $\Delta\langle r_n^2\rangle^{1/2}$ of the ratio R of the elastic scattering across section increased with decreasing pion energy and is most important in the angular region of the Coulomb nuclear interference and between the s-p interference and the first diffraction maximum. Because of the large myon background and the beam halos the forward angles are difficult to measure. For larger angles cross sections become rather small ($\sim$ 5mb/sr). In addition the beam intensity decreased by an order of magnitude from 50 to 30 MeV. Therefore a short spectrometer with large solid angle is needed.

At the 9.8m long M13 beam line at TRIUMF a small axial focusing quadrupole lence was added to the existing Büchner magnet spectrometer increasing the possible solid angle by a factor of 4 (2-4msr depending on the target spot). Using multiwire proportional chambers position and angle of of the scattered pions were measured in front and behind the magnet in order to determine the contribution of the myons. The resolution was limited predominantly by the energy width of the incoming π-beam. Because of beam intensity reasons it was kept as large as possible but allowing the save separation of the ground state and the 1. excited state in ^{32}S (2.24 MeV) and ^{36}S (3.29 MeV). The proton beam (up to 100μA), E_p = 540 MeV) was focused on a 10 cm thick H_2O production target. Only 50% of the flux of 2×10^{-6} π^-/sec hit the 192 mg/cm^2 ^{36}S target of 10 mm diameter. Elastic cross section angular distributions on a natural and a ^{36}S target have been measured at 8 different angles between 20° and 100°. Preliminary results of the on line analysis are shown in Fig. 1. A statistical error of 4.5% is expected for the final results.

After the final evaluation of the measured absolute cross section the determination of $\Delta\langle r_n^2\rangle^{1/2}$ can be done in a model independet way. Fig. 1 shows 3 curves representing calculations using the optical π-nucleus model by Stricker, Mc Manus and Carr[5] - SMC Parameter set 1. Proton and neutron fermi distributions have been assumed for sulfur. Charge distributions $\langle r_p^2\rangle^{1/2}$ = 3.219 fm for both sulfur isotops have been taken from ref. 6 determined from electron scattering on ^{32}S. In this preliminary analysis for the self conjugate nucleus ^{32}S it was assumed in addition that $\langle r_p^2\rangle^{1/2} = \langle r_n^2\rangle^{1/2}$. This curves for ^{36}S differ by 100 mfm in $\langle r_n^2\rangle^{1/2}$ from each other. The data points appear to be consistent with a radii difference of 100 mfm. For a final conclusion the elastic scattering data have to be fitted in a more accurate way.

It is planned to measure the charge distribution of ^{36}S in Mainz. In addition a ^{48}Ca target exists at TRIUMF. Using the QQD magnet spectrometer which is planned to become operational in 1982 - better by an order of magnitude concerning luminosity and resolution[7] compared to the existing Büchner magnet - further experiments with low energy $\pi\pm$ on $^{40,48}Ca$ are planned[4].

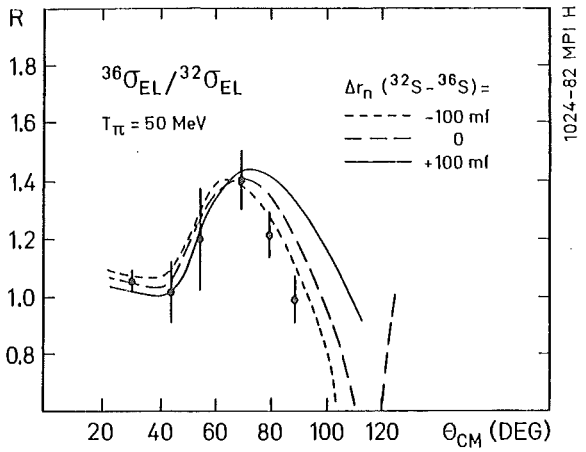

Fig. 1: Ratio of the elastic cross sections $R = d\sigma/d\Omega\ [^{36}S]/d\sigma/d\Omega\ [^{32}S]$. The measured data points at 55° and 100° remain to be analyzed. The curves represent optical model calculations with the SMC potential (see text). The solid line shows the calculation with $\langle r_n^2\ (^{35}S)\rangle^{1/2}$ = 3.119 fm with the broken and dotted lines are done for 3.219 and 3.319 respectively.

References

1) S. Iversen et al, Phys. Rev. Lett. 40 (1978) 17
2) R. R. Johnson et al, Phys. Rev. Lett. 43 (1979) 844
R. R. Johnson et al, submited to Phys. Rev. Lett.
3) B. Barnett et al, Phys. Lett. 97B (1980) 45
4) R. R. Johnson et al, PISCAT Proposal Exp-177 (1980)
5) K. Stricker, H. Mc Manus and J. Carr, Phys. Rev. C19 (1979) 929
6) K. Werle, Dissertation (1976), Mainz
7) S. Martin and C.-A. Wiedner, Improved Spectrometer Arrangement for PISCAT Experiments. TRIUMF (1980) unpublished

* University of British Columbia
** TRIUMF
*** Trieste
**** Colorado University
***** MPI Heidelberg

1.32. Charge transfer atomic collision by BIG KARL

I. Katayama, G.P.A. Berg, W. Hürlimann, S.A. Martin, J. Meißburger, W. Oelert, M. Rogge, J.G.M. Römer, J. Tain, B. Styczen[+] and G. Gaul[++]

Charge transfer at high energy remains still a challenging problem. The first order Born approximation (OBK calculation) does not provide correct cross sections. It has been pointed out that the second order term becomes relatively important[1]. Different theoretical approaches have been proposed[2], but because of lacking data it is not clear which one is favorable. Projectile energies from JULIC are just those where the high velocity asymptotic behaviour of the charge transfer can be tested (the energy of 22.5 MeV/A to 45 MeV/A corresponds to 30 to 40 V_o in atomic velocity units with $V_o = 2.18 \times 10^8$ cm/sec). During the preparation of a gas jet target system, solid targets of different mass and different thicknesses were used in the experiment. At high energy, it has been shown[3] that the charge exchange collision in solids is a consequence of successive single collision processes, i. e. electron loss from and electron capture into bound states on the moving projectile. The equilibrium charge fraction from the target is equal to $N \cdot \sigma_c/\sigma_s$, where N is beam intensity, σ_c and σ_s are cross sections of the electron capture and electron loss for the projectile atom, respectively. So if σ_s is measured independently, which is possible from target thickness dependence of the charge exchange yield, σ_c can be deduced even from solid targets. In the experiments $^3He^{2+}$ beams at 68 MeV and 130 MeV were used. The beam line was tuned in achromatic mode with a beam spot of 1 mm in diameter and a divergence angle of 0.2^o. Schematic geometry of the system is shown in fig. 1. BIG KARL was at zero degree and the primary

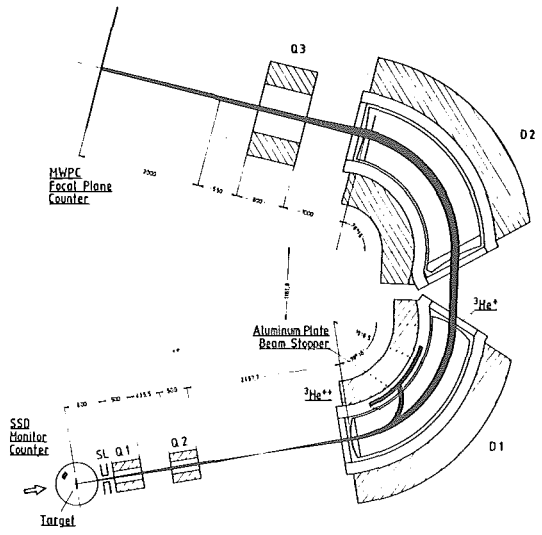

Fig. 1: Schematic view of the BIG KARL arrangement to measure the charge transfer atomic reaction

beam was integrated in an aluminium beam stopper in the middle of the first dipole magnet. Using a Si surface detector as a monitor detector at 135 degree, the beam collection efficiency was calibrated in the different runs. The efficiency determined in this way was found to be quite sensitive to the beam emittance and deviation from the midplane of the magnet. Beam line system was carefully adjusted so that this beam detection efficiency became as high as possible.

The dispersion of the BIG KARL was 26 cm per % momentum to get small vertical magnification. In fig. 2 the $^3He^+$

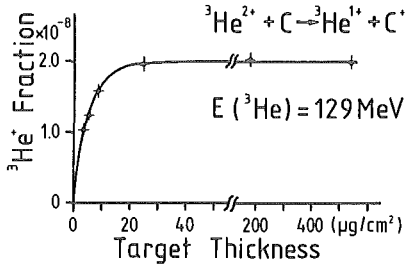

Fig. 2: Target thickness dependence of the $^3He^+$ yield from carbon

yield from the carbon foil at 130 MeV is plotted against the target thickness. A similar thickness effect was clearly observed at 68 MeV. The thickness was calibrated by energy loss measurement using α-source. From a least square fit σ_s is deduced to be $0.0204 \pm 0.0014\ a_o^2$ (a_o, Bohr radius) which agrees well with $0.0252\ a_o^2$ from Bohr theory[4]. The velocity dependence of the $^3He^{++}$ yield is shown in fig. 3. For better comparison to previously

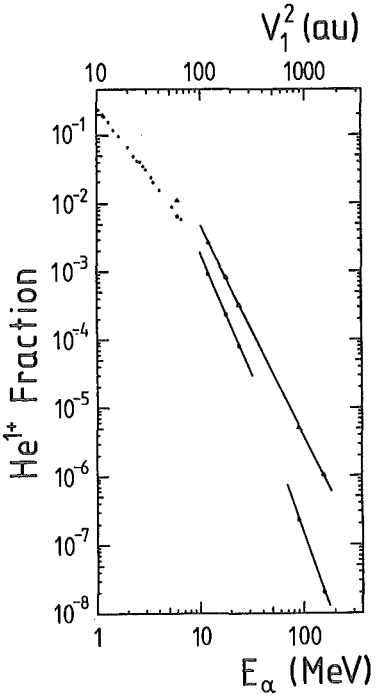

Fig. 3: Velocity dependence of the charge equilibrated $^4He^+$ yield from C (points and circles) and Au (triangles). The data for E_α = 1 - 24 MeV are from ref. 5,6. Data for E_α = 90 and 170 MeV are measured in this experiment. Solid lines are shown to guide the eye.

reported data, the $^3He^{++}$ energy is converted to corresponding α energies. For the gold targets, the velocity dependence of $V^{-5.0}$ above E_α = 10 MeV is well reproduced. For carbon, this velocity factor is $V^{-7.8 \pm 0.5}$ between 90 and 170 MeV

and $V^{-7.1}$ for energies from 10 MeV to 24 MeV[5]. The σ_c is obtained from the result in fig. 2 and fig. 3. They are shown in fig. 4 together with several theoretical predictions from ref. 1, 2 and 4. The vertical axis shows cross sections in unit of the OBK calculation. The present data is close to the second order Born calculation. The velocity dependence of the data as shown in the figure is, however, much larger than theoretically predicted. The experiment of charge transfer is further continued.

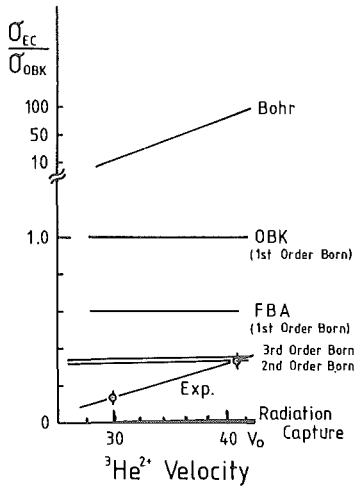

Fig. 4: Comparison of σ_c for C with theories (FBA includes the nucleus-nucleus interaction and OBK not).

References

1) R. Shakeshaft and L. Spuch, Rev. Mod. Phys. 51 (1979) 369

2) D. Belkic, R. Gayet and A. Salin, Phys. Report 56 (1979) 279

3) M.C. Cross, Phys. Rev. B15 (1977) 602

4) N. Bohr, K. Danske Vidensk, Selsk. Mat.-Fys. Meddr. 18 No. 8

5) A. Gladieux, A. Chateau-Thierry and B. Delaunay, J. Phys. B12 (1979) 3591

6) J.C. Armstrong et al., Proc. Phys. Soc. 86 (1965) 1283

+ Inst. of Physics, Jagiellonian Univ., Cracow, Poland

++ University of Münster, F.R. Germany

2. NUCLEAR SPECTROSCOPY

2.1. Identification and decay of ^{36}P

J.C. Hill[+], *H.R. Koch, K. Shizuma*

The nuclide ^{36}P has been previously observed[1] as a fragment from the reaction of 290 MeV ^{40}Ar on Th targets, thus proving its particle stability, but no further information was obtained. Recently the reaction $^{40}Ar(n,2p)^{39}S$ was used to identify and characterize ^{39}S, leading us to the assumption, that the (n,2p)-reaction is suitable for the production of ^{36}P from a ^{37}Cl target. We have observed the decay of ^{36}P to levels in ^{36}S. The half life of ^{36}P was measured and the knowledge on the level structure of ^{36}S was extended. Preliminary results have already been published[2].

The sources of ^{36}P were produced by the $^{37}Cl(n,2p)^{36}P$ reaction. The neutrons were generated by bombardment of a thick Be-target with 70 MeV deuterons from the JULIC cyclotron. The deuteron beam currents used ranged from 150 nA to 1.5 μA. The targets containing ^{37}Cl (solid PVC-cylinders) were irradiated with neutrons (< 35 MeV) behind the Be-beam stop. The PVC-targets were shot after irradiation by a compressed air "rabbit" system to a low background room, where gamma ray singles and coincidence spectra were measured with Ge(Li)-detectors. The transit time was ∿ 1 second. Lead absorbers of various thicknesses were placed between the sample and the detectors, in order to reduce the intense annihilation radiation from ^{34}Cl ($T_{1/2}$ = 1.5 s) produced in the $^{35}Cl(n,2n)^{34}Cl$ reaction. The gamma-ray lines, attributed to the decay of ^{36}P are given in table I. The coincidence relations are shown in table II.

Table I: ^{36}P γ ray energies and intensities

Energy (keV) this work	Energy (keV) Ref. 5	Relative[a] intensity	Placement
902.0±0.5[b]	901.5±0.4	77±19	3291-0
1638.1±0.8[b]	-	38±10	5831-4193
3290.7±0.3	3290.8±0.6	100±10	4193-3291

a: Intensities normalized to 100 for the 3291 keV γ ray.
b: Energies determined from γγ coincidence spectra.

Table II: γγ coincidences from ^{36}P decay

Gating transition (keV)	Definite coincidences
902	1638, 3291
1638	902, 3291
3291	902, 1638

The element assignment as ^{36}P decay is based on the observation of the 3291- and 902-keV γ rays which were observed in $^{34}S(t,p\gamma)^{36}S$ studies[3-5] and our detection of coincidences between these two gamma rays. The half life of 5.9 ± 0.4 s, which was determined from a least squares fit to the decay curve for the 3291 keV gamma ray (fig. 1) is in good agreement with the Gross theory of β-decay[6].

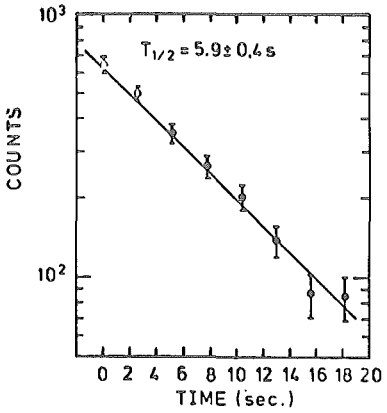

Fig. 1: Decay curve for the 3291 keV γ ray from ^{36}P decay.

The measured γ ray energies and intensities and coincidence information was used to construct a decay scheme for ^{36}P (fig. 2). The I^{π} assignment of $(3^-, 4^-)$ for the ^{36}P ground state is understandable in terms of a $\pi(s_{1/2})$ $\nu(f_{7/2})$ configuration with possibly a small amount of mixing from $\pi(d_{3/2})$ $\nu(f_{7/2})$.

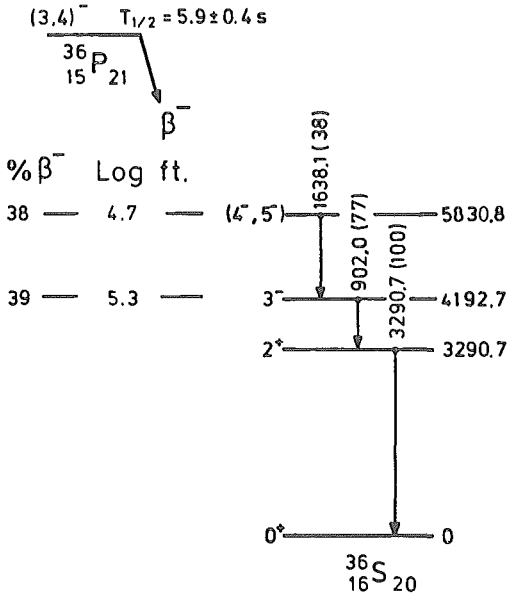

Fig. 2: Decay scheme for ^{36}P deduced from this work.

In the (t,pγ) studies 13 excited states in ^{36}S up to 7.12 MeV were found[3-5], whereas in our decay study only three excited states were observed, in spite of a large Q_β value. The β interaction in this case favors population of negative parity states whereas many positive parity states were populated in the reaction experiments.

Two simple mechanisms exist for allowed β^- decay to negative parity states in ^{36}S. In the first case the odd $f_{7/2}$ neutron in ^{36}P can decay to a $f_{7/2}$ proton in ^{36}S which can then couple with the $s_{1/2}$ proton to produce a proton p-h state. In the second case one member of the $s_{1/2}$ neutron pair in ^{36}P can decay to a $s_{1/2}$ proton in ^{36}P. The net effect is that a neutron pair is broken and a proton pair formed in ^{36}S leaving a neutron p-h state. In both cases only the states 3^- and 4^- can be formed. In order

to produce 2^- or 5^- states there must be mixing from the $d_{3/2}$ proton in the ^{36}P ground state or the ^{36}S negative parity states.

Since the 3^- state in ^{36}S at 4193 keV is a natural parity state populated in the (t,pγ) reaction[3-5] it probably is a neutron p-h state. In our case the simple mechanism outlined above implies that the β^- decay involves the transformation of a $s_{1/2}$ neutron in ^{36}P to a $s_{1/2}$ proton.

The state observed in this work at 5831 keV was not reported in (t,pγ)[3-5] studies. For this level we deduce from our decay scheme the assignment 4^- or 5^-. The nature of this state cannot be determined uniquely on the basis of the existing data.

References

1) A.G. Artukh, V.V. Avdeichikov, G.F. Gridnev, V.L. Mikheev, V.V. Volkov, and J. Wilczynski, Nucl. Phys. A176, 284 (1971)

2) J.C. Hill, H.R. Koch, and K. Shizuma, in Proceedings of the Fourth International Conference on Nuclei Far From Stability, Helsingør, Denmark, 1981, p. 372

3) N.G. Puttaswamy and J.L. Yntema, Phys. Rev. C 177, 1624 (1969)

4) W.S. Gray, P.J. Ellis, T. Wei, R.M. Polichar, and J. Jänecke, Nucl. Phys. A140, 494 (1970)

5) J.W. Olness, W.R. Harris, A. Gallmann, F. Jundt, D.E. Alburger, and D.H. Wilkinson, Phys. Rev. C 3, 2323 (1971)

6) K. Takahashi, M. Yamada, and T. Kondoh, Atomic Data Nucl. Data Tables 12, 101 (1973)

+ Iowa State University, Ames, Iowa, USA

2.2. Study of low spin states in $^{75,77}Se$ populated in slow neutron capture

Y. Tokunaga, H.G. Börner+, H. Seyfarth, G. Barreau+, K. Schreckenbach+, H. Faust+, R. Brissot+, Ch. Hofmeyer+, R. Weinreich++ and O.W.B. Schult

The study of the structures of nuclei with A ∿ 76 and Z ∿ 32 - 36 is of interest because of their transitional and rapidly changing character. This is indicated in particular by the low lying 0_2^+ states. In $^{76}_{34}Se_{42}$ the well isolated and almost degenerate 0^+, 2^+, 4^+ triplet at ∿ 2 x $E(2_1^+)$ suggests a harmonic vibrator. In ^{72}Se and ^{74}Se a nearly spherical ground state appears to coexist with a deformed excited band. For $^{76}_{36}Kr_{40}$, however, Hamilton et al.[1] have found a large ground state deformation and coexistence of a spherical 0_2^+ state. The Nilsson model even suggests oblate shape for Z,N ≃ 36 and prolate shape for Z,N ≃ 38 so that also prolate-oblate shape transitions are expected. As the spectroscopy of odd-A nuclei sometimes gives an even better view on the structures of transitional nuclei, Zell et al[2,3] have investigated $^{73,75,77}Se$ through (α,xnγ)-spectroscopy, where mainly high spin states are populated. In the present work we have used the (n,γ)- and (n,e⁻)-reaction in order to obtain with very high resolution complementary and complete information on the low spin levels of $^{75,77}Se$.

The lower portions of the (n,γ) decay schemes of $^{75,77}Se$ agree with the results of other studies. In the present work a number of weaker transitions were observed though. In ^{75}Se we have no evidence for a 741 keV level and find $5/2^+$ for the 628 keV state. In both nuclei all levels with $I < 7/2$ receive measurable (n,γ)-feeding so that complete level schemes exist up to ∿ 1 MeV in view of previous complementary high spin work[2,3].

Although the vibrational appearance of ^{76}Se would suggest vibration-particle coupling to occur in $^{75,77}Se$, the high spin studies have revealed the 427 and 747 keV states in ^{75}Se to belong to the |303↑| band and the 133 keV level as head of a quasi decoupled band. In ^{77}Se the 249 and 581 keV levels form the two lowest members of the |303↑| band. The 0, 239, 439 and 808 keV levels were assigned to 1/2, 3/2, 5/2 and 7/2 members of the |301↑| band. Thus both nuclei show a pronounced rotational character. However, in ^{75}Se as well as in ^{77}Se, a number of other low spin states exist that do not reveal a simple rotational structure. It is interesting to note that the energies of the 0^+ states of the even Se isotopes with mass A very strongly correlate with $E(5/2^+) - E(9/2^+)$ of the neighbours with mass A±1. Further structural analysis of the $^{75,77}Se$ level schemes is in progress.

With regard to the (n,γ) reaction we observe primary E2 transitions in ^{75}Se with $\langle I\gamma(E2)\rangle / \langle I\gamma(E1)\rangle$ ∿ 1/100. In ^{75}Se the (d,p) and (n,γ) intensities are strongly correlated. The correlation coefficient is α = 0.99 in contrast to ^{77}Se where α = -0.30.

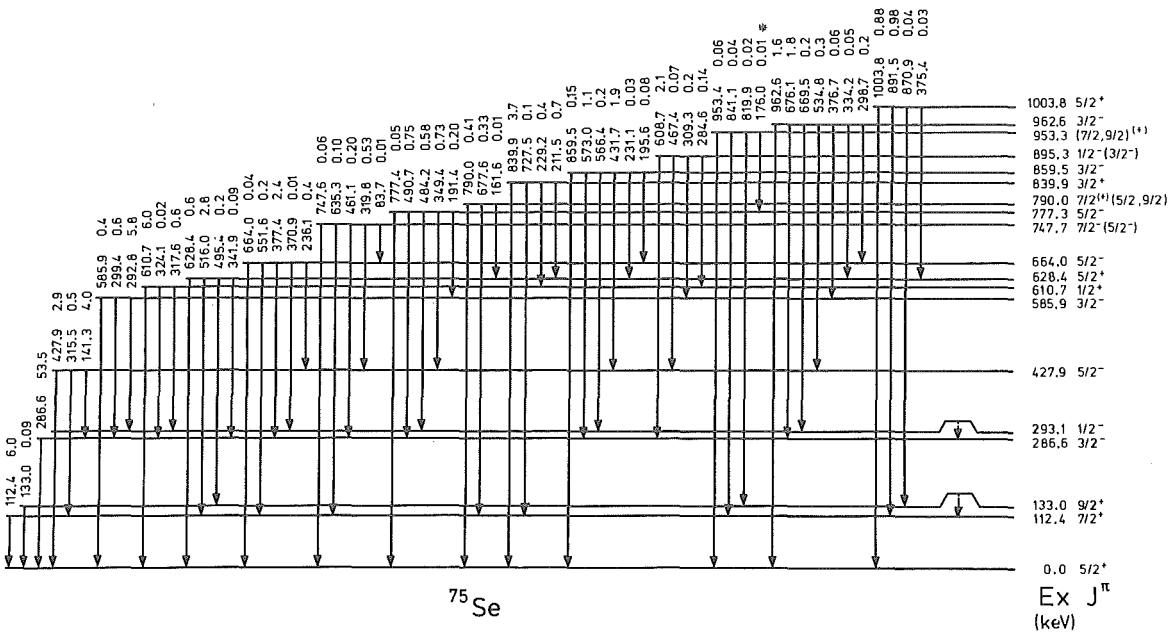

Fig. 1: Lower part of the preliminary ^{75}Se level diagram. Above each line is given its energy and intensity per 100 captured neutrons. An asterisk is used to label a questionable line. The (n,γ)-population rules out 5/2 for the 953 keV state and favours 3/2, 7/2 and 7/2 for the 839, 790 and 747 keV levels, respectively. The dashed 20.6 and 6.5 keV lines were not observed.

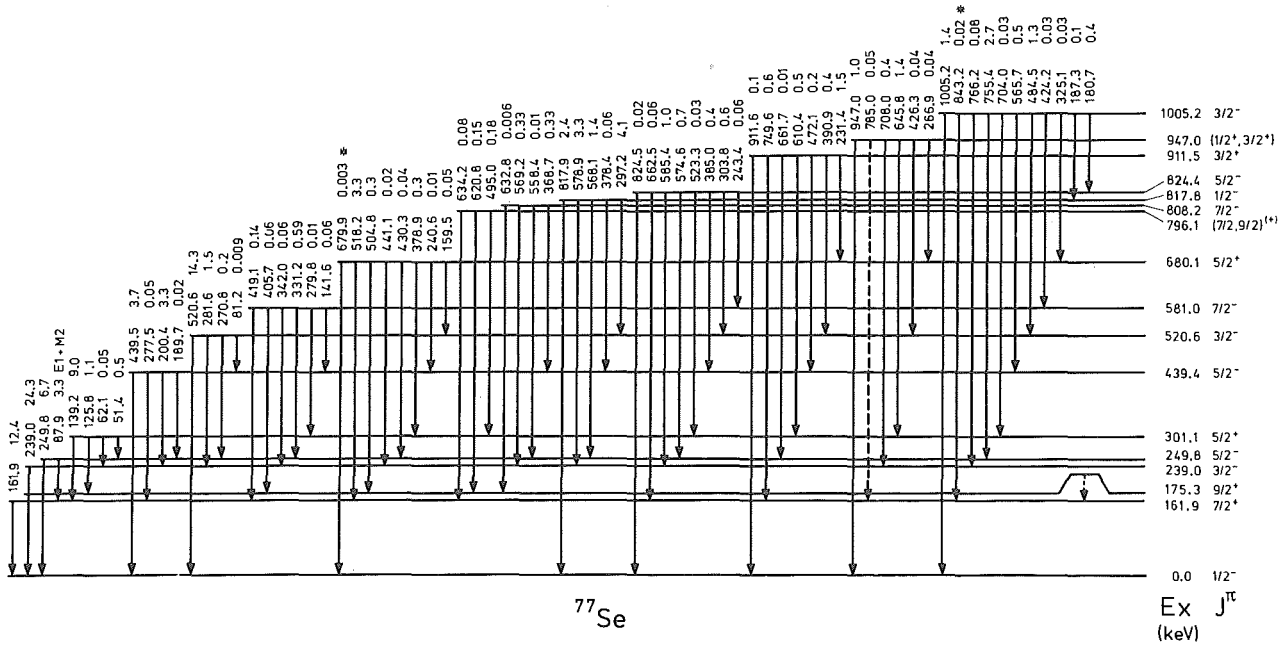

Fig. 2: Preliminary (n,γ)-decay scheme of ^{77}Se up to ∼ 1 MeV. The (n,γ)-population and (n,e$^-$)-data yield $9/2^+$, $5/2^+$ and $5/2^+$ for the 175, 301 and 680 keV states, respectively. The population of the 796 keV level favours $9/2^+$ and that of the 911 and 947 keV states is less than expected.

References

1) J.H. Hamilton, R.B. Piercey, R. Soundranayagam, A.V. Ramayya, C.F. Maguire, X.J. Sun, Z.Z. Zhao, J. Roth, L. Cleemann, J. Eberth, T. Heck, W. Neumann, M. Nolte, R.L. Robinson, H.J. Kim, S. Frauendorf, J. Döring, L. Funke, G. Winter, J.C. Wells, J. Lin, A.C. Rester and H.K. Carter, Proc. Int. Conf. on Nuclei far from Stability, Helsingør, 1981, CERN-Rep. p. 391

2) K.O. Zell, H.-G. Friedrichs, B. Heits, P. von Brentano, and C. Protop, Z. Phys. A272 (1975) 27

3) K.O. Zell, H.-G. Friedrichs, B. Heits, D. Hippe, H.W. Schuh and P. von Brentano, Z. Phys. A276 (1976) 371

+ Institut Laue-Langevin, Grenoble, France

++ Institut für Nuklearchemie, Kernforschungsanlage Jülich, FRG

2.3. A Rotational Band in ^{99}Y?

E. Monnand[+], J.A. Pinston[++], F. Schussler[+], G. Battistuzzi, H. Lawin, K. Shizuma, K. Sistemich, B. Pfeiffer[+++]

A new μs-isomer has been observed in $^{99}_{39}Y_{60}$. Its half-life was determined to (8.6 ± 0.8) μs through fission product, γ-ray coincidence measurements at the separator LOHENGRIN of the Institute Laue-Langevin, Grenoble. The assignment of the isomeric state to ^{99}Y was achieved with the mass determination from LOHENGRIN and with the nuclear charge identification from the separator JOSEF of the IKP.

The γ-radiation which is emitted in the depopulation of the isomeric level, was identified in the singles γ-ray spectra from LOHENGRIN. At JOSEF γ,γ coincidences were measured, and some examples for the results are shown in fig. 1. A partial level scheme is depicted in fig. 2. It does not yet contain all the isomeric γ-radiation and not all the levels, which are populated[1] in the β-decay of ^{99}Sr.

The levels up to 1595 keV exhibit the pattern of a rotational cascade: The energies of the levels can well be described with a rotational formula if K = 3/2 or 5/2 is assumed for the ground state[2]. If this interpretation of the levels in fig. 2 is correct, then ^{99}Y is the first odd mass nucleus around A = 100 where an extended rotational band has been observed.

A deformation of the nucleus ^{99}Y would not be unexpected, since a rotation-like structure has been observed earlier in the level scheme[3] of its isotope ^{98}Y and since evidence for deformed shapes have been found in its isotones ^{97}Rb, ref. 4, ^{98}Sr, ref. 5, ^{100}Zr, ref. 6,7.

References

1) B. Pfeiffer, E. Monnand, J.A. Pinston, F. Schussler, G. Jung, J. Münzel, H. Wollnik, Proc. 4th Int. Conf. on Nucl. Far From Stability, Helsingor 1981, Report CERN 81-09,p. 423

2) E. Monnand, J.A. Pinston, F. Schussler, G. Battistuzzi, H. Lawin, K. Shizuma, K. Sistemich, B. Pfeiffer, Report DRF/CENG 19 (1981)

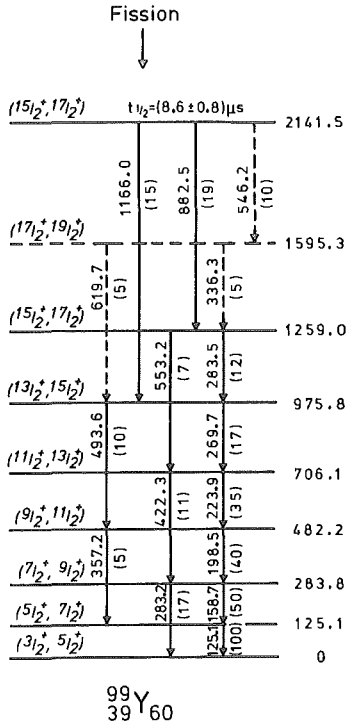

Fig. 2: Partial level scheme of ^{99}Y. The spin suggestions are deduced with assumption that there is a rotational band based on the ground state with K = 3/2 or 5/2.

3) J.W. Grüter, K. Sistemich, P. Armbruster, J. Eidens, K. Hübenthal, H. Lawin, Proc. Colloque sur les noyaux de transition, Orsay 1971 and K. Sistemich, J.W. Grüter, H. Lawin, J. Eidens, R. Fabbri, T.A. Khan, W.D. Lauppe, G. Sadler, H.A. Selic, M. Shaanan, Nucl. Instr. Meth., 130 (1975) 491

4) C. Thibault, F. Touchard, S. Büttgenbach, R. Klapisch, M. de Saint Simon, H.T. Duong, P. Jacquinot, P. Juncar, S. Liberman, P. Pillet, J. Pinard, J.L. Vialle, A. Pesnelle, G. Huber, Phys. Rev. C23 (1981) 2720

5) F. Schussler, J.A. Pinston, E. Monnand, A. Moussa, G. Jung, E. Koglin, B. Pfeiffer, R.V.F. Janssens, J. van Klinken, Nucl. Phys. A339 (1980) 415

6) R.C. Jared, H. Nifenecker, S.G. Thompson, Proc. IAEA Conf. on Physics and Chemistry of Fission, Rochester 1973, p. 211

7) T.A. Khan, W.-D. Lauppe, K. Sistemich, H. Lawin, H.A. Selic, Z. Physik A284 (1978) 313

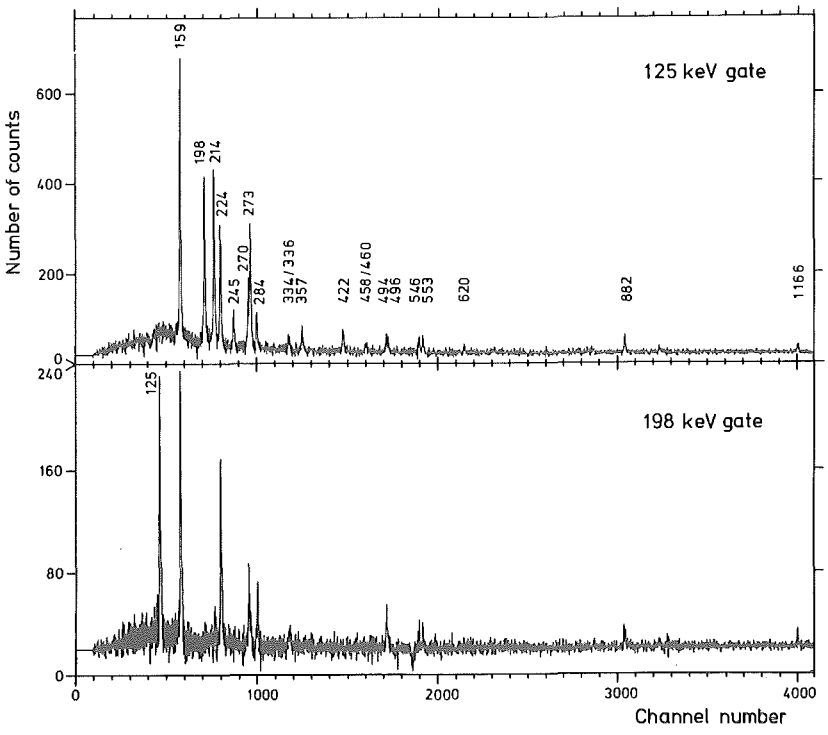

Fig. 1: Examples for the results of the γ,γ coincidence measurements. These spectra are measured with a 150 cm^3 Ge(Li) detector while digital windows were set on a large area intrinsic Ge-detector. The Compton background is subtracted.

2.4. Half-life of the 469 keV state in ^{99}Nb

G. Battistuzzi[+], K. Kawade[++], H. Lawin, K. Shizuma, K. Sistemich

The nucleus $^{99}_{41}Nb_{58}$ has one proton in excess to the subshell Z = 40. Its low lying levels are interpreted[1] as $p_{1/2}$ and $g_{9/2}$ proton states including the coupling of these orbits to excited levels in the neighbouring even, even cores ^{98}Zr or ^{100}Mo. In particular, the 469 keV level is supposed to be a $7/2^+$ state based on the coupling of the $g_{9/2}$ proton to the 2^+_1 state of ^{98}Zr or ^{100}Mo. The excitation energy favoured ^{100}Mo as the core ($E_{2_1^+}$ = 535 keV for ^{100}Mo while $E_{2_1^+}$ = 1223 keV for ^{98}Zr).

The reduced probability for the 469 keV transition into the ground state with $I^\pi = 9/2^+$ should, however, be a more sensitive test for the identification of the core underlying the levels in ^{99}Nb than the energies. If the above-mentioned interpretation of the 469 keV level is correct then the value of B(E2: $7/2^+ \rightarrow 9/2^+$) should be comparable to the reduced probability B(E2: $2^+_1 \rightarrow 0^+_1$) of the appropriate core.

In order to obtain the reduced transition probability in ^{99}Nb the half-life of the 469 keV state has been determined at the separator JOSEF. Delayed β,γ -coincidences have been measured with the experimental set-up described in ref. 2). Several runs have been performed and one example for the results is depicted in fig. 1. The positions of the centroids of the β,γ– coincidences for ^{99}Nb

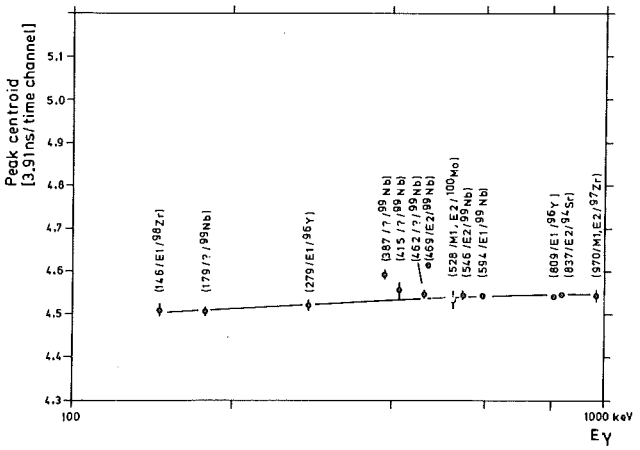

Fig. 1: The centroids of the timing distributions of the β,γ coincidences as a function of the γ-ray energy. The solid line served for interpolation purposes. The different points are marked by the energies and multipolarities of the γ-rays and by the isotope in which the transitions take place.

are shown together with the centroids of some probably prompt coincidences of neighbouring nuclei which were simultaneously studied. It is obvious that the 469 keV transition is delayed. This delay must be due to a half-life around 0.2 ns of the 469 keV state since the γ-transitions of 462 keV and 546 keV which feed into the 469 keV state, are prompt within the experimental uncertainties.

The average value for the half-life of the 469 keV level which has been deduced from all the available experimental information is

$$t_{1/2}(469\ \text{keV}) = (0.21 \pm 0.06)\ \text{ns}$$

Considering the deexcitation pattern for the 469 keV level and the measured value[1] of I(E2)/I(M1) = 6.25 for the 469 keV transition a value of

$$B(E2: 7/2^+ \rightarrow 9/2^+) = (89 \pm 28)\ e^2fm^4$$

is deduced. This value does not support the choice of ^{100}Mo as the core for particle vibrational coupling modes in ^{99}Nb since $B(E2: 2^+_1 \rightarrow 0^+_1) \sim 1000\ e^2fm^4$ in this case. Unfortunately the value of $B(E2: 2^+_1 \rightarrow 0^+_1)$ is not known for ^{98}Zr. But since the corresponding reduced transition probabilities for the lighter Zr isotopes with even mass lie all around 100 e^2fm^4, it is expected that the value for ^{98}Zr is of this order of magnitude. Hence ^{98}Zr seems to be the better candidate for being the core for the particle-vibrational coupling interpretation of the low lying levels in ^{99}Nb.

1) H.A. Selić, G. Sadler, T.A. Khan, W.-D. Lauppe, H. Lawin, K. Sistemich, E. Monnand, J. Blachot, J.P. Bocquet, F. Schussler, Z. Physik, A289 (1979) 197

2) K. Kawade, G. Battistuzzi, H. Lawin, H.A. Selic, K. Sistemich, F. Schussler, E. Monnand, J.A. Pinston, B. Pfeiffer, G. Jung, Z. Physik, in press

2.5. Decay of ^{102}Y to levels of ^{102}Zr

K. Shizuma[+], J.C. Hill[++], H. Lawin, M. Shaanan[+++], H.A. Selič and K. Sistemich

The neutron-rich Zr isotopes are of special interest as they show a very rapid transition from a spherical to a deformed nuclear shape. The heaviest isotope which has been studied in detail is ^{100}Zr[1]. A very low-lying 0_2^+-state was the most surprising result of these investigations. The only available information on ^{102}Zr was obtained through the study of the prompt γ-radiation of fission products[2]. Gamma rays of 151.9, 326.6 and 486 keV were attributed to this isotope as the transitions from the 2^+, 4^+, 6^+ levels of the ground state band. The resulting ratio E_{4^+}/E_{2^+} of 3.15 is close to the rigid rotor value. The study of ^{102}Zr through the β-decay of ^{102}Y is difficult because of the low fission yield and short half-life of the parent.

First results on this decay have now been obtained using the fission product separator JOSEF. Singles γ-ray, half-life, X,γ coincidence and preliminary γ,γ coincidence measurements were performed. The assignment of the 152 keV line (suggested in ref. 2) to the level scheme of ^{102}Zr was confirmed by measuring its intensity distribution of γ lines as a function of the magnetic rigidity Bρ of JOSEF. The position of the maximum of the Bρ-distribution agreed with that expected for ^{102}Y from a calibration of the separator. Moreover the 152 keV line was observed in coincidence with Zr K_α X rays.

A half-life for ^{102}Y was measured with a 30 cm^3 intrinsic Ge detector, which has excellent energy resolution. The detector was installed at the "on-line" position (deposit position of the moving tape) and the fission product beam was chopped through the high voltage supply of the fission product guide. The fission product beam passed through the guide for 0.6 sec and the decay of the γ-ray intensity was followed for next 2.2 sec while the beam was deflected. The 662 keV line of ^{137}Cs was measured simultaneously with fission product radiation for the purpose of deadtime correction (max. 10 %).

Figure 1 shows a growth and decay curve of 152 keV line. A half-life of 0.36 ± 0.04 sec was obtained from the least-squares fitting to the decay part. This value is much shorter than the early value[3], where a contamination of the 152 keV line through the 150.6 keV fraction (∿ 1.5 sec) was present. In contrast to ^{98}Y and ^{100}Y which have two isomers, only one half-life was observed for ^{102}Y. In an additional measurement with the detector in an "off-line"-position of JOSEF, the 152 keV fraction was not observed. This shows that the flattening of the decay curve at longer times is most probably of statistical origin and not to due to a long-lived component. The insert in fig. 1 shows that the 152 keV line has essentially disappeared 2.08 s after the end of the deposit of the fission products.

A γγ coincidence measurement was carried out over a period of about 170 hours using a 150 cm^3 and a 61 cm^3 Ge(Li) detector. The γ-ray energies of 151.9 keV ($2^+ \rightarrow 0^+$) and 326.5 keV ($4^+ \rightarrow 2^+$) agree well with former work[2], and the 2^+ level at 152 keV and the 4^+ level at 478 keV in ^{102}Zr were thus confirmed. Moreover 579 keV and 1090 keV lines were observed in coincidence with 152 keV line. Unfortunately the nature of the levels which are depopulated through the new γ transitions, is not yet known. It would be of particular interest to find out whether one of the new states is the 0_2^+-level. If the structure of ^{102}Zr is similar to that of ^{100}Zr, an excited 0_2^+ state should exist near the 2_1^+ level. If the ratio $E_{0_2^+}/E_{2_1^+}$ is a good indicator of nuclear deformation, the 0_2^+ state should lie higher (at (152 + 579) keV?). This level has been predicted to be at 840 keV[4]. Further investigation is in progress in order to construct the decay scheme of ^{102}Zr.

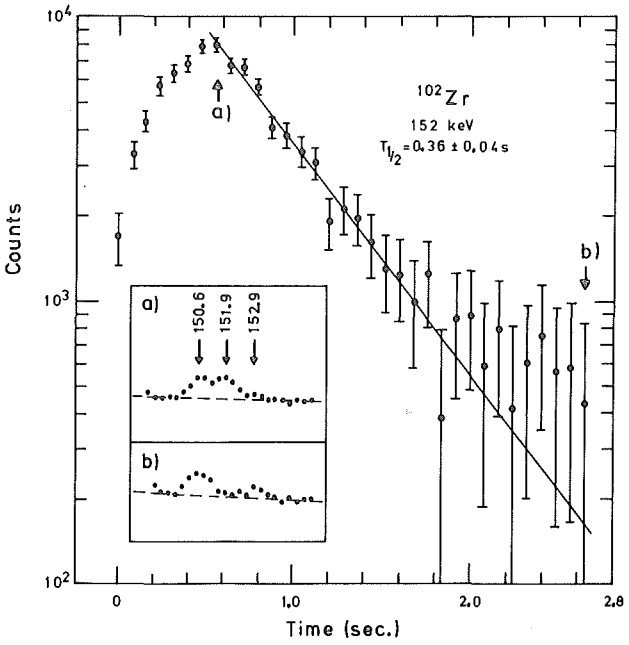

Fig. 1: Typical γ-ray decay curve for ^{102}Y → ^{102}Zr

[+] On leave from Hiroshima University, Hiroshima, Japan
[++] On leave from Iowa State University and Ames Laboratory DOE, Ames, USA
[+++] Soreq Nuclear Research Center, Yavne, Israel

References

1) T.A. Khan et al., Z. Physik A283 (1977) 105
2) E. Cheifetz et al., Phys. Rev. Lett. 25 (1970) 38
3) J.W. Grüter et al., Proc. Int. Conf. Nucl. Structure and Spectroscopy, Vol. 1 (1974) p. 89
4) K. Kumar et al., Phys. Rev. C16 (1977) 1235

2.6 The $^{107}Ag(n,\gamma)^{108}Ag$ Reaction

T. Mitsunari[+], *T.D. Mac Mahon*[+], *H. Seyfarth*, *K. Schreckenbach*[++], *W.R. Kane*[×], *I.A. Kondurov*[××], *P. Sushkov*[××], *Y. Loginov*[××], *M. Bogdanovic*[×××]

Since the introduction of the shell model, odd-odd nuclei have been characterized by the properties of the odd proton and odd neutron, leading to a proton-neutron multiplet structure. The residual proton-neutron force splits and mixes the multiplets, establishing the final physical situation. This simple treatment is applicable in the neighbourhood of double closed shell nuclei.

In transitional nuclei the odd-A nuclei are usually treated as one particle (quasiparticle) or cluster of particles (quasiparticles) coupled to a vibrator (harmonic or anharmonic) or to a rotor (axial or triaxial). After solving the problem of the neighbouring odd-A nuclei it is possible to construct the zero order proton-neutron multiplet structure in odd-odd nuclei. Calculations show[1] that the multiplets split into a parabolic structure, if plotted as a function of I(I+1).

As a contribution to the systematic study of trends in the structures of odd-odd nuclei in the region of the Z = 50 closed shell the $^{107}Ag(n,\gamma)^{108}Ag$ reaction has been studied in a variety of experiments:

(i) a high resolution study of about 500 γ-rays in the energy region 45 to 1200 keV using a curved crystal spectrometer at AEK, Risø.

(ii) singles γ-ray spectra measured using Ge(Li) detectors at the University of London Reactor Centre, and at the FRJ-2 reactor, KFA, Jülich.

(iii) low energy γ-rays (10 to 110 keV) recorded with Si(Li) detectors at the Leningrad Nuclear Physics Institute, Gatchina, and at the Technical University, Munich.

(iv) γ-γ coincidence spectra measured using Ge(Li) detectors at the FRJ-2 reactor, KFA Jülich; at the Leningrad Nuclear Physics Institute, Gatchina; and at the Boris Kidric Institute, Vinca.

(v) conversion electron spectra measured with the BILL spectrometer at the Institute Laue-Langevin, Grenoble.

(vi) γ-rays emitted following both single resonance (16 eV) and average resonance (2 keV and 24 keV) neutron capture studied at the Brookhaven National Laboratory, Upton, New York.

(vii) lifetimes of levels in ^{108}Ag measured at the Technical University, Munich.

Results of the above experiments have been combined to provide detailed and precise information about the level scheme of ^{108}Ag. Further details of the experimental techniques will be found in the paper to be submitted to the Journal of Physics G: Nuclear Physics.

A total of over 550 transitions in ^{108}Ag have been observed in the various experiments. Table 1 lists the properties of the energy levels in ^{108}Ag below 1 MeV which have been deduced from the experimental data.

It should be pointed out that the existence of the following levels, listed in the latest edition of the 'Table of Isotopes' [2] is not substantiated in the present work: 45.5, 287.5, 331.0, 451.2, 537.5 and 713 keV. In the present work a cascade of γ-rays, observed to be in coincidence with each other but not linked to the main part of the level scheme, are tentatively placed as feeding the 127 year isomeric state at 109.5 keV. The resulting tentative levels are at 155.90, 485.08, 587.39, 598.67 and 799.69 keV, and are included in Table 1.

Making use of the results of the $^{107}Ag(d,p)$ experiments[3] (a preliminary spectrum obtained from the $^{109}Ag(p,d)$ reaction[4] indicates what can be contributed by high-resolution charged particle spectroscopy) together with the I^π values determined here, allows the identification of certain multiplets. The 0^- component of the $\pi p^{-1}_{1/2}\,\nu s_{1/2}$ multiplet is assumed to be the 465.6 keV level, with 1^- components at 379.2, 606.5 and 679.1 keV. The ground state and isomeric state at 109.5 keV are assumed to be the 1^+ and 6^+ members of the $\pi(g_{9/2})^{-3}_{7/2}\,\nu d_{5/2}$ multiplet with 2^+, 3^+ and 4^+ levels at 206.6, 324.5 and 364.2 keV respectively. The 2^- first excited state at 79.1 keV and the 3^- state at 338.4 keV comprise the $\pi p^{-1}_{1/2}\,\nu d_{5/2}$ multiplet.

Table 1: Properties of low lying levels in ^{108}Ag. Column 1 lists the level energies in keV, with their errors in eV.

E_{ex}	I^π	E_{ex}	I^π	E_x	I^π
0.0	1^+	516.843(3)	3^-	715.815(4)	$2^-(1^-)$
79.140(2)	2^-	542.847(3)	$2^-,3^-$	718.789(10)	≤ 2
109.472(7)	6^+	563.813(2)	2^+	765.468(3)	2^-
155.902(6)	$5^+,6^+$	579.111(5)	0^-	779.728(4)	$2^-,3^-$
193.075(2)	1^+	587.389(3)	$3^-,4^-$	799.692(3)	$2^-,3^-$
206.612(2)	2^+	598.671(3)	$3^-,4^-$	803.731(5)	2^-
215.384(2)	3^+	606.532(2)	1^-	819.090(4)	2^-
294.561(2)	2^+	611.661(3)	$2^+,3^+$	857.501(14)	2^-
324.497(2)	3^+	616.942(3)	2^-	880.701(8)	2^+
338.419(2)	3^-	645.502(5)	$3^+(4^+)$	898.434(8)	1^-
364.239(3)	$4^+(3^+)$	656.356(10)	$3^-(4^-)$	899.943(4)	1^-
379.243(2)	1^-	656.653(4)	$3^+,4^+$	942.339(7)	$2^+,2^-,3^-$
408.363(2)	3^+	679.096(5)	1^-	959.851(17)	$2^+,2^-,3^-$
460.081(5)	$2^-,3^-,4^-$	700.869(7)	3^-	974.343(5)	$1^-,2^-$
465.641(3)	0^-	703.594(5)	$(2,3,4)^-,3^+$	994.591(9)	$1^-,2^-,3^-$
485.078(3)	$4^-,5^-$	705.693(6)	2^-		
508.478(2)	2^-	708.842(3)	2^-		

1) V. Paar, Nucl. Phys. A331(1979) 16

2) C.M. Lederer and V.S. Shirley (Eds) 'Table of Isotopes' 7th edition 1978 John Wiley and Sons Inc. New York

3) C.E. Brient et al., Phys. Rev. C6 (1972) 1837

4) G.P.A. Berg et al., contribution to this report (p. 4)

+ University of London Reactor Centre, Silwood Park, Ascot, Berkshire SL5 7PY, England

++ Institut Laue-Langevin, Grenoble, France

× Brookhaven National Laboratory, Upton, New York, USA

×× Leningrad Nuclear Physics Institute, Gatchina, USSR

××× Boris Kidric Institute of Nuclear Sciences, Belgrade, Yugoslavia

2.7. Level scheme of ^{110}Ag from the (n,γ) reaction

P.A. Sushkov[+], I.A. Kondurov[+], M. Bogdanovic[*], T. Mitsunari[++], T.D. Mac Mahon[++], H.A. Baader[××], D. Breitig[**], H.R. Koch, H. Seyfarth, O.W.B. Schult, H.G. Börner[×], R. Brissot[×], G. Barreau[×], S. Kerr[×], H. Faust[×], K. Schreckenbach[×]

An intensive study of odd-odd nuclei around the closed proton shell at Z = 50 has been carried out during the last few years. In this report a complex study of the ^{110}Ag level scheme from the (n,γ)-reaction is briefly presented. Gamma radiation in the energy range from 35 to 2000 keV was investigated with the bent crystal spectrometers at Risø and Grenoble and in the energy range from 15 to 110 keV with a Si(Li) detector based spectrometer at Gatchina. Conversion electrons from transitions in the energy range from 20 to 650 keV have been measured with the electron spectrometer BILL at Grenoble. The primary γ-ray spectrum was measured with the pair-spectrometer at JÜlich. Prompt γγ-coincidences were studied with two Ge(Li) detectors at spectrometers in Gatchina and JÜlich in the energy regions 15-600 and 50-7000 keV, respectively.

The last version of the ^{110}Ag level scheme[1] was carefully analyzed on the basis of these data. Numerous new levels were introduced. A rather complicated cascade with strong γ-transitions populating the long-lived isomeric state (117.5 keV, I = 6^+, $T_{1/2}$ = 250 d) was obtained on the basis of γγ-coincidence data[2]. This cascade is included in Fig. 1. The new levels are also connected through γ-transitions with previously known levels whose energies and spin and parity assignments are given on the left side. The energies and spin and parity assignments of all the levels, which were established in ^{110}Ag, are listed in the table.

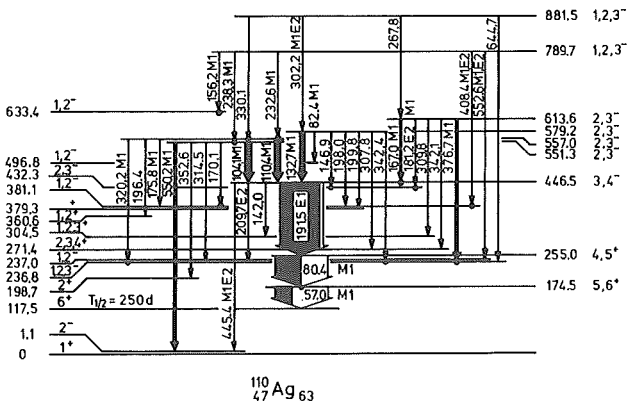

$^{110}_{47}Ag_{63}$

Fig. 1: Level scheme of ^{110}Ag including the new levels which are connected through a strong cascade with the 250 d isomer. The energies of these new levels are given on the right side of the figure.

Table 1: Levels in ^{110}Ag from the ^{109}Ag(n,γ)-reaction

Level energy keV(eV)	I^π	Level energy keV(eV)	I^π
0	1^+	539.795(3)	$1,2^+$
1.1142(20)	2^-	549.3829(22)	$1,2^+$
117.561(5)	6^+	551.360(3)	$2,3^-$
118.7210(18)	3^+	557.0684(24)	$2,3^-$
174.576(5)	$5,6^+$	579.295(3)	$2,3^-$
191.6247(21)	$2,3,4^+$	595.027(6)	$2,3^-$
198.6988(18)	2^+	613.641(3)	$2,3^-$
236.8536(22)	$1,2,3^-$	615.134(4)	$1,2,3^-$
237.0514(19)	$1,2^-$	633.441(3)	$0,1,2^-$
255.020(4)	$4,5^+$	653.918(5)	$1,2,3^-$
267.2212(18)	$1,2^+$	663.466(3)	$1,2,3^+$
267.259(3)	$2,3,4^+$	664.922(3)	$1,2,3^-$
271.4742(24)	$2,3,4^+$	683.148(7)	$2,3^+$
304.5300(21)	$1,2,3^+$	698.5532(25)	$0,1,2^+$
338.910(3)	$0,1,2^-$	706.1275(25)	$1,2^+$
360.6206(18)	$1,2^+$	725.802(5)	$1,2,3^-$
379.398(4)	$1,2,3^+$	748.576(4)	$1,2^+$
381.1978(20)	$1,2^-$	750.892(3)	$1,2^+$
424.707(3)	$1,2,3^-$	773.677(5)	$1,2^+$
432.373(3)	$2,3,4^-$	785.652(4)	$1,2^+$
446.5734(24)	$3,4^-$	789.703(3)	$1,2,3^-$
468.8489(20)	$2,3^+$	811.411(5)	$1,2^+$
471.241(4)	$1,2,3^+$	818.991(5)	$1,2^+$
485.7754(22)	$2,3^+$	881.552(5)	$1,2,3^-$
496.8802(23)	$1,2^-$	910.928(9)	$2,3^-$
525.666(4)	$1,2^-$	995.069(7)	$1,2^+$
527.514(3)	$2,3^+$	1013.015(11)	$1,2^+$
536.1832(21)	$1,2^+$	1097.558(11)	$1,2^+$

References

1) M. Bogdanovic, S.Koicki, J. Simic, B. Lalovic, D. Breitig, R. Koch, H.A. Baader, O.W.B. Schult, W.R. Kane and R.F. Casten, Fizika 11 (1979) 157

2) P.A. Sushkov, I.A. Kondurov and V.V. Martynov, Proc. XXXI Conf. on Nuclear Spectroscopy and Nuclear Structure 1981 (Leningrad: Nauka) p. 84

+ Leningrad Nuclear Physics Institute, Gatchina, USSR

* Boris Kidric Institute for Nuclear Science, Belgrade, Yugoslavia

++ University of London Reactor Centre, Ascot, Berkshire, England

× Institut Laue-Langevin, Grenoble, France

×× present address: Elektro Manufactur Zangenstein, Fa. Ernst Hanauer, Zangenstein, Germany

** present address: University of Ulm, Germany

2.8. High spin level structure of ^{133}La

T. Morek, H. Beuscher, B. Bochev, D.R. Haenni, T. Kutsarova, R.M. Lieder, M. Müller-Veggian, A. Neskakis

The previous knowledge about the structure of ^{133}La, deriving from decay studies[1,2,3] and in-beam investigation[4,5,6], could be largely extended using the ^{133}Cs(α,4n)^{133}La reaction at E_α = 55 MeV. The resulting level scheme is shown in fig. 1. The level structure of

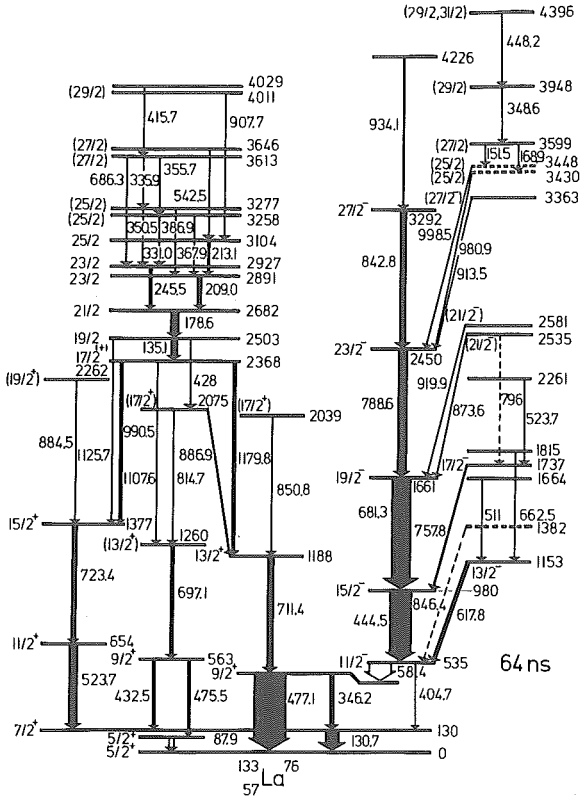

Figure 1: Level scheme of ^{133}La.

this odd proton nucleus shows interesting features. The orbitals near the Fermi surface are the $\pi h_{11/2}$, $\pi d_{5/2}$, $\pi g_{7/2}$. Bands based on these orbitals with negative and positive parity were established up to high spin states, i.e. $27/2^-$, $(17/2^+)$, $(19/2^+)$, $(17/2^+)$. The $11/2^-$ band exibits favoured and unfavoured states. Calculations have been performed in order to understand the $h_{11/2}$ proton band. The core-particle coupling model uses a "soft" core which is described by a collective hamiltonian with a γ-independent energy but γ-dependent inertial functions[7]. A good agreement between the experimental and calculated levels exists up to the $27/2^-$ state. Furthermore mixing ratios δ were extracted using the transition matrix elements and the experimental energies of the γ rays. There is a rather good agreement with the mixing ratios δ extracted from the angular distribution experiment. The $h_{11/2}$ band structure is interrupted at the excitation energy of 3599 keV and above this level. Three particle configurations are probably responsible for these levels. This fact would not be unexpected since 10^+ isomers with $[\nu h_{11/2}]^{-2}$ configuration were observed in the neighbouring even-even nuclei[8,9]. It is very probable that the states with spins (25/2),(27/2),(29/2),(29/2,31/2) have a $\{\pi h_{11/2}(\nu h_{11/2})^{-2}_{10^+}\}$ configuration. Furthermore one of the two 25/2 states (at 3430 and at 3448 keV excitation energy) has probably a $\{\pi h_{11/2}(\nu h_{11/2}\nu d_{3/2})_{7^-}\}_{25/2^+}$ configuration. Three positive collective bands based on the $5/2^+$ ground state, $5/2^+$ and $7/2^+$ states were found. The $g_{7/2}$ and $d_{5/2}$ orbitals near the Fermi surface have low Ω values so that bands with a decoupled structure are expected. It is interesting to see that for all three bands based on the $5/2^+$ ground state, $5/2^+$ and $7/2^+$ states the level spacings are very similar to those of the $2^+\to0^+$, $4^+\to2^+$, $6^+\to4^+$ in the core nucleus ^{132}Ba. The $5/2^+$ excited state at 87.9 keV is very probably due to the $g_{7/2}$ proton. A state with an intrinsic configuration at 2368 breaks the band structures. The I=17/2 state has probably a positive parity so that the possible configuration for it are:

i) $[\pi d_{5/2}(\pi g_{7/2})^2_{6^+}]$

ii) $[\pi d_{5/2}(\nu h_{11/2})^2_{10^+}]$ or

$[\pi g_{7/2}(\nu h_{11/2})^2_{10^+}]$

The possibility i) seems to be the most probable since a 6^+ state of configuration $[\pi g_{7/2}]^2$ or $[\pi g_{7/2}\pi d_{5/2}]$ has been experimentally observed in the ^{136}Ce nucleus[10]. States with I>17/2 have probably configuration of the type ii).

The investigation of the nucleus ^{133}La showed interesting features namely collective bands based on the $\pi h_{11/2}$, $\pi d_{5/2}$, $\pi g_{7/2}$ orbitals, as well as intrinsic states with three-particle configuration.

References

1) H. Abou-Leila, G. Gerschel, N. Perrin, Compt. Rend. 265 (1967) 1131

2) C. Gerschel, Nucl. Phys. A108 (1968) 337

3) E.A. Henry and R.A. Mayer, Phys. Rev. C18 (1978) 1814

4) J.R. Leigh, K. Nakai, K.H. Maier, F. Puhlhofer, F.S. Stephens, R.M. Diamond, Nucl. Phys. A213 (1973) 1

5) K. Nakai, P. Kleinheinz, J.R. Leigh, K.H. Maier, F.S. Stephens, R.M. Diamond, G. Lovhoiden, Phys. Lett. 44B (1973) 443

6) J. Chiba, R.S. Hayano, H. Sikimoto, H. Nakayama, K. Nakai, J. Phys. Soc. Jpn. 43 (1977) 1109

7) Ch. Droste, D. Chlebowska, J. Dobaczweski, F. Dönau, A. Kerek, G. Leander, J. Srebrny, W. Walus, Nucl. Phys. A341 (1980) 98

8) M. Müller-Veggian, H. Beuscher, R.M. Lieder, Y. Gono, D.R. Haenni, A. Neskakis, Z. Physik A290 (1979) 43

9) T. Morek, H. Beuscher, B. Bochev, D.R. Haenni, R.M. Lieder, T. Kutsarova, M. Müller-Veggian, A. Neskakis, Z. Physik A Atoms and Nuclei 298 (1980) 267

10) M. Müller-Veggian, Y. Gono, R.M. Lieder, A. Neskakis, C. Mayer-Böricke, Nucl. Phys. A304 (1978) 1

2.9. Structure of high spin states in ^{134}Ce

M. Müller-Veggian, H. Beuscher, D.R. Haenni, R.M. Lieder, A. Neskakis

The study[1] of the nucleus ^{134}Ce has been continued. The level scheme of ^{134}Ce is shown in fig. 1. The most interesting feature in this nucleus is the existence of two 10^+ states, one of them is an isomer and the other one is a collective state belonging the ground state cascade[2], which exibits backbending at the critical momentum I_c=10. The isotopes ^{128,130,132}Ce [2,3] show similarly backbending at the same angular momentum.

Furthermore the nucleus ^{134}Ce shows interesting bands. A well developed negative parity band with odd and even spin members up to I=13, 10 have been observed. Similar bands based on a 5^- state were observed in the neighbouring even-even nuclei ^{136}Ce [4], ^{138}Nd [5], ^{132,134}Ba [6,7]. The configuration of the 5^- state in ^{134}Ce is thought to be $(\nu h_{11/2}^{-1}(x)\nu s_{1/2}^{-1})_{5^-}$ or $(\nu h_{11/2}^{-1}(x)\nu d_{3/2}^{-1})_{5^-}$. A quasi-gamma band, which deexcites the 10^+ isomer can be seen in fig. 1. The characteristic spin sequence of γ bands could be observed. Furthermore the 3^+ state could be identified; its location is reasonable and agrees with theoretical prediction. The structure of the cascade on top of the 10^+ isomer is of special interest. This cascade established up to I=15 has a rotational character. The energies and the multipolarities of the γ rays are very similar to those of the transitions in the $h_{11/2}$ neutron band of ^{135}Ce. The level structures based on the 10^+ isomers in ^{136}Ce [4], in ^{138}Nd [5] are very similar to the ground state cascade in ^{137}Ce, ^{139}Nd [4,5].

This analogy suggests that the 10^+ isomer in ^{134}Ce has a $(\nu h_{11/2})^{-2}$ configuration. Furthermore this state must have an oblate deformation.

Goldberg et al.[6] performed g-factor measurement for the 10^+ isomer. The magnetic moment of the 10^+ state support the hypothesis that a decoupled $h_{11/2}$ neutron pair play the most important role in the configuration of this state. The backbending effect observed in the Ce nuclei (i.e. ^{128}Ce, $^{130\text{-}134}$Ce) has been attributed to the $h_{11/2}$ protons, using blocking arguments[7]. Calculations within the Bengtsson-Frauendorf model[8] explain the backbending of ^{130,132}Ce as due to the alignment of $h_{11/2}$ protons. The backbending in ^{134}Ce is very probably due to the $h_{11/2}$ neutrons. The alignment of the $h_{11/2}$ neutron is in fact expected to occur at higher energy than that of the $h_{11/2}$ proton in the framework of cranking model[8]. This model[8] predicts a sudden increase of the aligned angular momentum at a certain frequency caused by the backbending effect.

The big retardation of the 12^+ 10^+ transition in the ground state cascade for ^{134}Ce [9] ($R \approx 0.04$) deviates far from the rigid values. This suggests that for ^{134}Ce the backbending may be connected to a shape change. The $h_{11/2}$ neutrons which are the responsible for configuration of the 10^+ oblate isomer, are at the same time responsible for the structure of the 10^+ state in the ground state cascade. The 10^+ state has then very probably a different

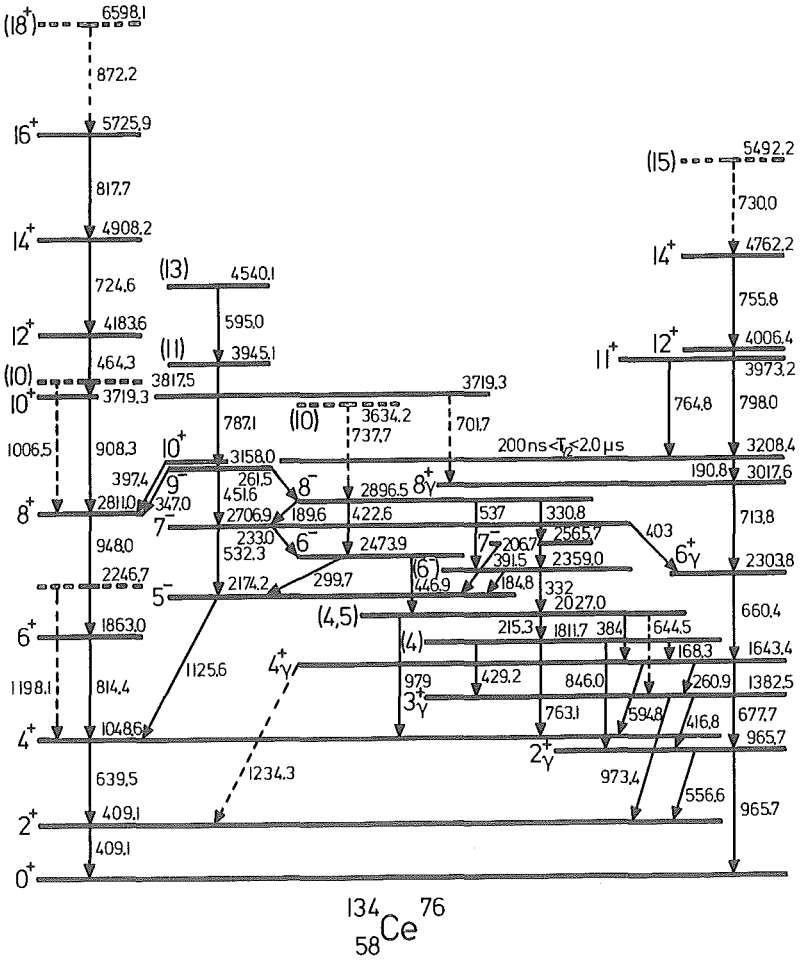

Figure 1: Level scheme of ^{134}Ce.

deformation. It may be therefore that for the nucleus ^{134}Ce the backbending is connected to a shape transition. Calculation of this type were performed by Gong-ou Xu and Jing-ye Zhang[10]. The g factor measurement of the 10^+ collective state[6] supports the assumption that the $h_{11/2}$ neutrons are responsible for the backbending of ^{134}Ce.

References

1) M. Müller-Veggian, et al., Annual Report 1980, Institut für Kernphysik der KFA Jülich, Jül-Spez-99 (1981) 49

2) W. Dehnhardt, S.J. Mills, M. Müller-Veggian, U. Neumann, D. Pelte, G. Poggi, B. Povh and P. Taras, Nucl. Phys. A225 (1974) 1

3) J. Gizon, A. Gizon, R.M. Diamond, F.S. Stephens, Nucl. Phys. A290 (1977) 272

4) M. Müller-Veggian, Y. Gono, R.M. Lieder, A. Neskakis, C. Mayer-Böricke, Nucl. Phys. A304 (1978) 1

5) M. Müller-Veggian, H. Beuscher, D.R. Haenni, R.M. Lieder, A. Neskakis and C. Mayer-Böricke, Nucl. Phys. A344 (1980) 89

6) M.B. Goldberg, C. Broude, A. Zemel, J. Gerber, G.J. Kumbartzki, K.-H. Speidel, Proc. Int. Conf. on Nucl. Behaviour of High angular momentum (Strasbourg, April 1980) p. 49

7) D. Ward, H. Bertschat, P.A. Butlar, P. Colombani, R.M. Diamond, F.S. Stephens, Phys. Lett. 56B (1975) 139

8) R. Bengtsson and S. Frauendorf, Nucl. Phys. A314 (1973) 27 and Nucl. Phys. A237 (1979) 139

9) D. Husar et al., Nucl. Phys. A292 (1977) 267

10) Gong-ou Xu, Jing-ye Zhang, Nucl. Phys. A343 (1980) 189

2.10. The Structure of the Heavy Ce-Isotopes

R.L. Gill[+], R.E. Chrien[+], M. Shmid[+], G.M. Gowdy[+], H.I. Liou[+], Y.Y. Chu[+], R.F. Casten[+], D.D. Warner[+], M.L. Stelts[0], D.S. Brenner[++], F.K. Wohn [+++], K. Sistemich, H. Yamamoto[+++], C. Chung, W.B. Walters, T.R. Yeh, R.F. Petry and R.A. Meyer[00]

The high beam intensity of the fission product separator TRISTAN[1] at the High Flux Beam Reactor of the Brookhaven National Laboratory enables the investigation of the level schemes of the neutron rich Ce-isotopes up to A = 148 through the β-decay of their La parents. These Ce-nuclei belong to the border at low Z of the region of the deformed rare earths and have not yet been studied in detail.

There were two major reasons to study these nuclei:

- Recent investigations of the Ba isotopes showed[2] that the onset of deformation takes place at N = 88 in this isotopic chain rather than at N = 90 as for Z$\gtrsim$60. The present experiments were undertaken in order to get information on the onset in the intermediate Ce-isotopes (Z = 58).
- The investigation of the Ce nuclei offers a possibility to check the predictive power of the IBA since calculations on these isotopes could be performed prior to the experiments with parameters which were deduced from fits to the neighbours.

The measurements provided extended level schemes[3]. The data on ^{148}Ce are shown in fig. 1 as an example. Only the 2_1^+, 4_1^+ and 6_1^+ (at 841 keV) levels were known earlier[4]. The spins and parities of the new levels are suggested from the deexcitation pattern and they are in accordance with the systematics for the N = 90 isotones[3].

The systematics of the Ce isotopes with even mass are shown in fig. 2. In contrast to the situation in Ba there is no indication that the deformation sets on prior to N = 90.

The calculations in IBA-2 fitted well[3] to the experimental data in ^{148}Ca but they were less satisfactory for the lighter isotopes. This is interpreted[5] as a consequence of the Z = 64 subshell closure which has to be taken into consideration for N $\lesssim$ 90 while its influence is less important for heavier isotopes.

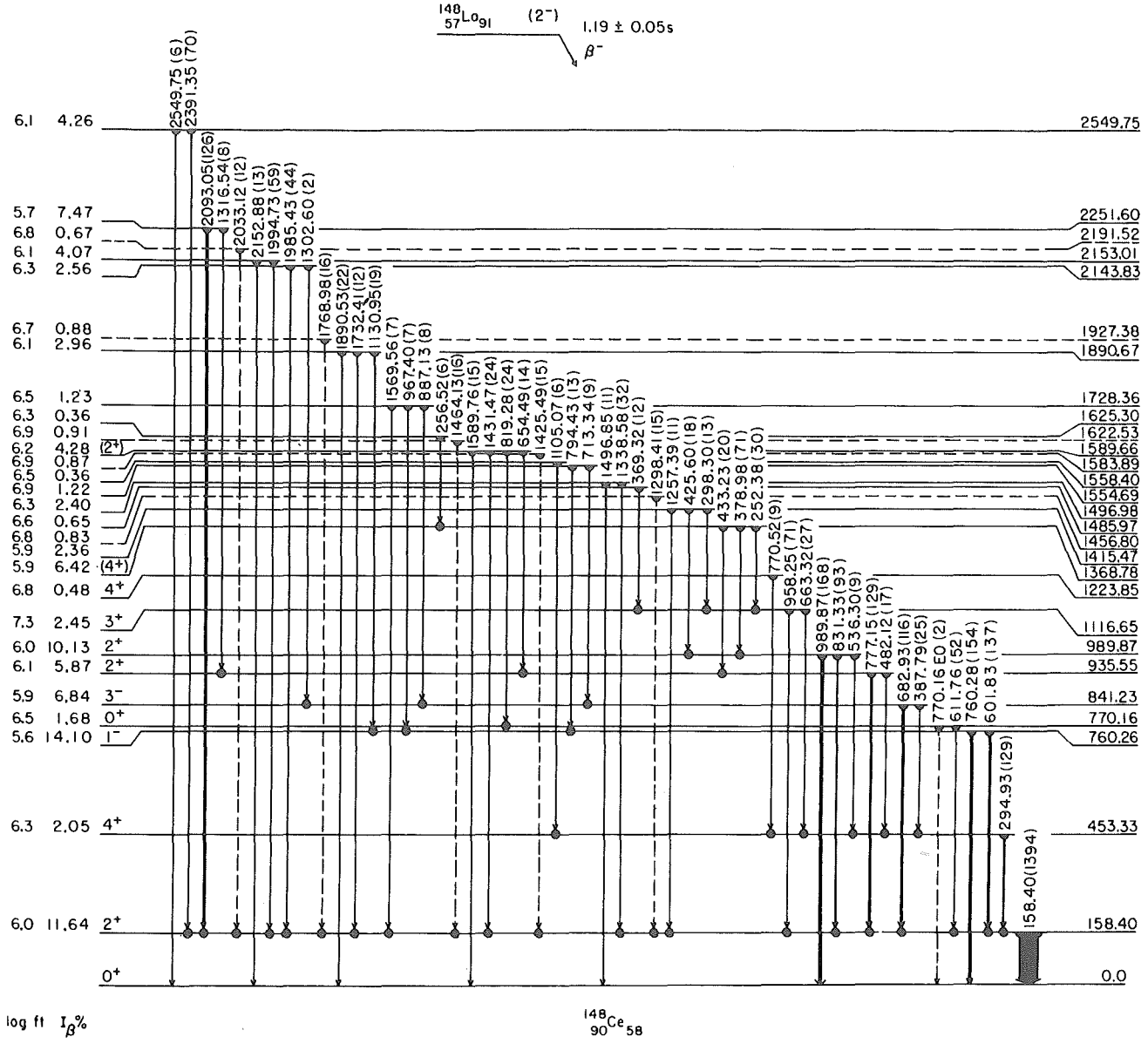

Fig. 1 The proposed level scheme of ^{148}Ce. The placement of all transitions is established through coincidence results.

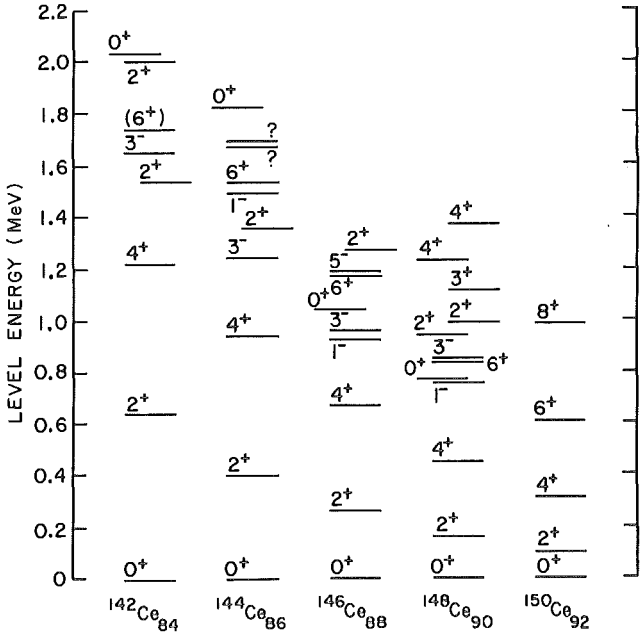

Fig. 2: The systematics of the Ce isotopes with even mass[3].

References

1) D.S. Brenner, R.E. Chrien, R.L. Gill, J.C. Hill and F.K. Wohn, Proc. Int. Sym. on Future Directions in Studies of Nuclei far from Stability, Nashville, Tennessee, Sept. 10 - 13 (1979)

2) S.M. Scott, D.D. Warner, W.D. Hamilton, P. Hungerford, G. Jung, K.D. Wunsch and B. Pfeiffer, J. of Phys. G 5 (1979) 487

3) R.L. Gill, R.E. Chrien, M. Shmid, G.M. Gowdy, H.I. Liou, M.L. Stelts, Y.Y. Chu, D.S. Brenner, F.W. Wohn, K. Sistemich, H. Yamamoto, C. Chung, W.B. Walters, T.R. Yeh, R.F. Petry and R.A. Meyer, Conf. Proc., CERN 81-09 (1981) 557-580

4) C.M. Lederer and V.S. Shirley, Table of Isotopes, Seventh Edition, A. Wiley Sons Inc., New York

5) R.L. Gill, R.F. Casten, D.D. Warner, D.S. Brenner and W.B. Walters, to be published

2.11. A 45 ns High-Spin Isomer in the Doubly Odd ^{150}Eu Nucleus

F. Soramel, J. Styczen, A. Ercan, P. Prokofjev and P. Kleinheinz

So far nothing was known on the energy levels in $^{150}_{63}Eu_{87}$ except that it has[1] two ß-decaying isomers with I^{π}, $T_{1/2} = 0^{(-)}$, 13h and $(4,5^-)$, 36y. We have investigated this nucleus at the IKP cyclotron through in-beam γ and e^- experiments using the (p,3n) reaction with proton beams between 26 and 35 MeV. The measurements included γ-ray singles excitation function and angular distribution studies, conversion electron singles measurements with a magnetic orange spectrometer and two-detector four-parameter γγ coincidence experiments using coaxial and planar Ge-detectors.

The level density in this nucleus with 6 valence particles, and only two neutrons away from ^{152}Eu, is quite high, and accordingly the prompt γ-ray spectra observed during beam bursts are highly complex and have not yet been successfully analyzed. The coincidence data however revealed that the nucleus has a low-lying high-spin isomer and four intense γ rays, 190.4, 247.9, 314.1 and 371.6 keV occur in its decay. Ten additional weak transitions were identified from prompt γγ coincidences measured between beam bursts. The isomeric half life was extracted from the four parameter γγ coincidence data as $T_{1/2}$ = 45(3) ns, the measurement is illustrated in fig.1.

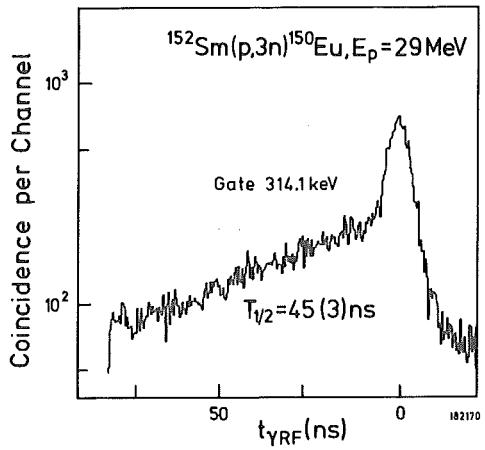

Fig. 1: Half life of the 589 keV isomer in ^{150}Eu extracted from the four-parameter γγ coincidence data.

The fig. 2 shows the decay scheme of the isomer. The three excited states at 190, 248, and 562 keV are specified from the comparison with in-beam intensities for the four strong transitions. The weak lines identify three additional levels at 360, 413 and 417 keV. In two cases (360 and 413 keV) where only two γ-rays connect with the level, their ordering could be determined from the γ-ray intensities observed in the pertinent in-beam coincidence spectra. The off-beam coincidence data clearly establish a 171.5 keV transition feeding the 417 keV state and the $t_{\gamma RF}$ time distribution of this line specifies the 589 keV state as the isomeric level. Its principal decay proceeds through an unobserved 26.8 keV transition feeding the 562 keV state.

Adopting $I^{\pi} = 5^-$ for the ground state in fig. 2 the measured angular distributions and α_K values uniquely determine 6^- for the 190 and 248 keV levels, and 6^+ for the 562 keV state. The 45 ns half life and the isomeric decay branching is only compatible with an $I^{\pi} = 8^+$ assignment, which gives 25 W.u. for the 26.8 keV isomeric E2 transition. From the remaining levels, only the 417 keV state can be specified as 7^-; the possible spin assignments for the other two weakly populated states are given in fig. 2.

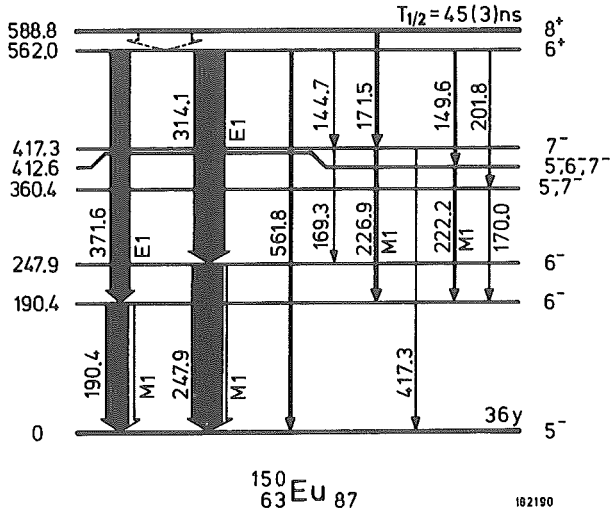

Fig. 2: Decay scheme of the 45 ns isomer in ^{150}Eu. Transition multipolarities obtained from α_K values are given. Proposed spin-parities are relative to the adopted 5^- ground state assignment.

At present it is difficult to propose structural assignments for the observed ^{150}Eu levels. One notes however that low-lying 5^-, 6^-, and 6^- levels have also been seen in the two neighbouring ^{148}Eu and ^{146}Eu odd odd isotopes[2,3] where they have been attributed to the couplings of the odd $f_{7/2}$ neutron to either the $d_{5/2}$ or $g_{7/2}$ proton hole. The nature of the higher-lying levels and also of the isomeric state is much less obvious. Since however the adjacent ^{151}Eu and ^{149}Sm nuclei are stable it is possible to obtain useful structure information from (p,d) and (^{3}He,d) single nucleon transfer experiments and we have therefore begun such measurements to investigate the ^{150}Eu levels further.

References

1) Table of isotopes, 7th edition, Eds. C.M. Lederer and V.S. Shirley (Wiley, 1978)

2) M. Piiparinen, R. Broda, Y. Nagai, P. Kleinheinz, and A. Pakkanen, Z. Physik A301, 231 (1981)

3) A. Ercan, R. Broda, M. Piiparinen, Y. Nagai, R. Pengo, and P. Kleinheinz, Z. Physik A295, 197 (1980)

2.12. The N=82 Gap in ^{146}Gd from β-decay Studies of Tb Isotopes

J. Styczen, P. Kleinheinz, M. Piiparinen, J. Blomqvist

There exists quite detailed knowledge on the proton particle-hole states in ^{146}Gd. These levels are strongly populated in the yrast decay[1], and their excitation energies are in accord with the ≃ 3.5 MeV Z=64 energy gap as derived from the difference of the ^{147}Tb and ^{146}Gd single proton separation energies. On the other hand it is well known that pairing is important at Z=64, and from an analysis of single proton quasi-particle energies[2,3] in the neighbouring ^{145}Eu and ^{147}Tb isotones a value of ∿ 2.5 MeV was derived for the energy gap in the single particle spectrum.

From the single neutron separation energies one obtains for ^{146}Gd an N=82 gap of ≃ 3.7 MeV, but nothing so far is known on the ^{146}Gd neutron particle hole excitations which should occur at about that excitation. Furthermore, the excitation energies in the neighbouring isotopes with one neutron lifted across N=82 (1p2h states in ^{145}Gd and 2p1h states in ^{147}Gd), which are crucial to determine the gap in the neutron single particle energies, are also not known. Many of these states have low spin and are therefore in general not populated in in-beam experiments.

We have therefore investigated the β-decay of the ^{145,146,147}Tb isotopes which are expected to populate specific neutron particle-hole excitations in the three Gd daughter nuclei. The parent activities were produced through (α,xn) reactions (x = 8, 9, 10) in bombardments of ^{152}Gd and ^{151}Eu targets with α-particle beams between 90 and 130 MeV from our cyclotron. Gamma-ray singles and two-detector coincidence measurements with various coaxial and planar Ge detectors were carried out during 20 to 40 sec beam pauses following similar irradiation periods during which the detectors were blocked.

Our results for ^{146}Tb decay are shown in Fig. 1. In contrast to earlier studies[4,5] we find negligible feed to the 3⁻ first excited state and the coincidence results locate three new levels in ^{146}Gd above 3.4 MeV.

From the shell model one expects for the ^{146}Tb parent nucleus a $\pi h_{11/2}\ \nu d_{3/2}^{-1}$ configuration which can couple to I^π = 4⁻, 5⁻, 6⁻ or 7⁻. The πν residual interaction will be repulsive for the two extreme couplings, which leaves 5⁻ and 6⁻ as the possible ^{146}Tb ground state spins. Since the β-decay proceeds through the allowed $\pi d_{5/2}^{-1} \rightarrow \nu d_{3/2}^{-1}$ GT transition a 6⁻ should lead to a strong population of the known ^{146}Gd $(\pi h_{11/2} d_{5/2}^{-1})7^-$ state at 2982 keV which is not observed. The decay instead proceeds strongly to the 5⁻ state of that configuration at 2658 keV and to two additional levels, at 2996 and 3099 keV, which we propose to be the associated I^π = 4⁻ and 6⁻ states, respectively, in accord with their γ-decay patterns. In particular identification of the previously overlooked 116.7 keV transition to the 2982 keV 7⁻ isomer from the 3099 keV state strongly supports its 6⁻ assignment. Furthermore, the observed β-decay intensities to these levels are in excellent agreement with the theoretically calculated ratios. These results unambiguously classify the ^{146}Tb parent state as 5⁻, in contrast to the conclusions of earlier works[4,5].

The clearly observed 1579 - 3140 keV coincidences establish a new level at 4719 keV. We attribute the feeding β-branch to the other expected GT transition, $\pi h_{11/2} \rightarrow \nu h_{9/2}$, which systematically occurs with essentially equal log ft values in other Tb isotopes in this region. This classifies the 4719 keV state as $\nu(h_{9/2} d_{3/2}^{-1})4^-$ neutron particle hole excitation. Only the 5⁻ multiplet member is predicted to be also fed in β-decay, but 14 times weaker than the 4⁻ state. The weakly fed level at 4828 keV, which decays to the 2996 keV 4⁻ state, is probably that 5⁻ multiplet member.

A weak 1297 - 1844 keV parallel decay branch proceeds from the 4⁻ state, where the transition ordering is determined from ^{144}Sm(α,2n) excitation function measurements[6] close to threshold. We interprete the intermediate 3423 keV level as $\nu f_{7/2} d_{3/2}^{-1}$ state, which is the lowest neutron particle hole excitation in ^{146}Gd. Its energy should be equal to the N=82 gap at Z=64, except for small contributions of collective or nucleon-nucleon interactions. The near-agreement with the ≃ 3.7 MeV N=82 gap as derived from the neutron separation energy difference is in accord with this view.

In our spectra we also observe weakly the known[6] 1972 keV $2^+ \rightarrow 0^+$ transition, and a 1059 keV line in coincidence with it. As no connecting transitions to any of the strongly β-fed levels could be found it remains unclear how the 2^+ state is fed. Most likely it is directly populated in β-decay of a low spin ^{146}Tb isomer involving the $d_{3/2}$(or $s_{1/2}$) proton particle, which is possibly produced at the present bombarding energies via precompound particle emission. Such a low spin ^{146}Tb activity has been identified[7] following β-decay of ^{146}Dy.

When we began our experiments the ^{145}Tb activity was not known. The mass identification was derived from excitation function and from X-ray coincidence measurements, and the ^{145}Tb half life was found as $T_{1/2}$ = 29 ± 4 sec. This value is in agreement with two independent determinations[8,9] reported in recent abstracts.

The ^{145}Tb decay scheme is shown in Fig. 2. From systematics we attribute I^π = 11/2⁻ to its ground state. Levels in ^{145}Gd have previously been investigated[10] through the ^{144}Sm(α,3n) reaction, but the energy levels observed in this study above 750 keV are not populated in ^{145}Tb decay. However, most of the levels seen in β-decay have been observed in concurrent ^{144}Sm(^{3}He,2n)γ and e⁻ measurements[11] which gave the spin-parity assignments shown in Fig. 2 for the levels between 1 and 2 MeV. The transition multipolarities quoted in the figure are also from the in-beam work. Our β-decay branchings are in accord with the 11/2⁻ ^{145}Tb parent spin. Strongly fed in β-decay is the 2382 keV ^{145}Gd level, and the log ft = 4.2 suggests a $\nu h_{9/2}\ j_o^{-2}$ configuration. The other 1p2h state, the $\nu f_{7/2} j_o^{-2}$ level at 1273 keV is known from the in-beam work[11].

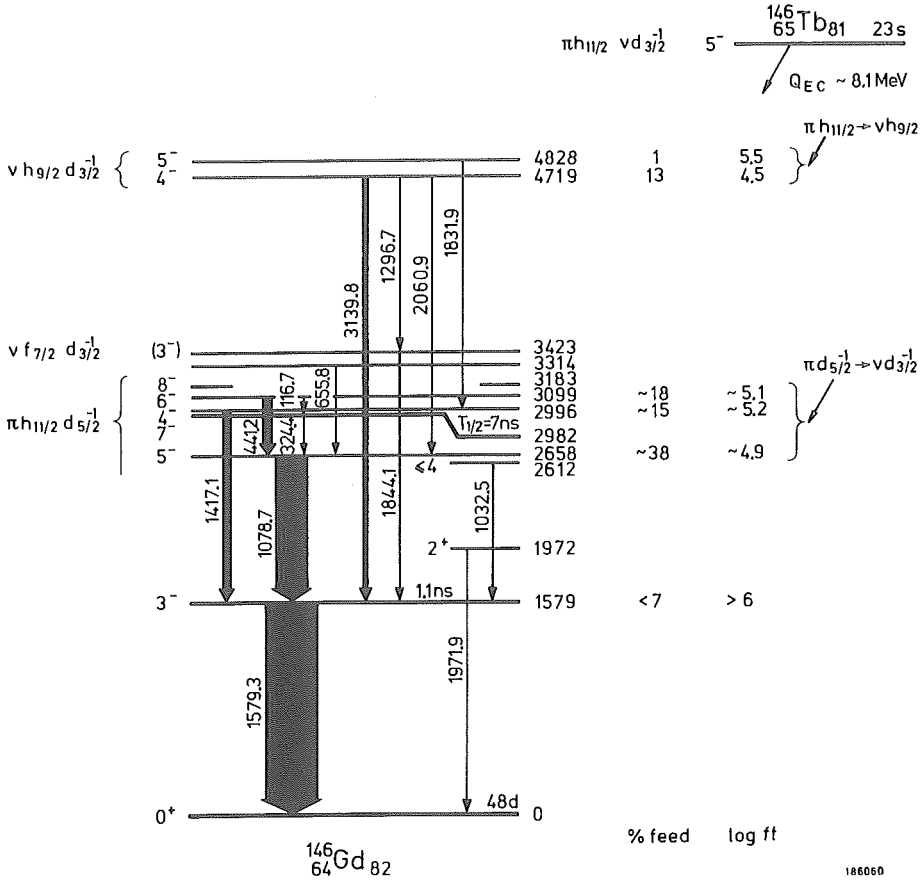

Fig. 1: Decay scheme of 23 s ^{146}Tb. For feeding of 1972 keV 2^+ state see text.

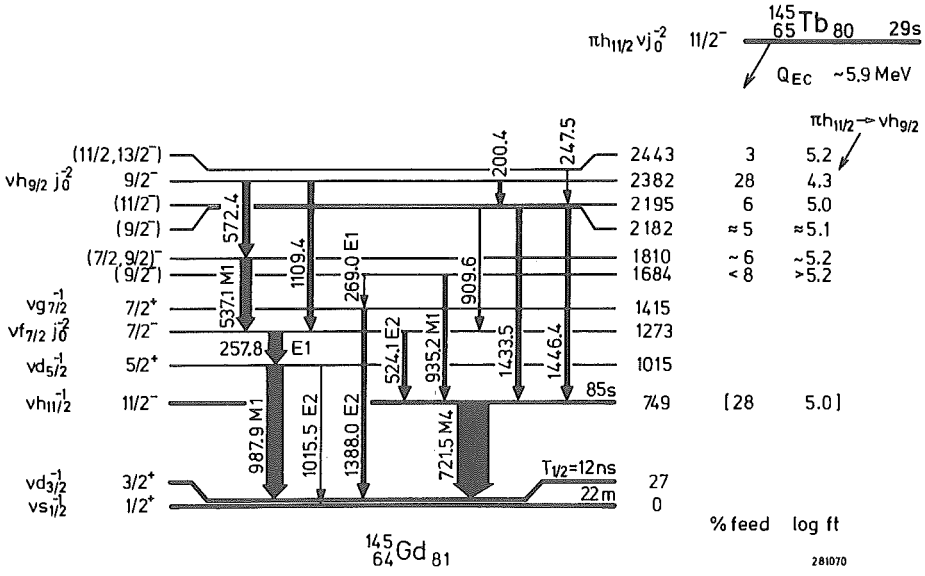

Fig. 2: Decay scheme of 29 s ^{145}Tb. The Q_{EC} value is derived from comparison with ^{147}Tb; it is assumed that the 0^+ neutron hole pair of ^{145}Tb will not affect the Q_{EC} ($\pi h_{11/2} \rightarrow \nu h_{9/2}$) value. The transition multipolarities are from the (^{3}He,3n) reaction study[11]. Due to recent modifications of the in-beam results[11] we have placed the 1446 keV transition feeding the 85 s isomer, in contrast to our earlier reported[13] scheme. The direct β-feed to the 85 s $11/2^-$ state is estimated from comparison with 1.8 min ^{147}Tb decay.

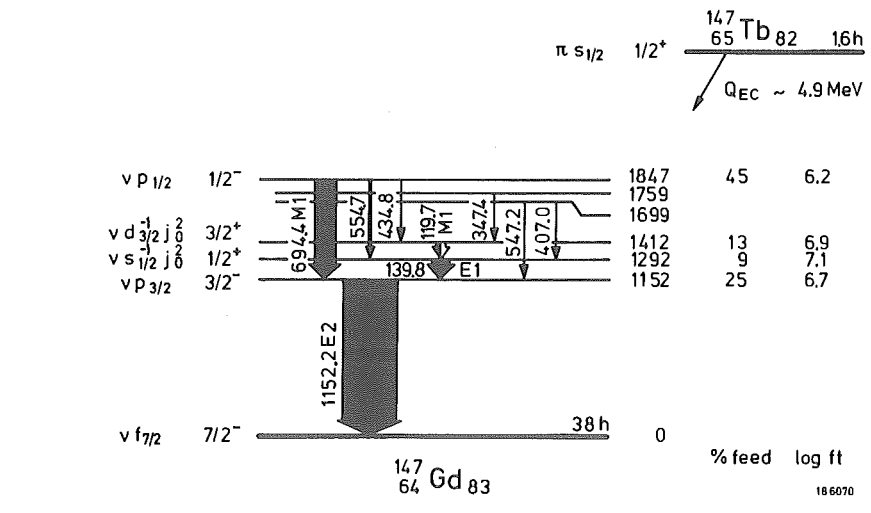

Fig. 3: Decay scheme of 1.6 h ^{147}Tb. The Q_{EC} value is from Ref. 12, assuming that the $1/2^+$ and $11/2^-$ ^{147}Tb β-activities lie close[3] in energy.

Our data on 1.6 h ^{147}Tb β decay are given in Fig. 3. The energy levels are in agreement with those reported[4] earlier, but the new $1/2^+$ assignment[3] for 1.6 h ^{147}Tb, together with new data on transition multipolarities lead to a revision of the ^{147}Gd spin parity assignments. In addition to the $\nu p_{3/2}$ state at 1152 keV now also the $\nu p_{1/2}$ level is identified at 1847 keV. We interpret the 1292 and 1412 keV levels respectively as $\nu s^{-1}_{1/2} j^2_0$ and $\nu d^{-1}_{3/2} j^2_0$ 2p1h excitations.

In conclusion, the present β-decay studies have located neutron particle hole states in ^{146}Gd and in the two neighbouring isotopes. These results provide the first spectroscopic information on the neutron gap in ^{146}Gd which is of crucial importance for calculation of high-spin isomers in this region involving neutron excitations across the shell. From a pairing analysis of our findings Chasman[14] derives a value of 3.05 MeV for the N=82 gap, which is significantly smaller than previously assumed.

References

1) P. Kleinheinz, R. Broda, P.J. Daly, S. Lunardi, M. Ogawa, J. Blomqvist, Z. Physik A290 (1979) 279

2) R.R. Chasman, Phys. Rev. C21 (1980) 456

3) Y. Nagai, J. Styczen, M. Piiparinen, P. Kleinheinz, D. Bazzacco, P. v. Brentano, K.O. Zell, J. Blomqvist, Phys. Rev. Lett. 47 (1981) 1259

4) E. Newman, K.S. Toth, D.C. Hensley, W.-D. Schmidt-Ott, Phys. Rev. C9 (1974) 674

5) K.S. Toth, Phys. Rev. C22 (1980) 1341

6) M. Ogawa, R. Broda, K. Zell, P.J. Daly, P. Kleinheinz, Phys. Rev. Lett. 41 (1978) 289

7) G. Colombo, R. Geier, H. Hick, P. Komninos, G. Korschinek, P. Kubik, H. Morinaga, E. Nolte, W. Schollmeier, DPG Verhandlungen 4/1981, ISSN 0420-0195 p. 775, and E. Nolte, private communication.

8) K.S. Toth, C.R. Bingham, D.C. Sousa, A.C. Kahler, D.R. Zolnowski, BAPS 25 (1980) No. 4

9) G.D. Alkhazov et al., Proc. XXXI Symp. Nucl. Spectr. and Nucl. Struct. Samarkand, April 1981, p. 97

10) D.R. Haenni, H. Beuscher, R.M. Lieder, M. Müller-Veggian, A. Neskakis, C. Mayer-Böricke, Proc. Conf. on Structure of Medium-Heavy Nuclei, Rhodos, (1979) p. 300

11) A. Pakkanen, J. Muhonen, M. Piiparinen, J. Blomqvist, Dept. of Physics, Univ. of Jyväskylä, Res. Report No. 5/1981 and Nucl. Phys. in press and P. v. Brentano, D. Bazzacco, C. Protop, Europhys. Conf. Nucl. and Atomic Phys. with Heavy Ions, Bucharest, 1981

12) J. Blomqvist, P. Kleinheinz, R. Broda, P.J. Daly to be published

13) J. Styczen, P. Kleinheinz, M. Piiparinen, J. Blomqvist, HECFOS, July 1981, CERN 81-09 p. 548

14) R.R. Chasman Preprint, Aug. 1981 submitted to Phys. Lett. B.

2.13. Two-Phonon Octupole Excitation in ^{147}Gd

P. Kleinheinz, J. Styczen, M. Piiparinen, J. Blomqvist[+] and M. Kortelahti[++]

In ^{146}Gd the octupole phonon lies 1 MeV lower than in ^{208}Pb, at 1.6 MeV, and in the neighbouring ^{147}Gd nucleus it occurs as low as 1 MeV. This low excitation makes this nucleus particularly favourable for a study of two-phonon octupole excitations.

Earlier we has observed[1] a $19/2^-$ level in ^{147}Gd at 2.572 MeV which decays through two stretched E3 transitions to the $f_{7/2}$ ground state (fig. 1). In ref. 1 we suggested that this level must have a significant $\nu f_{7/2} \times 3^- \times 3^-$ two-phonon contribution, but at that time the experimental data were insufficient to determine the properties of this state in detail. Since then, more quantitative knowledge has emerged on particle octupole coupling phenomena in this region[2,3]. These couplings will also strongly affect the two-phonon excitations.

We have now determined the strength of the 1575 keV $19/2^- \rightarrow 13/2^+$ E3 transition through a measurement of the $19/2^-$ level half life using the (^{3}He,3n) reaction where the direct side feeding to the state is $\sim$ 3 times larger than the population through the above-lying 5 ns isomer (fig. 1)

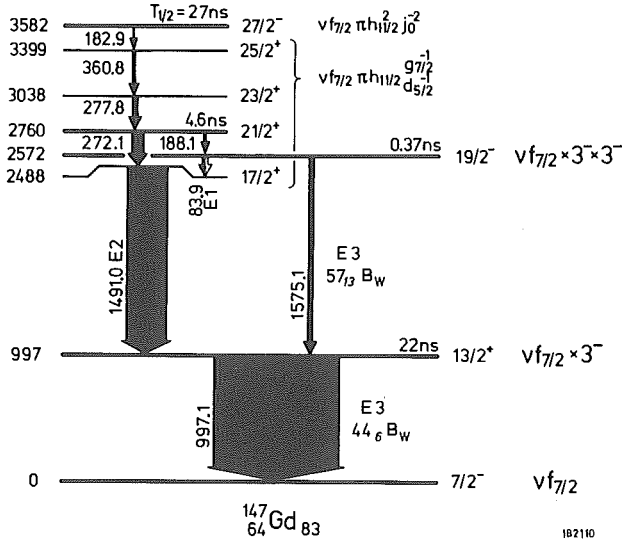

Fig. 1: High spin levels in ^{147}Gd with intensities as observed in (^{3}He,3n) at $E_{^3He}$ = 22 MeV.

This makes it possible to determine the half life from a singles measurement of the time delay of 1575 K electrons relative to the beam bursts. The conversion electrons were focussed in a magnetic lens spectrometer operated in swept-current mode and energy analyzed in a Si(Li) spectrometer[4]. From two independent measurements, with 22 MeV and 27 MeV ^{3}He beams we obtain the result

$$T_{1/2}(19/2^-, 2.572\ \text{MeV}) = 370 \pm 80\ \text{ps}.$$

Figure 2 shows the measured time centroids for 27 MeV beam energy, where the 1.579 MeV 3^- level of ^{146}Gd was also populated. For its half life we find $T_{1/2}(3^-, 1.579\ \text{MeV})$=

1.06(6) ns in perfect agreement with the earlier[5] result. Taking into account the 1575 to 84 keV branching ratio the measured $19/2^-$ half life gives

$$B(E3,\ 1575\ keV) = 57 \pm 13\ W.u.$$

This very high transition strength emphasizes the two-phonon character of the $19/2^-$ level.

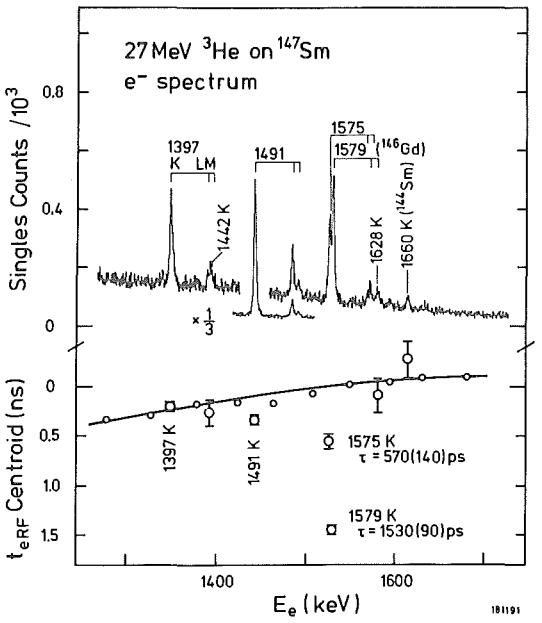

Fig. 2: Half life measurement for the 2.572 MeV $19/2^-$ state in ^{147}Gd. The electronic walk is obtained from prompt conversion lines (big dots) and from background electrons (small dots).

The simplest expectation is that the two-phonon state should occur at twice the energy of the one-phonon state and should decay with a rate twice as large as the one-phonon transition. It is apparent that the experimental findings deviate from these simple predictions for both energy and transition rate.

Two different phenomena are expected to affect the energy of the two-phonon state in ^{147}Gd. The first is associated with the coupling of the neutron $f_{7/2} \rightarrow i_{13/2}$ excitation to the octupole vibration, while the second reflects the action of the Pauli principle between the particle-hole components of the two phonons.

The $13/2^+$ level at 1.00 MeV has a considerable admixture of the $i_{13/2}$ single neutron state due to the large coupling matrix element $m = \langle i_{13/2}|H|f_{7/2} \times 3^-;\ 13/2\rangle$. The situation is basically similar to that observed in the N = 127 nucleus ^{209}Pb, where the corresponding single particle orbits are $\nu g_{9/2}$ and $\nu j_{15/2}$ (fig. 3). Whereas in ^{209}Pb the 1.42 MeV $15/2^-$ state is of ~70 % single particle character[6] with about 30 % admixture of $\nu g_{9/2} \times 3^-$, the situation is reversed in ^{147}Gd, where the octupole lies lower[3] in energy than the $\nu i_{13/2}$ single particle state.

When the difference δ between the single particle excitation energy and the phonon energy, $\delta = (\varepsilon_{13/2} - \varepsilon_{7/2}) - \hbar\omega_3$, is comparable to the coupling matrix element m, the energy E of the low-lying mixed state is obtained by diagonalizing the 2 x 2 Hamiltonian

$$E_{13/2} = \hbar\omega_3 - \frac{1}{2}\left(\sqrt{\delta^2 + 4m^2} - \delta\right).$$

Similarly, the energy of the lowest $19/2^-$ state is obtained by diagonalizing the Hamiltonian in the basis of the two states $f_{7/2} \times 3^- \times 3^-$ and $i_{13/2} \times 3^-$

$$E_{19/2} = 2\hbar\omega_3 - \frac{1}{2}\left(\sqrt{\delta^2 + 8m^2} - \delta\right).$$

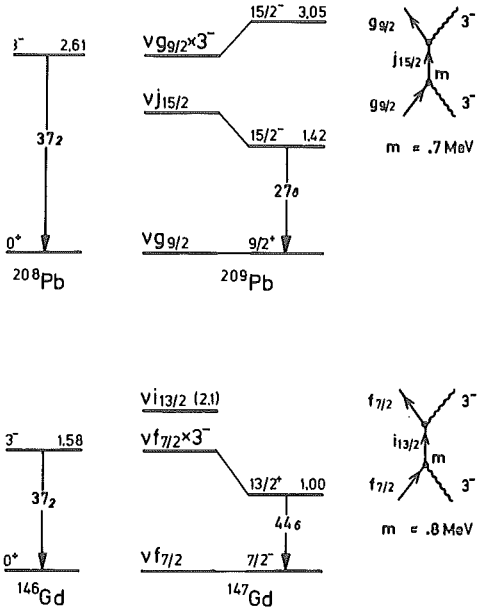

Fig. 3: Coupling of the valence neutron to the core octupole in ^{209}Pb and ^{147}Gd.

Whereas in second order perturbation theory the harmonic spectrum is preserved, the result is modified however for strong coupling, as in the present situation. $E_{19/2}$ is higher than 2 x $E_{13/2}$ by the amount

$$\delta E_{19/2} = \sqrt{\delta^2 + 4m^2} - \frac{1}{2}\left(\sqrt{\delta^2 + 8m^2} + \delta\right).$$

The unperturbed $\nu i_{13/2}$ energy in ^{147}Gd (and hence δ) is not well known experimentally. However, as discussed in ref. 3, systematics of the N = 83 isotones and other indirect spectroscopic evidence suggest approximately 2.1 MeV for the $f_{7/2}$ to $i_{13/2}$ single particle energy separation, which is indicated in fig. 3. Thus using δ = 0.52 MeV, the observed $E_{13/2}$ = 1.00 MeV excitation is reproduced with m = 0.8 MeV. These values give $E_{19/2}$ = +0.26 MeV.

The second effect is associated with the microscopic composition of the octupole phonon. In the $\pi h_{11/2} \times 3^-$ particle-phonon multiplet in ^{147}Tb it was seen[2] clearly that the $\pi h_{11/2}\, d_{7/2}^{-1}$ particle hole component occurs with large probability in the 3^- core state. The $17/2^+$ and $15/2^+$ members of this multiplet are separated by the large energy of 772 keV. This can be understood as an effect of the Pauli principle where the $h_{11/2}$ proton particle in the phonon interferes with the $h_{11/2}$ valence proton. The associated particle-phonon interaction matrix element

M in the exchange process (fig. 4) is obtained from the 772 keV $17/2^+$ to $15/2^+$ splitting to be

$$M \simeq 1.1 \text{ MeV}.$$

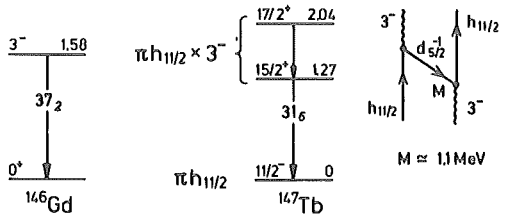

Fig. 4: Coupling of the $h_{11/2}$ valence proton of ^{147}Tb to the core octupole.

The two-phonon exchange process, which is analogous to the exchange coupling in fig. 4, is illustrated in the fourth order diagram of fig. 5a. The large $\pi h_{11/2} d_{5/2}^{-1}$ components in the two octupole phonons interact by exchanging the particle (or the hole). The interaction vertices in figs. 4 and 5 are the same, and we can therefore use the empirical values of M and Δ which describe the Pauli effect in the ^{147}Tb case to evaluate the energy shift δE_I corresponding to the diagram in fig. 5a. The shift is given by the expression

$$\delta E_I = 98\ X\ (\tfrac{11}{2}\ \tfrac{5}{2}\ 3;\ \tfrac{5}{2}\ \tfrac{11}{2}\ 3;\ 3\ 3\ I) \times \frac{M^4}{\Delta^3}$$

where I is the coupled angular momentum of the two phonons. For the case I = 6 the geometric coefficient is 98 X = + 0.846 giving the energy shift

$$\delta E_6 \simeq 0.846 \times \frac{1.1^4}{1.5^3} \text{ MeV} = +0.41 \text{ MeV}.$$

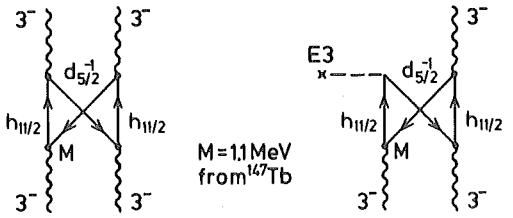

Fig. 5: a) Phonon-phonon coupling in ^{146}Gd; b) Diagram representing the correction to the two-phonon to one-phonon E3 transition amplitude.

This shift can also be adopted for the $19/2^-$ state of ^{147}Gd, neglecting the $\nu i_{13/2} \times 3^-$ content in that state. This approximation may be of similar quality as the use of fourth order perturbation theory in describing the $3^- \times 3^-$ coupling.

Summing up the two contributions the total energy shift ΔE for the $19/2^-$ state is

$$\delta E = \delta E_{19/2} + \delta E_6 = (0.26 + 0.41) \text{ MeV} = 0.67 \text{ MeV},$$

which compares well with the experimental shift

$$\delta E_{exp} = (E_{19/2} - E_{13/2}) - (E_{13/2} - E_{7/2}) = 0.58 \text{ MeV}.$$

Processes similar to those causing the energy shifts discussed above will also give rise to a reduction of the 19/2 to 13/2 E3 strength. The main effect comes from the third order diagram in fig. 5b. The transition rate between the two-phonon and one-phonon states changes by

$$\delta B(E3, I \to 3) = -392\ X(\tfrac{11}{2}\ \tfrac{5}{2}\ 3;\ \tfrac{5}{2}\ \tfrac{11}{2}\ 3;\ 3\ 3\ I) \times \frac{M^3}{\Delta^2}$$

$$\times \sqrt{B(E3, 3 \to 0) \times B(E3, h_{11/2}\, d_{5/2}^{-1} \to 0)}.$$

Using the estimate $B(E3, h_{11/2}\, d_{5/2}^{-1} \to 0) = 5$ W.u. the reduction in the case I = 6 is $B(E3, 6 \to 3) = -18$ W.u. This is of the correct order of magnitude to explain the observed deviation from the harmonic expectation.

The present data provide the first clear indication of a two-phonon octupole state. It has been shown that the large departure of the two-phonon excitation from harmonic vibration (twice the one-phonon energy, and twice the transition rate) can be quantitatively understood in terms of the microscopic composition of the states, and can be derived from other observed features of the octupole vibrations in this region.

+ Research Institute of Physics, Stockholm, Sweden
++ University of Jyväskylä, Finland

References

1) P. Kleinheinz, R. Broda, P.J. Daly, S. Lunardi, M. Ogawa, J. Blomqvist, Z. Physik A290, 279 (1979)
2) R. Broda, M. Behar, P. Kleinheinz, P.J. Daly, J. Blomqvist, Z. Physik A293, 135 (1979)
3) P.J. Daly, P. Kleinheinz, R. Broda, S. Lunardi, H. Backe, J. Blomqvist, Z. Physik A298, 173 (1980)
4) M. Luontama, J. Kantele, R. Julin, A. Passoja, T. Poikolainen, M. Pyvänäinen, Nucl. Instr. & Meth. 159, 339 (1979)
5) P. Kleinheinz, M. Ogawa, R. Broda, P.J. Daly, D. Haenni, H. Beuscher, A. Kleinrahm, Z. Physik A286, 27 (1978)
6) A. Bohr and B. Mottelson, Nuclear Structure Vol. II (Benjamin 1975) p. 564 ff.

2.14. Study of Side Bands in ^{180}Os

A. Neskakis, R.M. Lieder, G. Sletten, H. Beuscher, B. Bochev, D.R. Haenni and M. Müller-Veggian*

The study of the level scheme of ^{180}Os has been continued. Timing spectra have been measured at the Jülich Isochronous cyclotron using the ^{180}W(α,4n) reaction at 54 MeV. Conversion electron spectra where studied at the Niels Bohr Institute Tandem Van de Graaff accelerator using the ^{168}Er(^{16}O,4n) reaction at 83 MeV. These studies were carried out to complement previous investigations. In the earlier experiment γ-γ coincidences and γ-ray angular distributions have been measured. In these investigations ^{180}Os was produced at the Jülich isochronous cyclotron using the ^{182}W(α,6n) and ^{182}W(^{3}He,5n) reactions at beam energies of 80 and 50 MeV, respectively.

The level scheme of ^{180}Os as resulting from the present experiments is shown in Fig. 1. The yrast band was established up to the 20^+ level. Furthermore, four side bands have been observed. One of them is based on an isomer which was not reported before. Our assignment of levels to the yrast band differs above I=14 from that given by Dracoulis et al.[1]. They considered those levels as yrast states which we assigned to band 4 (cf. Fig. 1). Dracoulis et al.[1] based their assignments on

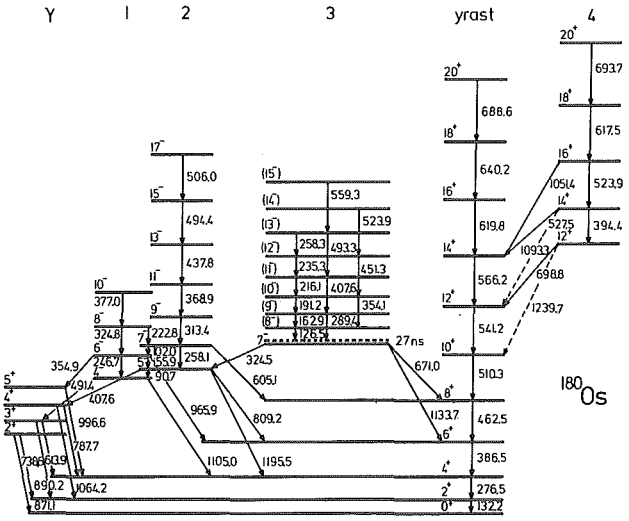

Figure 1: Partial level scheme of ^{180}Os. All transitions were placed considering coincidence data except for those indicated by dashed lines. They were observed in γ-ray singles spectra.

the assumption that the 527.5 and 698.8 keV γ rays are stretched E2 transitions since their angular distributions have large positive anisotropies. In the present study we determined the conversion coefficients of these lines and found that they are of mixed M1/E2 character. The angular distributions and conversion coefficients of the 527.5 and 698.8 keV lines can, therefore, only be understood if they connect levels of same spin yielding the spin assignments given in Fig. 1. They are considered as interband transitions deexciting band 4 into the yrast band. Our spin assignments are supported by the observation of the 1051.4, 1093.3 and 1239.7 keV transitions, which connect levels of band 4 and the yrast band with spin differences ΔI=2.

The bands 1 and 2 were established up to spins of I=10 and I=17, respectively. The low-spin members of bands 1 and 2 are connected by low-energy γ rays which are interpreted as cascade transitions. Spin-parity assignments result from angular-distribution and conversion-electron measurements.

Band 3 is a strongly coupled band based on an isomer with a half life of 27±5 ns. This band is deexcited by the 324.5 keV line of stretched quadrupole character (ΔI=2) into band 2 and by stretched dipole transitions (ΔI=1) of 671.0 and 1133.7 keV into the yrast band. We consider the 324.5 keV γ ray to have E2 character since enhanced M2 transitions are not known. This γ ray would be enhanced by a factor of 4.1 with respect to the Weisskopf estimate if it was a M2 transition. Therefore, a spin and parity of 7^- was assigned to the level deexcited by these transitions. We assume that the 7^- state is the isomer and forms the band head. However, it cannot be excluded completely that a transition of small energy exists, deexciting the isomer into the 7^- state, which escaped detection. Therefore, a hypothetical level is included in Fig. 1 as a dashed line and the spin-parity assignments of the band members are given in brackets. The K quantum number may be K=7 or 8.

In order to understand the nature of the isomeric band, its inertial parameter $(E_I-E_{I-1})/2I$ has been plotted as a function of I^2 in Fig. 2 as well as that of the isomeric $K^\pi=8^-$ band in ^{182}Os and the (7^-) band in ^{178}W (ref. 2). It can be seen that the inertial parameters of the isomeric bands in ^{180}Os and ^{178}W increase strongly with I^2 for small spins whereas that of the 8^- band in ^{182}Os is almost constant. The fact that the inertial parameter is larger for ^{180}Os than for ^{178}W may be caused by a decrease of the deformation. It may be concluded that the bands in ^{180}Os and ^{178}W have the same configuration which is different from that of the 8^- band in ^{182}Os. Therefore, a K=7 assignment is proposed for the isomeric band in ^{180}Os. It may have a $(\nu 7/2^+|633|(x)\ \nu 7/2^-|514|)_{7^-}$ configuration as suggested by Dors et al.[3] for the (7^-) band in ^{178}W. In order to support this suggestion the gyromagnetic ratio g_K has been deduced for band 3. From the dipole-quadrupole mixing ratios δ of the cascade transitions, the quantity $(g_K-g_R)^2/Q_0^2$ was determined to be $(3.8\pm1.6)\cdot10^{-4}$. Assuming a rotational g factor g_R=0.22 0.02 and an intrinsic quadrupole moment Q_0=6.0±0.6 (ref. 4) we found g_K=0.10±0.04. This value

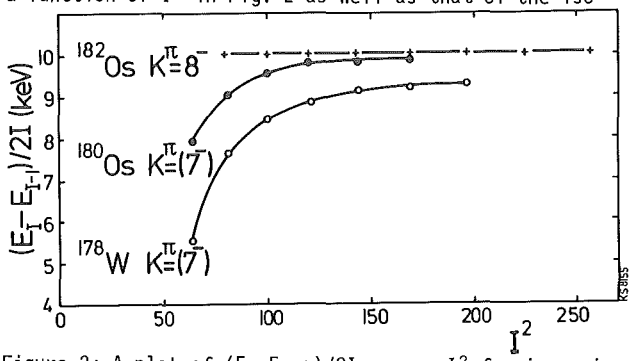

Figure 2: A plot of $(E_I-E_{I-1})/2I$ versus I^2 for isomeric bands in ^{178}W and ^{180,182}Os.

agrees approximately with the theoretical prediction for the above configuration[3] supporting our assignments.

References

1) G. Dracoulis, C. Fahlander, M.P. Fewell, Phys. Rev. Lett. 45 (1980) 1831; G. Dracoulis, J. Physique L-10, suppl. 12, 41 (1980) 66

2) R.M. Lieder, G. Sletten, J. Borggreen, J. Pedersen, Nucl. Phys. to be published; R.M. Lieder, Proc. Workshop on Nuclear Structure, Trieste, 1981, Nucl. Phys. to be published

3) C.L. Dors, J.M. Bernthal, T.L. Khoo, C.H. King, Nucl. Phys. A314 (1979) 61

4) K. Kumar, M. Baranger, Nucl. Phys. A110 (1968) 529

*Niels Bohr Institute, Copenhagen

2.15. Interpretation of side bands in ^{180}Os in the framework of the cranked shell model

A. Neskakis, R.M. Lieder, G. Sletten, H. Beuscher, B. Bochev, D.R. Haenni and M. Müller-Veggian*

The features of side bands in deformed nuclei have in many cases been successfully interpreted in the framework of the cranked shell model[1] yielding new information on the band-crossing phenomenon. In ^{182}Os eight side bands have been observed[2]. Three of these bands show a backbending effect whereas the other bands behave regularly in some cases even up to rather large rotational frequencies. The interpretation of the latter effect in terms of the cranked shell model revealed properties hitherto unknown[2]. To obtain more information about these new features it is important to analyse the side bands in the neighbouring nucleus ^{180}Os in the same way.

In order to interprete the bands observed in ^{180}Os in terms of the cranked shell model[1] the aligned angular momentum i has been plotted for all bands versus the rotational frequency $\hbar\omega$ in Fig. 1. The reference band used

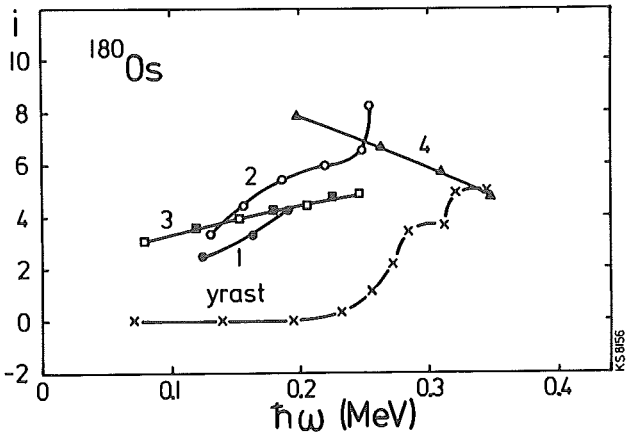

Figure 1: Alignment plot for all bands observed in ^{180}Os.

in the calculation of i was the ground (g) band which has been fitted by the Harris formula (Θ_0=21.7 MeV$^{-1}\hbar^2$, Θ_1=171.4 MeV$^{-3}\hbar^4$). The yrast band does not show a backbending effect like ^{182,184,186}Os but forward-bending. This behaviour can be understood if a strong interaction of $\approx$ 320 keV exists between the g band and the s band being a two-quasiparticle band consisting of a pair of rotation-aligned $i_{13/2}$ quasineutrons. This result is in agreement with predictions of the cranked shell model[1] but contradicts to the conclusions of Dracoulis et al.[3]. The aligned angular momentum of the yrast band shows a kink at a rotational frequency of $\approx$ 0.3 MeV which may result from an intersection with a four-quasiparticle band.

The negative-parity bands 1 and 2 in ^{180}Os have a similar structure as the bands 2 and 3 in ^{182}Os (ref. 2) indicating that they may have the same nature, viz. a $\nu 9/2^+|624|(x)\nu 7/2^-|514|$configuration. Band 2 in ^{180}Os shows a backbending effect at a frequency of $\hbar\omega \approx$ 0.25 MeV whereas the corresponding band 2 in ^{182}Os has no bandcrossing below $\hbar\omega \approx$ 0.33 MeV. This variation in crossing frequency may be attributed to a change of

the hexadecapole deformation ε_4 between ^{180}Os and ^{182}Os (ref. 4).

Band 4 is of special interest since it has a large aligned angular momentum already at small rotational frequencies and shows no band crossing up to $\hbar\omega \approx 0.35$ MeV. The decrease of aligned angular momentum with increasing frequency is probably unreal and caused by the chosen reference. Band 4 in ^{180}Os may correspond to band 6 in ^{182}Os of $\nu 9/2^+|624|(x)\nu 7/2^+|633|$ configuration[2]. The latter band shows no backbending up to $\hbar\omega \approx 0.38$ MeV, a fact which has been attributed in the framework of the cranked shell model to a new type of interaction[2]. A similar interpretation may apply to band 4 in ^{180}Os.

References

1) R. Bengtsson and S. Frauendorf, Nucl. Phys. A314 (1979) 27 and A327 (1979) 139

2) R.M. Lieder, G. Sletten, J. Borggreen, J. Pedersen, Nucl. Phys. to be published; R.M. Lieder, Proc. Workshop on Nuclear Structure, Trieste, 1981, Nucl. Phys. to be published; R.M. Lieder, G. Sletten, J. Borggreen and J. Pedersen, contribution to this Annual Report

3) G. Dracoulis, C. Fahlander, M.P. Fewell, Phys. Rev. Lett. 45 (1980) 1831; G. Dracoulis, J. Physique L-10, suppl. 12, 41 (1980) 66

4) J.D. Garrett, S. Frauendorf, to be published

*Niels Bohr Institute, Copenhagen

2.16. Blocking effects in side bands of ^{182}Os

R.M. Lieder, G. Sletten, J. Borggreen*, and J. Pedersen**

The level scheme of ^{182}Os is given in a separate contribution to this annual report[1]. Here the interesting feature of the positive-parity bands 6 and 7 shall be discussed that they show no backbending effect up to frequencies of $\hbar\omega = 0.38$ MeV as can be seen in fig. 1.

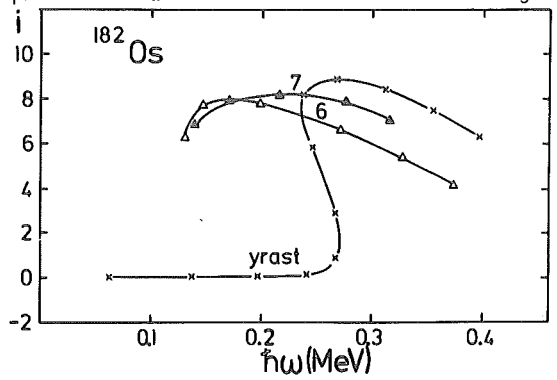

Figure 1: Plot of the aligned angular momentum i vs. the rotational frequency $\hbar\omega$ for selected bands observed in ^{182}Os.

Furthermore they have aligned angular momenta which are almost as large as those of the s band. Also, the dependence of the aligned angular momenta on the rotational frequency is similar for these three bands. Since interband transitions exist between band 7 and 6 they are considered to form the two sequences with signatures of $|\alpha|=1$ and $\alpha=0$ of a band of one and the same configuration. These features of bands 6 and 7 can be understood in a plausible way assuming that they are formed by two $i_{13/2}$ quasineutrons of $9/2^+[624]$ and $7/2^+[633]$ configurations[2]. To understand the absence of crossings in bands 6 and 7, the experimental quasiparticle energies are compared in fig. 2 with those of the calcula-

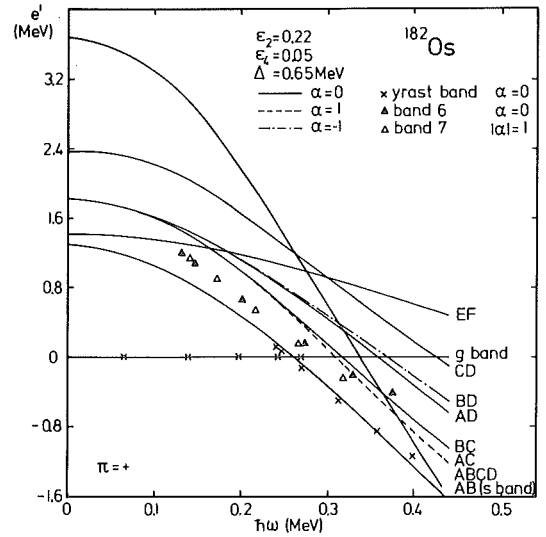

Figure 2: Plot of calculated quasiparticle energies as function of the rotational frequency for two- and four-quasineutron levels of positive parity. The g band serves as reference. The experimental quasiparticle energies of bands 6, 7 in ^{182}Os are included.

ted lowest-lying two- and four-quasineutron levels of positive parity. In this calculation the g band has been used as reference. Bands 6 and 7 may be identified with

the levels BC and AC, respectively. The fact that band 7 ($|\alpha|=1$) shows no crossing can be understood in the following way (cf. fig. 2): With the help of the levels A, B, C, D of $i_{13/2}$ quasineutron configuration only two-quasineutron levels but no four-quasineutron levels of $\alpha=\pm1$ can be constructed, viz. the levels AC and BD. In order to obtain levels which could interact with AC or BD other configurations have to be involved which lie higher in quasiparticle energy. The resulting crossings are consequently expected to lie at considerably larger frequencies. This effect may be called double blocking since levels deriving from two different $i_{13/2}$ quasineutron orbitals of $9/2^+[624]$ and $7/2^+[633]$ configurations are occupied. Such an explanation cannot be applied to band 6 ($\alpha=0$) since a four-quasineutron level ABCD of signature $\alpha=0$ exists which crosses the two-quasineutron level BC of same signature at the frequency $\hbar\omega_{AD}$ = 0.36 MeV. Band 6, however, does not show any crossing up to the rotational frequency $\hbar\omega$ = 0.38 MeV.

The absence of a crossing in band 6 can be understood if one interprets the quasiparticle diagram of fig. 3 in

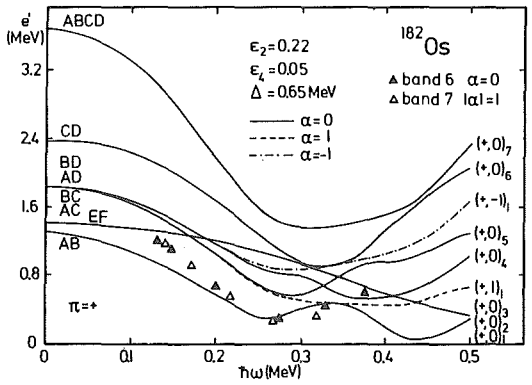

Figure 3: Plot of calculated quasiparticle energies as function of rotational frequency for levels of positive parity for even numbers of quasiparticles. The yrast band labelled as $(+,0)_1$ serves as reference. The experimental energies of bands 6, 7 in ^{182}Os are included.

ref. 1 in a new way as suggested by Bohr and Mottelson[3]. Their proposal concerns the use of an appropriate reference band. Sofar the g band was used as reference. This choice has the disadvantage that the g band levels are not any more yrast states beyond the crossing of the yrast band. Bohr and Mottelson suggested, therefore, to use the quasiparticle vacuum as reference which is in general identical with the yrast band. The theoretical quasiparticle energies for many-quasiparticle configurations can be directly derived from fig. 3 in ref. 1 by adding the quasiparticle energies of the single-quasiparticle levels.

In fig. 3 the quasiparticle energies of the lowest-lying quasineutron levels of positive parity for even numbers of quasiparticles are plotted vs. the rotational frequency. These levels are labelled by their parity and signature quantum numbers and by an index which counts the levels of same quantum numbers. The yrast band with $e'(\hbar\omega)=0$ is labelled $(+,0)_1$. On the left hand side the configurations are indicated by letters, being applicable only for small rotational frequencies. Fig. 3 furthermore contains the experimental quasiparticle energies of bands 6, 7 in ^{182}Os. Band 7 can be identified with the level $(+,1)_1$ which derives from the configuration AC in agreement with the previous interpretation. No new aspect results. A new situation arises, however, for band 6. For small frequencies band 6 can be identified with the level $(+,0)_5$ of configuration BC. This level is crossed at a frequency of $\hbar\omega$=0.33 MeV by the level $(+,0)_4$. If an interaction between these two levels would occur, they would repell each other producing new trajectories. For an interaction strength of $\approx$ 150 keV the lower-lying of the two new trajectories would obtain a similar frequency dependence of the quasiparticle energy as the level $(+,1)_1$ indicating that the band crossing predicted previously on the basis of fig. 2 vanishes. In this way the absence of backbending in band 6 could be explained. Such an interaction is not contained in the cranked shell model calculations of Bengtsson and Frauendorf[4]. Therefore, the existence of a new type of interaction is proposed here. It may be a two-body interaction. For a detailed comparision of the features of bands 6 and 7 with theoretical predictions, calculations taking into account the proposed new interaction have to be carried out.

References

1) R.M. Lieder, G. Sletten, J. Borggreen and J. Pedersen, Separate contibution to this annual report

2) R.M. Lieder, G. Sletten, J. Borggreen and J. Pedersen, Nucl. Phys. A375 (1982) 291

3) A. Bohr and B.R. Mottelson, private communcation, 1981

4) R. Bengtsson and S. Frauendorf, Nucl. Phys. A327 (1979) 139

*Niels Bohr Institute, Copenhagen

2.17. Negative-parity side bands in ^{182}Os

R.M. Lieder, G. Sletten, J. Borggreen*, and J. Pedersen**

The study of ^{182}Os has been continued. The level scheme of ^{182}Os is shown in fig. 1. Eight side bands have been established. Bands 1 and 8 have the characters of strongly coupled bands, i.e., the spin sequence is $\Delta I=1$ and crossover as well as cascade transitions exist. Bands 2 to 7 consist of stretched E2 cascades. They can be identified as rotation-aligned bands. The side bands in ^{182}Os start at spins ranging from I=4 to I=12. Except for band 8, the lowest-lying states of the respective bands are considered not to be their band heads. If they were band heads, the bands should have large K values and the transitions to the yrast band, which has K=0, should be K forbidden. The band heads should then have long half lives as observed only in case of band 8. Furthermore, the transition probabilities of the interband transitions are considerably reduced by the K forbiddenes with respect to that of the intraband transitions. However, several members of each of the bands 1 to 7 decay into the yrast or γ bands. The K values of these bands are therefore probably $K \lesssim 2$. It should be mentioned that for rotation-aligned bands K is not a good quantum number.

It is of special interest to compare the features of bands 2, 3 and 8 since they most probably consist of quasi neutrons of same configuration. Configurations can be assigned to bands 2 and 3, if considered together, on the basis of the band structure, the dipole-quadrupole mixing ratios of the cascade (interband) transitions and the parity. A comparision with the level scheme of the neighbouring odd-mass isotope ^{181}Os (ref. 1) indicates that bands 2 and 3, if taken together, have a band structure similar so that of the Coriolis-mixed band formed by a $i_{13/2}$ quasineutron of predominantly $9/2^+[624]$ configuration. In both cases two sequences of stretched E2 transitions exist. Only the low-spin members of the bands are connected by cascade transitions. The dipole-quadrupole mixing ratios of the cascade transitions between bands 2 and 3 have similar values as those of the Coriolis-mixed band in ^{181}Os, viz. on average $\delta = -0.4 \pm 0.3$ and $\delta = -0.3 \pm 0.2$, respectively. The dipole-quadrupole mixing ratio δ depends on the transition matrix elements and hence in a sensitive way on the intrinsic configuration of the band. It may be concluded, therefore, that the configurations of bands 2 and 3 contain a quasineutron of $9/2^+[624]$ nature. Assuming that the low-spin branches of bands 2 and 3 are of two-quasineutron nature, the second quasineutron must have the opposite parity in order to obtain the negative parity observed experimentally for bands 2 and 3. Since they form at small spins the second excited two-quasiparticle bands above the yrast line the other quasineutron may have a $7/2^-[514]$ configuration, considering that this is the ground state configuration of ^{181}Os. Band 8 is known to consist of $9/2^+[624]$ and $7/2^-[514]$ quasineutrons as well[2]. The K value of band 8, K=8, can only be reproduced, if these quasineutrons are coupled parallel. For bands 2 and 3 they must be coupled (almost) antiparallel to reproduce the small K value. It is, therefore, worthwhile to compare the features of these bands.

Here the features of the side bands shall be interpreted in terms of the cranked shell model[3], which considers the motion of independent quasiparticles in a deformed potential rotating with the frequency $\hbar\omega$. The aligned angular momenta and quasiparticle energies of these bands are shown in fig. 2. They were calculated using the g band as reference. In the upper portion of fig. 2 it can be seen that the quasiparticle energy of band 8 is $\approx$ 0.5 MeV larger than those of bands 2 and 3. The aligned angular momenta, however, are at small frequencies very similar for all these bands as can be seen in the lower portion of fig. 2. An interesting result is that bands 2 and 8 do not show a crossing effect up to a frequency of $\approx$ 0.32 MeV.

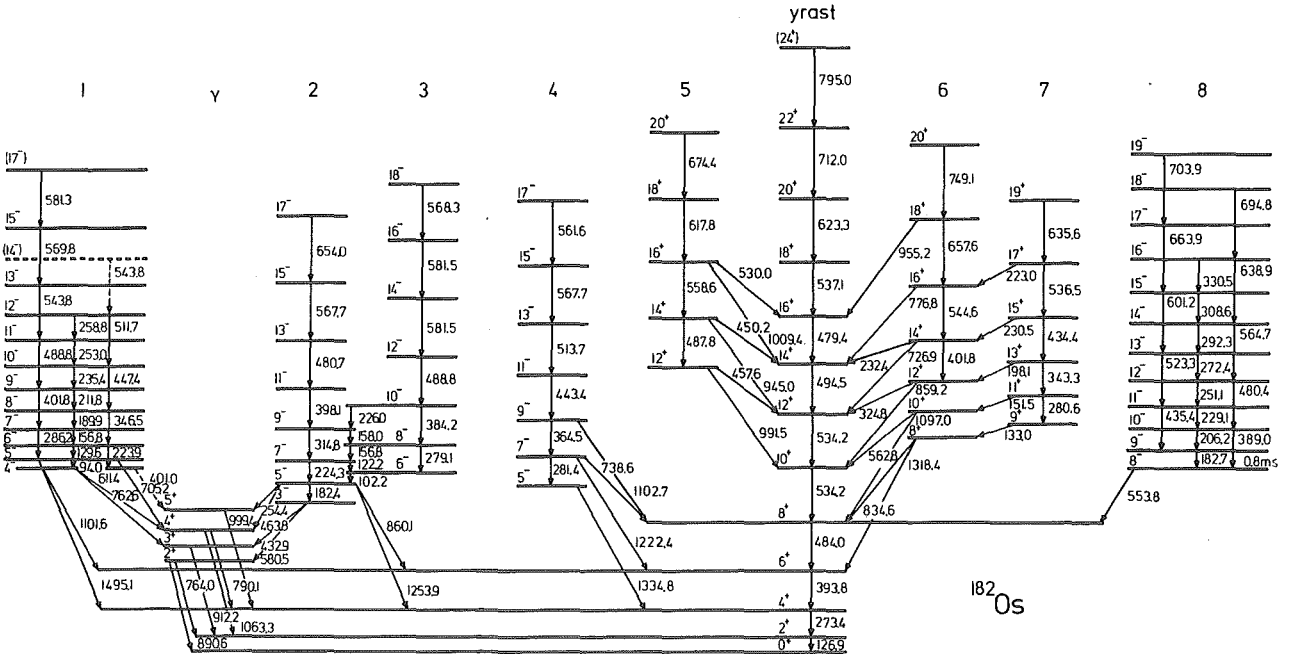

Figure 1: Partial level scheme of ^{182}Os. Uncertain placements are indicated by dahsed lines.

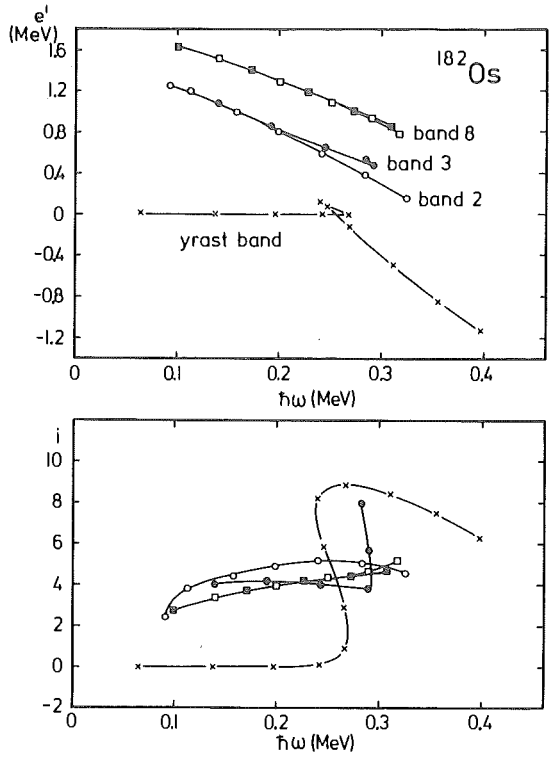

Figure 2: Plots of the quasiparticle energy e' and the aligned angular momentum i vs. the rotational frequency $\hbar\omega$ for selected bands in ^{182}Os.

In order to find an interpretation of these features calculations in the framework of the cranked shell model have been made[3]. As result of these calculations the quasineutron energies e' are plotted as function of the rotational frequency $\hbar\omega$ in fig. 3. Some of the levels in

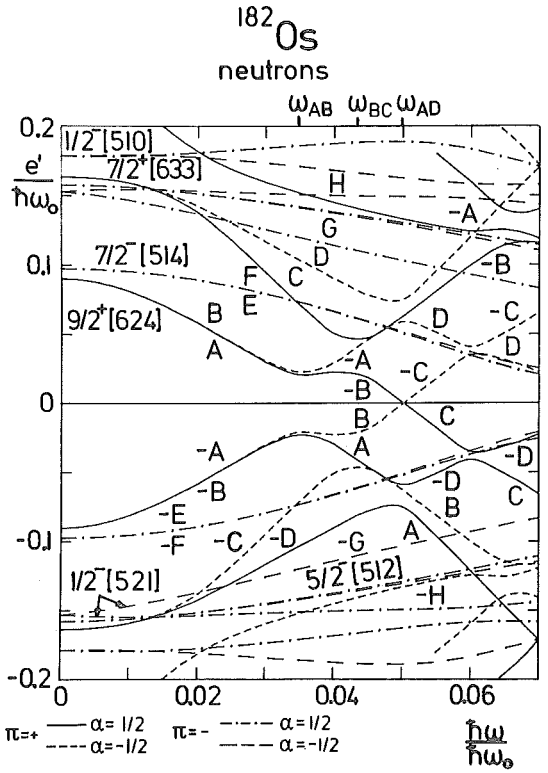

Figure 3: Calculated quasiparticle energies as function of rotational frequency for ^{182}Os. The energy unit is $\hbar\omega_0$ = 7.23 MeV. The parameters are ε_2 = 0.218, ε_4 = 0.045, Δ = 0.09 $\hbar\omega_0$ and λ = 6.72 $\hbar\omega_0$.

fig. 3 are labelled with letters to identify their configurations. In addition some of the states are identified by their asymptotic Nilsson quantum numbers, which are only meaningful at $\hbar\omega$ = 0. All levels show a splitting into two trajectories, which can be populated by only one quasiparticle each. The levels are characterized by two quantum numbers, viz. the parity π and the signature α. They result from the fact that the Hamiltonian is symmetric against inversion as well as against reflection about the x axis by 180°, respectively. The signature of single-quasiparticle states in $\alpha=\pm\frac{1}{2}$. Since quasiparticles are considered in the cranked shell model two solutions exist for each configuration. They are labelled in fig. 3, e.g., A and -A, respectively. If the level A is occupied, then the conjugate level -A, obtained by reflection about e'=0 and by changing the signature from α to $-\alpha$ must be free.

In order to compare the experimental quasiparticle energies e' of bands 2, 3 and 8 with the theoretical predictions, two- and four-quasineutron trajectories have to be calculated. In this calculation the g band has to be used as reference as well. This is achieved by reconstructing the unperturbed single quasiparticle orbits being indicated in fig. 3 by a labelling using letters. In fig. 4 the

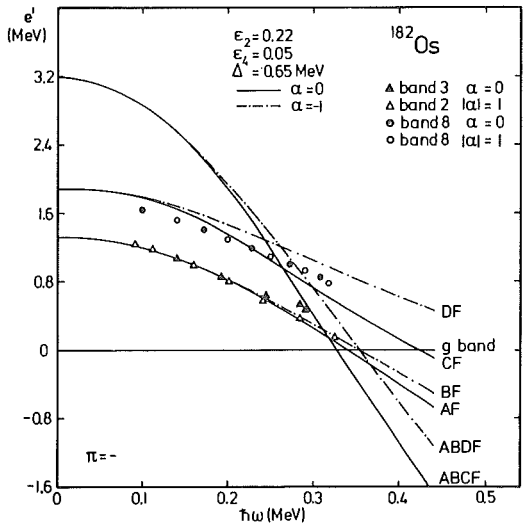

Figure 4: Plot of calculated quasiparticle energies as function of the rotational frequency for two and four-quasineutron levels of negative parity. The g band serves as reference. The experimental quasiparticle energies of bands 2, 3 and 8 in ^{182}Os are included.

quasiparticle energies of the lowest-lying two- and four-quasineutron levels of negative parity are plotted vs. the rotational frequency. They are obtained by adding the quasiparticle energies of the appropriate reconstructed single-quasiparticle levels. The experimental values for bands 2, 3 and 8 are included in fig. 4. The bands 2 and 3 lie lowest in quasiparticle energy and they may be identified at low spins with levels AF and BF, respectively, for the following reason: Band 3 (α = 0) shows a crossing at $\hbar\omega_2$ = 0.29 MeV in good agreement with the frequency $\hbar\omega_{BC}$ = 0.31 MeV at which the level ABCF (α=0) intersects the level AF (α=0). Band 2 ($|\alpha|$=1) has no crossing up to a frequency of $\hbar\omega$ = 0.33 MeV as expected if identified with the level BF (α=-1) since the intersection with level ABDF takes place only at the frequency $\hbar\omega_{AD}$ = 0.36 MeV. A serious discrepancy exists for band 8. Considering that band 8 shows no crossing up to a frequency of $\hbar\omega$ = 0.32 MeV

one would expect that, if an intersection exists at all, it may be caused by the AD crossing since the corresponding frequency is $\hbar\omega_{AD}$ = 0.36 MeV. However, the quasiparticle energy of band 8 is ≈ 0.5 MeV larger than that of the corresponding levels BF and BE, not even taking into account that level BF has already been used to interpret band 2. Considering the quasiparticle energies, the two sequences of different signature of band 8 could be identified with the levels CF (α=0) and CE (α=1), which almost coalesce. These levels are crossed by the levels ABCF and ABCE, respectively, at the frequency $\hbar\omega_{AB}$ = 0.25 MeV in clear disagreement with the experimental observations for band 8. An alternative explanation may be that band 8 has another configuration than assigned to it. However, an $i_{13/2}$ quasineutron should be involved in the configuration since the backbending of band 8 is blocked. More experimental and theoretical work seems necessary to understand the nature of band 8.

References

1) A. Neskakis, R.M. Lieder, M. Müller-Veggian, H. Beuscher, W.F. Davidson and C. Mayer-Böricke, Nucl. Phys. A261 (1976) 189

2) J. Burde, R.M. Diamond and F.S. Stephens, Nucl. Phys. 85 (1966) 481; J. Borggreen, N.J.S. Hansen, J. Pedersen, L. Westgaard, J. Zylicz and S. Bjørnholm, Nucl. Phys. A96 (1967) 561

3) R. Bengtsson and S. Frauendorf, Nucl. Phys. A327 (1979) 139

*Niels Bohr Institute, Copenhagen

2.18. High-Spin States in ^{188}Au

A. Neskakis, R.M. Lieder, H. Beuscher, B. Bochev, T. Venkova, D. Haenni, T. Morek and M. Müller-Veggian

Recently high-spin states of the odd-odd nuclei ^{190,192,194}Au have been studied[1]. This investigation has been extended to ^{188}Au in order to get more information about the structure of these nuclei. The high-spin states in ^{188}Au were populated using the (α,7n) reaction. A target prepared by gluing metallic powder of ^{191}Ir isotopically enriched to 89 % on a Mylar backing was bombarded with 90 MeV α-particles from the Jülich isochronous cyclotron JULIC. The resulting γ radiation was studied by means of standard in-beam γ spectroscopy. The level scheme of ^{188}Au resulting from these measurements is shown in fig. 1. For systematic reasons it seems plausible to assume that the high-spin isomer in ^{188}Au has spin and parity (11^-) (Ref. 1). The decay of the (11^-) isomer is not known. As can be seen in fig. 1 there are two rotational bands above the (11^-) isomer in ^{188}Au. The arguments for the assignments of the observed levels to two bands are the same as for ^{190,192,194}Au (ref. 1). The bands are built on intrinsic states with J^π of (11^-) and (12^-) and are connected by interband transitions with spin differences of ΔI=1. It has been proposed[1] that the corresponding bands in ^{190,192,194}Au are rotational-

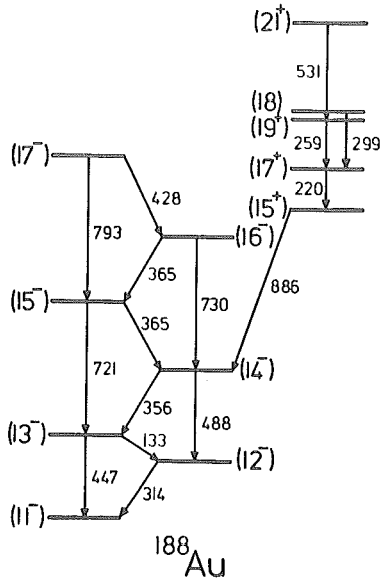

Figure 1: Partial level scheme of ^{188}Au.

aligned bands of $(\pi h_{11/2}^{-1}\ \nu i_{13/2}^{-1})$ configuration. A comparison of both bands in ^{188}Au with those of ^{190,192,194}Au (ref. 1) band with the rotation-algined $h_{11/2}$ proton-hole bands in ^{187,189,191,193,195}Au (ref.2) shows that the excitation energies of corresponding states are remarkably similar. This indicates that the bands in ^{188}Au have a $(\pi h_{11/2}^{-1}\ \nu i_{13/2}^{-1})$ configuration as well.

The observation of two rotation aligned bands based on the (11^-) and (12^-) states in the odd-odd nuclei ^{190,192,194}Au is in agreement with the predictions of Toki et al.[3]. The experimental trends in the level systematics of these nuclei and the electromagnetic properties, viz. mixing ratios and branching ratios, extend to ^{188}Au. This indicates that the same interpretation applies also for ^{188}Au in agreement with theoretical predictions[3].

As can be seen in fig. 1 also a side band is observed in ^{188}Au. The angular distribution of the 886 keV transition indicates pure dipole character for this transition corresponding to the 854.5-, 863.5- and 1058.3 keV transitions in ^{190,192,194}Au respectively. Tentatively a spin and parity of (15^+) has, therefore, been assigned to the band head of the side band. It may have a $(\pi h_{11/2}^{-1}\ \nu i_{13/2}^{-1}\ \nu f_{7/2}^{-1})$ configuration[1].

References

1) A. Neskakis et al., Phys. Lett. 80B (1979) 194; A. Neskakis et al., Nucl. Phys., to be published

2) P.O. Tjøm et al., Nucl. Phys. A231 (1974) 397; M.A. Deleplanque et al., J. Phys. (Paris), Lett. 36 (1975) L. 205; Y. Gono et al., Phys. Rev. Lett. 37 (1976) 1123

3) H. Toki et al., Phys. Lett. 66B (1977) 310; H. Toki et al., Z. Physik A292 (1979) 79; H.L. Yadav et al., Phys. Lett. 81B (1979) 119

2.19. Curved Crystal Study of De-excitation Gamma Rays in ^{184}W Following Neutron Capture

W.F. Davidson[+], *C.W. Reich*[++], *R.C. Greenwood*[++], *and H.R. Koch*

Earlier studies of the ^{184}W level scheme from radioactive decay of the two ^{184}Re isomers[1] and from the $^{183}W(n,\gamma)$ reaction[2] have provided a rather detailed picture of the rotational-band structure of this nucleus in the region below ∼ 2 MeV. The analysis of these data permitted a number of conclusions to be drawn regarding the nature and the strength of the coupling among the different bands of both collective and two-quasiparticle character. One of the interesting features to emerge from these studies was the observation of low-energy γ rays which could be assigned as transitions between excited positive-parity collective bands. To provide more definite information on these possible low-energy γ rays and hence to address the question of the existence of non-zero E2 matrix elements between the collective positive-parity bands in ^{184}W, we have remeasured the secondary γ-ray spectrum emitted following thermal-neutron capture in ^{183}W.

The capture γ-ray spectrum was studied using the curved crystal γ-ray spectrometers installed at the High Flux Reactor of the ILL in Grenoble. Approximately 150 γ-ray transitions, from ∼ 85 keV to 2.33 MeV, were assigned to ^{184}W. A partial level scheme of ^{184}W, showing the first four excited positive-parity bands and their de-exciting γ-ray transitions as observed in this study, is shown in Fig. 1. Especially noteworthy is the observation of a number of transitions connecting the various excited bands. Of the nine such γ rays shown in Fig. 1, only three (those from the 1386 keV state to 2^+ and 3^+ and the one from 1322 keV to 2^+) were previously reported and one (from 1431 keV to 3^+) was only tentatively placed in the earlier (n,γ) study[2]. Three new transitions to the ground-state band are also observed. The placement of two of these (from 1523 keV to 4^+_g and 1322 keV to 2^+_g) is considered definite, while that of one of them (from the tentative 4^+ level at 1359 keV to 4^+_g) is considered as uncertain.

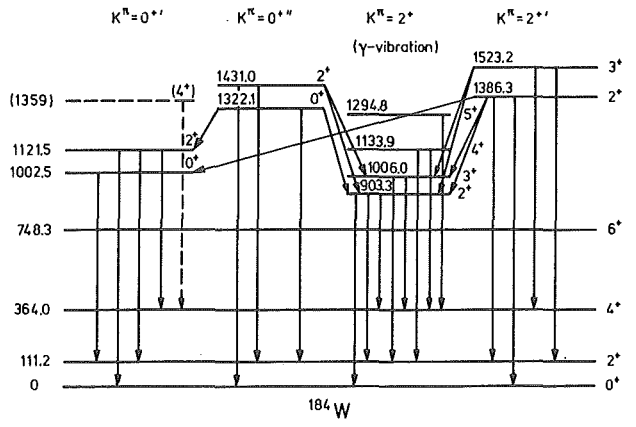

Fig. 1: $K^\pi = 0^+$ and 2^+ bands below ∼ 1.5 MeV in ^{184}W

The transitions connecting the different excited bands are intrinsically rather strong. For those involving excited 0^+ states, where E2 multipolarities can be assigned with confidence, the B(E2) values, relative to those of transitions to the ground-state band, are quite large. From the 1322 keV, $0^{+'}$ state, for example, we calculate

$B(E2; 1322 \rightarrow 1121)/B(E2; 1322 \rightarrow 2^+_g) \sim 960$, and
$B(E2; 1322 \rightarrow 903)/B(E2; 1322 \rightarrow 2^+_g) \sim 230$.

For the 1386 keV, $2^{+'}$ state, we find $B(E2; 1386 \rightarrow 1002)/B(E2; 1386 \rightarrow 0^+) = 5.2$. From the measured B(E2) value of the 1386 keV ground state transition we calculate $B(E2; 1386 \rightarrow 1002) = 0.022e^2 \cdot b^2$, a relatively large value.

These E2-transition-rate data are presently being analyzed, using both a phenomenological five-band mixing approach and the results of IBA-model calculations, to see if non-zero values for the E2 matrix elements between the excited bands are required to explain these interband B(E2) values.

[+] Division of Physics, National Research Council of Canada, Ottawa, Canada KIA OR6 and Institut Laue-Langevin, 38042 Grenoble, France

[++] Idaho National Engineering Laboratory, EG&G Idaho, Inc. Idaho Falls, Idaho 83415, USA

References

1) D.J. McMillan, R.C. Greenwood, C.W. Reich and R.G. Helmer, Nucl. Phys. A223 (1974) 29

2) R.C. Greenwood and C.W. Reich, Nucl. Phys. A223 (1974) 66

2.20 Search for the two-photon decay of a light penetrating particle - axion ? - at a nuclear reactor

H. Bechteler, H. Faissner*, E. Frenzel**, H.R. Koch, O. Schult, H. Seyfarth, R. Yogeshwar**

Starting from gauge symmetry considerations, Weinberg[1] and Wilczek[2] have proposed the existence of a light, neutral, and long-lived pseudoscalar boson, called axion. Its experimental verification would constitute strong evidence in favor of the gauge-theory nature of the fundamental interactions. Analysis of earlier neutrino experiments in terms of model predictions (Donnelly et al.[3], Vuilleumier et al.[4]) could not give a definite answer to this question. These results, however, like those from additional decay experiments (Bechis et al.[5], Faissner et al.[6], Zehnder[7]) are compatible with an axion mass of < 1 MeV. Appropriate two-photon events have indeed been observed in experiments at the CERN PS (Faissner[8]) and at SIN (Faissner et al.[9]).

Since axion production should compete with electromagnetic decay, nuclear reactors may produce a significant axion flux due to de-ecxitation of nuclei after fission, ß-decay, and interaction with neutrons (Weinberg[1], Donnelly et al.[3], Wilson and Selinger[10]).

In order to search for two coincident γ rays originating from the decay of a light penetrating particle we have carried out a first measurement using a rather simple set-up which has been installed at the light water moderated research reactor MERLIN, KFA Jülich (10MW thermal power). Fig. 1 shows the detector telescope pointing to the reactor core center 573 cm from the left outer face of the concrete shielding. A lead absorber blocks the line-of-sight between detectors A and B. The shape of the toroidal decay volume between the Pb wall at the left of Fig. 1 and counter A is determined by kinematics,

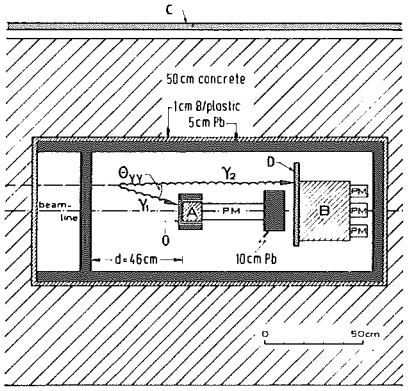

Fig.1: Set-up with NaI(Tl) counters A (4"ϕ x 4") and B (10"ϕ x 10"). C and D are plastic vetocounters. The present shielding was limited by the maximum admissible load of the reactor platform.

geometry, and detection efficiency. As additional shielding the vetocounter D around A is surrounded by a 1.2 cm thick lead tube. A fast-slow coincidence system is used to store the energy information of the coincidence events (0.6 MeV ≤ $E_{\gamma 1}$, $E_{\gamma 2}$ ≤ 6 MeV) on magnetic tape event by event for off-line analysis.

Beyond only looking for a reactor ON/OFF effect in the coincidences at a fixed geometry the following modifications of the set-up have been made: (i) movement of the lead wall in front of A with A and B fixed, i.e. variation of the length of the decay volume only, (ii) movement of A with the positions of B and the lead wall fixed, i.e. variation of the length of the decay volume together with the relative position of both detectors, and (iii) installation of additional shielding. The reactor ON/OFF effect has been investigated for a total of six different set-ups (Table 1).

In Fig. 2 we show examples of the obtained spectra. The fast coincidence signal AB was vetoed by 6 µs signals from counters D and/or C and gated by the energy signals (0.6 ≤ E_A,E_B ≤ 6 MeV). In Table 1 all reactor ON-OFF difference spectra, obtained with 6 different set-ups (schematically given in the top of the table) are listed together with the total reactor ON-OFF effect (coincidence counts/h for 0.6 ≤ E_A,E_B ≤ 6 MeV). In Fig. 3 a sum-energy spectrum is depicted as difference of the reactor ON and OFF spectra.

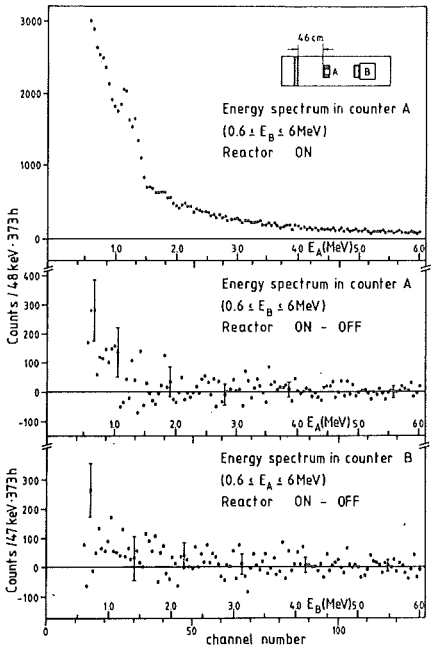

Fig.2: Coincidence spectrum registrated with counter A in set-up no. 1 and with reactor ON (upper part) and difference spectra reactor ON-OFF for counter A (center) and counter B (bottom).

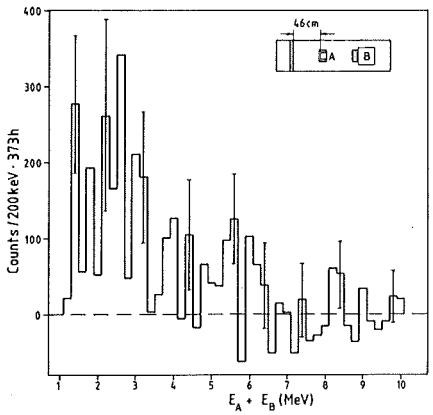

Fig.3: Sum-energy spectrum obtained with set-up no. 1.

The present data indicate a reactor ON-OFF effect for the set-ups no. 1 and no. 5 with significant decay volumina. No reactor ON-OFF effect of statistical significance is observed for the set-ups no. 3 and no. 4 with vanishing decay volume. The same holds for set-up no. 2 (16 cm length of decay volume) and no. 6 (73 cm length of decay volume, Pb tube of 46 cm length in front of counter A).

In addition Monte-Carlo (MC) investigations have been performed. Assuming isotropic 2-γ decay in the rest frame of a decaying particle, the detection efficiency of the two-detector set-up was determined under the condition that each of the two γ quanta enters the unshielded front area of one of the counters A and B. In addition the decay angle (and energy distributions) were restricted by the electronical thresholds. Fig. 4 shows efficiency curves obtained under the assumption of 250 keV mass of the decaying particle. These calculated values do not yet take

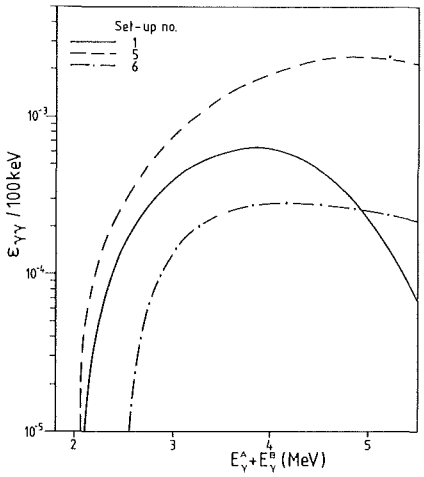

Fig. 4: 2-γ efficiencies (relative units) from Monte-Carlo calculations for various set-ups (electronical threshold: $E_\gamma^A + E_\gamma^B = 1.2$ MeV).

Set-up no.	1	2	3	4	5	6
	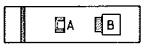				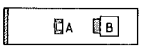	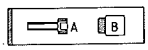
Length of decay volume (cm)	46	16	0	0	73	73 (Pb tube: 46 cm long, 10 cm inner ϕ, 0.5 cm thick)
Measuring time (h) Reactor ON (OFF)	372.8(115.7)	262.8(258.7)	303.0(118.8)	166.1(240.2)	124.5(232.2)	112.5(135.3)
E_A (MeV)	Coincidence spectra reactor ON-OFF for counter A (counts/h, $0.6 \leq E_B \leq 6.0$ MeV)					
0.6 - 1.0	3.78 ± 0.79	-0.28 ± 0.63	0.09 ± 0.54	-1.42 ± 0.94	2.88 ± 0.81	0.71 ± 0.91
1.0 - 1.5	0.68 ± 0.69	0.83 ± 0.53	0.49 ± 0.45	-0.24 ± 0.83	1.90 ± 0.71	-1.57 ± 0.80
1.5 - 2.0	0.25 ± 0.45	0.15 ± 0.37	-0.26 ± 0.33	0.78 ± 0.38	0.80 ± 0.43	1.41 ± 0.49
2.0 - 2.5	0.33 ± 0.35	-0.41 ± 0.29	-0.17 ± 0.26	0.06 ± 0.30	0.57 ± 0.34	-0.33 ± 0.37
2.5 - 3.0	0.17 ± 0.30	0.30 ± 0.25	0.21 ± 0.22	0.08 ± 0.25	0.21 ± 0.29	0.55 ± 0.33
3.0 - 3.5	0.25 ± 0.27	-0.05 ± 0.22	0.16 ± 0.19	0.06 ± 0.22	0.18 ± 0.27	0.29 ± 0.28
3.5 - 4.0	0.61 ± 0.22	0.15 ± 0.19	0.10 ± 0.17	0.26 ± 0.19	0.30 ± 0.22	0.22 ± 0.24
4.0 - 5.0	0.19 ± 0.28	0.33 ± 0.24	-0.21 ± 0.21	0.13 ± 0.23	0.43 ± 0.27	0.28 ± 0.30
5.0 - 6.0	0.01 ± 0.24	0.38 ± 0.20	0.15 ± 0.17	-0.21 ± 0.19	0.16 ± 0.23	0.24 ± 0.25
E_B (MeV)	Coincidence spectra reactor ON-OFF for counter B (counts/h, $0.6 \leq E_A \leq 6.0$ MeV)					
0.6 - 1.0	1.76 ± 0.71	0.26 ± 0.59	0.66 ± 0.51	0.05 ± 0.83	2.70 ± 0.71	0.60 ± 0.81
1.0 - 1.5	1.80 ± 0.72	0.51 ± 0.56	0.45 ± 0.49	-0.43 ± 0.87	2.32 ± 0.76	-1.18 ± 0.84
1.5 - 2.0	1.00 ± 0.43	-0.14 ± 0.35	0.11 ± 0.31	-0.07 ± 0.35	0.06 ± 0.42	0.79 ± 0.46
2.0 - 2.5	0.52 ± 0.38	0.58 ± 0.31	0.02 ± 0.27	0.06 ± 0.32	0.93 ± 0.37	0.67 ± 0.41
2.5 - 3.0	0.47 ± 0.33	0.14 ± 0.26	-0.25 ± 0.24	0.23 ± 0.28	0.63 ± 0.33	0.47 ± 0.36
3.0 - 3.5	-0.05 ± 0.29	-0.08 ± 0.22	0.04 ± 0.19	0.02 ± 0.23	0.64 ± 0.27	-0.20 ± 0.30
3.5 - 4.0	0.28 ± 0.26	-0.34 ± 0.20	-0.52 ± 0.18	0.28 ± 0.21	0.26 ± 0.27	0.15 ± 0.28
4.0 - 5.0	0.59 ± 0.31	-0.19 ± 0.24	0.04 ± 0.21	0.62 ± 0.26	-0.02 ± 0.31	0.08 ± 0.35
5.0 - 6.0	-0.10 ± 0.28	0.02 ± 0.21	0.00 ± 0.18	-0.21 ± 0.23	-0.01 ± 0.27	0.44 ± 0.29
Total reactor ON-OFF effect (counts/h, $0.6 \leq E_A, E_B \leq 6.0$ MeV)						
	6.28 ± 1.33	0.75 ± 1.07	0.55 + 0.93	0.55 ± 1.12	7.41 ± 1.34	1.80 ± 1.50

Table 1: Resulting coincidence spectra (difference reactor ON-OFF) for the 6 experimental set-ups (cuts through the coincidence matrices) and total reactor ON-OFF effects. The errors are statistical-errors only.

into account the intrinsic efficiency of the NaI(Tl) counters. The results of the MC calculations suggest that the telescope counter arrangements are favouring γ-ray energy sums $E_\gamma^A + E_\gamma^B > 2$ MeV. For set-up no. 1 the MC simulation yields $< E_\gamma^B/E_\gamma^A >= 1.9 \pm 0.5$ and $< (E_\gamma^B/E_\gamma^A)^{1/2} > = 1.4 \pm 0.2$ for (2.2 ± 0.2) MeV total energy of the decaying particle the mass of which is assumed as 200 keV. With a ^{60}Co source placed in the decay volume 20 cm from counter A the peak/total ratio in both detectors was found to be equal within 15%. Taking into account this result the measured ratios $<E_B/E_A> = 1.4 \pm 0.7$ and $<(E_B/E_A)^{1/2}> = 1.1 \pm 0.3$ for $E_A + E_B = (2.2 \pm 0.2)$ MeV agree with those from the MC calculation. The latter yields $<E_\gamma^B/E_\gamma^A>= 2.6 \pm 1.3$ and $< (E_\gamma^B/E_\gamma^A)^{1/2} > = 1.6 \pm 0.4$ under the assumption of a white energy spectrum of the decaying particle (m = 200 keV, $1.2 \leq E_\gamma^A + E_\gamma^B \leq 10$ MeV) in agreement with the experimental values 2.2 ± 1.9 and 1.3 ± 0.7, respectively. In Fig.5 the experimental distribution of $(E_B/E_A)^{1/2}$ is plotted for $E_A + E_B = (2.2 \pm 0.2)$ MeV together with MC distributions of $(E_\gamma^B/E_\gamma^A)^{1/2}$ for $E_\gamma^A + E_\gamma^B = (2.2 \pm 0.2)$ MeV and different masses of the decaying particle.

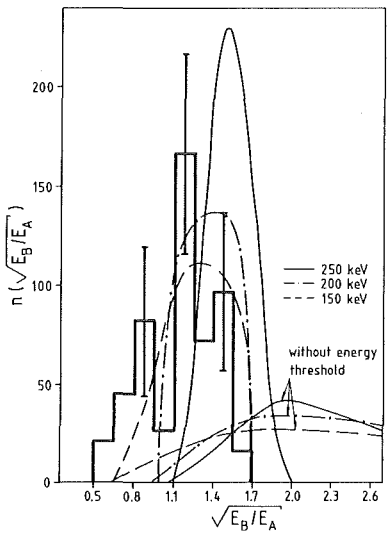

Fig. 5: Experimental distribution of $\sqrt{E_B/E_A}$ for $E_A + E_B = (2.2 \pm 0.2)$ MeV compared with MC curves for different masses of the decaying particle (the curves with and without energy threshold have areas normalized to that of the experimental distribution).

Fig. 6 contains the corresponding distributions for $1.2 \leq E_A + E_B \leq 10$ MeV and a white energy spectrum underlying the MC calculations. Reasonable agreement would be achieved for a mass of the decaying particle of ∿ 200 keV.

Whereas in a preliminary experiment at the High Flux Reactor ILL, Grenoble[14] a reactor ON-OFF effect has also been observed, other measurements at the Nuclear Power Plants at Bugey, France[15] and Goesgen, Switzerland[16] indicate contradictary results. Our present results (partly already presented elsewhere [11-13]) do not yet allow unambiguous conclusions. For this reason our experiments are pursued with a turnable set-up which due to its direction-sensitivity allows to view at or past the reactor core at constant reactor power.

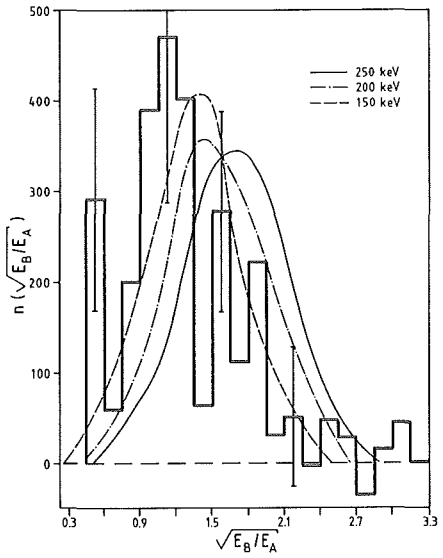

Fig. 6: Experimental distribution of $\sqrt{E_B/E_A}$ for $1.2 \leq E_A + E_B \leq 10$ MeV compared with MC curves for different masses of the decaying particle calculated for a white energy spectrum ($1.2 \leq E_\gamma^A + E_\gamma^B \leq 10$ MeV).

References

1) S. Weinberg, Phys. Rev. Letters 40 (1978) 223
2) F. Wilczek, Phys. Rev. Letters 40 (1978) 279
3) T.W. Donnelly et al., Phys. Rev. D18 (1978) 1607
4) J.L. Vuilleumier et al., Phys. Letters 101B (1981)341
5) D.J. Bechis et al., Phys. Rev. Letters 42 (1979) 1511
6) H. Faissner et. al., Phys. Letters 96B (1980) 201
7) A. Zehnder, Phys. Letters 104B (1981) 494
8) H. Faissner, Report to the Neutrino Conference 1980 (Erice, Italy), to be published
9) H. Faissner et al., Phys. Letters 103B (1981) 234
10) R. Wilson and J. Selinger (1981), private communication
11) H. Faissner, Proc. Int. Neutrino Conf., Maui, Hawaii, USA (1981), Ed. R.J. Cence, in press
12) W.R. Ermer, H. Faissner, E. Frenzel, E. Hermens, H.R. Koch, O. Schult, H. Seyfarth, R. Yogeshwar, Proc. Symp. on Neutron-Capture Gamma-Ray Spectroscopy and Related Topics, Grenoble, France (1981). Ed.T.von Egidy, in press
13) H. Faissner, Proc. 1981 Int. Symp. on Lepton and Photon Interactions at High Energies, Bonn, F.R.G. Ed.W. Pfeil (1982), p. 797
14) H.G. Börner and S.A. Kerr (1981), private communication
15) J.F. Cavaignac et al. (1982), private communication
16) A. Zehnder, K. Gabathuler, J.L. Vuilleumier (1982), private communication

* III. Physikalisches Institut, Technische Hochschule Aachen, Fed. Rep. Germany

** Now with Bundeswehr-Hochschule München, Fed.Rep.Germany

II. THEORETICAL NUCLEAR PHYSICS

3. NUCLEAR STRUCTURE

3.1. Higher Compression Modes

R. de Haro, S. Krewald, J. Speth

Compression modes have been suggested long ago as a possible oscillation mode of nuclei[1]. Since then more refined studies have been performed, leading to predictions, to a very good degree of accuracy of the monopole compression mode (breathing mode)[2] and of the isoscalar dipole (squeezing mode)[3]. The monopole is now experimentally a well known state[4] and recently sound experimental indications of the isoscalar dipole compression mode in ^{208}Pb have been presented[5].

The question raised here concerns the existence of other compression states at higher energies or higher multipolarities.

These states certainly would not be excited by an electromagnetic operator $\hat{Q}_J = \Sigma_i\, e/2(1-\tau^i) r_i^J Y_{JM}(\Omega_i)$. Its model structure (the transition density for a compression mode must have at least one node in the radial coordinate) is such that

$$\int_0^R \rho_J^{compr.}(r)\, r^{J+2}\, dr \approx 0$$

Therefore, one can think of taking other kinds of operators, other than $\hat{Q}_J$, for which the contribution does not vanish.

Just like in the case of the monopole, we take now the higher order operators in the expansion in r, that means, operators of the form

$$\hat{C}_{J,k} = \sum_i \frac{e}{2} (1-\tau^i) r_i^{J+2k}\, Y_{JM}(\Omega_i) \qquad k=0,1,2,\ldots$$

For every value of k one is able to write a corresponding linearly weighted sum rule[6].

That way one can calculate the nuclear response to each of these operators and compare the different curves for the exhaustion of the corresponding EWSR[7,8].

The information we look for now is if and where there is a much steeper slope for the curve corresponding to the operator $\hat{C}_{J,k}$ in comparison to that for $\hat{C}_{J,k=0}$.

In fig. 1a, b, c we see the percent exhaustion of the EWSR corresponding to $\hat{C}_{J,k=1}$ (dotted line), and that for $\hat{C}_{J,k=0}$ (full line), for 0^+ (top), 1^- (middle) and 2^+ (bottom), in ^{208}Pb.

For the isoscalar dipole, for $\hat{C}_{1,0}$ we get only a flat curve raising slowly to 4 % (which should be exactly zero if our projection out of the spurious state were exact). However, for the $\hat{C}_{1,1}$ operator a clear and steep growth of the exhausted percentage of the isoscalar EWSR is to be seen around 23.3 MeV (centroid of the distribution) and we can identify it to be the isoscalar dipole state, with a decay width of 3.0 MeV. Both values are in good agreement with experiment. We note also that for such a high-lying state the decay width is already half the total experimental width.

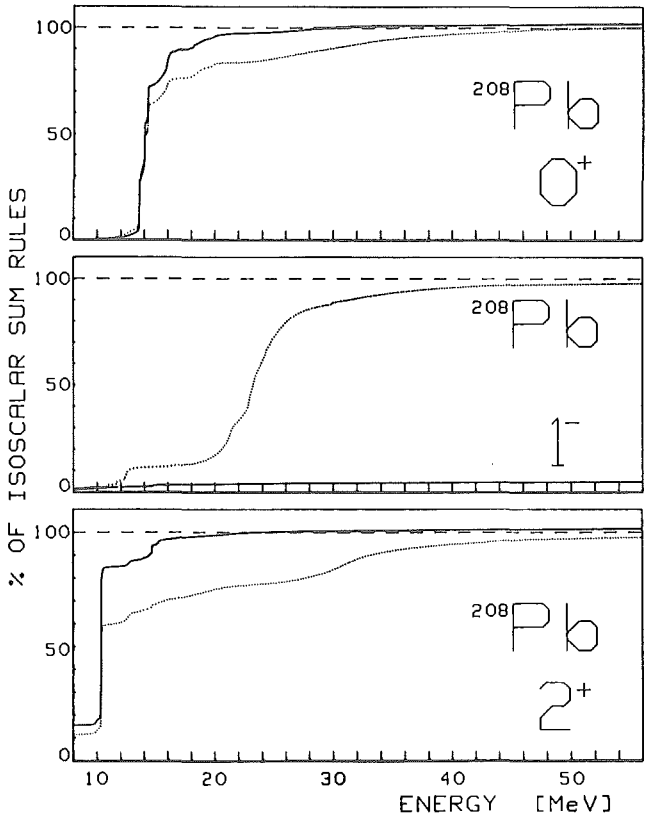

Fig. 1: Percentage exhaustion of the isoscalar EWSR for the given multipolarity J, for the operators $C_{J,k=0}$ (full line) and $C_{J,k=1}$ (dotted line) against the upper integration energy. a: monopole; b: dipole; c: quadrupole.

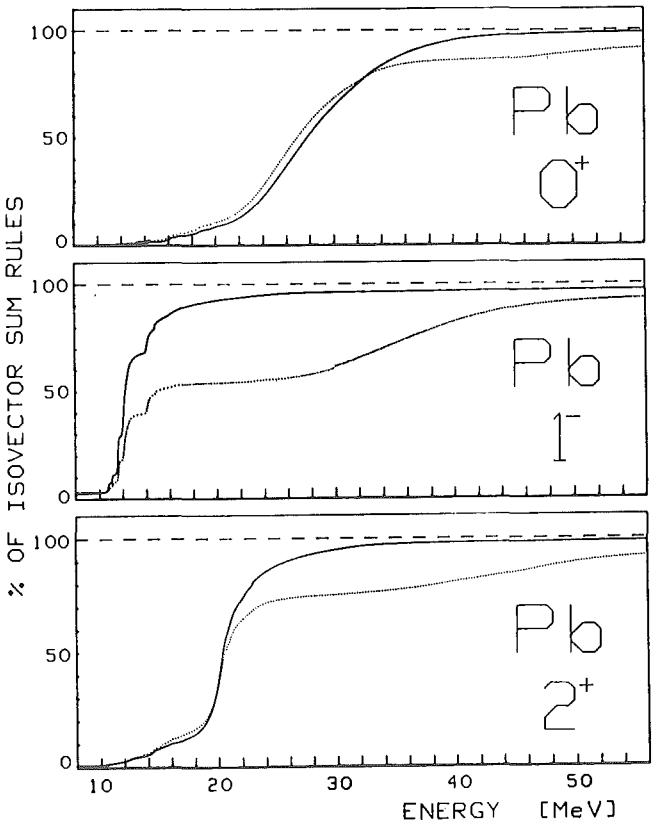

Fig. 2: Percentage exhaustion of the isovector EWSR for the given multipolarity J, for the operators $C_{J,k=0}$ (full line) and $C_{J,k=1}$ (dotted line) against the upper integration energy. a: monopole; b: dipole; c: quadrupole.

The other multipolarities can be analyzed in a similar way and also for the isovector components.
We can then recognize some fairly concentrated compression modes like the isovector dipole at E=36 MeV and with a decay width Γ^{d} = 7 MeV, the second isoscalar monopole around E=30 MeV, Γ=13 MeV and the isoscalar quadrupole at 31 MeV, Γ=6 MeV.

For a final analysis of those modes one should also calculate the spreading width of those states in order to see if they and which of them allow experimental observation beyond the already quoted isoscalar monopole and dipole.

References

1) A. Bohr, B. Mottelson, Nuclear Structure, Vol. II, Benjamin Inc. (1975).

2) P. Ring, J. Speth, Nucl. Phys. A235 (1974) 315.

3) J. Wambach, V. Klemt, J. Speth, Phys. Lett. 77B (1978) 245.

4) J. Speth, A. van der Woude, Rep. Prog. Phys. 44 (1981) 719.

5) H.P. Morsch, M. Rogge, P. Turek, C. Mayer-Böricke, Phys. Rev. Lett. 45 (1980) 337;
M. Buenerd, Comm. Int. Nucl. Phys. Workshop, Trieste, Italy (1981).

6) R. de Haro, S. Krewald, J. Speth, to be published.

7) R. de Haro, S. Krewald, J. Speth, submitted to Nucl. Phys.

8) R. de Haro, S. Krewald, J. Speth, comm. in this report.

3.2. Isospin Projection and Sum Rules for High Multipolarity Giant Resonances

R. de Haro, S. Krewald, J. Speth

The Fourier-Bessel RPA[1] has been used to study the giant resonances in magic nuclei. Particularly in ^{208}Pb, a systematic calculation of those states has been made to very high multipolarities[2]. One of the central questions here concerns the existence and location of concentrated strength, especially for the higher multipoles.

In the frame of a 1p-1h RPA, in which only the decay width of the resonances can be taken into account, the calculated states turn out to be very sharp. Inspection of the strength distribution as response to an electromagnetic multipole operator tells us that for the higher multipoles the resonances are described by a succession of peaks. Figure 1a, showing the proton transition density for the hexadecapole in ^{208}Pb, is a typical example.

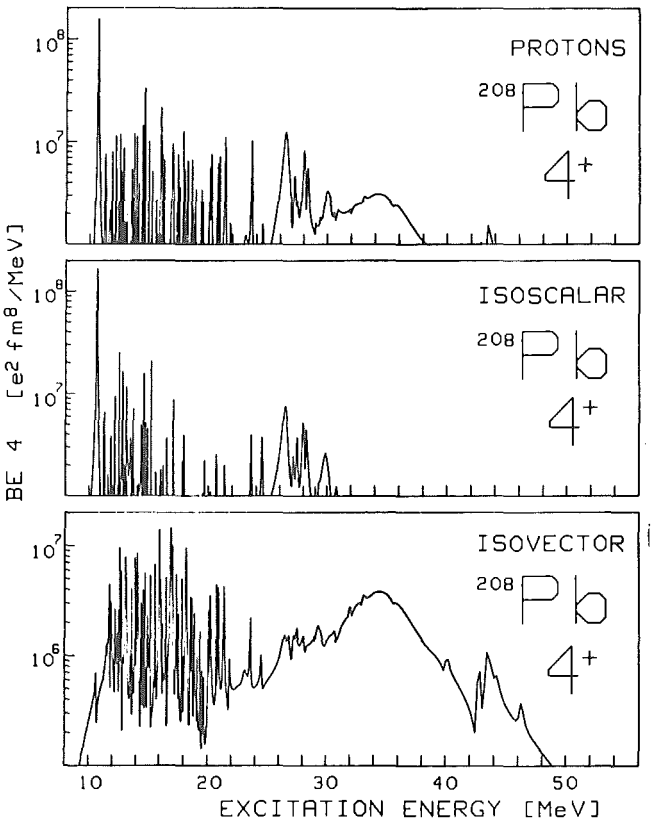

Fig. 1: Hexadecapole transition probability in units of e^2fm^8/MeV against the excitation energy in MeV for ^{208}Pb decomposed in proton (top), isoscalar (middle) and isovector (bottom) contributions.

If one projects now the nuclear response in isoscalar and isovector components (fig. 1b and 1c) a clearer picture is obtained, especially if one thinks about pure isospin probes like the α-particles. Comparison of the different pictures, together with the knowledge of the neutron response function allows an at least qualitative understanding of the states, without recurring to the detailed wave function.

However, almost no light has been shed on the concentration of strength. Let us now build up the curves

describing the qualitative exhaustion of the corresponding energy weighted sum rules (EWSR) for the proton transition probability and for each isospin component, like in fig. 2a, b, c. In fig. 2a, the ordinate represents

$$\frac{100}{S_\pi^{TH}(J)} \left[S_\pi^C(J,E) + S_\pi^B(J) \right]$$

where

$$S_\pi^{TH}(J) = \frac{(hc)^2}{2mc^2} \frac{J\ (2J+1)^2}{4\pi} \cdot Z \cdot \langle r^{2J-2} \rangle_{\pi\text{-g.s.}}$$

is the classical linearly weighted sum rule. For each multipolarity J we can build classical EWSR also for the isoscalar $S_{T=0}^{TH}(J)$ and the isovector $S_{T=1}^{TH}(J)$ components, where the expected value $\langle r^{2J-2} \rangle_{g.s.}$ runs over the whole ground state (protons and neutrons). Furthermore

$$S_\pi^C(J,E) = \int_{\text{continuum threshold}}^{E} B^\pi EJ(\omega) \cdot \omega \cdot d\omega$$

and

$$S_\pi^B(J) = \sum_{i=1}^{\text{last bound state}} E_i \cdot BEJ(E_i)$$

From the slope and relative increase of these curves one can conclude about the existence of concentrated strength. The steeper the curve, the more concentrated the strength.

The isoscalar hexadecapole (fig. 2b), for instance, shows only around 11 MeV fairly concentrated strength, coherently with former results[3], exhausting about 15 % of the corresponding EWSR. Somehow concentrated strength one can also find from 26 to 32 MeV, exhausting 30 % of the isoscalar EWSR.

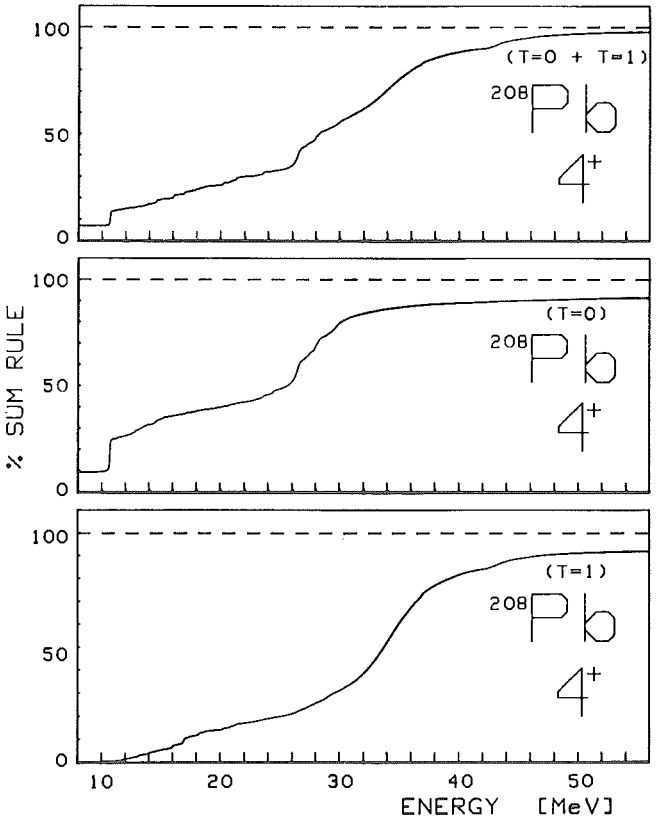

Fig. 2: Percentage exhaustion of the linearly weighted sum rule for the hexadecapole in ^{208}Pb as a function of the upper integration energy E in MeV. The upper curve shows the proton, the middle one the isoscalar and the lowest one the isovector contribution.

In our calculation, complete ph-spaces (exhausting every possible coupling possibility to a given multipolarity) have been used, assuring the saturation of the EWSR.

References

1) Jül-Spez-99, Februar 1981.

2) R. de Haro, S. Krewald, J. Speth, submitted to Nucl. Phys.

3) J.S. Dehesa, S. Krewald, J. Speth, A. Faessler, Phys. Rev. C15 (1977) 1858.

3.3. The Role of the Δ_{33}-Resonance in Low-Energy Nuclear Physics

J. Speth, S. Krewald, T. Suzuki[+]

The Gamow-Teller giant resonance was recently discovered in a (p,n) charge-exchange, reaction using high energy protons[1]. The spin-isospin transition strength, summed over all states, was systematically found to exhaust only approximately 50 % of the Ikeda sum rule[2]. Likewise, in inelastic electron and proton scattering, only a small fraction of the expected M1 strength has been found so far, particularly in heavy nuclei. Since conventional nuclear degrees of freedom only redistribute the strength but do not change the sum rule, the Δ_{33}-resonance was invoked to explain the missing strength[3]. The Δ_{33}-resonance, coupled with a nucleon hole, can move part of the isovector $\sigma\tau$-strength into an energy region approximately 300 MeV above the low-lying excitations of the nucleus. The major reason why this mechanism may have a significant effect despite this enormous energy gap is due to the Pauli principle. Since there is no Pauli blocking for the Δ_{33}-resonance, virtually all nucleons can share in building Δ-h states. Therefore the sheer number of possible configurations is able to bridge the gap. A similar effect appears in the quenching of the axial vector coupling constant g_A. We propose a model, which explicitly includes the Δ_{33}-resonance into the wave function:

$$\Psi^J = \Big(\sum_{NN'} X^J_{NN'} a^+_N a_{N'} + \sum_{\Delta N''} X^J_{\Delta N''} a^+_\Delta a_{n''} \Big) |g.s.\rangle$$

The major improvement with respect to other approaches, such as schematic models, nuclear matter estimates, or the effective operator formalism[3], is that now the effect of Δ-h configurations on the excitation energies, transition probabilities and cross sections can be evaluated. The interaction consists of one pion-exchange, rho-meson exchange and a residual phenomenological Landau parameter g'_0. A breakdown of typical matrix elements is shown in fig. 1. Short range correlations are treated by a Jastrow correlation function. All details are found in ref. 4). The results are displayed in table 1. It is found that by far the largest amount of quenching occurs for states with low spin. This has to be expected, since the one-pion and ρ-meson exchange weakens the residual particle-hole interaction for increasing momentum transfer. A detailed discussion of the amount of quenching seen in various reactions is given in the following contributions.

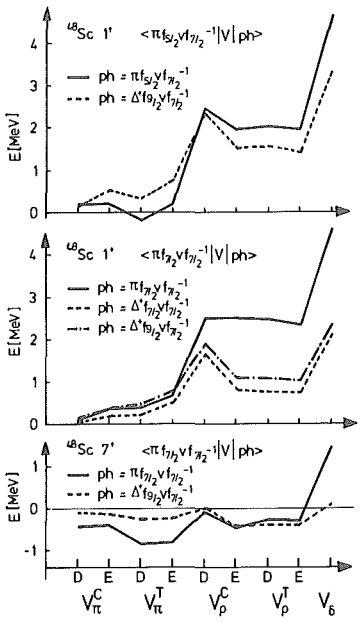

Fig. 1: Sum of the interaction matrix elements for various particle-hole and Δ-hole configurations in ^{48}Sc. Starting with the direct matrix element of the central part of the one-pion exchange interaction, each contribution from the various components of the interaction is added up, D denoting direct, and E exchange contributions. There is a big cancellation between D and E for the short range interaction, which would be exact in the case of a δ-function. Therefore it is essential to develop a microscopic model for the $\delta g'_0$ term. The big advantage of the present approach is that $\delta g'_0$ is entirely determined from the experimental excitation energies.

References

1) C.D. Goodman et al., Phys. Rev. Lett. 44 (1980) 1755.
2) K. Ikeda, Prog. Theor. Phys. 31 (1964) 434.
3) M. Rho, Nucl. Phys. A231 (1974) 493;
I. Towner and F.C. Khanna, Phys. Rev. Lett. 42 (1979) 51;
W. Knüpfer, M. Dillig, A. Richter, Phys. Lett. 95B (1980) 349;
A. Bohr, B. Mottelson, Phys. Lett. 100B (1981) 10;
A. Härtling et al., Phys. Lett. 104B (1981) 261;
G.E. Brown and M. Rho, preprint.
4) T. Suzuki, S. Krewald, J. Speth, Phys. Lett. 107B (1981) 9.

Nucleus	J^π	E_{exp}(MeV)	B_{exp}	E_N(MeV)	B_N	$E_{N+\Delta}$(MeV)	$B_{N+\Delta}$	Q(%)
^{48}Sc	1^+	3.02		3.02	2.42	2.96	1.88	22
^{48}Sc	1^+	11.0		11.08	21.09	10.86	14.97	29
^{48}Sc	7^+	1.6		1.41	36.62	1.65	33.2	9
^{48}Ca	1^+	10.23	5.2	10.21	8.20	10.16	5.29	36
^{16}O	0^-	12.80		13.17	0.13	13.35	0.12	8
	2^-	12.97	197±37	13.16	168	13.13	126	25
		19.04	338±68	20.25	915	20.48	813	11
		20.36	467±156					
	4^-	18.98		19.41	$5.6\cdot10^5$	19.75	$5.14\cdot10^5$	8

Table 1: Summary of the calculations for energies and B(ML) values, without ($\delta g'_0$ = 0.4) and with ($\delta g'_0$ = 0.5) the Δ_{33}-degree of freedom. Q is the quenching factor $(B_{N+\Delta}-B_N)/B_N \cdot 100$.

[+] Niels Bohr Institute, Copenhagen, Denmark

3.4. Experimental Signatures of the Δ_{33}-Hole Quenching Mechanism in Pionic States

T. Suzuki[+], *S. Krewald, J. Speth*

The Δ_{33}-resonance was recently proposed to be responsible for the reduction of magnetic strength in many nuclei. In this contribution, we apply the Δ-h model of the previous report to inelastic electron scattering. Since the Δ-hole configurations couple to nucleon particle-hole configurations mainly through the one-pion and the rho-meson exchange, the following qualitative behaviour of the quenching may be expected: the interaction is strongest for small momentum transfer, therefore states of small spin should suffer the most dramatic amount of quenching. At large momentum transfer, the Δ-h coupling is very weak and therefore virtually no quenching may be expected. Since this behaviour is fully confirmed from the B(ML) values, one might expect that this effect should be particularly clean in the (ee') experimental form factor of the 1^+ state in ^{48}Ca at 10.227 MeV. When one inspects the form factor displayed in fig. 1, however, one finds a very smooth decrease of the amount of

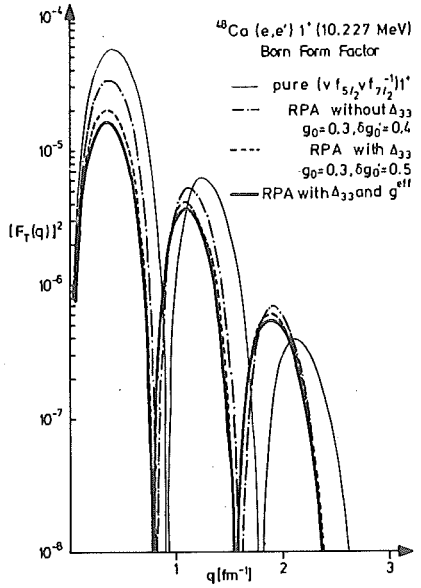

Fig. 1: Theoretical form factors of the inelastic electron scattering to the 1^+, 10.23 MeV state in ^{48}Ca, calculated in Born approximation. The dashed and dash-dotted results correspond to RPA calculations with and without inclusion of Δ-h configurations, respectively. The thin line is the corresponding result of using a pure neutron $f_{5/2}f_{7/2}^{-1}$ configuration. In all three cases the bare magnetic operator was used. In order to simulate the many-particle many-hole effects, we also performed a nucleon-hole, Δ-hole RPA calculation using an effective operator (thick line) which gives rise to $B(M,1)\uparrow = 4.27\ \mu_K^2$.

quenching. In fact, the reduction of the form factor is 39 %, 22 % and 13 % in the first, resond, and third maximum, respectively. There are two effects which explain this behaviour qualitatively: (i) The operator for electron scattering is of the form $\sigma\times\nabla$, therefore it is more sensitive to the q-dependence of the ρ-meson. Because of the large mass of the ρ-meson, the ρ-interaction decreases only very smoothly with increasing q. (ii) The M1-operator has no radial dependence, therefore it is only sensitive to diagonal matrix elements. The (e,e') operator, however, has a radial dependence which gets more important with increasing momentum transfer. In summary, our investigations show that the (angular) momentum dependence is a possible experimental signature of the Δ-hole quenching effect, which is fully effective, however, only in hadron induced reactions.

[+] Niels Bohr Institute, Copenhagen, Denmark

3.5. Fragmentation of the M1-Strength in ^{58}Ni and ^{60}Ni

J.B. McGrory[+] *and J. Speth*

One of the best cases for the investigation of isoscalar and isovector 1^+-strength would be the doubly closed shell nucleus ^{56}Ni. Here the proton and neutron spin-orbit partners $f_{5/2}$-$f_{7/2}^{-1}$ give rise to a $\Delta T=0$ and $\Delta T=1$ 1^+-resonance within the TDA or RPA. The $\Delta T=0$ state would be a unique possibility in order to investigate the isoscalar spin-flip part of the particle-hole interaction. Because of the short lifetime of ^{56}Ni there is little hope to investigate these 1^+-states in (e,e') and (p,p'). As targets of ^{58}Ni and ^{60}Ni isotopes exist we investigated the influence of the additional neutrons on the 1^+-states in those nuclei.

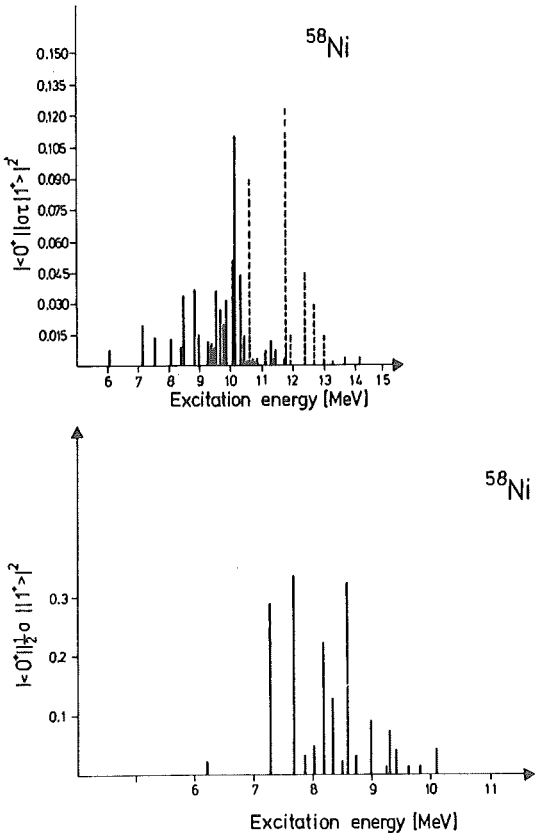

Fig. 1: Isovector (upper part) and isoscalar (lower part) 1^+-strength in ^{58}Ni.

The present work is an extension of a similar calculation of the Ca-isotopes[1]. Our model space includes all states with $f_{7/2}^{16}\times(p_{3/2},p_{1/2},f_{5/2})^{A-56}$ and $f_{7/2}^{15}\times(p_{3/2},p_{1/2},f_{5/2})^{A-55}$. We also used a Kuo-Brown interaction constructed for a ^{40}Ca core. Within this model one gets a single isoscalar and a single isovector state in ^{56}Ni at 5.9 MeV and 8.3 MeV, respectively. Practically all the M1-strength is

concentrated in the upper state. The additional two neutrons in ^{58}Ni give rise to very large fragmentation of the corresponding 1^+-strength. In the upper part of fig. 1 we show the isovector 1^+-strength ($\sigma\cdot\tau$) in ^{58}Ni where the full lines indicate T=1 and the dotted lines T=2 states. The lower part of that figure shows the distribution of the isoscalar 1^+-strength (1/2) which is also strongly fragmented. The splitting gets larger if one adds more neutrons as shown in fig. 2. This

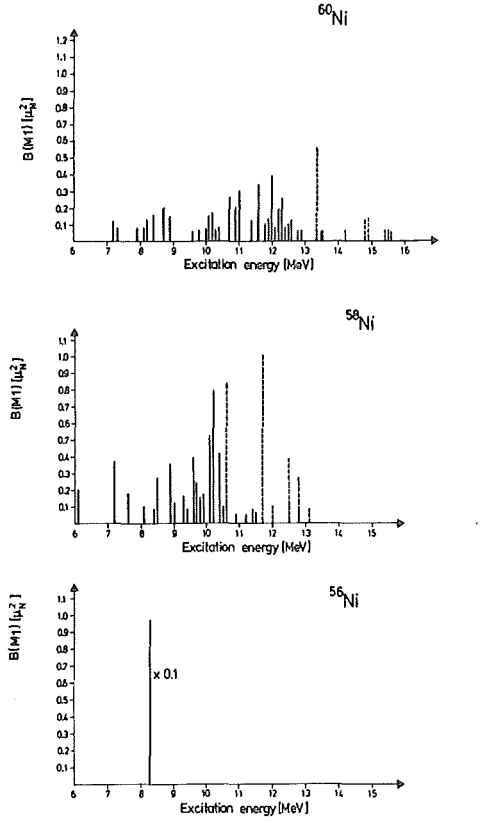

Fig. 2: Isovector M1-strength distribution in various Ni-isotopes.

theoretical result of the $\Delta T=1$ excitations is in qualitative agreement with the experimental findings of Marty et al.[2]. The strong fragmentation of the isoscalar strength makes an experimental detection probably very difficult.

References

1) J.B. McGrory and B.H. Wildenthal, Phys. Lett. 103B (1981) 173.

2) N. Marty, private communication.

+ Oak Ridge National Lab., Oak Ridge, Tenn., USA

3.6. The Effect of the Δ(1232)-Isobar in ^{48}Ca(p,n)-Cross Sections

F. Osterfeld, S. Krewald, J. Speth

Recent (p,n) experiments[1] at intermediate energies have demonstrated that a significant part of the total Gamow-Teller (GT) strength is concentrated in one collective state which appears energetically somewhat above the isobaric analogues of the target ground states. From the theoretically expected total GT-strength, however, only 30-50 % is found in these experiments. Several authors[2] have suggested that this so-called quenching of the total GT-strength is due to the admixture of Δ(1232) isobar-nucleon hole (ΔN^{-1}) excitations into the proton particle-neutron hole (PN^{-1}) Gamow-Teller state.

Here we present for the first time a microscopic analysis of (p,n) cross sections to GT-states which includes Δ(1232)-isobar degrees of freedom explicitly in both the structure and the reaction calculations. The structure calculations are based on the random phase approximation (RPA) and have been performed in the same way at described in ref. 3. The generalized RPA wave function including isobar degrees of freedom is then given by

$$\Psi^J = \left[\sum_{p,N} X^J_{PN}\, a^+_p\, a_N + \sum_{\Delta N} X^J_{\Delta N}\, a^+_\Delta\, a_N\right] |g.s.> \qquad (1)$$

In order to calculate (p,n)-cross sections from the wave function of eq. (1) we have extended the fast speed DWBA-code FROST-MARS[4] to allow also for the excitation of the (ΔN^{-1})-components in Ψ^J (see fig. 1). Both direct and

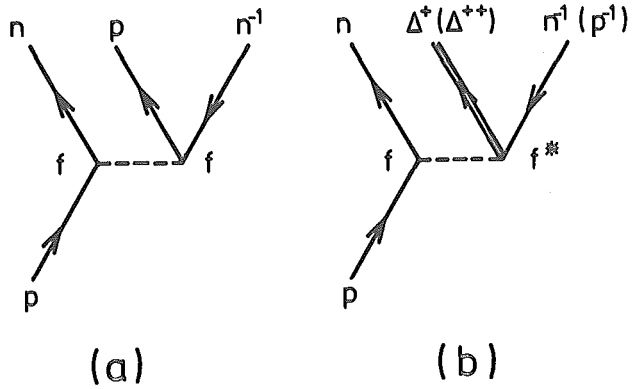

Fig. 1: Graphical representation of reaction processes included in the DWIA calculations. Only direct graphs are shown.

knockout exchange amplitudes are calculated exactly. The exact treatment of exchange for the (ΔN^{-1})-excitations is very important since direct and exchange amplitudes interfere destructively for a finite range projectile-isobar effective interaction.

In fig. 2 we show differential cross sections of ^{48}Ca(p,n)-reactions leading to the three 1^+-states in ^{48}Sc. The theoretical cross sections are antisymmetrized DWIA-calculations using the G3Y-interaction of Love for the effective projectile-target nucleon interaction. For the effective projectile-isobar interaction (see fig. 1) we simply used the real S=1, T=1 part of the G3Y-interaction in which we replaced the spin (σ) and isospin (τ)

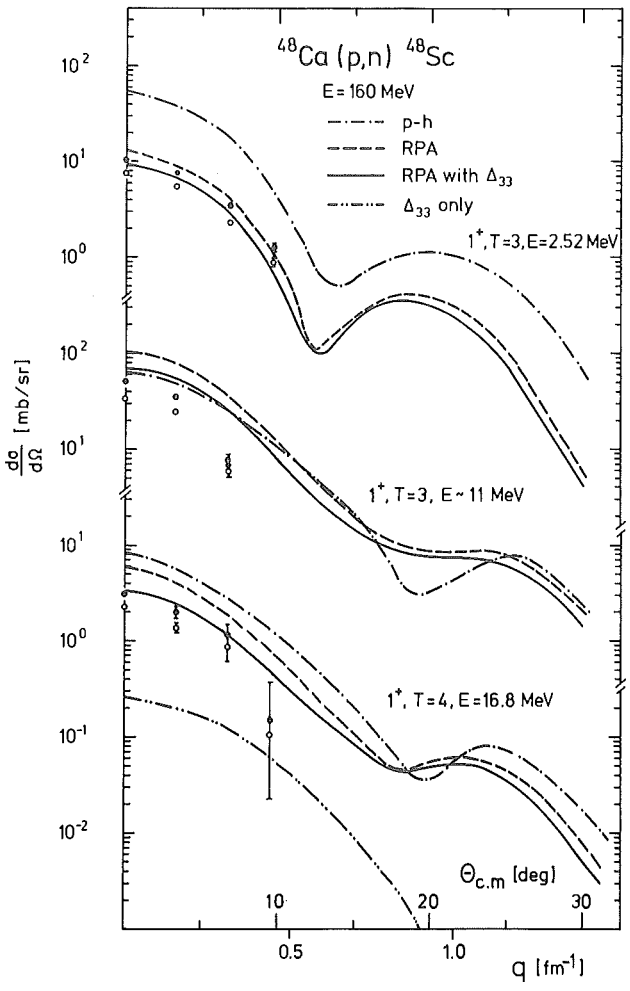

Fig. 2: Differential cross section for the ^{48}Ca(p,n)^{48}Sc 1^+ reactions. The open circles are the data of ref. 7. The full points are the same data but with the normalization of ref. 8.

operators by the transition operators S and T. For the nucleon-isobar coupling constant we assumed $f^* = 2f$ [6].

The theoretical cross sections in fig. 2 are compared to two sets of data. The open circles correspond to the data of ref. 7 and the full points are the same data but with the normalization of ref. 8.

Cross sections for the three 1^+-states at E_x = 2.52 MeV, E_x = 11 MeV, and E_x = 16.8 MeV in ^{48}Sc are shown. We compare results obtained either with pure particle-hole, standard RPA, or generalized RPA wave functions (including Δ isobars) with the data. By comparison of the results for "p-h" and "RPA" one can see that the residual ph-interaction redistributes the GT-strength in that it shifts a large amount of strength from the low to the high excitation energy region. The theoretical cross section to the low-lying 1^+-state calculated with simple "ph"-wave functions is strongly reduced when RPA wave functions are used, while that for the high-lying 1^+, T=3-state is enhanced. This is due mainly to the repulsive ph-interaction which pushes a large fraction of the low-lying $\sigma\tau$-strength to higher energies. The introduction of Δ isobars, which means coupling of these (low-lying) 1^+-states to (ΔN^{-1})-states at ~300 MeV excitation energy, has a similar effect in that now part of the GT-strength is robbed from the low-lying states and shifted to the high energy region at 300 MeV. This effect can clearly be seen by comparing the cross sections based on RPA with those obtained with "RPA with Δ". For the 1^+, 2.52 MeV-state the quenching at 0^o amounts to ~28 %, and that of the 1^+, T=3-state at ~11 MeV amounts to 30 %.

In the lower part of fig. 2 we analyze data of the 1^+, T=4, 16.8 MeV state in ^{48}Sc. The wave function of this state was obtained by simply applying the T_--lowering operator onto the 1^+, T=4 state in ^{48}Ca. In the case of "RPA with Δ" the wave function has then basically the following form:

$$|1^+,T=4,{}^{48}Sc\rangle = \sqrt{\frac{1}{2T_o}}|PN^{-1}\rangle + \sqrt{\frac{3}{2T_o}}|\Delta^{++}P^{-1}\rangle + \sqrt{\frac{4}{2T_o}}|\Delta^{+}N^{-1}\rangle + |2p\text{-}2h\rangle + |1p1\Delta\text{-}2h\rangle + \ldots , \quad (2)$$

with T_o=4 being the isospin of the 1^+-state in the parent nucleus ^{48}Ca. Under the assumption of a direct reaction mechanism only the 1p-1h and the 1Δ-1h components of the wave function of eq. (2) can be directly excited. Since the isospin factors of the $|\Delta^{++}P^{-1}\rangle$ and $|\Delta^{+}N^{-1}\rangle$ configurations are by a factor of $\sqrt{3}$ or 2, respectively, larger than that for the $|PN^{-1}\rangle$ configuration and since the $|PN^{-1}\rangle$ and $|\Delta N^{-1}\rangle$ excitations interfere destructively we have a particularly strong quenching effect for the $T_>$-GT states. This can actually be seen from the 1^+, T=4 cross sections in fig. 2. The quenching amounts to ~50 %. In the lower part of fig. 2 we show also the contribution to the 1^+, T=4 cross section which is due to the (ΔN^{-1})-component in the wave function. This contribution is only a factor of ~10 smaller than that due to the (PN^{-1})-configurations. In our calculations we find 59 % of the total GT-strength in the three 1^+-states (multiplying the 1^+, 11 MeV cross section with the factor 7/8) while experimentally Gaarde et al.[8] find 45±7.5 %.

References

1) D.E. Bainum et al., Phys. Rev. Lett. 44 (1980) 751; C.D. Goodman et al., Phys. Rev. Lett. 44 (1980) 1755.

2) M. Rho, Nucl. Phys. A231 (1974) 493; K. Ohta and M. Wakamatsu, Nucl. Phys. A234 (1974) 445; J. Delorme, M. Ericson, A. Figureau, and C. Thévenet, Ann. Phys. 102 (1976) 273; E. Oset and M. Rho, Phys. Rev. Lett. 42 (1979) 42; I.S. Towner and F.C. Khanna, Phys. Rev. Lett. 42 (1979) 51; W. Knüpfer, M. Dillig, and A. Richter, Phys. Lett. 95B (1980) 349; A. Härting et al., Phys. Lett. 104B (1981) 261; H. Toki and W. Weise, Phys. Lett. 97B (1980) 12; S. Krewald, F. Osterfeld, J. Speth, and G.E. Brown, Phys. Rev. Lett. 46 (1981) 103; A. Bohr and B.R. Mottelson, Phys. Lett. 100B (1981) 10; G.E. Brown and M. Rho, Nucl. Phys. (in press).

3) T. Suzuki, S. Krewald, J. Speth, Phys. Lett. 107B (1981) 9.

4) F. Osterfeld, FROST-MARS-Code, unpublished.

5) W.G. Love, in: The (p,n) reaction and the nucleon-nucleon force, eds. C.D. Goodman et al. (Plenum, New York, 1980) p. 30; F. Petrovich, W.G. Love, Nucl. Phys. A354 (1981) 499c.

6) G.F. Chew and F.E. Low, Phys. Rev. 101 (1956) 1570.

7. B.D. Anderson et al., Phys. Rev. Lett. 45 (1980) 699; J.W. Watson et al., Phys. Rev. C23 (1981) 2373.

8) C. Gaarde et al., Phys. Lett. B (in press).

3.7. Electron Scattering Coincidence Experiments to Study Higher Multipole Resonances

G. Co', S. Krewald, J. Speth

The advent of high-duty cycle electron accelerators makes the investigation of giant resonances with coincidence experiments attractive. The hope is that sufficient experimental information can be gathered in order to disentangle the various multipolarities. In Born approximation, the (ee'p) cross section (Coulomb scattering only) factorizes into the Mott cross section σ_M and the square of the inelastic form factor, which is the Fourier transform of the charge transition density[1]:

$$\frac{d^4\sigma}{d\Omega_\ell d\varepsilon_\ell d\Omega_p d\varepsilon_p} = \sigma_M \frac{q_\mu^4}{q^4} \cdot |F(\vec{p},\vec{q})|^2$$

$$\text{with} \quad F(\vec{p}\vec{q}) = \langle A-1,\vec{p}|\rho(\vec{q})|A\rangle \qquad (1)$$

where $\vec{q}$ denotes the momentum transfer of the electron onto the nucleus and $\vec{p}$ is the momentum of the outgoing proton. If the residual nucleus is described by a pure hole state $\psi_h(\vec{r})$, the inelastic form factor is

$$F(\vec{p}\vec{q}) = \int d^3r\, \chi_{\vec{p}}^{(-)*}(\vec{r})\psi_h(\vec{r})e^{i\vec{q}\cdot\vec{r}} \qquad (2)$$

In most applications, the distorted wave is approximated by a plane wave[1,2]. In this approximation, the inelastic form factor is proportional to the momentum distribution of the hole state. For the region of relatively small energy transfer to the nucleus, however, distortion effects may play a crucial role at least for the outgoing proton. Therefore we propose to incorporate the distortion effects directly into the nuclear wave function by using the continuum random-phase wave function

$$|A-1,\vec{p}\rangle = \sum_{ph} \int d\varepsilon_{\vec{p}}\, X_{ph}(\varepsilon) a_{\vec{p}}^{+}(\varepsilon) b_h^{+}|0\rangle \qquad (3)$$

Here the particle states $a_{\vec{p}}^{+}(\varepsilon)$ are identical to the distorted waves obtained from the nuclear mean field. The wave function (3) contains both direct knock-out processes as well as core-polarization effects. The analytic derivation of the inelastic form factors is in progress.

References

1) T. de Forest, Jr., Ann. Phys. 45 (1967) 365.
2) Y. Balashov et al., Nucl. Phys. A345 (1980) 367.

3.8. Meson Exchange Current Effects in Heavy Nuclei

S. Krewald, J.S. Dehesa[+], T.W. Donnelly[++]

The existence of meson exchange currents in nuclei is an immediate consequence of charge conservation, which requires an isovector static exchange current in the lowest order (1/M) of a nonrelativistic reduction. As first derived by Villars[1], the one-pion exchange current consists of a "pionic" exchange current (the photon interacts with a pion) and a "seagull"-current (the photon interacts with an antiparticle). Particularly clean evidence for the importance of exchange currents is obtained in deuterium[2]. In heavier nuclei, the problem is that the nuclear wave functions are too poorly known to draw unambiguous conclusions, though the importance of exchange current effects particularly at large momentum transfer has been stressed[3]. This situation has changed after the discovery of magnetic high spin states[4] which are relatively pure particle-hole states with possible admixtures of phonons. Here the nuclear structure may be explored at small q-transfer, and then be used to study meson-exchange effects at large q-transfer.

Though practical calculations of exchange current effects are pretty much routine, the existing methods are based on harmonic oscillators and therefore cannot be expanded to heavier nuclei. We propose here a new approach based on a direct evaluation of the Feynman diagrams. The basic idea is not to use Feynman's parameter integral to combine the product of two propagators, but rather to work with the product of two q-space integrals. The resulting formulae reduce to an effective one-body operator in the limit of large meson-masses. As an example, the seagull-current gives the following form factor for an RPA-wave function:

$$\langle JM|T(q)|0\rangle = e_\pi \frac{f^2}{\mu^2} \int_0^\infty dr\, r^2\, j_J(qr) \sum_{ph} X_{ph}^{J\,*}$$

$$+ \sqrt{\frac{(2j_p+1)(2j_h+1)}{4\pi\, J(J+1)}}\,(-)^{j_p-1/2} \begin{pmatrix} j_p & j_h & J \\ 1/2 & -1/2 & 0 \end{pmatrix} (\varkappa_p+\varkappa_h)$$

$$\times \left(\frac{d}{dr} + \frac{\varkappa_p+\varkappa_h+2}{r}\right) R_p^*(r) R_h(r) \rho_{t'}(r)$$

with $\varkappa_i = (\ell_i - j_i)(2j_i+1)$. The proton (neutron) ground state density is denoted by $\rho_{t'}(r)$. The following qualitative conclusions can be drawn already at the present stage in the case of the high spin states:

(i) the q-dependence of the form factor due to meson-exchange currents will be very much like the one obtained from the convection and the spin current.

(ii) an enhancement at large q-transfer has to be expected, because the 1p1h nucleon wave functions are multiplied with the nuclear density, which introduces large Fourier components into the form factor.

The fact that mesonic corrections give rise to a modified orbital g-factor g_ℓ (and spin g factor g_s) has been known[5] for a long time and is proved in this

contribution directly in a finite nucleus, using an analytical limit. Numerical applications of the full approach are in preparation[6].

References

1) F. Villars, Helv. Phys. Acta 20 (1947) 476.

2) D.O. Riska and G.E. Brown, Phys. Lett. 38B (1972) 193.

3) J. Dubach, J.H. Koch, T.W. Donnelly, Nucl. Phys. A271 (1976) 279;
J.L. Friar, Ann. Phys. 104 (1977) 380.

4) J. Lichtenstadt et al., Phys. Rev. C20 (1979) 497.

5) H. Migazawa, Prog. Theor. Phys. 6 (1951) 801.

6) S. Krewald, J.S. Dehesa, J. Speth, T.W. Donnelly, to be published.

+ Univ. de Granada, Spain

++ MIT, Cambridge, Mass., USA

3.9. Pionic $\Delta\ell$=1 Charge Exchange Modes in Heavy Mass Nuclei

F. Osterfeld, S. Krewald, H. Dermawan, J. Speth

In the past year, new experimental information has been obtained on "collective magnetic resonances" in medium and heavy mass nuclei using the (p,n) reaction. The most prominent peak is identified as the T_o-1 component of the Gamow-Teller resonances (GTR, 1^+, $\Delta\ell$=0, Δs=1). The structure of this GTR is very similar to the well known isobaric analogical state (0^+,IAS). Both resonances can be described in the framework of the RPA theory as a superposition of proton particle-neutron hole states. Besides the GTR the charge exchange ^{208}Pb(p,n)^{208}Bi experiments[1] revealed another broad bump. The authors of ref. 1 concluded that this resonance is a spin-isospin flip dipole mode ($\Delta\ell$=1, Δs=1). We investigate the nature of this $\Delta\ell$=1 resonance in more detail. We show that this $\Delta\ell$=1 resonance is a superposition of all possible $\Delta\ell$=1, Δs=1 modes with spin-parity 0^-, 1^- and 2^-, and one of $\Delta\ell$=1, Δs=0 mode with spin-parity 1^-. We also explain the rather broad width of the $\Delta\ell$=1 resonance of 10 MeV and the shift of its centroid energy which is located at 21.5 MeV in the 160 MeV ^{208}Pb(p,n) experiment[1] and at around 25 MeV in an experiment with 45 MeV incident proton energy[2].

The structure calculations reported here are based on the random phase approximation (RPA) and have been performed in the same way as described in refs. 3,4. For the residual p-h interaction we used the generalized Landau-Migdal interaction which includes the finite range π- and ρ-exchange potentials.

The results of the RPA calculations for charge exchange modes with spin parity 0^+ through 2^- are presented in table 1. Only the collective states which produce an appreciable fraction of the total (p,n) cross section are listed in the table.

J^π	Δs	E_x [MeV]	$d\sigma/d\Omega$ (5^o) at E_p = 160 MeV [mb]	$d\sigma/d\Omega$ (7.5^o) at E_p = 45 MeV [mb]
0^-	1	23.73	2.433	0.0733
1^-	1	20.33	0.533	0.0304
1^-	1	23.00	2.067	0.0668
1^-	1	23.47	5.667	0.1633
1^-	0+1	25.43	0.6+0.6	0.3302+0.0197
1^-	0	28.14	2.05	1.32
2^-	1	17.80	1.267	0.069
2^-	1	18.33	1.733	0.808
2^-	1	19.75	2.5	0.1067
2^-	1	21.35	0.967	0.0414
2^-	1	21.62	2.2	0.078
2^-	1	23.44	0.383	0.0101
2^-	1	25.88	1.533	0.0217

Table 1: The excitation energies are measured with respect to the ground state of ^{208}Bi.

The cross section calculations have been performed with the fast speed DWBA code FROST-MARS[5] which includes knock-out exchange amplitudes exactly.

For the effective projectile-target nucleon interaction

we use the G3Y interaction[6] at E_p = 160 MeV and M3Y interaction at E_p = 45 MeV [7].

In the calculation of the 1^-, $\Delta s=0$ cross section at E_p = 45 MeV we also include the imaginary form factor from the collective model following the procedure of ref. 8.

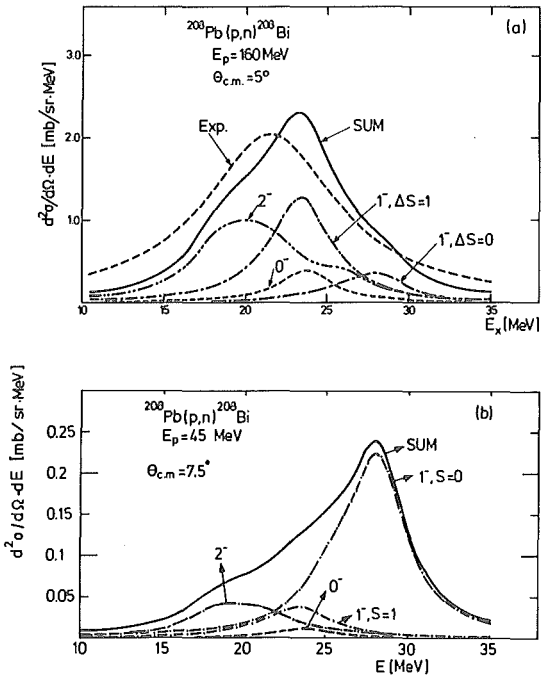

Fig. 1: Charge exchange spectra for 160 MeV and 45 MeV incident proton energies scattered from ^{208}Pb. In the upper part the theoretical spectra are compared with the experimental data of ref. 1. The 0^-, the 1^- ($\Delta s=1$) and the 2^- cross sections have been reduced by a factor of 3 in order to account for quenching effects.

In fig. 1a and 1b we show the spectra of ^{208}Pb(p,n) reactions for E_p = 160 MeV and 45 MeV. The theoretical results in fig. 1a are compared with the experimental data of Horen et al.[1]. We have assumed an experimental cross section of 32 mb/sr for the $\Delta\ell=1$ resonances at $\Theta_{c.m.} = 5^0$ and have folded this value into a Breit-Wigner form with the experimental width of 10 MeV. The theoretical (p,n) cross sections have been folded into the same way with a width of 4.1 MeV (as the width of GTR) for each state. The cross sections to $\Delta s=1$ states have been reduced by a factor of 3 in order to account for the quenching effect. The theoretical spectrum agrees remarkably well with the experimental one. The 45 MeV data[2] are unfortunately not background subtracted and have a strong γ contamination in the centre of experimental peak; therefore we are not able to compare our results with the data. There seems, however, to be a qualitative agreement.

From fig. 1a one can see that the $\Delta s=1$ contributions to the spectrum are dominant at 160 MeV proton energy ($V_{\sigma\tau} > V_\tau$ for $E_p > 100$ MeV). In the 45 MeV spectrum (fig. 1b), however, the contributions of the 1^-, $\Delta s=0$ state are dominant while the contributions of the spin-flip states are comparatively small. Since the 1^-, $\Delta s=0$ resonance is located roughly 5 MeV above the 1^-, $\Delta s=1$ resonance (and 2^- resonance) and since they are differently strongly excited at 45 MeV and 160 MeV one finds a shift in the centroid energy of the two spectra by about 2.5 MeV. The centroid energy shift of $\Delta\ell=1$ resonances has actually been found from a comparison of the 160 MeV data of ref. 1 and of the 45 MeV data of ref. 2.

In summary, we have shown that the experimentally observed $\Delta\ell=1$ resonance in the ^{208}Pb(p,n)^{208}Bi reaction is a superposition of all possible $\Delta\ell=1$, $\Delta s=1$ modes with spin-parity 0^-, 1^-, 2^- and of one $\Delta\ell=1$, $\Delta s=0$ mode with spin-parity 1^-.

References

1) D.J. Horen et al., Phys. Lett. 95B (1980) 27.

2) W.A. Sterrenburg et al., Phys. Rev. Lett. 45 (1980) 1839.

3) J. Speth, V. Klemt, J. Wambach, G.E. Brown, Nucl. Phys. A343 (1980) 382.

4) S. Krewald, F. Osterfeld, J. Speth, G.E. Brown, Phys. Rev. Lett. 46 (1981) 103.

5) F. Osterfeld, FROST-MARS-Code, unpublished.

6) W.G. Love, in: The (p,n) Reaction and Nucleon-Nucleon Force, eds. C.D. Goodman et al., (Plenum, New York, 1980) p. 30.

7) G.F. Bertsch et al., Nucl. Phys. A284 (1977) 399.

8) G. Baur, V.A. Madsen, F. Osterfeld, Phys. Rev. C17 (1978) 819.

3.10. Spin Polarization in the Ground State of ^{207}Pb

J. Wambach[+]

Recently a physically intuitive model for the spin parts of the particle-hole interaction based on the long range parts of the one boson exchange potential has been developed[1]. The Fermi liquid parameters of this interaction show remarkable similarities with more sophisticated interactions (G-matrices), especially in the tensor channels. We may hope that the extrapolation from the Landau limit is reasonable. Transverse electromagnetic excitations are a tool to investigate high momentum spin correlations in the nucleus. The model interaction predicts that those are weak since short range repulsion gets cancelled by the attractive one-pion-exchange as the momentum transfer in the p-h scattering increases. We have investigated the ground state dipole moment distribution of ^{207}Pb. The magnetic moment $\mu^{exp} = .59\ \mu_0$ is very close to the Schmidt value $.637\ \mu_0$. The reason is that the coupling of the $3p_{1/2^-}$ hole to the spin-orbit partners is very small (it vanishes in a zero range limit). Higher shells do not contribute in the long wave length limit either. As the momentum transfer to the nucleus increases the form factor $F(q) \sim \langle 0|M^1(q)|1^+\rangle$ gets polarization contributions from coherent $2\hbar\omega$-states which decrease the shell model form factor. The suppresion is however not as large as recently claimed[2] (fig. 1).

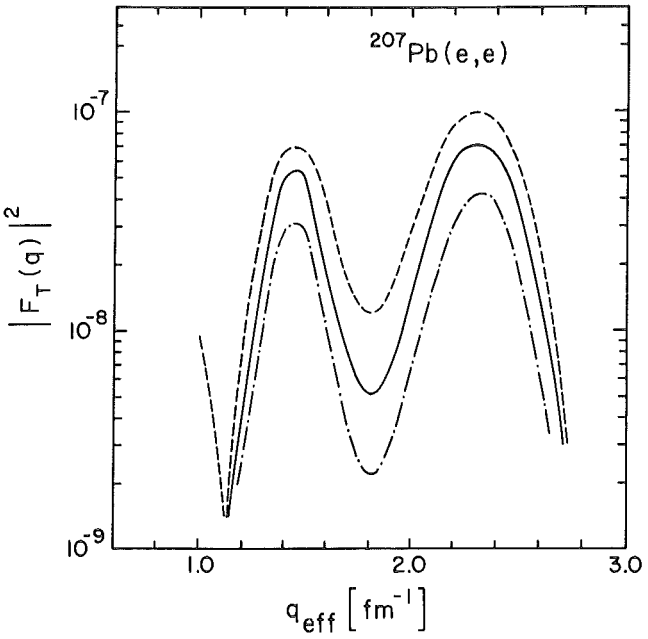

Fig. 1: Transverse magnetic DWBA form factor of ^{207}Pb as a function of $q_{eff} = (1 + 4Z\alpha/3EA^{-1/3})$. The dashed line is the shell model prediction. The dash-dotted line was taken from ref. 2.

References

1) M.R. Anastasio and G.E. Brown, Nucl. Phys. A285 (1977) 127.

2) J. Hamamoto, J. Lichtenstadt and G.F. Bertsch, Phys. Lett. 93B (1980) 213.

[+] SUNY at Stony Brook, Stony Brook, N.Y., USA

3.11. Two-Particle Two-Hole Damping of "Giant 1^+-States" in ^{208}Pb

J. Wambach[+]

One particle-one hole calculations in ^{208}Pb consistently predict giant $2\hbar\omega$ 1^+ isovector excitations with roughly 50 % of the $[\sigma Y_0]^{1^+}$ and $[\sigma Y_2]^{1^+}$ RPA strength[1,2]. These states have not been detected so far even though the transverse (e,e') cross section is large[1]. Because of the high excitation energy considerable 2p-2h damping is expected (around 30 MeV the density of states is larger than 10^4/MeV). Within a quasiphonon model[3] we have analyzed the coupling of the 1p-1h collective state to 2p-2h degrees of freedom. As suggested in ref. 4 the average p-h gaps from an adjusted static mean field should be enlarged to take into account the lower density of states from dynamical correlations in a self-consistent potential with G-matrices. We used the scaling prescription[4] with $m^*/m = .64$ (Reid value). For large $G_0' = 1.8$ the giant $1^+\Delta T=1$ resonance has an excitation energy of 35 MeV (the D1 force of Gogny[2] gives similar results). The calculated 2p-2h energy shift ΔE_0 is small and shows a typical principal value behaviour[4]. The strength function in fig. 1 shows complete damping into more complicated configurations.

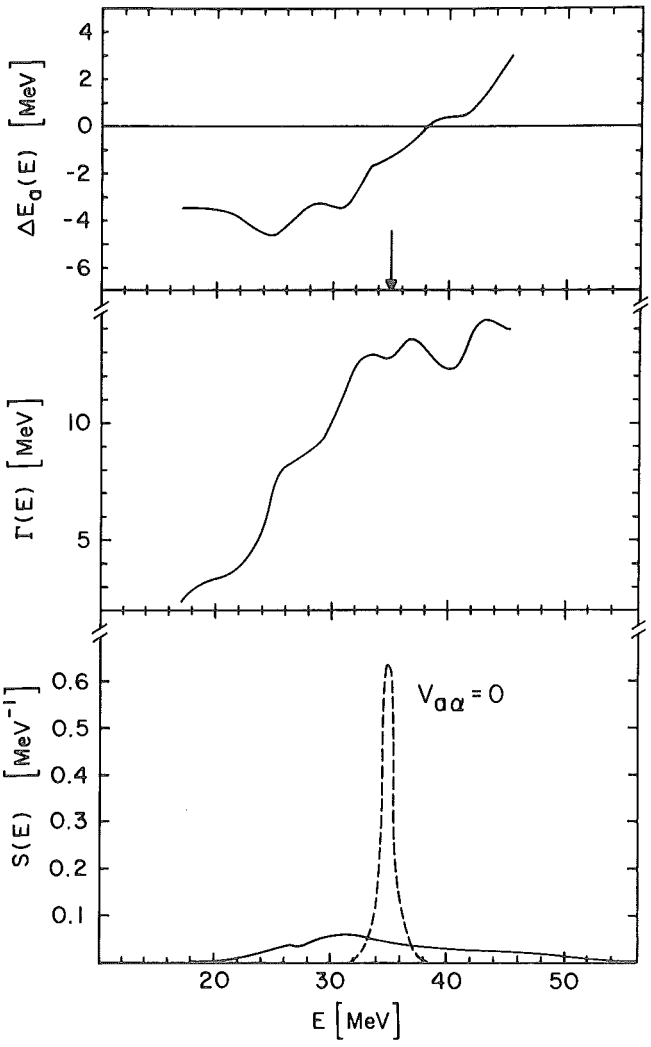

Fig. 1: 2p-2h energy shift ΔE, width Γ and strength function S(E) for the $2\hbar\omega$ 1^+ T=1 giant resonance in ^{208}Pb. The dotted line indicates the unperturbed 1p-1h state.

References

1) J. Speth et al., Phys. Lett. 63B (1976) 257.
2) J.P. Blaizot and L. Sips, Nucl. Phys. A337 (1980) 586.
3) J. Wambach, Li Chu-Hsia and V. Mishra, to be published.
4) G.E. Brown, J.S. Dehesa and J. Speth, Nucl. Phys. A330 (1979) 290.

+ SUNY at Stony Brook, Stony Brook, N.Y., USA

3.12. Quasiparticle Effective Masses in Finite Nuclei

J. Wambach[+], *V. Mishra*[+], *Li Chu-Hsia*[++]

The dynamics of the nuclear mean field of single particle motion is most conveniently described by the effective mass m^*/m, insisting that a quasiparticle obeys the same dispersion relation as a free particle. In a translationally invariant system this is simply the kinetic energy of a particle with mass m^*

$$\varepsilon_k = \frac{k^2}{2m^*} \tag{1}$$

Utilizing the definition of m^*/m

$$\frac{m^*}{m} = k \frac{dk}{d\varepsilon_k} \tag{2}$$

and the dispersion relation for a "dressed" particle which is obtained from the poles of the single particle Greens function

$$\varepsilon_k = \frac{k^2}{2m} + \mathrm{Re}\,\Sigma\,(k,\varepsilon_k) \tag{3}$$

one readily derives the standard expression[1]

$$\frac{m^*}{m} = (1 - \frac{\partial \mathrm{Re}\Sigma}{\partial \varepsilon})/(1 + \frac{m}{k^2}\frac{\partial \mathrm{Re}\Sigma}{\partial k})_{\varepsilon=\varepsilon_k} \equiv \frac{\bar{m}}{m} \cdot \frac{\hat{m}}{m} \tag{4}$$

The k-mass $\frac{\hat{m}}{m}$ stems from the nonlocality of the mean field and is smaller than one, while the E-mass $\frac{\bar{m}}{m}$ arises from the true energy dependence of Σ. It is one in the HF-approximation. In nuclear matter $\frac{\bar{m}}{m}$ is enhanced near the Fermi surface because the HF state can decay into 2p-1h states. We have analyzed if similar enhancements can be obtained in nuclei for orbits near the Fermi surface. Of course the mean field Σ is nonlocal in the linear momentum for a non-uniform system and the effective mass is a priori not a well defined quasiparticle quantity. However the nuclear matter notions can be carried over adopting a state-dependent effective mass for each single particle orbit α. By definition

$$(\frac{m^*}{m})_\alpha = (1 - \frac{\partial \mathrm{Re}\Sigma_{\alpha\alpha}}{\partial \varepsilon})/(1 + \frac{m}{k^2}\frac{\partial \mathrm{Re}\Sigma_{\alpha\alpha}}{\partial k}) \tag{5.a}$$

$$\sum_{\alpha\alpha} = \langle \alpha | \Sigma(\omega) | \alpha \rangle \tag{5.b}$$

We have evaluated the matrix elements $\Sigma_{\alpha\alpha}$ in coupling HF-states to RPA-vibrations in ^{208}Pb and computed the E-mass $(\frac{\bar{m}}{m})_\alpha$ together with the change in single particle energy in the first oscillator shell for particle states

$$\varepsilon_\alpha = \varepsilon_\alpha^{HF} + \sum_{\alpha\alpha} (\varepsilon_\alpha) \tag{6}$$

The results are listed in table 1. It is instructive to extract a frequency dependent average E-mass near the Fermi surface

$$\frac{\bar{m}}{m}(\varepsilon) = \sum_\alpha \frac{(2j_\alpha+1)(\frac{\bar{m}}{m}(\varepsilon))_\alpha}{\sum_\alpha 2j_\alpha+1} \tag{7}$$

which is displayed in fig. 1. As the frequency increases $\frac{\bar{m}}{m}(\varepsilon)$ increases, which means the particles get heavier (the k-mass does not change much on the energy scale considered). The system tries to resist the imposed frequency change. At a large enough frequency however a rapid change in $\frac{m^*}{m}$ takes place and the coupling to p-h states (dominantly surface modes) vanishes. This "shake off" of the surface modes takes place at $\sim 1/4\ \varepsilon_F$ and is probably much more pronounced than in infinite nuclear matter.

proton				neutron			
n&j	$(\frac{\bar{m}}{m})_\alpha$	ε_α^0	ε_α	n&j	$(\frac{\bar{m}}{m})_\alpha$	ε_α^0	ε_α
$3p_{1/2}$	1.66	8.34	6.1	$3d_{3/2}$	1.16	6.57	5.9
$3p_{3/2}$	1.84	7.58	5.6	$2g_{7/2}$	1.27	6.5	5.45
$2f_{5/2}$	1.66	7.17	5.3	$4s_{1/2}$	1.07	5.84	5.4
$1i_{13/2}$	1.41	5.58	4.25	$3d_{5/2}$	1.07	5.17	4.7
$2f_{7/2}$	1.22	4.41	3.2	$1j_{15/2}$	1.52	4.97	4.2
$1h_{9/2}$	1.04	3.14	2.7	$1i_{11/2}$	1.20	4.04	3.85
				$2g_{9/2}$	1.15	2.88	2.55
Average	1.37			Average	1.27		

Table 1

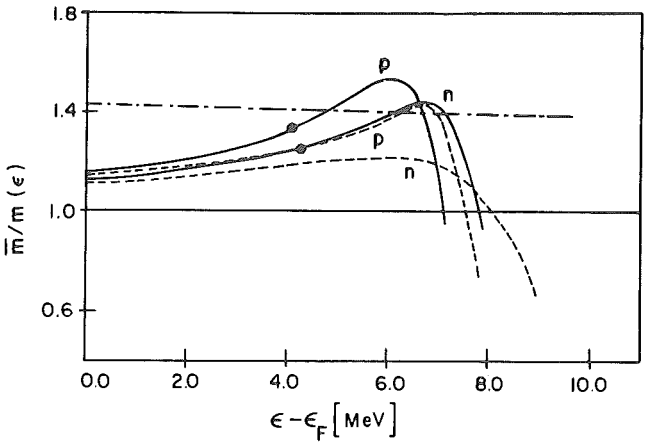

Figure 1

References

1) J.P. Lejeune et al., Phys. Rep. 25C (1976) 83.

+ SUNY at Stony Brook, Stony Brook, N.Y., USA

++ Inst. of Atomic Energy, Academia Sinica, Beijing, The Peoples Republic of China

3.13. Spin-Isospin Sum Rules Based on the Quark Model

G.E. Brown[+], *H.R. Fiebig*[+], *J. Wambach*[+]

Recent observations of Gamow-Teller and M1 states in proton-nucleus reactions at intermediate energies ($\lesssim$ 200 MeV) indicate that both nuclear shell model and internal nucleon degrees of freedom can be excited by an effective spin dependent isovector force[1]. It is thus straightforward to ask whether it is possible to describe the overall, say M1 transition strength including the internal degrees of freedom in a model independent way.

An appropriate tool would be a sum rule which only depends on parameters that are "fundamental" from the nuclear physicist's point of view such as, e.g., particle masses, meson coupling constant, bag radii and any kind of QCD ingredients.

To get a rough preliminary idea one may describe baryons in a quark model where, non-relativistically, the quarks acquire effective masses. The Hamiltonian

$$H_{GLA} = \sum_q m_q + \frac{B}{2} \sum_{q \neq p} \frac{\vec{\sigma}^q \cdot \vec{\sigma}^p}{m_q \; m_p} \qquad (1)$$

with $m_q = m_Q$ = 360 MeV for non-strange, $m_q = m_s$ = 540 MeV for strange quarks and B = 50 MeV × m_Q provides a good fit to low lying baryon masses[2]. In this picture the magnetic moment is

$$M_z = \sum_q \frac{\hbar e}{2 m_q c} \frac{1}{2} (\tau_z^q + \frac{1}{3}) \sigma_z^q \qquad (2)$$

Calculation of $\Sigma_{M1} = 1/2 \times \langle \phi_o | [M_z, [H_{GLA}, M_z]] | \phi_o \rangle$ with $|\phi_o\rangle$ being a Slater determinant for a spin saturated nucleus of mass A yields the energy weighted sum rule

$$\sum_{M1} = \sum_n (E_n - E_o) |\langle \phi_n | M_z | \phi_o \rangle|^2 = (\frac{m_N}{m_Q})^2 \frac{2B}{m_Q^2} \; 8 \; A \; \mu_o^2 = 1780 \; \mu_o^2 \text{ MeV } A \; , \qquad (3)$$

here m_N = 930 MeV and $\mu_o = e\hbar/2m_N c$. The transition merely leads to a state where a nucleon simply is substituted with an isobar. The model is, so far, rather trivial and one may wish to look at a system of communicating hadrons.

Therefore consider a state $|\psi_o\rangle$ with $N^{-1}\Delta$-correlations and excited states

$$|\psi_n\rangle = \sum_{N\Delta} (x_{\Delta N}^{(n)} \; C_\Delta^+ \; C_N - y_{\Delta N}^{(n)} \; C_N^+ \; C_\Delta) |\psi_o\rangle \qquad (4)$$

where the sum is over spin, isospin and orbital quantum numbers. For a schematic calculation the particle-hole interaction may be chosen to be $\xi \times f(1,2) S(1) \cdot S(2) \; \vec{T}(1) \cdot \vec{T}(2)$ where in case of a ΔN-vertex S and $\vec{T}$ are transition spin and isospin, respectively, and conventional spin and isospin otherwise; f(1,2) accounts for different coupling strength of NN-, NΔ- and $\Delta\Delta$-vertices determined from the constituent quark model (cf. e.g. ref. 3). The RPA-equations yield a coherent T=S=1 state which exhausts the sum rule (3). The figure shows Σ_{M1}

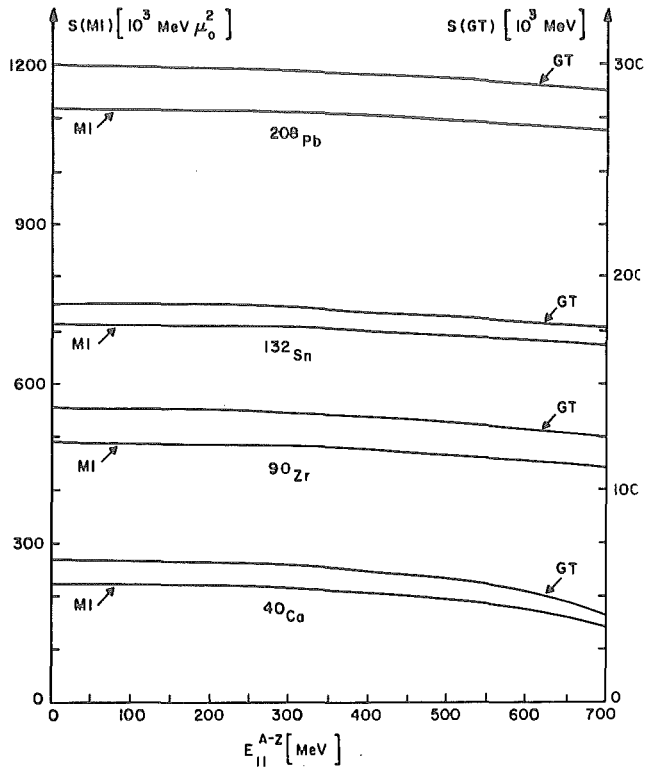

for various nuclei as a function of the energy shift E_{coh} (rather than ξ). (A sum rule for the Gamow-Teller operator is also given.) Σ_{M1} and Σ_{GT} are remarkably stable even for unrealistic values of E_{coh}. (One may expect $E_{coh} \gtrsim$ 300 MeV.)

Of course, the above rough estimates only give the order of magnitude. A realistic theory of sum rules proposed here should account for (a) the "confined-quark" structure of baryons, (b) the meson fields filling the remainder volume of a nucleus[4] and (c) many-body effects such as short range correlations.

References

1) D.J. Horen et al., Phys. Lett. 95B (1980) 27;
A. Bohr and B.R. Mottelson, Phys. Lett. 100B (1981) 10;
G.E. Brown and M. Rho, preprint 1981;
C. Gaarde et al., preprint 1981.

2) S.L. Glashow, Physica 96A (1979) 27.

3) G.E. Brown and W. Weise, Phys. Rep. 22C (1975) 279.

4) G.E. Brown and M. Rho, to be published in "Comments on Nuclear and Particle Physics".

[+] SUNY at Stony Brook, Stony Brook, N.Y., USA

3.14. Charge-Exchange Resonances in Deformed Nuclei

D. Zawischa[+] *and J. Speth*

Within the quasi-particle RPA we have calculated the isobaric analogical states and Gamow-Teller ($\Delta\ell$=0) resonances in ^{162}Dy and ^{238}U. Both resonances can be excited in charge-exchange reactions, e.g. in (p,n). Due to the repulsive particle-hole interaction in the $\tau\cdot\tau$- and $\sigma\cdot\sigma\tau\cdot\tau$-channel we obtain rather collective states in which most of the corresponding transition strength is concentrated. For the same reason those states are also shifted to higher energies compared to the unperturbed quasi-particle energies. In figs. 1 and 2 we show the results of ^{162}Dy and ^{238}U, respectively. In both cases the isobaric analogical states (dashed line in the lower part of the figure) and the Gamow-Teller resonance (full line in the lower part) are practically degenerated. It is interesting to see that the $K^{\pi}=0^{+}$ and 1^{+} components of the Gamow-Teller resonance are only little separated from each other. From a simple comparison with the electric dipole resonance one would expect a much larger splitting due to the nuclear deformation. Therefore we obtain from our calculation only a broadening of the Gamow-Teller resonances in deformed nuclei but no splitting into two separated components. This theoretical result is in agreement with the experimental results in the rare earth region[1].

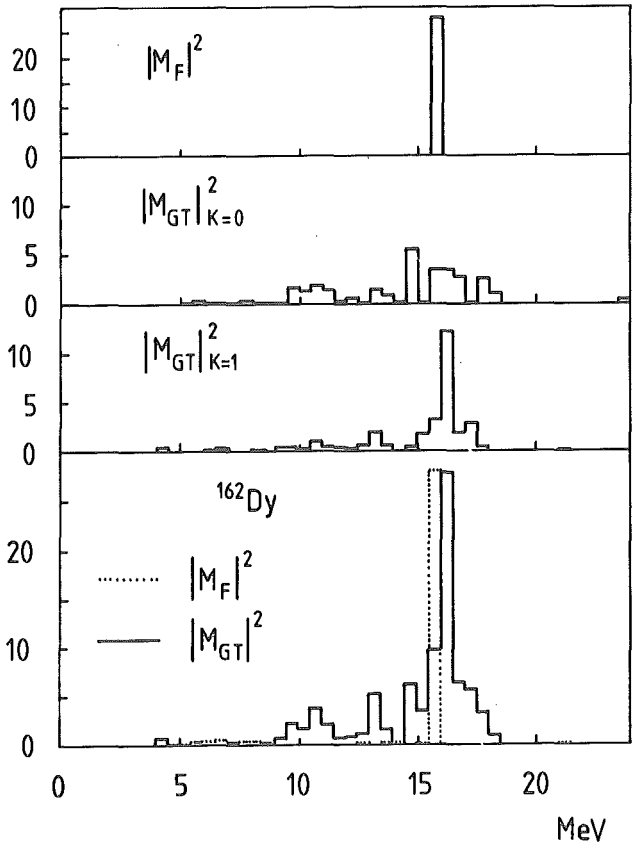

Fig. 1: Isobaric analogical and Gamow-Teller resonances in ^{162}Dy. The lower part of the figure shows the transition strengths, summed over all final states in intervals of 0.5 MeV. On top of this the various contributions are given separately.

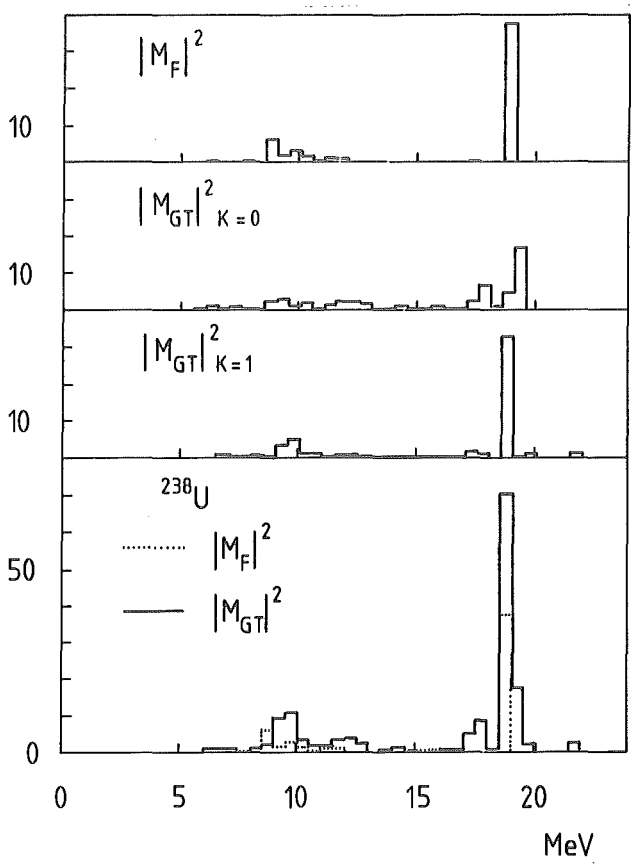

Fig. 2: The same as in fig. 1 for the nucleus ^{238}U.

Reference

1) C. Gaarde et al., preprint.

[+] Inst. f. Theor. Physik, Univ. Hannover

3.15. Electric Giant Resonances in ^{238}U

D. Zawischa[+] and J. Speth

Previous calculations of electric giant resonances in the rare earth region[1] have been extended into the Uranium region. The major changes compared with ref. 1) are: (i) the size of the particle-hole configuration space which has now a dimension of 350. This space includes 74 %, 99 %, and 90 % of the energy weighted sum rule strength for E0, E1, and E2, respectively. (ii) the particle-hole interaction which includes now also the spin-dependent components which have been left out in the earlier attempt.

The results in ^{238}U are qualitatively similar to the results in the rare earth region. Fig. 1 shows the result of the giant electric dipole resonance. The full line indicates the total transition strength whereas the dotted line denotes the partial contribution of the $K^\pi = 0^-$ states. The theoretical result agrees well with the experimental one.

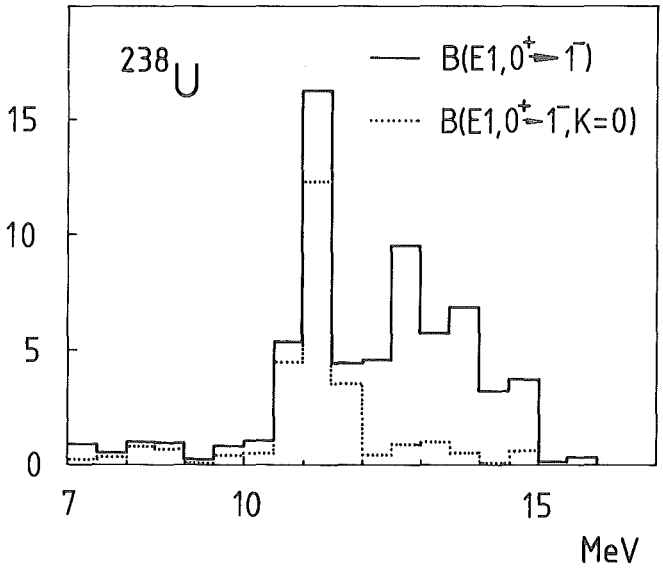

Fig. 1: Giant dipole resonance in ^{238}U.

In fig. 2 we show the results of the monopole (dotted line) and the quadrupole (full line) resonances. The transition strength around 10 MeV and 15 MeV is of isoscalar character whereas the quadrupole strength beyond 15 MeV and the monopole strength around 25 MeV is of isovector character. In the upper part of the figure we show separately the $K^\pi = 0^+$, 1^+, and 2^+ strength, respectively. As pointed out previously the $K^\pi = 0^+$ component is a mixture of quadrupole and monopole strength. This fact gives rise to a splitting of the monopole resonance. In the lower part of fig. 2 the total B(E0) and B(E2) strength is shown. As in the rare earth region the $K^\pi = 0^+$, 1^+ and 2^+ components of the giant quadrupole resonance are very close, therefore giving rise for a broadening of the resonance only. The splitting of the components is too small to be resolved experimentally. The theoretical results are in good qualitative agreement with experiments[2].

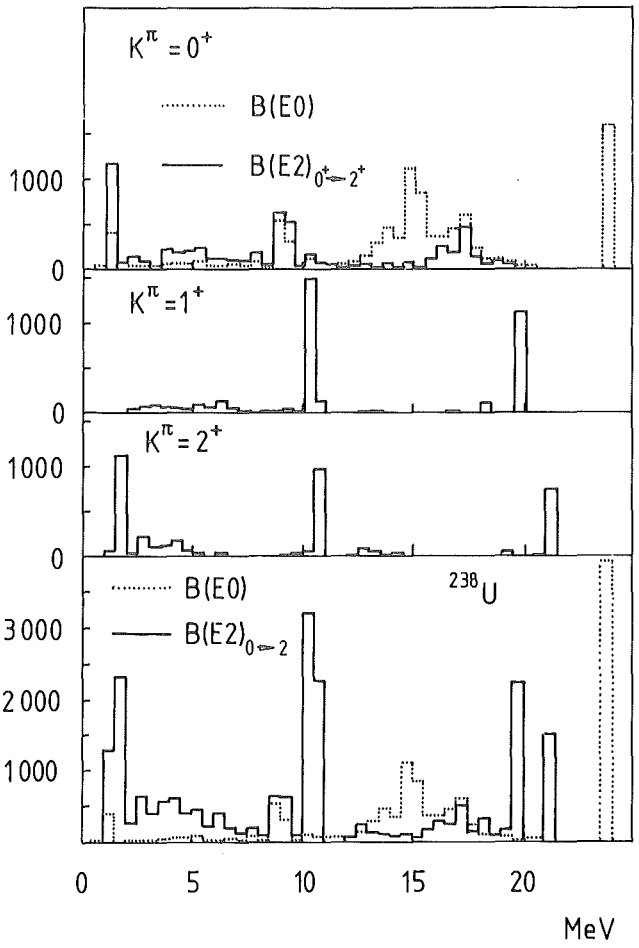

Fig. 2: Monopole and quadrupole transition strength distribution in ^{238}U.

References

1) D. Zawischa, J. Speth, D. Pal, Nucl. Phys. A311 (1978) 445.

2) H.P. Morsch, private communication.

[+] Inst. f. Theor. Physik, Univ. Hannover

3.16. MONSTER - A Code for the Microscopic Description of Deformed Even-Even Nuclei

F. Grümmer, K.W. Schmid[+]

Given a finite single particle basis and an appropriate effective Hamiltonian one may calculate the exact eigenstates of the A-nucleon system within this model space by a shell model configuration mixing calculation (SCM)[1]. However, because of the enormous size of the matrices to be diagonalized, the SCM-approach is restricted to rather small model spaces. Consequently most heavy nuclei, as for example those of the rare earth region, cannot be studied using the SCM-procedure. Equally not accessible to SCM-calculations are furthermore, with only a few exceptions, all those problems, which a priori require the use of several major shells as single particle basis, like for example the description of negative parity states in s-d shell nuclei or the investigation of the highly excited giant multipole resonances. Hence here as well as for many other problems suitable approximations to the complete SCM-expansion of the nuclear wave functions have to be found.

Such an approximation is provided by the "projected quasiparticle model" (PQPM)[2]. In this model the nuclear wave functions are approximated by linear combinations of the particle-number and spin-projected deformed HFB-vacuum and the two-quasiparticle excitations with respect to it.

$$|\alpha;N,Z,I,M\rangle = f^{NZI}_{0;\alpha}|\phi_0;N,Z,I,M\rangle + \sum_{\mu\nu} f^{NZI}_{\mu\nu;\alpha}|\phi_{\mu\nu};N,Z,I,M\rangle \qquad (1)$$

Essential to this approach is that the required symmetries are restored before the diagonalization of the many nucleon Hamiltonian. This means that with

$$|\phi_0;N,Z,I,M\rangle = \hat{P}(IM)\hat{Q}(N)\hat{Q}(Z)|HFB\rangle$$

and (2)

$$|\phi_{\mu\nu};N,Z,I,M\rangle = \hat{P}(IM)\hat{Q}(N)\hat{Q}(Z)\beta^+_\mu\beta^+_\nu|HFB\rangle$$

the matrix equations

$$(H - EN)f = 0 \qquad (3)$$

where H and N denote the Hamiltonian and overlap matrices in the nonorthogonal configuration space (2), has to be solved. In this way spin dependent correlations are taken into account and problems with rotational spurious admixtures are avoided. Furthermore spurious admixtures due to center of mass excitations can be removed at least approximately by a separate treatment of the center of mass Hamiltonian.

With the wave functions (1) being given, then for arbitrary initial and final states the spectroscopic amplitudes

$$S^{iKL^\pi}_{fi} = \langle\alpha_f;N,Z,I_f||[c^+_i c_k]^{L^\pi}||\alpha_i;N,Z,I_i\rangle \qquad (4)$$

can be calculated. These yield the moments and transitions of the considered states and furthermore also transition densities, which may be directly used for example in DWBA-analysis of inelastic scattering experiments and such allow a crucial test of the quality of the nuclear structure description by our wave functions.

As far as light nuclei are considered, the PQPM-approach can be considered as the natural extension of the PHM-model[3] which has been used lately with some success for the description of the giant multipole resonances as well as for low excited states in light deformed N=Z nuclei. Our new approach makes also the N≠Z nuclei accessible to realistic microscopic calculations in large basis systems. However, the PQHM-approach also contains all the essential ingrediences necessary to describe heavier nuclei. We consider it as very satisfying that here the same microscopic approach can be used as for light nuclei.

In the meantime a computer code ("MONSTER") has been developed, which allows to use the PQPM-model for rather general applications. It can handle rather large single nucleon basis systems as well as realistic two body interactions of any type. First results obtained with this code will soon be available.

References

1) R.R. Whitehead, A. Watt, B.J. Cole and I. Morrison, Adv. Nucl. Phys. 2 (1977) 123.

2) F. Grümmer, K.W. Schmid and A. Faessler, Z. Physik A300 (1981) 77.

3) K.W. Schmid and G. DoDang, Phys. Rev. C18 (1978) 1003.

[+] Inst. für Theor. Physik, Univ. Tübingen

3.17. Preliminary Calculations for ^{146}Gd

C. Conci, V. Klemt

From the experimental point of view the structure of the doubly even nucleus $^{146}_{64}Gd_{82}$ is well known[1].

We present in this contribution some preliminary calculations performed in the framework of the RPA theory using a generalized particle-hole interaction which includes, in addition to the zero-range terms of the Landau-Migdal theory, also explicitly the contributions of the one-pion and one-rho exchange potentials[2].

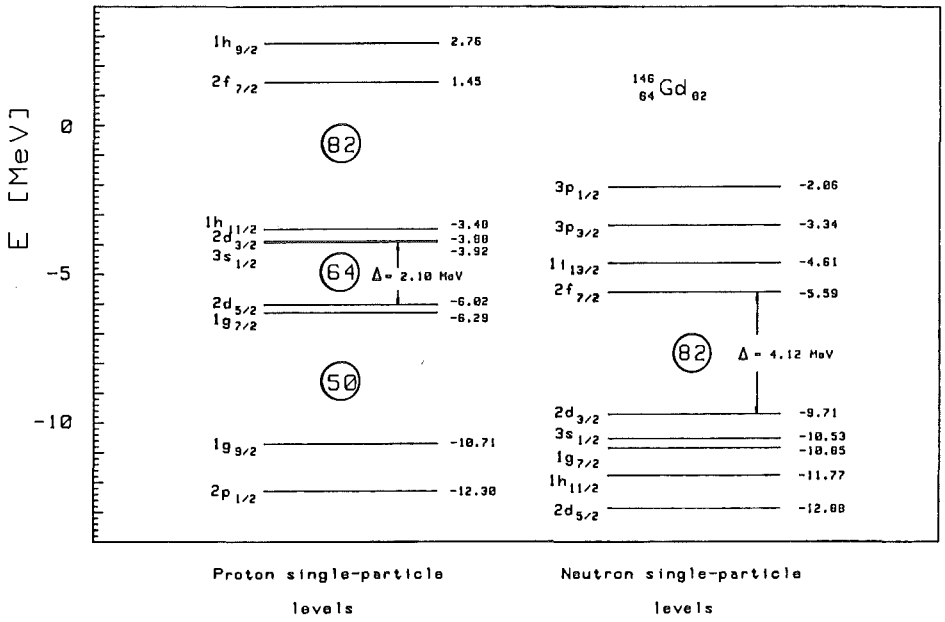

Fig. 1: Single-particle levels for ^{146}Gd around the Fermi surface obtained from a Woods-Saxon potential.

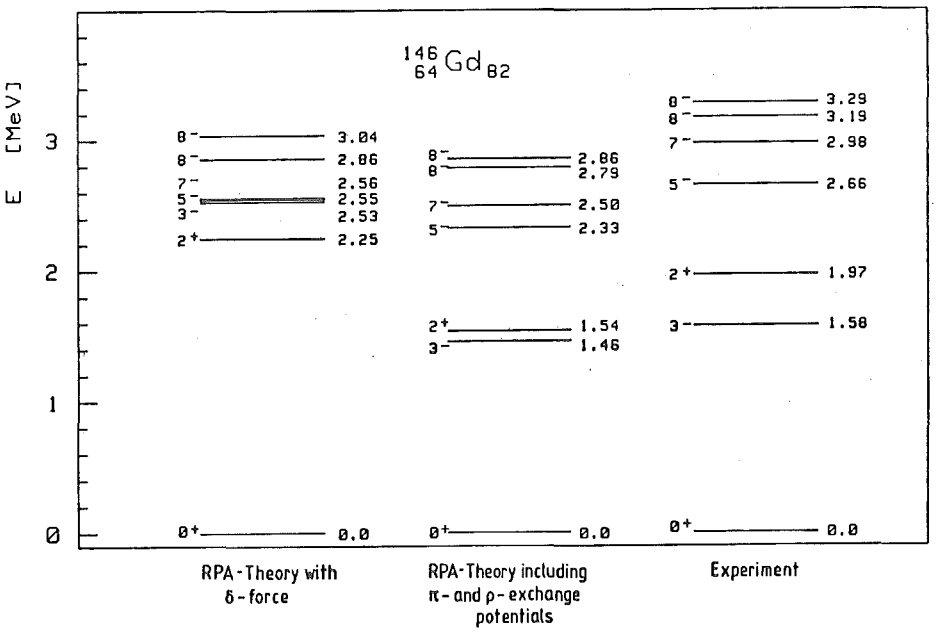

Fig. 2: Low-lying level scheme of ^{146}Gd. (The values of the interpolation radii are 6.63 fm.)

The unperturbed single-particle levels, given in fig. 1, are obtained from a Woods-Saxon potential. The excitation energies and the structure of the low-lying excited states obtained in our calculations are shown in fig. 2 and table 1, respectively.

The comparison between the level scheme obtained using only a δ-force (with the interpolation raddi of ref. 3 readjusted according to the $A^{1/3}$ law) and that one using the tensor force show that only the last one gives the right level sequence and gives also quite good values for the excitation energies.

The calculations using the tensor force reproduce the fact that the ^{146}Gd appears to be the only doubly even nucleus besides ^{208}Pb with a first excited 3^- state and that the dominant configuration contributing to the octupole excitation is the proton particle-hole $\pi h_{11/2}{}^{-}\pi d_{5/2}^{-1}$.

The results written down in table 1 show also that the 3^- state is characterized by a mixture of many 1p-1h excitations, typical for a collective vibration, and that the 2^+ level involves mostly 1p-1h excitations, in particular $\pi s_{1/2}{}^{-}\pi d_{5/2}^{-1}$ and $\pi d_{3/2}{}^{-}\pi g_{7/2}^{-1}$ components.

The other states with negative parity, 5^-, 7^-, 8^-, are given from the particle-hole proton configurations $\pi h_{11/2}{}^{-}\pi d_{5/2}^{-1}$ and $\pi h_{11/2}{}^{-}\pi g_{7/2}^{-1}$. This result is due to the fact that the first proton high-j level, i.e. $h_{11/2}$, is located immediately above the Fermi surface, whereas the neutron high-j orbitals are far away from the N=82 gap.

The analysis of the data confirms the assumption that in order to get better agreement with experiment one has to include realistic one-boson exchange interactions in addition to contact forces.

Furthermore it suggests that one should go beyond RPA, since the structure of ^{146}Gd is more complex than that of fully magic nuclei.

J^π	E	main config.	E_{ph}	X_{ph}
3^-	1.46	$\pi h_{11/2}{}^{-1}\pi d_{5/2}^{-1}$	2.54	-0.910
		$\nu i_{13/2}{}^{-1}\nu h_{11/2}^{-1}$	7.15	0.239
		$\nu f_{7/2}{}^{-1}\nu s_{1/2}^{-1}$	4.94	-0.168
		$\pi h_{11/2}{}^{-1}\pi g_{7/2}^{-1}$	2.81	-0.126
2^+	1.54	$\pi d_{3/2}{}^{-1}\pi g_{7/2}^{-1}$	2.41	-0.687
		$\pi s_{1/2}{}^{-1}\pi d_{5/2}^{-1}$	2.10	-0.666
5^-	2.33	$\pi h_{11/2}{}^{-1}\pi d_{5/2}^{-1}$	2.54	-0.961
		$\pi h_{11/2}{}^{-1}\pi g_{7/2}^{-1}$	2.81	-0.140
7^-	2.50	$\pi h_{11/2}{}^{-1}\pi d_{5/2}^{-1}$	2.54	-0.989
		$\pi h_{11/2}{}^{-1}\pi g_{7/2}^{-1}$	2.81	-0.140
8^-	2.79	$\pi h_{11/2}{}^{-1}\pi g_{7/2}^{-1}$	2.81	-0.955
		$\pi h_{11/2}{}^{-1}\pi d_{5/2}^{-1}$	2.54	-0.2915
8^-	2.86	$\pi h_{11/2}{}^{-1}\pi d_{5/2}^{-1}$	2.54	-0.957
		$\pi h_{11/2}{}^{-1}\pi g_{7/2}^{-1}$	2.81	0.290

Table 1: Main configurations (and the respective ph-energies in MeV and amplitudes) of the low-lying levels of ^{146}Gd obtained with the inclusion of π- and ρ-exchange potentials.

References

1) P. Kleinheinz et al., Z. Physik A290 (1979) 279.

2) J. Speth et al., Nucl. Phys. A343 (1980) 382.

3) G.A. Rinker and J. Speth, Nucl. Phys. A306 (1978) 360.

3.18. A New Method to Treat Even- and Odd-Particle Nuclei Consistently in the Framework of Landau-Migdal's Theory

V. Klemt

The motion of a Fermi particle in a medium is described by the Green function

$$G_{12}(\omega) = \sum_s \frac{\langle\phi_0|a_1|\phi_s\rangle\langle\phi_s|a_2^+|\phi_0\rangle}{\omega-E_s+i\eta} + \sum_r \frac{\langle\phi_0|a_2^+|\phi_r\rangle\langle\phi_r|a_1|\phi_0\rangle}{\omega+E_r-i\eta} \qquad (1)$$

Here $E_s = E_s(A+1)-E_0(A)$ and $E_r = E_r(A-1)-E_0(A)$ are the energies (ground state and excited) of the even-odd nuclei neighbouring to even-even ones with particle number A. The numbers 1, 2, ... define an arbitrary single-particle basis. The Green function can be used to define the mass operator by[1)]

$$\sum_3 \left[\omega\delta_{13}-t_{13}-M_{13}(\omega)\right]G_{32}(\omega) = \delta_{12} , \qquad (2)$$

which shows that the poles of the Green function can be found by solving (for each E_s kept fixed as the argument of M) the eigenvalue equation

$$E_\lambda\delta_{\lambda\lambda'} - t_{\lambda\lambda'} - M_{\lambda\lambda'}(E_s) = 0 . \qquad (3)$$

One of the eigenvalues, $E_\lambda=E_s$, will then be identical with a true energy of an even-odd nucleus, while the others are unphysical. One of the single-particle eigenvectors, $|\lambda\rangle = |\sigma\rangle$, corresponding to the eigenvalue E_s has a physical meaning, too. In fact it can be shown that the state $a_\sigma^+|\phi_0(A)\rangle$ has maximum overlap (of all possible states of the type $a_i^+|\phi_0(A)\rangle$ with i=1,2,3,...) with the true eigenstate $|\phi_s(A+1)\rangle$. This provides us with a model-independent definition of the single-particle strength

$$z_s = |\langle\phi_s|a^+|\phi_0\rangle|^2 = \left[1-M'_{\sigma\sigma}(E_s)\right]^{-1} . \qquad (4)$$

In Landau's theory however it is not the mass operator but the particle-hole-irreducible part F of the T-matrix which is considered the basic amplitude. It is true that there exists a differential relationship, $F = \delta M/\delta G$, which describes Landau's amplitude as a functional derivative of the mass operator But though this relation has been used by several authors[2,3)] for a consistent treatment of even-even and even-odd nuclei, a relation that would give the mass operator in terms of the Landau amplitude would be by far more preferable.

It is easy to see that for a Hamiltonian of the form

$$H = \sum_{12} t_{12}a_1^+a_2 + \frac{1}{2}\sum_{1234} V_{1234}a_1^+a_2^+a_4a_3$$

there holds the identity

$$H = \frac{1}{2}\sum_{12}\left(t_{12}a_1^+a_2 - a_1^+[H,a_1]\delta_{12}\right) = \frac{1}{2}\sum_{12}\left(t_{12}a_1^+a_2 + ia_1^+\dot{a}_1\delta_{12}\right) , \qquad (5)$$

which makes it look somewhat single-particle-like. In fact eq. (5) can be used to derive an exact relation for the ground state energy[4],

$$E_o = \frac{1}{2} \sum_{12} \int \frac{d\Omega}{2\pi i} (t_{12}+\Omega\delta_{12})G_{21}(\Omega) \ , \qquad (6)$$

which contains, in spite of the interaction between the particles, only the single-particle Green function. Applying eq. (5) to an even-odd (magic ±1) nucleus leads to an expression including the two-particle Green function.

The final relation, which is effectively a response equation with the Hamiltonian as the external field, reads[5,6]:

$$E_\lambda \langle 1|\lambda\rangle = \frac{1}{2} z_s \sum_{2} \{t_{12}+E_s\delta_{12} + \\ + \sum_{343'4'} \int \frac{d\Omega}{2\pi i} T_{14'23'}(E_s,\Omega,0)G_{44'}(\Omega)G_{3'3}(\Omega) \qquad (7) \\ (t_{34}+\Omega\delta_{34})\}\langle 2|\lambda\rangle$$

It is shown thereby that the mass operator on energy shell can be described by an expression that contains the T-matrix (which is defined via the bound part of the two-body Green function by G^{II}_{bound} = GGTGG in a short-hand notation) as the basic many-body amplitude. Since the T-matrix, as is well known, also governs equations of Bethe-Salpeter type, eq. (7) provides us with a method to deal with even-even and even-odd systems consistently. The formalism, as presented up to now, is of course not yet complete. First, since eq. (7) is only an on-shell relation one cannot form the derivative of the mass operator from it as would be needed to get the single-particle strength from eq. (4). But a Ward identity for the particle-number operator is complementary to eq. (7),

$$1-z_s = z_s \sum_{1234} \langle\sigma|1\rangle\langle 2|\sigma\rangle \int \frac{d\Omega}{2\pi i} T_{1423}(E_s,\Omega,0) \\ \sum_{5} G_{54}(\Omega)G_{35}(\Omega) \ , \qquad (8)$$

and gives exactly the desired information. Secondly one has to derive equations for the T-matrix in terms of its irreducible kernel K[5,6], which finally will turn out to be the basic interaction amplitude and, thirdly, one has to generalize the Bethe-Salpeter equations for even-even nuclei so that they include retardation effects[6].

The formalism outlined above represents a generalization of Landau's theory to finite systems which enables one to treat even-even and even-odd systems consistently starting with one fundamental interaction amplitude K. No additional parameters appear in the treatment of the mass operator. This avoids double-counting problems which appear in other formalisms[7], probably due to the omission of irreducible three-body terms, which never come into play in our theory.

References

1) A.B. Migdal, Theory of Finite Fermi Systems and Applications to Atomic Nuclei, Interscience Publishers, New York 1967.

2) B.L. Birbrair, G.D. Alkhazov, L.P. Lapina, V.A. Sadovnikova, Sov. J. Nucl. Phys. 28 (1978) 321.

3) E.E. Saperstein, S.A. Fayans, V.A. Khodel, Sov. J. Part. Nucl. 9 (1978) 91.

4) V. Galitskii, A.B. Migdal, Sov. Phys. JETP 7 (1958) 96.

5) V. Klemt, Proc. 4th Int. Conf. on Nuclei far from Stability, Helsingør, 1981, CERN, Service d'information scientifique, Geneva.

6) V. Klemt, elsewhere in this report and to be published.

7) G.F. Bertsch, P.F. Bortignon, R.A. Broglia, C.H. Dasso, Phys. Lett. 80B (1979) 161.

3.19. On the Necessity of Generalizing RPA Equations to Include Retardation Effects

V. Klemt

While the low-energy structure of even-odd nuclei is governed by Dyson's equation, even-even (and odd-odd) nuclei are analogously described by Bethe-Salpeter equations[1]. In the Landau-Migdal theory the irreducible kernel F of this equation (in particle-hole direction) is considered to be the basic interaction amplitude. It is generally assumed to be approximately energy-independent and roughly the same for all nuclei. Landau-renormalization[1] allows to incorporate the single-particle strength factors into the amplitude F, thus leading to equations that differ from the well-known RPA only in the interpretation of the entering physical quantities (e.g. energy denominators taken from the experimentally known spectrum of the neighbouring even-odd nuclei).

Now it is well known that the surface of finite nuclei (especially of the lighter ones) tarnishes the appealing simplicity of this picture. To proceed beyond the limitations of the RPA, as proposed by the author[2,3], requires first a more detailed description of the even-odd states, including the coupling of the single-particle degrees of freedom to the collective ones, and secondly a treatment of the Bethe-Salpeter equation that avoids the above-mentioned simplifying assumptions. In fact, while Landau's amplitude F is irreducible in the direction of one particle-hole channel, it is neither so in the particle-hole channel nor in the particle-particle channel. One has therefore to assume an energy-dependence of F at least in these both cross channels.

If we define the many-body T-matrix via the two-particle Green function by

$$G^{II}_{1423}(\Omega,\Omega',\omega) = 2\pi\ \delta(\omega)G_{12}(\Omega)G_{43}(\Omega') \\ - 2\pi\ \delta(\Omega-\Omega')G_{13}(\Omega+\omega/2)G_{42}(\Omega-\omega/2) \qquad (1) \\ + i \sum_{1'2'3'4'} G_{11'}(\Omega+\omega/2)G_{44'}(\Omega'-\omega/2) \\ T_{1'4'2'3'}(\Omega,\Omega',\omega)G_{2'2}(\Omega-\omega/2)G_{3'3}(\Omega'+\omega/2)$$

and further introduce the response function R by

$$R_{1234}(\Omega,\Omega',\omega) = G^{II}_{1423}(\Omega,\Omega',\omega) \qquad (2) \\ - 2\pi\ \delta(\omega)G_{12}(\Omega)G_{43}(\Omega') \ ,$$

it can be shown that the T-matrix can be expanded in the following way:

$$T_{1423}(\Omega,\Omega',\omega) = K_{1423}(\Omega,\Omega',\omega)$$

$$+ i \sum_{1'2'3'4'} \int \frac{d\Omega''}{2\pi} \int \frac{d\Omega'''}{2\pi},$$

$$F_{121'2'}(\Omega,\Omega'',\omega) R_{1'2'3'4'}(\Omega'',\Omega''',\omega) F_{3'4'34}(\Omega''',\Omega',\omega)$$

$$- i \sum_{1'2'3'4'} \int \frac{d\varepsilon}{2\pi} \int \frac{d\varepsilon'}{2\pi}$$

$$F_{131'3'}((\Omega+\Omega'+\omega)/2,\varepsilon,\Omega-\Omega') R_{1'3'2'4'}(\varepsilon,\varepsilon',\Omega-\Omega') \qquad (3)$$

$$\times F_{2'4'24}(\varepsilon',(\Omega+\Omega'-\omega)/2,\Omega-\Omega')$$

$$+ \frac{i}{4} \sum_{1'2'3'4'} \int \frac{d\varepsilon}{2\pi} \int \frac{d\varepsilon'}{2\pi}$$

$$I_{141'4'}((\Omega-\Omega'+\omega)/2,\varepsilon,\Omega+\Omega') G^{II}_{1'4'2'3'}(\varepsilon,\varepsilon',\Omega+\Omega')$$

$$\times I_{2'3'23}(\varepsilon',(\Omega-\Omega'-\omega)/2,\Omega+\Omega')$$

In this equation the matrix K is the totally (in all three channels) irreducible kernel, which now is to play the part of the fundamental effective interaction, while F is only irreducible in one particle-hole and I in the particle-particle channel. From this general equation one can easily deduce the relations for F and I, which read (in shorthand notation):

$$\begin{aligned} F &= K - i \tilde{F}\tilde{R}\tilde{F} + \frac{i}{4} I G^{II} I \\ \tilde{F} &= K + i FRF + \frac{i}{4} I G^{II} I \qquad (4) \\ I &= K + i FRF - i \tilde{F}\tilde{R}\tilde{F}, \end{aligned}$$

where the tilde indicates the cross channel.

Through the two-particle Green function G^{II} there enter overlap amplitudes of the type

$$\langle \phi_s(A+1) | a_i^+ | \phi_\mu(A) \rangle,$$

where μ indicates an excited state of the even-even and s a state of the even-odd nucleus. It is exactly this type of amplitudes for which equations can be derived. One of these reads:

$$\langle \phi_s | a_i^+ | \phi_\mu \rangle = \sum_{1234} \int \frac{d\Omega}{2\pi i} \langle \phi_s | a_1^+ | \phi_o \rangle$$

$$F_{1234}(E_s - E_\mu/2, \Omega - E_\mu/2, E_\mu)$$

$$\times \Big(\sum_{s'} \frac{\langle \phi_o | a_2 | \phi_{s'} \rangle \langle \phi_{s'} | a_i^+ | \phi_o \rangle}{E_s - E_{s'} - E_\mu} \qquad (5)$$

$$+ \sum_{r'} \frac{\langle \phi_o | a_i^+ | \phi_{r'} \rangle \langle \phi_{r'} | a_2 | \phi_o \rangle}{E_s + E_{r'} - E_\mu}$$

$$\times \Big(\sum_{s''} \frac{\langle \phi_o | a_3 | \phi_{s''} \rangle \langle \phi_{s''} | a_4^+ | \phi_\mu \rangle}{\Omega - E_{s''} + i\eta}$$

$$+ \sum_{r''} \frac{\langle \phi_o | a_4^+ | \phi_{r''} \rangle \langle \phi_{r''} | a_3 | \phi_\mu \rangle}{\Omega - E_\mu + E_{r''} - i\eta} \Big)$$

If F would be energy independent, one could perform the integration over Ω and finally end up with the RPA equation. One can conclude therefore that it is the retardation effect of this energy dependence which prevents one from getting equations for amplitudes of the type

$$\langle \phi_o | a_i a_j^+ | \phi_\mu \rangle$$

as in the RPA. One may say that the particle j in general is allowed to move relatively to the hole i. Analogous equations hold for amplitudes including states of A±2-particle nuclei. The norm of the amplitudes of eq. (5) is determined by

$$\sum_r \langle \phi_\mu | a_i^+ | \phi_r \rangle \langle \phi_r | a_i | \phi_\mu \rangle + \sum_s \langle \phi_\mu | a_i | \phi_s \rangle \langle \phi_s | a_i^+ | \phi_\mu \rangle = 1 \qquad (6)$$

resulting from the anticommutation relations for Fermion field operators.

References

1) A.B. Migdal, Theory of Finite Fermi Systems and Applications to Atomic Nuclei, Interscience Publishers, New York 1967.

2) V. Klemt, Proc. 4th Int. Conf. on Nuclei far from Stability, Helsingør, 1981, CERN, Service d'information scientifique, Geneva.

3) V. Klemt, elsewhere in this report and to be published.

4. NUCLEAR REACTIONS

4.1. Investigation of Finite Range Effects in (d,t) and (d,^{3}He) Reactions

R. Shyam[+] *and M.A. Nagarajan*[+]

In the analysis of ($\vec{d}$,t) and ($\vec{d}$,^{3}He) reactions, the zero range distorted wave Born approximation with finite range effects taken into account by means of a local energy approximation (LEA) has been extensively used. Whereas in case of (d,p) reactions the range of validity of LEA has been tested very extensively[1], no such investigation has been made for the ($\vec{d}$,t) and ($\vec{d}$,^{3}He) reactions.

We have performed full finite range DWBA calculations for ($\vec{d}$,t) and ($\vec{d}$,^{3}He) reactions on a number of target nuclei ranging from ^{12}C to ^{208}Pb for incident deuteron energies ranging between 9-130 MeV. The form factors for projectile and ejectile overlaps (referred to as V(r)) required in finite range calculations have been obtained by using the Phillips 3-nucleon wave function[2], which consists of a totally symmetric S-state and mixed symmetry S' and D states. We have also performed zero range DWBA calculations with finite range effects being taken into account by LEA. The zero range normalization constant D_0 and finite range parameter β required in these calculations have been calculated from V(r) to obtain a consistent comparison of the finite range calculations with zero range calculations.

At lower incident deuteron energies, finite range effects are not important as far as the shape of the angular distribution is concerned. However, the absolute magnitude of the cross section is altered by a factor of 1.35. Also finite range has no effect on the vector analyzing powers at these energies. However, for tensor analyzing powers while finite range and zero range results agree with each other at lower angles, at angles beyond 90^0 finite range reduces the tensor analyzing power (T_{20}) by nearly 30 %.

At high deuteron incident energies, finite range affects the cross section at angles beyond 20^0. In fig. 1 we show the result of our calculations for ^{54}Fe($\vec{d}$,^{3}He)^{53}Mn reaction at E_d = 80 MeV. The experimental data has been taken from ref. 3). Full lines represent the full finite range calculation with S and D states of the form factor V(r), dashed lines the full finite range calculations with only S state of V(r) and dotted lines represent the zero range calculations. As can be seen the effect of finite range is strongest for angular momentum mismatched ($1/2^+$) transition. Also for vector and tensor analyzing powers finite range is very important at these high energies.

Thus the result of our investigation is fairly good to account for the finite range effects as far as the shape of the angular distributions and vector analyzing powers is concerned. However the renormalization of the absolute magnitude of the cross section introduced by finite range effects still persists. At higher incident[5] energies, on the other hand, even the shapes of the angular distributions are not properly accounted by LEA.

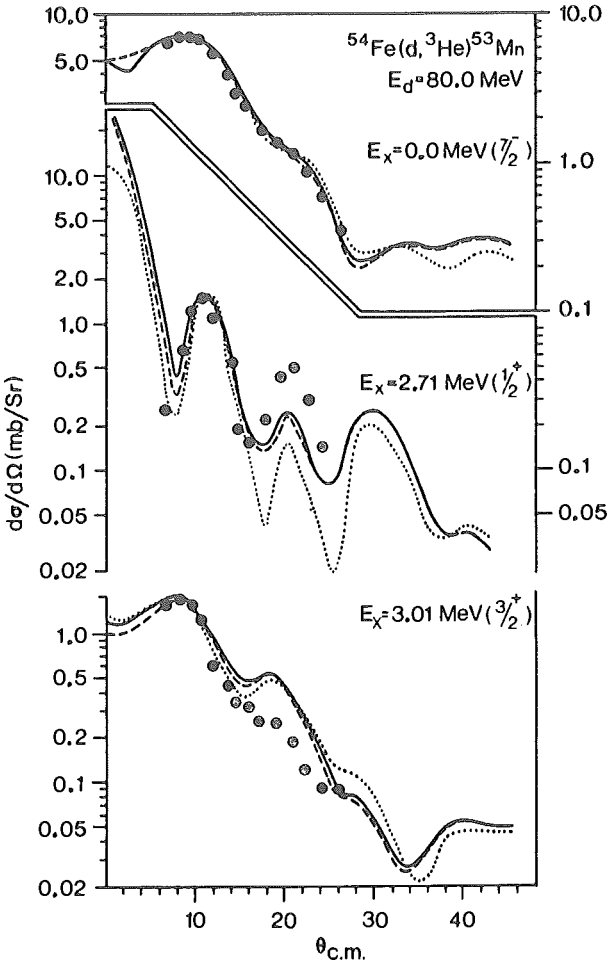

Figure 1

References

1) J.K. Dickens, R.M. Drisko, F.G. Perey and G.R. Satchler, Phys. Lett. 15 (1965) 337.

2) A.C. Phillips and F. Roig, Nucl. Phys. A234 (1979) 378.

3) N.G. Puttaswamy, W. Oelert, A. Djaloeis, C. Mayer-Böricke and P. Turek, JÜl-Spez-99 (1980) 18.

4) A.A. Ioannides, M.A. Nagarajan and R. Shyam, Phys. Lett. 103B (1981) 187.

5) M.A. Nagarajan and R. Shyam, Phys. Rev. C, rapid comm. (to be published.)

[+] Science Research Council, Daresbury Lab., England

4.2. Semiclassical Treatment of Light-Ion Induced Alignment of the L_3-Subshell in Heavy Atoms[+]

F. Rösel[++], *D. Trautmann*[++], *G. Baur*

Recently, the study of alignment in ion atom collisions has become very active. (For an up to date review see ref. 1).) It provides a powerful test for theories of inner shell ionization since they are sensitive to the magnetic substate population, while cross section measurements are determined by an incoherent sum of magnetic substate populations. Theories for inner shell ionization become more and more accurate[2] and therefore such experiments are definitely called for.

We compare recent results for L_3-subshell alignment[3,4,5] in light ion collisions with the semiclassical theory for inner shell ionization[6] where Coulomb deflection effects are exactly taken into account. Whereas simple plane wave theories[7] give rather good agreement at the higher energies (for a relative projectile velocity $V = v_p/v_{L_3} \gtrsim 0.3$, where v_p is the projectile velocity and v_{L_3} the classical orbiting velocity of the L_3 electron as calculated from the experimental binding energy E_{L_3}), strong and systematic deviations show up at the lower energies ($V \lesssim 0.3$). Estimates of Coulomb deflection effects[8,9] have shown that these can account for the observed differences. Therefore, calculations where these Coulomb deflection effects are exactly taken into account are important.

In fig. 1 we show alignment measurements for the reactions p+Au and p+Ag[4] as a function of the square of the relative velocity V. Quite good agreement with the theory is obtained, especially for small bombarding energies where Coulomb deflection effects become important. Calculations based on the Born approximation[3,7,9] show large discrepancies with experiments in this energy region. Of course, this could be expected from recent estimates of this Coulomb deflection effect[8,9]. As a side remark we mention that our results for the total ionization cross section for different L_k subshells are also in agreement with relevant experimental data[10-14]. Furthermore, we note that according to eq. (5) recoil effects are completely taken into account. However, they are negligible for the total alignment in all the cases investigated here.

In conclusion we have shown that discrepancies between calculations in Born approximation and experimental results for small bombarding energies are due to Coulomb deflection effects, which was already claimed by several authors. The influence of the projectile charge on the alignment is small and therefore additional effects have to be considered for an explanation of the experimental results using heavier ions as projectiles. Furthermore we have shown that for an accurate description of the alignment Hartree-Fock wave functions for the electron are necessary to overcome the problem with the effective charge. This may be especially important for impact parameter dependent alignment measurements.

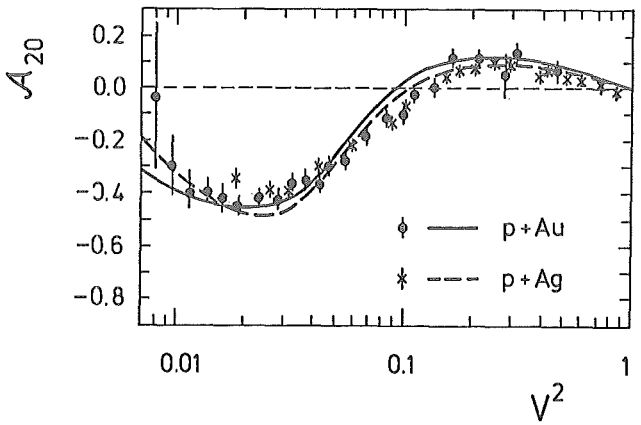

Fig. 1: The L_3-shell alignment for the two systems p+Au (full line) and p+Ag (dashed line) is shown as a function of the square of relative projectile velocity V. Experimental data are from refs. 4,5).

References

1) W. Mehlhorn, Proc. Int. Seminar on High-Energy Ion-Atom Collision Processes, Debrecen (1981) and further references contained therein.

2) See e.g. Proc. Workshop on Theories of Inner Shell Ionization by Heavy Particles, Nucl. Instr. and Methods 169 (1980) 249.

3) W. Jitschin, H. Kleinpoppen, R. Hippler, H.O. Lutz, J. Phys. B12 (1979) 4077.

4) W. Jitschin, A. Kaschuba, H. Kleinpoppen, H.O. Lutz, Z. Physik A (1981) to be published.

5) J. Palinkás, B. Schlenk, A. Valek, J. Phys. B14 (1981) 1157.

6) D. Trautmann, F. Rösel, Nucl. Instr. and Methods 169 (1980) 259 and further references contained therein.

7) V.V. Sizov, N.M. Kabachnik, J. Phys. B13 (1980) 1601.

8) W. Jitschin, H.O. Lutz, H. Kleinpoppen, X-80 Conference Stirling, Book of Abstracts (1980) p. 32.

9) J. Palinkás, L. Sarkadi, B. Schlenk, J. Phys. B13 (1980) 3829.

10) S. Datz, J.L. Duggan, L.C. Feldmann, E. Laegsgaard, J.U. Andersen, Phys. Rev. A9 (1974) 192.

11) C.N. Chang, J.F. Morgan, S.L. Blatt, Phys. Rev. A11 (1975) 607.

12) J.R. Chen, Phys. Rev. A15 (1977) 487.

13) C.V. Barros Leite, N.V. de Castro Fario, A.G. de Pinho, Phys. Rev. A15 (1977) 943.

14) L. Sarkadi, T. Mukoyama, J. Phys. B13 (1980) 2255.

[+] Z. Physik A, in press

[++] Inst. für Physik, Univ. Basel

4.3. Recoil Effects in Atomic Inner Shell Ionization

F. Rösel[+], *D. Trautmann*[+], *G. Baur*

In recent years there has been an increasing interest in the theory of inner shell ionization[1]. Since the interactions responsible for the ionization process are well understood, a comparison of the theoretical calculations with experimental data gives a direct measure of the quality of the approximations involved in the theory. One of these approximations is the semiclassical description (SCA)[2]. One assumes that the projectile moves on a classical hyperbolic trajectory in the field of the target nucleus whereas the electron is described quantum-mechanically. Furthermore, in cases where $Z_p/Z_t \ll 1$ or $(V_{collision}/V_e)^2 > 1$ the ionization can be treated as direct Coulomb ionization process where the electron projectile interaction is to a good approximation given in first order theory[3]. The electron is described by relativistic Hartree-Fock Slater wave functions to include screening effects or by relativistic Dirac functions using a screening parameter θ. However binding effects can be taken into account only in an approximate way.

It has long been realized[4] that not only the interaction of the projectile with the target, but also the recoil of the target nucleus in a nuclear collision can give rise to ionization. An especially pure example in this context is the ionization due to neutron induced reactions[5]: the (charged) target nucleus receives a kick in the nuclear reaction and may "shake off" an inner (or outer) shell electron.

In a slightly different context, the importance of recoil effects in the treatment of Migdal[5] for ionization after α-decay was pointed out by Levinger[6] who found that Migdal's result for dipole electronic transitions is reduced by a factor of 25 (for the case of ^{208}Pb) because of nuclear recoil.

The importance of recoil effects was stressed again by Ciochetti and Molinari[7]. A treatment in the accelerated target system, where non-Newtonian forces arise, was given by Amundsen[8], Andersen et al.[9] and Kocbach et al.[10] and by Kleber and Unterseer[11].

We treat the recoil effects in the SCA model of refs. 12) and 13). The starting point of this approach is the full quantal first order DWBA expression for the T-matrix. As it is usual, the c.m. system is used as a frame of reference, where recoil effects are treated simply. It is not necessary to go into a moving frame of reference. The quantal expressions are then transformed into the semiclassical ones where average quantities for the classical relative motion of the projectile and the target nucleus occur in a simple way.

We found that recoil effects are especially important for close collisions (backward scattering) which probe the form factor for small distances. As it is expected recoil effects are especially important for small target charges, and due to the importance of higher multipole orders for small bombarding energies, recoil effects are important for all bombarding energies. For energies well above the Coulomb barrier they may become important due to strong nuclear forces. It would be interesting to study ionization by neutron impact which is caused in this case solely by the recoil effect.

A detailed account of this work will be published in ref. 14).

References

1) See e.g. Proc. Workshop on Theories of Inner Shell Ionization by Heavy Particles, Nucl. Instr. and Methods 169 (1980) 249-317.

2) D. Trautmann and F. Rösel, Nucl. Instr. and Methods 169 (1980) 259 and further references contained therein.

3) D.H. Madison and E. Merzbacher, in B. Craseman (ed.): Atomic Inner Shell Processes, Academic Press, New York (1975), p. 1.

4) See e.g. A.B. Migdal, Qualitative Methods in Quantum Theory, W.A. Benjamin, Inc., Reading, Mass. (1977), p. 109.

5) A.B. Migdal, J. Phys. (USSR) 4 (1941) 449.

6) J.S. Levinger, Phys. Rev. 90 (1953) 11.

7) G. Ciochetti and A. Molinari, Nuov. Cim. 40B (1965) 69.

8) P.A. Amundsen, J. Phys. B11 (1978) 3197.

9) J.U. Andersen, L. Kocbach, E. Laegsgaard, M. Lund and C.P. Moak, J. Phys. B9 (1977) 3247.

10) L. Kocbach, J.U. Andersen, E. Laegsgaard and M. Lund, Proc. ICPEAC, Paris (1977), p. 42.

11) M. Kleber and K. Unterseer, Z. Physik A292 (1979) 311.

12) M. Pauli and D. Trautmann, J. Phys. B11 (1978) 667.

13) M. Pauli, F. Rösel and D. Trautmann, J. Phys. B11 (1978) 2511.

14) F. Rösel, D. Trautmann and G. Baur, Nucl. Instr. and Methods, in press.

[+] Inst. für Physik, Univ. Basel

4.4. Coulomb-Dissociation at Relativistic and Non-relativistic Energies

G. Baur, B. Hoffmann

Coulomb-dissociation of nuclei with low incident energies is hindered because of the large adiabaticity parameter ξ

$$\xi = \eta_f - \eta_i \qquad (1)$$

which characterizes the excitation in regions unstable against particle emission. Nevertheless such a process was observed experimentally and explained theoretically in the low energy part of proton spectra, measured in 15 MeV deuteron induced reactions on heavy target nuclei (especially ^{232}Th). This is described in detail in refs. 1) and 2). The well-known quantal and semi-classical methods of Coulomb-excitation (ref. 3)) could be used to calculate these processes. At energies above the Coulomb-barrier, nuclear absorption effects are taken into account in the strong absorption model. Using the strong absorption model, angular distributions of excitations of giant resonances can be calculated rather simply. They compare quite well with the much more laborious DWBA-calculations (ref. 4) and fig. 1).

Matsuoka et al. (ref. 5)) reported an in intriguing A-dependence of the (d,p) total breakup cross section of E_o = 56 MeV deuterons. For peripheral breakup processes we expect

$$\sigma \propto A^{1/3} \qquad (2)$$

(Serber model) whereas the experimental result is $27(A^{1/3}+0.8)^2$ mb. These authors conclude that all partial waves up to the grazing one contribute to the breakup cross section. Our calculations show that Coulomb-dissociation at distances $R > R_{nucl}$ contribute (significantly) to the total breakup cross section. This can be seen in fig. 2 taken from ref. 2). A related effect was observed for relativistic heavy ion fragmentation (Heckman et al., ref. 6)).

Since the adiabatic cutoff which reduces the cross sections becomes less effective at higher energies (especially due to relativistic effects), we extended our calculations to much higher energies. The total cross section for d on Th is shown in fig. 3. After a maximum around 100 MeV and a minimum around 2 GeV the cross section rises again due to relativistic effects. We compared the relativistic Coulomb-excitation theory of ref. 7) to the Weizsäcker-Williams method of virtual quanta. For E1 excitation both methods yield the same result only if the full Weizsäcker-Williams method (eq. (15.54) of ref. 8)) is used. At not too high energies it is important to include the modification of the impact parameter due to Coulomb repulsion.

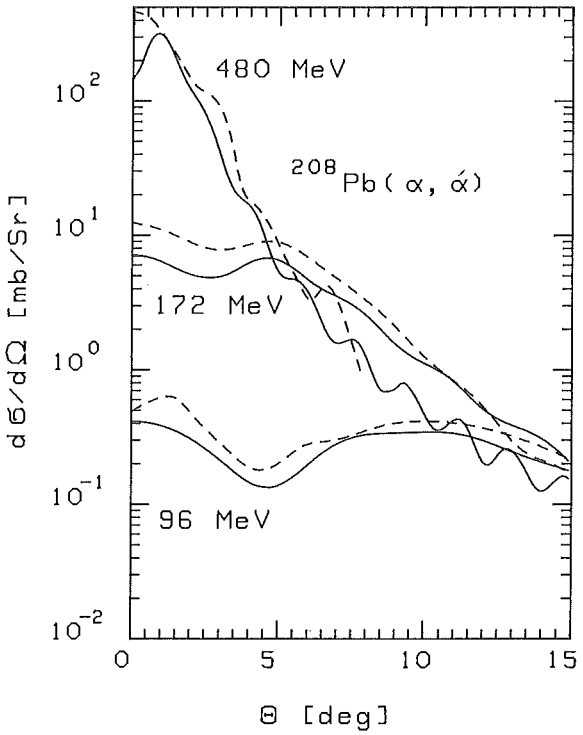

Fig. 1: Comparison of calculated differential cross section for excitation of the giant dipole resonance in Pb with alpha particles using the strong absorption model (___) and standard DWBA calculations (ref. 4)) (---). The excitation energy was assumed to be 13.5 MeV, the B(E1)-value was taken to be 100 % of the energy-weighted sum rule.

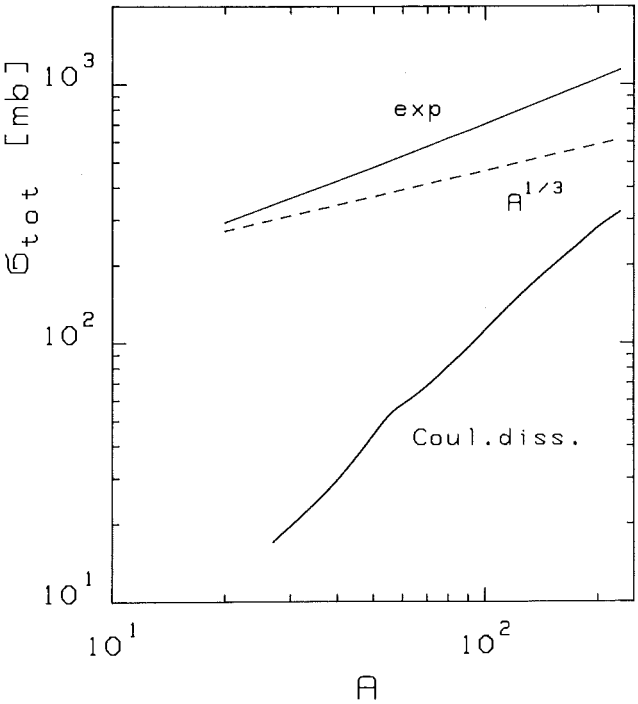

Fig. 2: Total cross section for the reaction A(d,p) with deuterons of 56 MeV. The curve labelled "exp" shows the fitted values determined experimentally by Matsuoka et al.[4]). For large A (large Z) the Coulomb-dissociation becomes more and more important and together with a nuclear breakup component, assumed to be proportional to $A^{1/3}$ (Serber model), it nearly adds up to the experimental value.

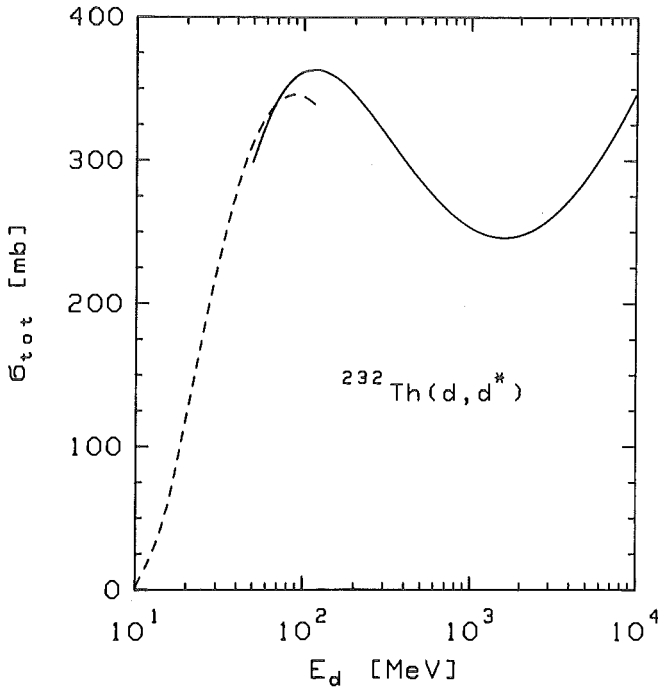

Fig. 3: Total cross section of Coulomb-dissociation for deuterons on Thorium as a function of the incident energy. --- strong absorption model, ___ relativistic Coulomb excitation.

References

1) J. Kleinfeller, J. Bisplinghoff, J. Ernst, T. Mayer-Kuckuk, G. Baur, B. Hoffmann, R. Shyam, F. Rösel, D. Trautmann, Nucl. Phys. A370 (1981) 205.

2) B. Hoffmann, Jül-Spez-131 (1981).

3) K. Alder, A. Winther, Electromagnetic Excitation, North-Holland, Amsterdam-Oxford (1975).

4) M. Buenerd, D. Lebrun, preprint 1981.

5) N. Matsuoka et al., Nucl. Phys. A345 (1980) 1.

6) H. Heckman et al., Proc. Int. Conf. Nucl. Physics, Berkeley, USA, 24-30.8.1980, Report LBL-11118 (1980) p. 220.

7) K. Alder, A. Winther, Nucl. Phys. A319 (1979) 293.

8) J.D. Jackson, Classical Electrodynamics, John Wiley & Sons, New York (1975).

5. HEAVY ION REACTIONS

5.1. Comparison of Concepts: ATDHF and Functional Integrals

K. Goeke, P.-G. Reinhard[+], H. Reinhardt[++]

There have been suggested various theories for the microscopic and parameterfree description of large amplitude collective motion. If one requires quantum effects there are basically two approaches, i.e. the quantized adiabatic time dependent Hartree-Fock (ATDHF)[1] and the path-integral-approach (PIA)[2]. It will be shown in this report that the multitude of periodic TDHF-trajectories $|\phi_T(t)>$, with period T, is for slow motions clearly related to the collective path $|\phi_{qp}>$ as it results from ATDHF[3]. The multitude $\{|\phi_T(t)>\}$ of those solutions (associated to a certain collective model) we shall call a branch. We will assume that a branch contains an HF point and that all quantities calculated from $\phi_T(t)$ will be distinguishable in T and also distinguishable in the energy $E = <\phi_T(t)|H|\phi_T(t)>$ and that there is a unique relation between E and T. Hence any Slater determinant, which is member of a branch, is uniquely characterized by giving E and t, i.e. $|\phi_E(t)>$. This labelling in E and t has the convenience that E and t are something like canonically conjugate quantities. This establishes immediately a bridge between a branch $\{|\phi_E(t)>\}$ and a path $\{|\phi_{qp}>\}$ since both multitudes are characterized by two real parameters which can be understood as classical canonical conjugate variables. Within the branch $\{|\phi_E(t)>\}$ a periodic trajectory $|\phi_E(t)>$ represents an actual classical motion. This is characterized within the path $\{|\phi_{qp}>\}$ by $q = q(t,E)$ and $p = p(t,E)$ with obey the classical equations of motion. Hence the members of a branch and of a path can be related by

$$|\phi_E(t)> \propto |\phi_{q(t,E),p(t,E)}>$$

with a reverse relation $E = E(q,p)$ and $t = t(q,p)$. One actually can construct the mapping explicitly such that the equation of motion for the periodic trajectories following from PIA corresponds to classical canonical Hamiltonian equations:

$$(i\frac{\partial}{\partial t} - h[\rho])|\phi_E(t)> = -\varepsilon|\phi_E(t)>$$

Replace $\partial/\partial t$ by $\dot{q}\frac{\partial}{\partial q} + \dot{p}\frac{\partial}{\partial p}$. If we define the hermitian 1p-1h operators P and Q as

$$\hat{P}|\phi^{PIA}_{qp}> = i(\frac{\partial}{\partial q})_{1p\text{-}1h}|\phi^{PIA}_{qp}>$$

$$\hat{Q}|\phi^{PIA}_{qp}> = -i(\frac{\partial}{\partial p})_{1p\text{-}1h}|\phi^{PIA}_{qp}>$$

one obtains from the 1p-1h projection

$$(\dot{q}\hat{P} - \dot{p}\hat{Q} - h_{1p\text{-}1h})|\phi^{PIA}_{qp}> = 0$$

Multiplying from left with $<\phi^{PIA}_{qp}|\hat{P}$ and $<\phi^{PIA}_{qp}|\hat{Q}$ yields after few manipulations

$$\dot{p} = -i<[\hat{P},H]> = -\partial_q \mathcal{H}$$

$$\dot{q} = i<[\hat{Q},H]> = \partial_p \mathcal{H}$$

where

$$\mathcal{H}(q,p) = <\phi^{PIA}_{qp}|H|\phi^{PIA}_{qp}>$$

These are obviously classical Hamiltonian equations. Apparently we have one dimensional classical mechanics, in which any bound motion is periodic. This is consistent with the periodicity of the trajectories $|\phi_E(t)>$.

In order to establish a connection of a branch to an adiabatic path one has first to transform from (q,p) to a new (q',p') such that the trajectories $|\phi_E(t)>$ correspond to q'(E,t) and p'(E,t) which show turning points, i.e. which have two times t_a and t_b at which $p'(E,t_a) = p'(E,t_b) = 0$. We furthermore assume that the states $|\phi^{PIA}_{q',p'=0}> = |\phi^{PIA}_{q'}>$ are time even, which simplifies the calculational techniques. Actually the path $\{|\phi_{q'p'}>\}$ is fully identical to $\{|\phi_E(t)>\}$ and it may have any complicated q'- and p'-dependence. An adiabatic collective path, however, as it is used in ATDHF, is assumed to have the special structure of a separation ansatz (we omit henceforth the primes at the coordinates q' and p')

$$|\phi^{ATDHF}_{qp}> = \exp\left[i\, p\, Q(q)^{ATDHF}\right]|\phi^{ATDHF}_{q}>$$

where $Q^{ATDHF}(q)$ is a 1p-1h operator with respect to $|\phi^{ATDHF}_q>$ corresponding of course to the derivative with respect to p at p=0

$$Q^{ATDHF}(q)|\phi^{ATDHF}_q> = (i\frac{\partial}{\partial p})_{1p\text{-}1h}|\phi^{ATDHF}_{qp}>_{p=0}$$

Apparently an adiabatic $\{|\phi^{ATDHF}_{qp}>\}$ is a useful object if it can be constructed in such a way that it is as close as possible to the $\{|\phi^{PIA}_{qp}>\}$. We shall see in the next section that this yields precisely the ATDHF equations for the collective path $|\phi^{ATDHF}_{qp}>$. It remains then, however, to check how good it is to approximate the ϕ^{PIA}_{qp} by an adiabatic ϕ^{ATDHF}_{qp}. This can be done by extending in PIA the adiabatic expansion to second order and investigating the additional contributions to the ϕ^{ATDHF}_{qp}. Actually this procedure will reveal a validity condition, which will be identical to the one derived in quantized ATDHF. Obviously for each single point $|\phi^{PIA}_{q_0p_0}>$ one can find a 1p-1h operator Q^{PIA} such that $|\phi^{PIA}_{q_0p_0}> \sim \exp\left[i\, p_o\, Q^{PIA}\right]|\phi^{PIA}_{q_0p_0}>$. However, in general this operator will also depend on p_o, $Q^{PIA} = Q^{PIA}(q_o,p_o)$, since one cannot assume that the same operator $Q^{PIA}(q_o)$ can expand the whole range of $|\phi^{PIA}_{q_0p_0}>$ for all p_o values. In other words, the ATDHF-ansatz is adiabatic in the sense that it describes the p-dependence of the path by an extrapolation from the p-dependence at small p. Hence an adiabatic path is only a valid approximation if $\partial Q^{PIA}/\partial p$ is small. This is precisely the quantity on which the ATDHF validity condition is based.

References

1) K. Goeke and P.-G. Reinhard, Ann. Phys. 112 (1978) 328; P.-G. Reinhard, J. Maruhn, K. Goeke, Phys. Rev. Lett. 44 (1980) 1740.

2) H. Reinhardt, Nucl. Phys. A346 (1980) 1.

3) K. Goeke, P.-G. Reinhard, H. Reinhardt, Nucl. Phys. 1982, to be published.

[+] Inst. f. Kernphysik, Univ. Mainz

[++] ZfK Rossendorf, Dresden, DDR

5.2. Adiabaticity in the Path Integral Approach

P.-G. Reinhard[+], *H. Reinhardt*[++], *K. Goeke*

As one has seen, the essential link between ATDHF[1] and PIA[2] is established by realizing that the concept of a branch $\{|\phi_E(t)>\}$ and the concept of a path $\{|\phi_{qp}>\}$ are equivalent in that they can be mapped one to one

$$\{|\phi_E(t)>\} \leftrightarrow \{|\phi_{qp}>\} \tag{1}$$

by

$$q = q(E,t) \ , \ p = p(E,t) \tag{2}$$

where q(E,t) and p(E,t) are given by the canonical equations of motion. We now want to derive the equations-of-path of ATDHF from the equations-of-motion for a branch of PIA together with the mapping (1). We will do this in an adiabatic expansion in powers of p. This will allow to establish a precise correspondence to ATDHF and, later on, to study the quantization process. We have to fulfil the EOM

$$i\partial_t\rho - [h(\rho),\rho] = 0 \tag{3}$$

with

$$\rho(t+T) = \rho(t) \tag{4}$$

We assume that we have given an approximate solution $\bar{\rho}$

$$\delta = i\partial_t\bar{\rho} - [h(\bar{\rho}),\bar{\rho}] \simeq 0 \tag{5}$$

$$\bar{\rho}(t+T) = \bar{\rho}(t) \quad \text{and} \quad \bar{\rho}^2 = \bar{\rho}$$

where the mismatch δ is small. We expand the exact solution

$$\rho(t) = \bar{\rho}(t) + i[\hat{R}(t),\bar{\rho}(t)] + \ldots \tag{6}$$

where $\hat{R}$ is a hermitian 1p-1h operator first order in δ with period T. This guarantees that the boundary conditions (4) are fulfilled up to first order. Inserting expansion (6) into eq. (3) we obtain

$$[\mathrm{Tr}\, V[\hat{R},\bar{\rho}],\bar{\rho}] + [h(\bar{\rho}),\hat{R}] - i\partial_t\hat{R},\bar{\rho}] = i[\hat{D},\bar{\rho}] \tag{7}$$

where $\hat{D}$ is a 1p-1h operator and given in terms of the δ of eq. (5) as

$$\delta = i[\hat{D},\bar{\rho}] \tag{8}$$

Eq. (7) is a linear response equation for branches determining the improvement $\hat{R}$ as response to the mismatch $\hat{D}$.

In the above formulae all quantities are a function of time t and period T or energy E respectively. We equivalently can consider them as functions of q and p (the time dependency of which is given by eq. (2), i.e. $\rho = \rho(q,p)$, $\bar{\rho} = \bar{\rho}(q,p)$, $R = R(q,p)$ and $D = D(q,p)$. This translates the eqs. (3)-(7) in a straightforward manner.

For an adiabatic motion we assume now p and $\dot{p}$ to be small allowing an expansion of eq. (7) in powers of p and $\dot{p}$. The key argument is now that the path $\{|\phi_{qp}>\}$, or $\{\bar{\rho}(q,p)\}$ equivalently, is an object independent of time and independent of an actual motion. An actual motion $\varepsilon_E(t)$ can take place in $\{|\phi_{qp}>\}$ by inserting an actual classical solution for q(E,t) and p(E,t). We may look for various motions at various energies E, all have to be described by the same path. In simple words: $\{|\phi_{qp}>\}$ and $|\phi_E(t)>$ correspond to each other like a rail and a car moving on it, respectively. This is precisely the decoupling property we demand $\{|\phi_{qp}>\}$ to fulfil. To vary E for a given q means to vary p. Thus we have to consider p as an independent variable and one has to fulfil eq. (7) for each power separately. One has to take into account that $\dot{p} = \dot{p}(q,p)$ due to the Hamiltonian equations in q and p.

We call a path adiabatic, if its members can be parametrized as

$$\bar{\rho}(q,p) = \exp(ip\hat{Q}(q))\bar{\rho}(q)\exp(-ip\hat{Q}(q)) \tag{9}$$

That means an adiabatic path is completely determined by its first two terms of a p^n expansion (please note that the Q and the $\bar{\rho}(q)$ are functions only of q; no further p^2-, p^4-, etc.-dependency is allowed therein).

We now want to find an optimal adiabatic path, i.e. a path in the form which comes as close as possible to the "exact" path given by the PIA equations and the subsequent mapping (E,t) $\leftrightarrow$ (q,p): The term "close" has a priori no unique meaning. It depends on the range of q and p for which one wants to fit the adiabatic path. In the spirit of an adiabatic expansion we define the optimal adiabatic path to be that one which is identical with the p^0 and p^1 term of the "exact" one. That means in the perturbation theory for paths the optimal adiabatic path is signified as the path for which no correction $\hat{R}$ in order p^0 and p^1 arises. Thus we obtain the equations for the path by requiring

$$\hat{R}(q) = 0 \ , \ \partial_p\hat{R}(q) = 0 \tag{10}$$

The p^0 and p^1 parts then yield

$$p^0: \quad [h(\bar{\rho}(q)) - \partial_q\mathcal{V}\hat{Q}(q),\bar{\rho}(q)] = 0 \tag{11a}$$

$$p^1: \quad [[H,\hat{Q}(q)]_{ph} + \frac{i}{\mathcal{A}}\hat{P}(q),\bar{\rho}(q)] = 0 \tag{11b}$$

These are just the well known ATDHF equations written here in density matrix representation. Hence we obtain the remarkable result that the implementation of an adiabatic concept into the path integral approach to periodic motion yields precisely the collective path as has been derived previously by means of ATDHF and GCM.

The ATDHF equations can be reformulated as a differential equation for the path $\partial_q|\phi_q> = [H,h(\rho(q))_{ph}]|\phi_q>$. Thus we have an initial value problem: For any given starting point $|\phi_{q_0}>$ we can find a solution to the ATDHF equations. However, it is clear that out of the multitude of ATDHF solutions only one solution can come closest to the "exact" path from PIA. This optimal path will be the one

which remains most stable if we subject it to the full dynamics. We have already exploited PIA up to order p^0 and p^1. Thus we have to look at the correction which comes from the p^2-term. This is described by the response $\partial_p^2\hat{R}(q)$ and given, after exploiting the above equations, as

$$[[H,\partial_p Q(q)]_{ph},\bar{p}] = [\partial_q Q(q)/\mathcal{M}-[[H,Q(q)],Q(q)],\bar{p}(q)] \quad (12)$$

The optimal path is then the one for which along the actual motion the necessary correction by $\partial_p^2\hat{R}$ is smallest, i.e. for which

$$\int_0^T dt\ \frac{1}{4}\,p^4(t)\langle\phi_{q(t)}|(\partial_p Q(q(t))^2|\phi_{q(t)}\rangle = \text{Minimum} \quad (13)$$

This is precisely the form of the validity condition as it has been derived in ref. 3. It is a condition on the path, via $\partial_p^2\hat{R}$, and on the actual collective motion, via $p^4(t)$.

In summary the present section shows that one can perform an adiabatic approximation to the path-integral-approach. The result is a collective path being identical to the one obtained in ATDHF. It should be pointed out that the formal steps in the present section used only the 1p-1h elements of the density matrix and never its 1h-1h elements. This shows that the construction of the path, corresponding to 1p-1h, and the quantization, corresponding to 1h-1h, are of different footing[4].

References

1) K. Goeke, P.-G. Reinhard, Ann. Phys. 112 (1980) 328.

2) H. Reinhardt, Nucl. Phys. A346 (1980) 1.

3) P.-G. Reinhard and K. Goeke, Nucl. Phys. A312 (1978) 121.

4) K. Goeke, P.-G. Reinhard, H. Reinhardt, Nucl. Phys. 1982, to be published.

+ Inst. f. Kernphysik, Univ. Mainz

++ ZfK Rossendorf, Dresden, DDR

5.3. Quantization of TDHF-Fields

H. Reinhardt[+], *K. Goeke, P.-G. Reinhard*[++]

In the ATDHF theory[1] we obtain a consistently quantized collective Hamiltonian $H_C(q,\frac{d}{dq})$. Thus, within the given path $\{|\phi_{qp}\rangle\}$ we solve the full quantum mechanics. The path integral approaches (PIA), on the other hand, determine the eigenstates within a given branch $\{|\phi_E(t)\rangle\}$ by stationary phase condition, similar to the Bohr-Sommerfeld quantization rule. Obviously, with respect to the quantization within a given collective path ATDHF is more general and hence one has to solve the collective Hamiltonian in a semiclassical approximation in order to compare with the path integral approach. In the following we show the equivalence of the quantized ATDHF in its semiclassical limit and the path integral approach in the adiabatic and semiclassical limit by studying the quantization within the latter theory, rewriting it as a semiclassical quantization for one dimensional collective dynamics (represented by q and p) and comparing the Hamiltonian therein with the ATDHF-Hamiltonian.

As we have seen before, in the PIA the two basic problems decouple, viz. 1. finding a branch of periodic paths $\{|\phi_E 6t)\rangle\}$ with $T=T(E)$, and 2. finding the quantized energies within this branch. We thus can assume the first step to be completed, yielding a branch $|\phi_E(t)\rangle$ for which

$$(i\partial_t - h(\rho))|\phi_E(t)\rangle = -\varepsilon|\phi_E(t)\rangle \quad (1)$$

$$|\phi_E(t+T)\rangle = |\phi_E(t)\rangle \quad (2)$$

and the period T is a function of E (or vice versa). The semiclassical PIA-quantization proceeds now as follows: The classical action along the periodic TDHF trajectories is then given with

$$S(T) = \int_0^T dt\langle\phi_{E(T)}(t)|i\partial_t-\hat{H}|\phi_{E(T)}(t)\rangle \quad (3)$$

In order to trace the equivalence to a semiclassical quantization of collective dynamics in q and p we transform the branch to the path representation. As outlined in report 1 we can map the branch $\{|\phi_E(t)\rangle\}$ onto a collective path $\{|\phi_{qp}\rangle\}$ such that

$$S = \int_0^T dt(\dot{q}p - \mathcal{H}(q,p)) \quad (4)$$

where we have to insert the $q_E(t)$ and $p_E(t)$. The derivation of the second term in eq. (4) is obvious whereas the first term needs a little more care: We first rewrite

$$\int_0^T dt\langle\phi_{qp}|i\partial_t|\phi_{qp}\rangle = \int_0^T dt(\dot{q}\langle\hat{P}\rangle-\dot{p}\langle\hat{Q}\rangle) \quad (5)$$

and now have to specify the hole-hole matrix elements of the operators $\hat{P}$ and $\hat{Q}$. One can show that one has to choose either $\langle P\rangle = p$ and $\langle\hat{Q}\rangle = 0$ or $\langle P\rangle = 0$ and $\langle Q\rangle = q$ or any intermediate choice $\langle P\rangle = xp$ and $\langle\hat{Q}\rangle = (1-x)q$. For any choice of x, with $0\le x\le 1$, we obtain $\int dt\,\dot{q}p$ by partial integration of the $\dot{p}$-term. Altogether we end up with the action (4) to be evaluated along a solution $q_E(t)$ and $p_E(t)$. This yields just the semiclassical quantization rule for a system whose dynamics is governed by a Hamiltonian $\mathcal{H}(q,p)$. In the adiabatic limit we expand

$$\mathcal{H}(q,p) \approx \frac{p^2}{2\mathcal{M}(q)} + \mathcal{V}(q) \quad (6)$$

Thus we see that the quantization in PIA at that level involves a Hamiltonian $\mathcal{H}(q,p)$ which is the classical limit of the quantum mechanical Hamiltonian $H_c(q,\frac{d}{dq})$ of the ATDHF approach if one ignores the quantum corrections $\mathcal{E}(q)$, which is consistent in a strict classical limit. Thus we obtain the satisfying result that a semiclassical quantization of the collective ATDHF-Hamiltonian yields precisely the quantization condition of PIA in the adiabatic limit, if in both theories the quantum corrections are neglected.

The quantum fluctuations in PIA give an additional contribution to the action which can be expressed by the fluctuation spectrum and the pure 1p-1h excitation as

$$\Delta S = \frac{1}{2}\sum_k{}' \omega_k T - \frac{1}{2}\sum_{ph} \omega_{ph}^{(o)} T \qquad (7)$$

This can actually be rewritten by means of the operators Q and P, where $Q|\phi\rangle = -\partial_p|\phi\rangle$ and $P|\phi\rangle = i\partial_q|\phi\rangle$ are the usual collective operators and λ is the width, $\lambda = 2\langle\phi_q|P^2|\phi_q\rangle \simeq (2\langle\phi_q|Q^2|\phi_q\rangle)^{-1}$. Inserting this into the local form we obtain finally

$$\Delta S = -\frac{1}{4}\int_o^T dt(\langle\phi|[Q,[h,Q]]|\phi\rangle 2\langle\phi|P^2|\phi\rangle + \langle\phi|[P,[h,P]]|\phi\rangle 2\langle\phi|Q^2|\phi\rangle) \qquad (8)$$

$$= -\int_o^T dt\,(\frac{\lambda}{4\mathcal{M}_o} + \frac{\partial_q^2 \mathcal{V}_o}{4\lambda})$$

where

$$\lambda = 2\langle\phi_q|P^2|\phi_q\rangle \simeq (2\langle\phi_q|Q^2|\phi_q\rangle)^{-1} \qquad (9)$$

$$\frac{1}{\mathcal{M}_o(q)} = \langle\phi_q|[Q,[h,Q]]|\phi_q\rangle \qquad (10)$$

$$\mathcal{V}_o(q) = \langle\phi_q|h|\phi_q\rangle \qquad (11)$$

and all quantities are functions of q, time dependent via q=q(t). Obviously, this ΔS has approximately the form of the zero-point energy $\mathcal{Z}(q)$ of ATDHF. We finally obtain

$$S+\Delta S = \int_o^T dt(qp - H(q,p)) \qquad (12)$$

where

$$H(q,p) = \mathcal{H}(q,p) - \mathcal{Z}^{PIA}(q) \qquad (13)$$

with

$$Z^{PIA}(q) = \frac{\lambda_o(q)}{4M_o(q)} + \frac{\partial^2 \mathcal{V}_o(q)}{4\lambda_o(q)} \qquad (14)$$

The PIA expression differs from the corresponding one of quantized ATDHF in that it is lacking the residual two body interaction in eq. (14). One can interpret this result in the following way: In the zero-point-energy subtraction in PIA the selfconsistent Peierls-Thouless cranking mass, which is used in quantized ATDHF, is replaced by the Inglis-cranking mass. This is a widely used approximation in microscopic collective theories.

The collective potential $\mathcal{V}_o(q)$ is given by $\langle\phi_q|h|\phi_q\rangle$ and not by $\langle\phi_q|H|\phi_q\rangle$ as the ATDHF potential $\mathcal{V}(q)$ is. However, the corresponding potential zero point energy correction is in general much smaller than the kinetic zero point energy correction and one may perhaps neglect the difference between $\mathcal{V}(q)$ and $\mathcal{V}_o(q)$ in eq. (14). These features are interesting with regard to the PIA. They seem to be connected to the problem of deriving Hartree-Fock from PIA rather than pure Hartree. It will be an interesting point for further studies under which conditions the PIA leads to quantum corrections which include the residual two body interaction.

In summary: If one evaluates a semiclassical solution to the quantized ATDHF collective Hamiltonian (i.e. WKB), then one obtains two prescriptions for the energies depending on whether one includes the zero point corrections $\mathcal{Z}(q)$ in ATDHF or not. The first case is exactly matched in PIA if one performs there an adiabatic expansion and sticks to the pure classical limit. The second case is matched in PIA by including the quantum fluctuation. This, however, is only approximately the case since in the present formulation of PIA the residual two body interaction is ignored in contrast to quantized ATDHF.

References

1) K. Goeke and P.-G. Reinhard, Ann. Phys. 112 (1978) 328; P.-G. Reinhard, K. Goeke, Phys. Rev. C20 (1979) 1546.

2) H. Reinhardt, Nucl. Phys. A346 (1980) 1.

3) K. Goeke, P.-G. Reinhard, H. Reinhardt, Nucl. Phys. 1982, to be published.

+ ZfK Rossendorf, Dresden, DDR

++ Inst. f. Kernphysik, Univ. Mainz

5.4. Quantized ATDHF Calculations for ^{8}Be

F. Grümmer, K. Goeke, P.-G. Reinhard+

The quantized ATDHF theory[1] for the optimal collective path, mass and potential in the way suggested in ref. 2 can be exposed as follows. The equations of motion are transformed to a simple differential equation

$$\frac{\partial}{\partial q}\phi_q = C(q)[H,H_{ph}(q)]\phi_q$$

with $C(q) = \mathcal{M}(q)(\partial V/\partial q)^{-1}$. Here the $\{\phi_q\}$ is the multitude of Slater determinants to characterize the collective motion and from which the collective mass, $\mathcal{M}(q)$, and the classical potential energy surface, V(q), is to be extracted. The $H_{ph}(q)$ is an operator consisting out of the 1p-1h elements of the full microscopic Hamiltonian H with respect to ϕ_q. The two body interaction used is given by

$$V(r_1,r_2) = t_o\,\delta(r_1-r_2) + \frac{1}{6}t_3\,\rho(\frac{r_1+r_2}{2})\,\delta(r_1-r_2) + V_y + V_{Coul}$$

where V_y is a Yukawa potential and V_{Coul} the Coulomb interaction. From the latter ones only the direct part is used and evaluated by means of successive over-relaxation techniques. For the calculation a three dimensional grid in r-space is used with 16x16x24 meshpoints. In order to evaluate the collective Hamiltonian (to be used e.g. for fission and fusion events) the V(q) is to be corrected by zero point energies Z(q) associated to spurious rotations and translations of the total system and to spurious relative motions.

These zero point energies are asymptotically identical, see fig. 3. The mass parameter in fig. 2 shows a clear increase in the overlapping region indicating the re-arrangements in the internal wave function. The classical V(q) is given in fig. 1. Scattering cross sections and the evaluation of resonances in the

potential are presently under investigation. Furthermore the code is being applied to heavier systems.

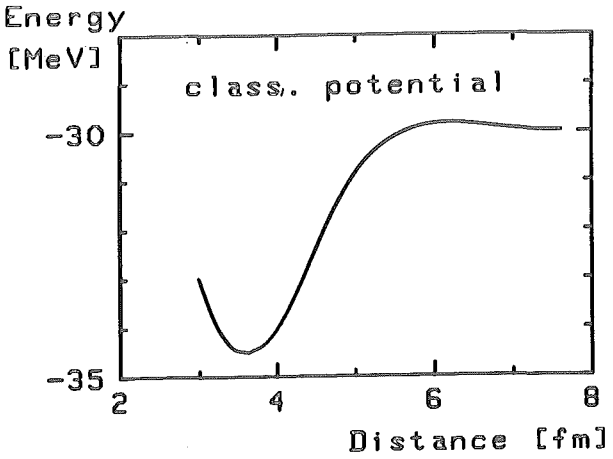

Figure 1

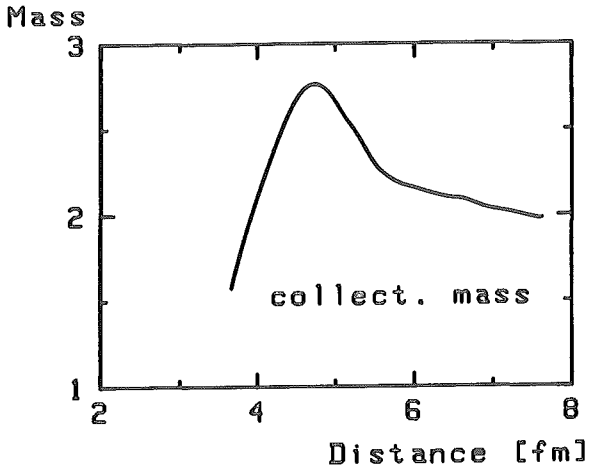

Figure 2

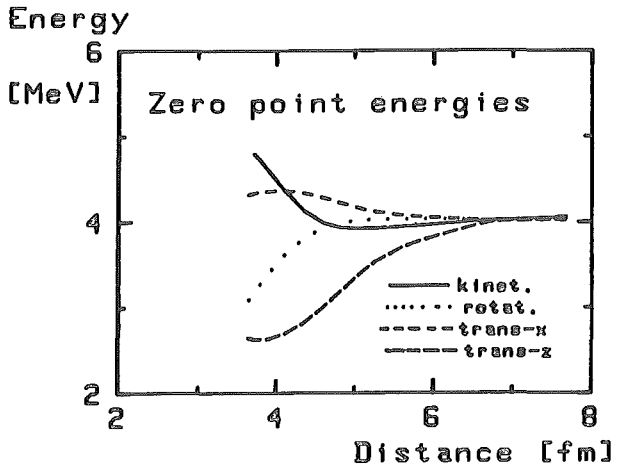

Figure 3

References

1) K. Goeke, P.-G. Reinhard, Ann. Phys. 112 (1978) 328.

2) P.-G. Reinhard, J. Maruhn, K. Goeke, Phys. Rev. Lett. 44 (1980) 1740.

+ Inst. f. Theor. Physik, Univ. Mainz

III. SOLAR ENERGY

6.1. Development of a Simple Test Unit for Comparative Testing of Solar Collectors

B. Sack, H.J. Stein

Thermal performance testing of collectors plays a control role in solar energy applications since such tests provide the necessary data for system design and the prediction of system performance. The test of the efficiency curve also forms the diagnostic basis for reliability and durability tests. Equation (1) describes the steady-state efficiency η of the collector as a function of the driving forces (operating variables) and the collector design parameters (characteristic collector parameters).

$$\eta = F'(\alpha\tau) - F'U_m \frac{\vartheta_m - \vartheta_a}{G} = \frac{\dot{Q}_{use}}{AG} \qquad (1)$$

$\dot{Q}_{use}$	= useful heat extracted from the collector	W
A	= collector area	m^2
G	= global irradiance in the plane of the collector	$W\,m^{-2}$
$(\alpha\tau)$	= absorption transmission product of cover and absorber, "optical efficiency"	
U_m	= overall heat-transfer coefficient from the fluid to the surrounding	$W\,m^{-2}K^{-1}$
ϑ_m	= mean fluid temperature	^oC
ϑ_a	= ambient (air) temperature	^oC
F'	= absorber efficiency factor describing the influence of the heat-transfer coefficient between the absorber plate and the fluid	

The collector efficiency curve can be determined by measuring G and $\dot{Q}_{use}$ at different collector temperatures.

$$\dot{Q}_{use} = \dot{m} c_p (\vartheta_o - \vartheta_e) \qquad (2)$$

$\dot{m}$	= mass flow	$(kg\,s^{-1})$
c_p	= specific heat of the heat transfer medium	$(J\,kg^{-1}K^{-1})$
ϑ_e	= collector entrance temperature	(^oC)
ϑ_o	= collector outlet temperature	(^oC)

Standard test procedures like ASHRAE 93-77 or DIN 4757, part 4 (draft), prescribe the test conditions to be observed, the quantities to be measured, and the accuracy requirements for the measurements.

The collector has to be in a stationary operational mode in order to avoid transient heat capacity effects (instantaneous efficiency determination). This requires stability of

- mass flow	1 %
- fluid entrance temperature	0.1, (0.5) K
- solar irradiance	2 %

The environmental conditions are

- level of global irradiance	$\geq 600\ W\,m^{-2}$
- diffuse part of global irradiance	20 to 40 %
- angle of incidence of the direct solar radiation	0 to 15 degree
- air velocity	0 to 4 ms^{-1}

To be measured are

- the collector entrance temperature	ϑ_e, $\pm$ 0.3 K
- the fluid temperature difference across the collector	$\vartheta_o - \vartheta_e$, $\pm$ 0.1 K
- the mass flow rate of the heat-transfer fluid	$\dot{m}$, $\pm$ 1 %
- the global irradiance in the plane of the collector entrance area (according to WMO class 1 specifications)	$\dot{G}$, $\pm$ 3 %
- the ambient air temperature	ϑ_a, $\pm$ 0.5 K
- the air velocity above the collector front cover	v, $\pm$ 0.5 ms^{-1}

Although these test conditions are restrictive enough for the practical feasibility of testing, the scatter of data obtained at different laboratories might be extremely high. This is demonstrated in Fig. 1 showing a typical result of a round-robin test exercise.[1)]

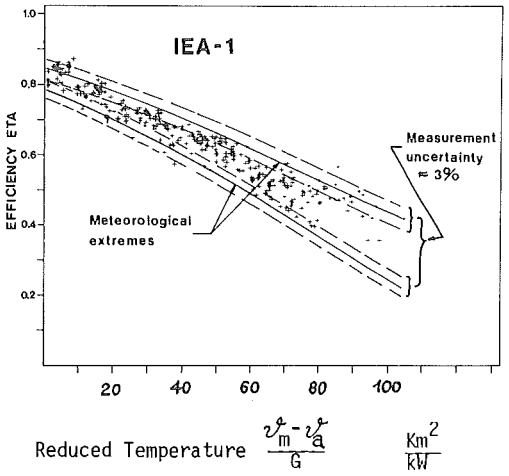

Fig. 1: Result obtained by 12 laboratories in a round-robin test exercise on a single-glass, selective-absorber collector. Data scatter is caused by varying meteorological conditions as well as measuring errors.

These data were obtained outdoors using the ASHRAE procedure. The reasons for the unacceptable high data scatter are both varying meteorological conditions and measuring errors. The analysis of the test data made clear that different air velocities and the inaccuracies of the pyranometers were the dominating error causes.

These facts are immediately leading to the idea of comparative testing. If two collectors are measured at the same time the environmental conditions are the same. If one uses the principle of series connection of collectors one also avoids the accurate measurement of the flow rate and the complicated determination of the specific heat of the heat-transfer fluid in cases where other fluids than water are used.

Naturally, one should not expect that results from different locations would show less data scatter, however, if one used a well-known "reference" collector, the data of the collector under test can always be referred to that reference collector. It is obvious that the problem is now shifted to the availability of an appropriate reference collector.

Fig. 2 shows the scheme of a comparative test loop with series connection of reference and test collector.[2)] A

stable, but variable collector entrance temperature is obtained by using regulated heat exchangers in the cooling water loops. It is important to note that a registration (not an accurate measurement) of the basic operational variables is still needed, i.e. global irradiance, air temperature, collector entrance temperature,

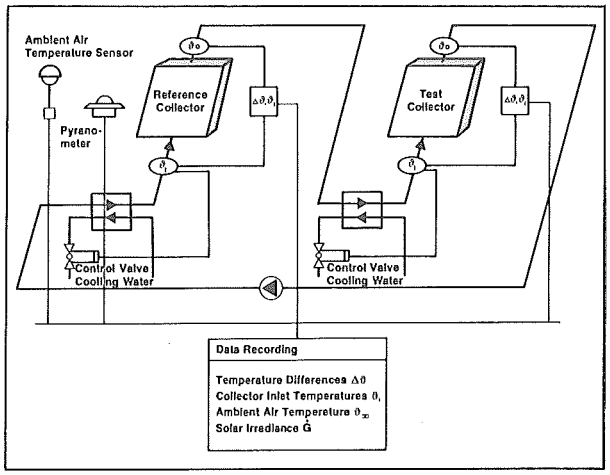

Fig. 2: Scheme of a collector test loop for comparative testing. Two or more collectors are connected in series. The heating up of the loop to a certain operating temperature shall be achieved by solar radiation absorbed by the collectors.

and last not least the air velocity have to be monitored. This is necessary in order to know the "Arbeitspunkt" of the collector. The only remaining requirement is the accurate measurement of the fluid temperature difference $\Delta\vartheta$ across the collectors. The use of the mean fluid temperature ϑ_m for the definition of the collector efficiency is important in this context, since it allows also collectors with different areas to be compared. In most cases the arithmetic mean $\vartheta_m = 0.5\ (\vartheta_e + \vartheta_o)$ is sufficiently precise, otherwise the logarithmic mean temperature

$$\vartheta_m - \vartheta_a = \vartheta_o - \vartheta_e / \ln \frac{\vartheta_o - \vartheta_a}{\vartheta_e - \vartheta_a}$$

has to be taken.

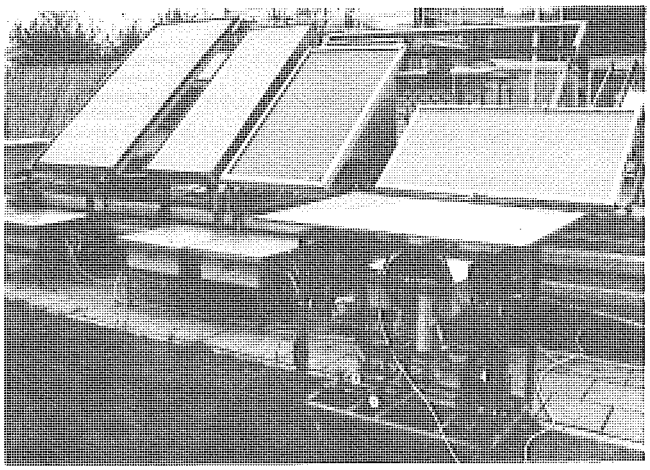

Fig.3: View of the collector test unit according to the scheme of Fig. 2 installed at the collector test field of KFA-IKP.

Fig. 3 shows a technical solution of this principle of comparative collector testing. This test unit, as installed at the collector test field of KFA-IKP, is designed on a modular basis. It consists of a rack allowing four collectors to be connected in series, the pump unit, and four individual cooling-water-regulated heat exchangers in between the collectors. Inlet and outlet temperatures are measured with platinum resistors (Pt-100) and recorded on a 12-channel strip-chart recorder. Global irradiance, air temperature, and air speed are recorded simultaneously. This collector test unit is foreseen to be used by several partner institutes in foreign countries which are cooperating with KFA-IKP in the field of collector testing on a bilateral basis, as, e.g., University of Ljubljana/Yugoslavia, Universities of Joao Pessoa and Porto Alegre/Brasil.[3)]

The practical experience with this test unit has shown that in view of a reliable and easy operation, technical modifications of the regulation of the collector inlet temperatures and the temperature difference measurement across the collectors are necessary. Fig. 4 shows the prototype of a very simple and cheap solution. Here, the principle of mixing the warm fluid coming from the collector with cooled down fluid from the heat exchanger is applied. An electric heater in the hot branch holds the

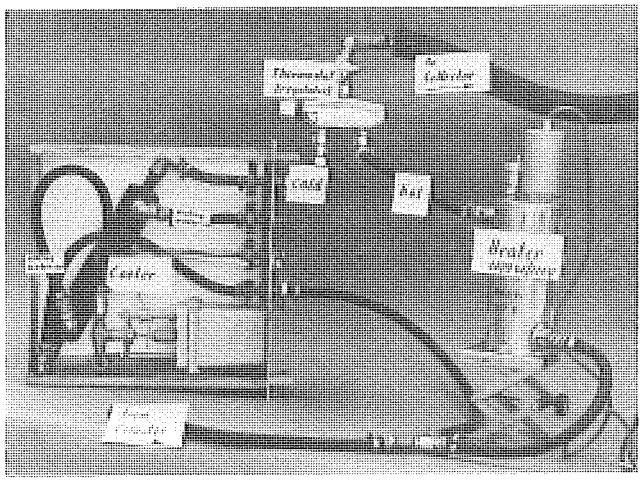

Fig. 4: Prototype of a simple and cheap regulation of collector entrance temperatures based on the principle of mixing cold and warm fluid.

adjusted fluid temperature also when there is less solar radiation and guarantees a quick change of the temperature level. As a mixing valve a usual shower thermostat is used. The operational results were encouraging. A stability of the collector entrance temperature, within 1.0 K, could be maintained over a broad range of temperatures also under fluctuating solar radiation. In order to improve the critical $\Delta\vartheta$ measurement, specifically designed Pt-100-based temperature difference amplifiers[4)] will be used in the future. With this improvement we hope to reach the goal having on hand a versatile and relatively simple and cheap collector test apparatus.

Fig. 5 demonstrates what can be expected for the practical feasibility of collector testing. This is the result of a three days measurement outdoors applying collector inlet temperatures of 20, 40, and 60 °C. Here, as a measure for the efficiency, the reduced temperature difference $\Delta\vartheta/A$, $\Delta\vartheta = \vartheta_o - \vartheta_e$ is plotted against the reduced

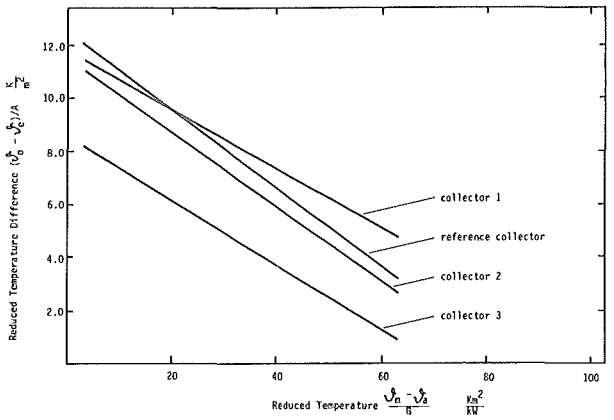

Fig. 5: Typical test result of comparative collector testing. As a relative measure for the efficiency, the reduced temperature difference $(\vartheta_o - \vartheta_e)/A$ is plotted against the reduced temperature $(\vartheta_m - \vartheta_a)/G$. The thermal quality of collectors under test can be immediately compared to the reference collector.

temperature $(\vartheta_m - \vartheta_a)/G$. Such a plot immediately gives insight into the thermal quality of the three collectors under test against the reference collector. In this case, the reference collector was a single-glass, blackpaint, rollbond-absorber collector. The other collectors were all of the double-cover, non-selective-absorber type. It is interesting to observe large differences of the maximum conversion efficiency as well as of the thermal losses, both due to different construction and material. For instance, collectors 1 and 2 have double glass covers, collector 3 has a double plastic cover which shows a strongly reduced optical transmissivity after a two years exposure to natural weathering.

References

1) H.D. Talarek, IEA Round Robin Testing, Annual Report 1980 of KFA-IKP, JÜl-Spez-99, p.136.

2) A. Boettcher, G. Scheidler, Sonnenenergie II, Umschau-Verlag, ISBN 3-524-10018, p. 175.

3) The equipment is funded by the German Minister for Research and Technology (BMFT) under contract number ET 4172 B.

4) H. Labus, High Resolution ΔT-amplifier, Annual Report 1980 of KFA-IKP, JÜl-Spez-99, p. 140.

6.2. Thermal Performance of Heat Absorbers

K. Maßmeyer, R. Posorski

The outdoor test facilities for heat absorbers as described in the Annual Report 1980[1] have been operational since June 1981. Calorimetric measurements concerning the useful energy output of absorber plates were carried out together with simultaneous recording of meteorological data under the seasonal range of weather conditions.

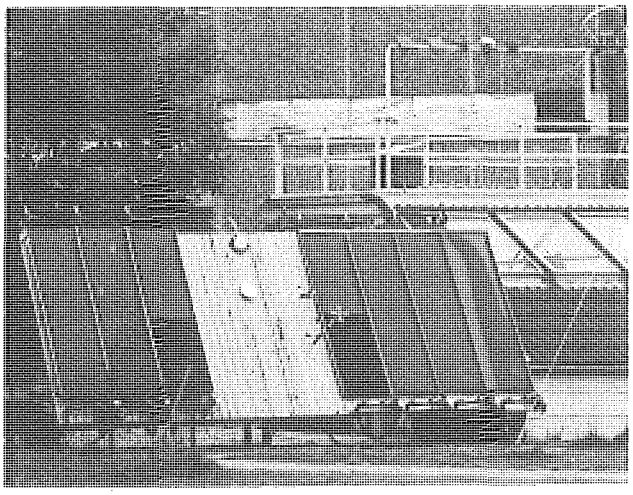

Fig. 1: View of operating test loops with inclined absorber plates (60°) oriented to the south

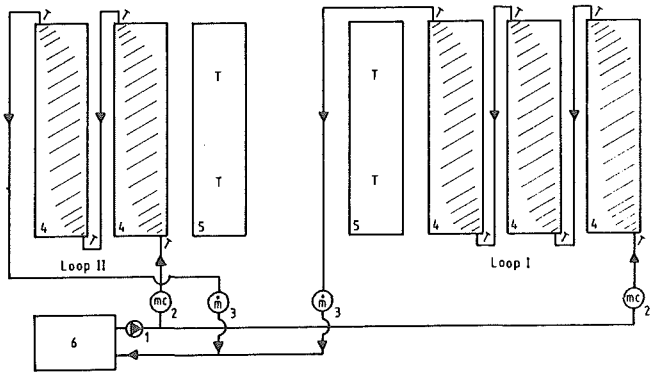

Fig. 2: Scheme of test loops (1-circuit pump; 2-flow controller; 3-flowmeter; 4-absorber with circulating fluid; 5-absorber in no-flow condition; 6-thermostate controlled buffer bath; T temperature sensors).

Two test loops were supplied with controlled constant mass-flow and a constant inlet temperature.

Loop I consists of 3 absorber plates connected in series with thermal insulation on the rear sides.

Loop II consists of 2 absorber plates connected in series, elevated from the supporting plane (14 cm) to allow heat exchange, likewise on the rear side of the plate (see Fig. 1 and 2).

A MADAS system[2] was used for data acquisition. Mean values for each parameter were calculated on periods of 10 min based on instantenous measurements with a sampling rate of 25 sec.

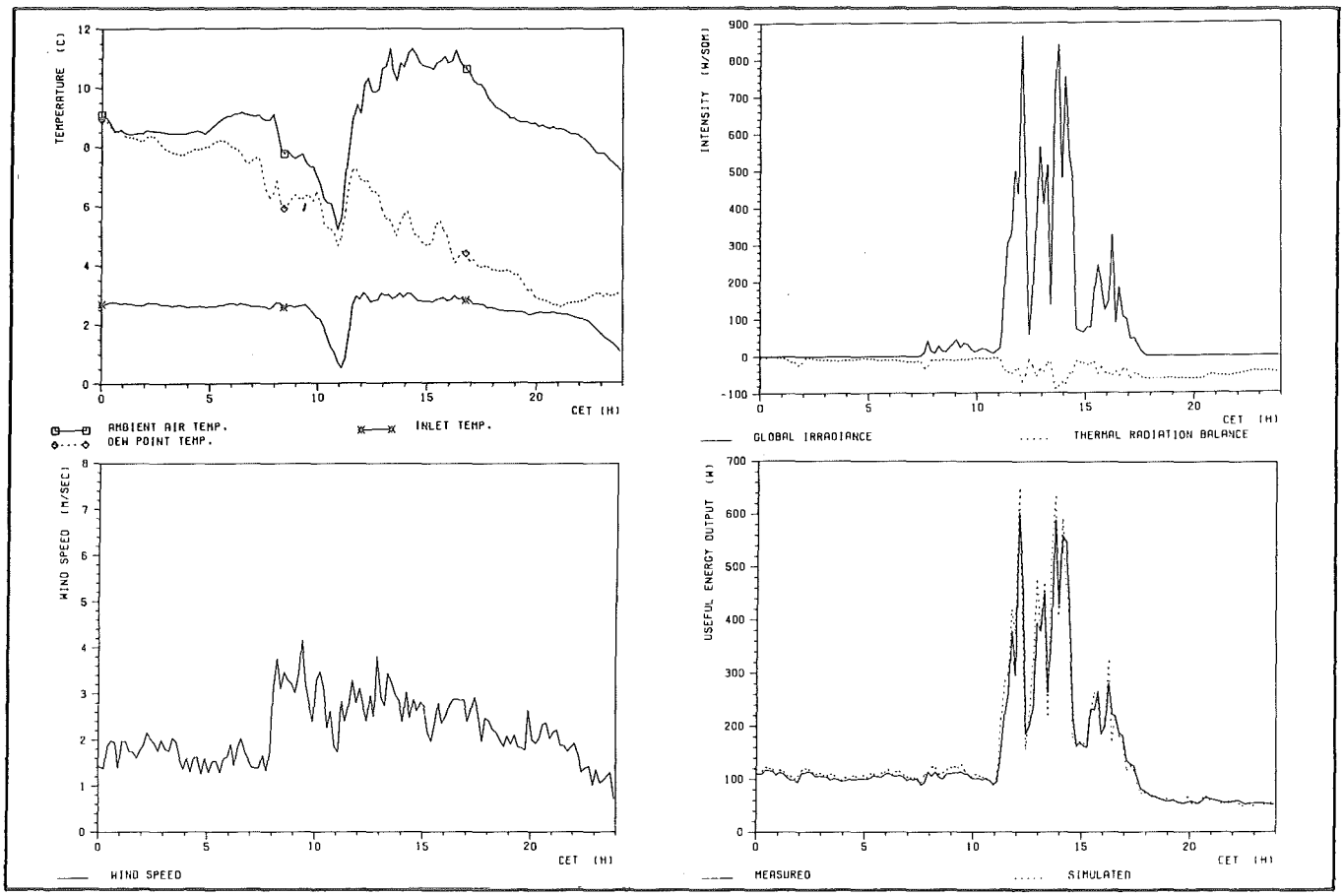

Fig. 3: Meteorological conditions and comparison of measured and calculated useful energy output on October 11, 1981

The all-day performance of an absorber plate which is insulated on the rear side is shown together with the meteorological parameters in Fig. 3.

Apart from the measurements on the thermal performance of absorber plates a model[3] was developed to simulate the heat transfer mechanisms on the absorber plates in order to predict their useful energy output under varying weather and operating conditions.

The model takes into consideration the heat transfer of

- absorbed global irradiance
- thermal radiation balance
- natural and forced convection
- condensation of water vapour on the absorber surface.

Time (CET)	0 - 1h	12 - 13h	18 - 19h
absorbed global irr. (W)	/	330	/
thermal radiation bal. (W)	9	- 29	- 29
nat. and forced conv. (W)	52	31	89
condensation (W)	52	16	5
useful energy output (W)	113	348	65

Table 1: Contributions of the heat transfer mechanism to the useful energy output shown in Fig. 3 for three periods with different meteorological conditions.

In its present state the model does not take ice or hoarfrost formation into account.

In the case of all other operating conditions investigated we found an accuracy of ± 10 % compared with the measured results.

Future work will deal with heat transfer measurements with ice and hoar frost formation as well as the defrosting performance of the plates.
At the beginning of 1982 four vertically oriented northward facing absorber plates will be connected to the fluid circuit shown in Fig. 2.

Further investigations on all-day performance will be conducted with an inlet temperature showing a constant temperature shift related to the ambient air temperature.

References

1) R. Wagner, An outdoor test facility for heat absorbers, JÜl-Spez-99, 143, 1981.

2) J.W. Grüter, K.-P. Kruck, H. Labus, Madas a microprocessor aided data acquisition system, JÜl-Spez-15, 131, 1978.

3) K. Maßmeyer, R. Posorski, Wärmeübergänge am Energieabsorber, to be published 1982.

6.3. Round Robin Testing of Evacuated Tubular Collectors

H. D. Talarek

While the basic insight into the useability of collector testing procedures was gained from round robin tests of flat-plate collectors[1], the testing of evacuated tubular collectors was hoped to verify the maturity reached. However, the recent results from round robin testing of the evacuated tubular collector (coded as IEA-3) do reveal a usual too large scatter to be acceptable. The collector was tested with a white diffuse reflective backboard by 8 laboratories outdoors and by 6 laboratories with a simulator. The analysis of the data was conducted in the same way as previously done for the flat-plate collectors. The environmental impact on collector performance is expected and shown to be less prominent as compared to flat-plate collectors but the data scatter is large (Fig. 1).

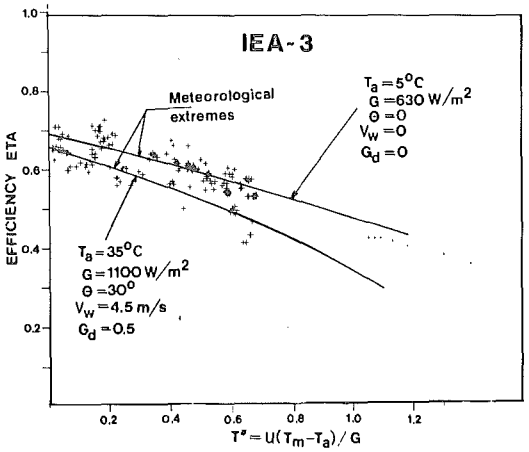

Fig. 1: Efficiency data of the IEA-3 collector enclosed by extremes of collector performance.

The test results with simulators from 6 laboratories suggest that again a systematic bias in radiation measurements exists between laboratories rather than a bias from the calorimetric measurements as the slopes are nearly parallel (Fig. 2). This is supported by a comparison of heat loss measurements for the IEA-1 collector.

Summarizing the results from various round robin tests it is concluded that a high standard of measuring technique is required for thermal performance testing and that a code of practice for the use of pyranometers in solar energy application has to be developed in order to make the test standards operational.[2]

Nomenclature for all figures:

T_a = ambient temperature

T_m = mean fluid temperature

G = insolation

U = normalizing coefficient 10 $W/m^{2}.{}^oK$

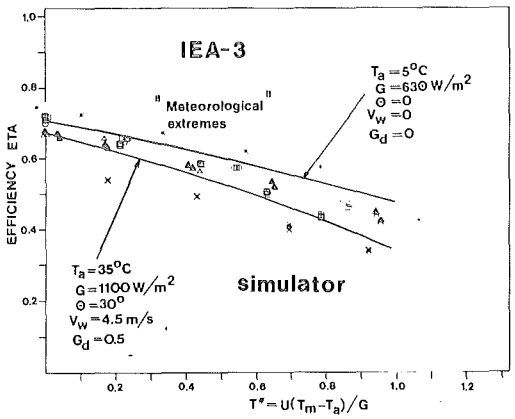

Fig. 2: Efficiency data of the IEA-3 collector (simulator)

References

1) H.D. Talarek, Results and Analysis of IEA Round Robin Testing, Technical Report III.A.1, Kernforschungsanlage Jülich GmbH, 1979

2) H.D. Talarek, IEA-Round Robin Testing of Solar Collectors, Poster Presentation at the Solar World Forum, Brighton, England, 1981

6.4. Pyranometry

H. D. Talarek

As the comparison of thermal performance data of collectors has questioned the accuracy of global radiation measurements in solar applications, an attempt was made to resolve the problem into its essential elements: A sequence of pyranometer comparisons and recalibrations was conducted at three different laboratories. An initial comparison took place in Davos/Switzerland[1], followed by outdoor and indoor calibrations in Canada and in the U.S.A.[2].

Figure 1 shows in a very direct and almost heuristic way the essential result from the round robin intercomparative pyranometer testing.

The standard calibration practices reveal about the same "spectrum" of instrument constants, while systematic laboratory-to-laboratory discrepancies are apparent. The obvious conclusion is that the problem encountered is twofold:

- The "spectrum" of instrument constants can possibly be explained by the characteristics of the particular instruments.
- The disagreement between laboratories is possibly due to different standard indoor or outdoor calibration practices.

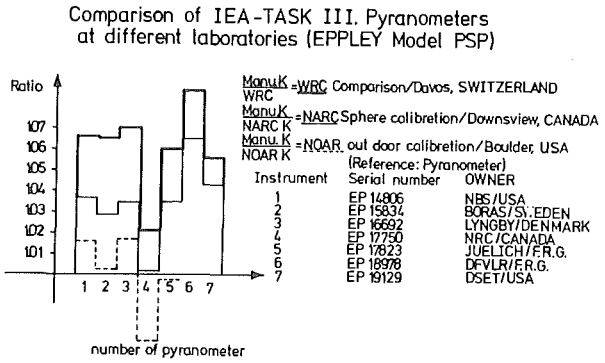

Figure 1: Calibration constants of Eppley PSP Pyranometers (3 laboratories, 3 methods).

These problems can be eased if

- the uncertainty of the performance characteristics of individual instruments,
- the diversity of calibration procedures for pyranometers practised by meteorological offices, manufacturers and others

are diminished.

Participants within Task III of the IEA project "Solar Heating and Cooling Systems" have addressed the uncertainty of the performance characteristic by design and conduct of an experiment which is to compare the performance of pyranometers that are well characterized beforehand. This is to test the hypothesis that the characterization of an individual pyranometer can be used to correct the instrument's reading to achieve an adequate accuracy of global radiation measurements.

References

1) C. Fröhlich, Results of a Pyranometer Comparison, Davos, March 5 and 6, 1980, Solar Heating and Cooling Program, IEA-Task III Report

2) Draft Report: International Energy Agency Conference on Pyranometer Measurements, March 16-20, 1981, Boulder, Colorado, SERI/TR-642-1156/Golden, Colorado

6.5. Heat Output Calculations With Reduced Meteorological Data Sets[+)]

H. R. Koch, W. Scheller, A. Pilatte[++)]

Systems which make use of solar energy can be most perfectly designed using complete short interval meteorological data sets, in which the correlation between the various parameters and their time sequence are preserved. The use of reduced meteorological data sets makes the computations easier but the results may be less valuable. The subject of the work presented in this paper is a study on the precision of the heat output calculations of solar converters when different types of reduced weather data are used. The collector heat output is the energy which is fed into the pipes leading in general to a storage tank. Of course, this energy does not determine alone the quality of a solar system. But the solar converter is, among the components of a solar system, the one whose performance is most strongly related with weather conditions. The fraction of the collector energy which is finally used by the energy consumer and which replaces other energy resources this fraction can only be computed regarding the interaction of all the components of the system and must be the subject of further research. In the present study we have computed collector heat outputs assuming in a first step the simplest action of the system on the collector: we regard constant inlet temperatures and constant flow rates leading to operating temperatures of the collector which vary only by some degrees.

In order to classify the differences which may appear in heat output determinations we must have a quality scale. We have learnt from the round robin collector tests of the IEA[1)] and the EC[2)] that the variance of η-determinations is in the order of 5 % for test procedures with defined meteorological conditions. Considering these differences one may define, of course, somewhat arbitrarily the following quality scale for the computation of the heat output of collectors of long periods during which all types of weather conditions may appear:

deviation	quality
<10 %	good
<20 %	sufficient
>20 %	questionable

The reference heat output of a collector which is used as a standard in the comparison of computed results can be obtained through precise measurements or through a detailed simulation calculation based on the short interval weather data and the physical properties of the collector. We may assume that the result of a detailed simulation calculation is by far more precise than results of simplified methods provided that the correct collector parameters are known. The simulation programme used for our work is the COL2 programme of the Faculté Polytechnique de Mons.

The methods of data reduction applied within action 3.4 of the CEC Solar Programme are shown schematically in Fig. 1.

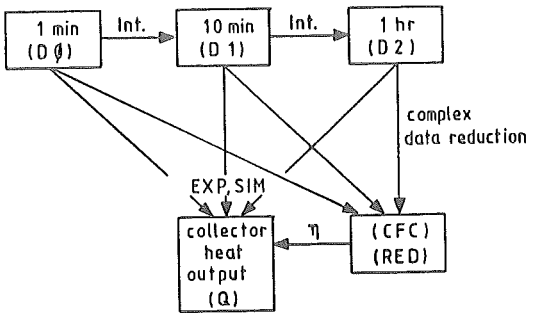

Fig. 1: Flow diagram for the applied data reduction methods.

The transformation of data sets D0 to D1 and D2 is a simple integration leading to longer time steps. The transformations D0, D1, or D2 → CFC or RED are more complex reductions which were described previously (3,4). The Cumulative Frequency Curves ("CFC") are studied by the Ecole des Mines in Paris and will not be discussed here. The "RED"-function (Radiation Energy Distribution) is a simplified version of the MURD-function. The latter is applied in Switzerland by Kesselring and his coworkers[5)]. The method is based on the assumption that the collector efficiency η is in good approximation only a function of the reduced temperature $T^+ = U_o(T_c-T_a)/G$ (U_o = 10 W/(m^2·K), T_c = mean collector temperature, T_a = temperature of ambient air, G = irradiance on the collector plane). The value of the RED-function for a certain $T^{+\prime}$ is the sum of G for all intervals for which T^+ falls within a slice between $T^{+\prime}$ and $T^{+\prime}+\Delta T^+$. For normalization this sum is divided by ΔT^+. The collector heat output for the period which was used for the computation of the RED-function is given as $Q(T_c) = \Sigma\ RED(T^+) \times \eta(T^+)\cdot\Delta T^+$, where the summation comprises all T^+-slices. This mode of proceeding is applicable for fixed collector temperatures T_c.

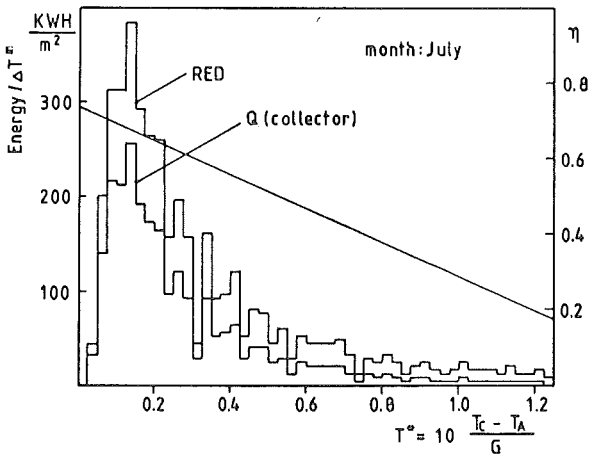

Fig. 2: Example of the application of the RED-funcion (T_c = 30°, Q = Σ RED·η·ΔT^+) for the month of July of the Belgian Reference Year. The RED function refers to the global radiation on a south oriented plane of the slope 51°.

Fig. 2 illustrates how Q is derived from the RED- and η-curves. It can be shown easily that the same heat output is obtained when the most primitive simulation calculation is performed using the original data and the efficiency $\eta(T^+)$ for each of the intervals of the investigated period:

$$Q = \Sigma\, G.\eta(T^+)$$

Therefore, the applicability of the RED-function can be studied through an investigation of the applicability of an efficiency η which depends only on T^+, for all day heat output calculations. In the following limitations of the $\eta(T^+)$-concept are briefly discussed, in order to show that a careful study is needed.

Deviations between $\eta(T^+)$ and the real efficiency are introduced through the following effects:

a) Wind speed.

b) The efficiency η is only valid for the global radiation G fixed in the test procedure. The heat loss coefficient usually is given as $\alpha = a_1'+a_2'\cdot\Delta T$. The coefficient of the quadratic term of the η-curve ($\eta = a_0+a_1T^+ + a_2\cdot T^{+2}$), derived from α depends on G:

$$a_1 = a_1'/U_o; \quad a_2 = a_2'\cdot G/U_o^2$$

This effect vanishes only if a constant heat loss coefficient is used corresponding to a linear η-curve.

c) Radiation incident at angles $<45^o$ is overestimated.

d) The dynamical behaviour of the collector due to its heat capacity leads to an overestimation of the heat output.

As discussed before, the value of the RED-funcion concept can be deduced from a determination of the all-day validity of the efficiency $\eta(T^+)$. This question has been studied in two ways:

a) Comparison with Experiment

For a period of 9 days in August 81, the heat output of a flat-plate collector (type: Viessmann Acredal-s, 2 covers) was measured at Jülich in time steps of 1 minute and compared with $Q = \eta(T^+)\cdot G$. In the terms of Fig. 1 we have compared

$$DO \xrightarrow{EXP} Q \text{ with } D1 \rightarrow RED \xrightarrow{\eta(T^+)} Q.$$

The latter process is equivalent with

$$D1 \xrightarrow{\eta(T^+)} Q$$

for constant collector temperatures. Fig. 3 and 4 show the results for the 2nd (varying insolation) and the 6th of August (permanent insolation). We observe in both cases the expected delay of the collector heat output when the insolation changes. The deviation of 5 % in Fig. 4 which is most clearly seen during the long period of constant irradiance at noon is probably due to a difference between the real $\eta(T^+)$-curve of our collector and that we used in our calculation which had been determined for this collector type in a standard BSE collector test at our institute. We could have adapted, of course, easily the η-curve according to our measurements. But keeping to our quality scale we can very well tolerate the deviation.

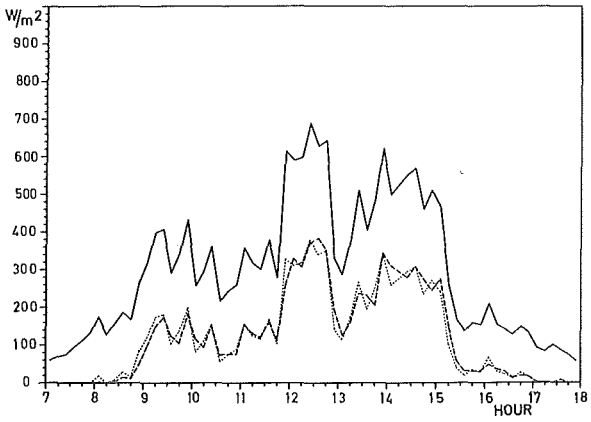

Fig. 3: Global radiation on the collector plane (——), measured collector energy (---) and computed energy (···) $Q = \eta(T^+)\cdot G$ for August 2, 1981, at Jülich.

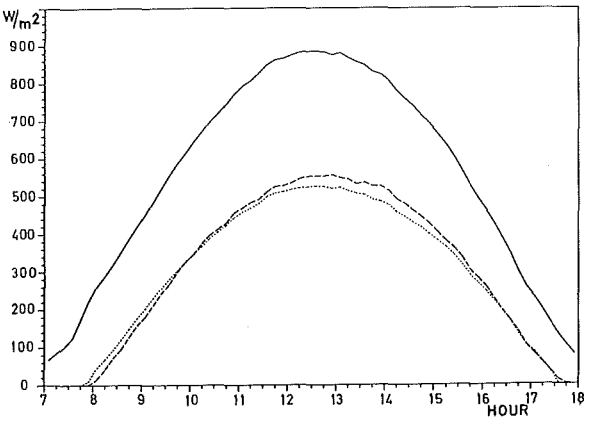

Fig. 4: Same as Fig. 3 for August 6, 1981.

b) Comparison with Detailed Simulation Calculations

The energy output of the CEC4-collector (Dru-collector) was determined for the inlet temperatures 10, 30, and 50 ^oC using as meteorological input parameters the Belgian Reference Year (CEC Solar Energy Programme).

The process of data reduction can be described in terms of Fig. 1 by

$$D2 \rightarrow RED \xrightarrow{\eta(T^+)} Q.$$

The reference energies were obtained with the help of a simualtion calculation. The monthly collector energies obtained with the two methods are given in Fig.5. The differences amount up to 15 %.

These deviations are due to effects inherent in the method itself, but eventually also to an imperfect correspondence of the basic physical parameters which were used in the simualtion calculation with the efficiency curve $\eta(T^+)$. But, nevertheless, we conclude that for fixed temperatures the RED function method yields in the average for flat-plate collectors energies with good precision (deviation <10 %).

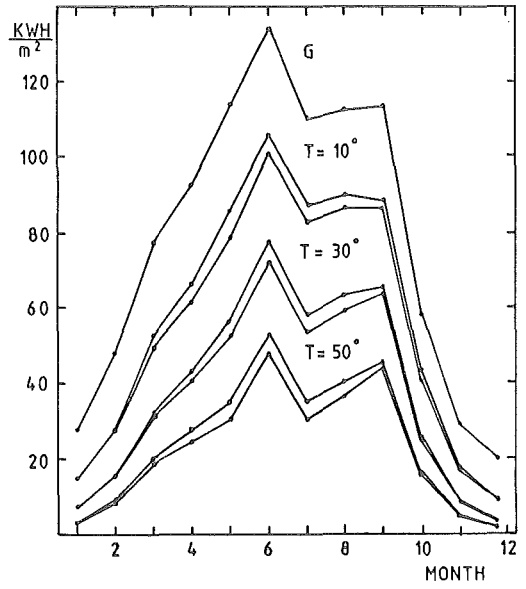

Fig. 5: Monthly heat output of the Dru-collector (slope = 51°) during the Belgian Reference Year. For every inlet temperature the upper curve is the result of the RED-function method, the lower was obtained with the help of the simulation programme COL2 (Faculté Polytechnique de Mons).

References

1) Results and analysis of IEA round robin testing. IEA-report task III, KFA Jülich, 1979

2) Results and analysis of the round robin testing of the fourth solar collector in the European Community programme, edited by A. Derrick, University College, Cardiff, U.K., 1980

3) J. Adnot, B. Bourges, D. Campana, R. Gicquel, Utilisation de courbes de fréquences cumulées d'irradiation globale pour le calcul des installations solaires, Report of Ecole de Mines de Paris, 1978

4) H. R. Koch, K. Maßmeyer, W. Scheller, Contribution to the Workshop "Time and Correlation Structures of Meteorological and Radiometric Data for Solar Energy Applications, Dec. 17-19, 1980, Paris, Publication by the CEC in progress

5) P. Kesselring, A. Duppenthaler, The layout of solar hot water systems using statistical meteo- and heat demand data, Contribution to the ISES 1979 International Congress on Solar Energy, May 28 - June 1, Atlanta, Georgia, U.S.A.

+) Work performed within the Solar Research Programme F of the European Community, action 3.4

++) Faculté Polytechnique de Mons, Belgium

IV. TECHNICAL DEVELOPMENT

7. ISOCHRONOUS CYCLOTRON

7.1. Cyclotron Operation and Improvement

L. Aldea, H.G. Böge, W. Bräutigam, H. Borsch, R. Brings, R. Fiedler, I. Jannakos, C. Mayer-Böricke, J. Reich, A. Retz, U. Rindfleisch, N. Rotert, G. Schlienkamp, H. Schwan, P. Wucherer

At the end of September 1981 it was a period of ten years[1] that the cyclotron JULIC runs in regular operation around the clock. For normally 45 to 46 weeks a year the machine is operated in 21 8 hours shifts per week with a scheduled interruption of 11 hours every two weeks for maintenance and repair. Figure 1 illustrates the operating record of JULIC during the past decade. With only minor

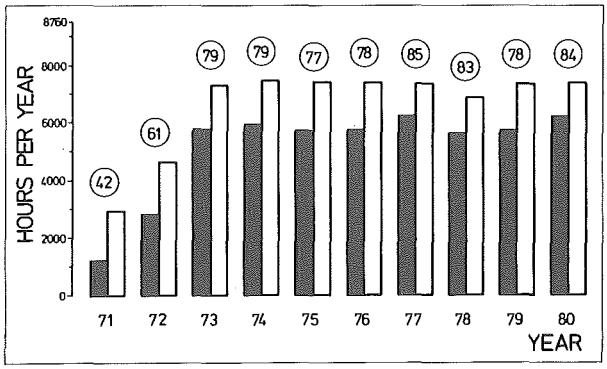

Figure 1: Operating record at JULIC during the past decade: □ scheduled operating time ▩ cyclotron being operational ○ quotient of ▩ / □ in percent.

variations during the years about 20 % of the available machine time have been used by guests from German and foreign universities and other organisations, 10 % by other institutes of the Kernforschungsanlage and 70 % by scientists of the Institut für Kernphysik for nuclear reaction and spectroscopy experiments as well as for beam and apparatus development (typically 6 %). In total 90 % of the machine time was devoted to basic nuclear physics and 10 % to isotope production and other applied topics.

The cyclotron time distribution in 1981 is given in Table 1. A brief summary of some technical improvements and modifications is described in the following. They had to be realized mainly during the regular annual shut down period of 7 weeks in August/September.

1. The exchange of the RF-resonator cooling plates which started in 1980 was continued. In difference to the elements, which were installed in 1980, we now use copper plated Aluminium sheet metal with soft soldered copper tubes instead of stainless steel tubes to facilitate the realization of the complicated cooling platterns. The exchange of the cooling plates is intended to be completed as soon as it becomes necessary.

2. To improve stability and reproducibility of the RF amplitude first measures have been taken: New amplitude pick ups have been installed and calibrated. The associated precise RF detection circuits will be completed in early 1982. A specially adapted power amplifier for the control of the series tube in the RF power supply was installed to allow the implementation of several superposed regulation loops. This is a first step on the way to improve the ripple suppression as well as the long term stability of the RF amplitude.

CYCLOTRON OPERATION		
Cyclotron tuning and beam handling	594 h	8.4 %
Beam on target	4893 h	68.8 %
Beam time for experiments	5487 h	77.1 %
Beam development, testing new components	411 h	5.8 %
CYCLOTRON OPERATIONAL	5898 h	82.9 %
SCHEDULED MAINTENANCE	237 h	3.3 %
SYSTEM FAILURES	982 h	13.8 %
SCHEDULED OPERATING TIME	7117 h	100.0 %
BEAM TIME DISTRIBUTION		
Guest scientists (U. Bonn, TH Darmstadt, U. Hamburg, MPI Heidelberg, KfK Karlsruhe, U. Köln, U. Krakau, TH München, U. Münster, IPN Orsay, U. Tübingen)	1390 h	25.3 %
Scientists of KFA (excluding IKP (ICH1-IME,-IRA)	616 h	11.2 %
Scientists of IKP	3481 h	63.5 %
Beam time for experiments	5487 h	100.0 %

Table 1: Cyclotron time distribution in 1981.

3. Extraction elements have been readjusted and modified for better external beam quality and increased intensity. The compensated iron channels have been readjusted on the base of actual magnetic fields. The focussing channel is now completely water cooled and carries the diaphragms defining the trajectory for minimum beam distortion (see chapter 7.2.). Both elements have been equipped with graphite shielded high power entrance and exit diaphragms for increased beam intensity. A field mapping was taken in the region of the septum deflector to allow a check of the actual septum geometry.

4. In a several weeks procedure all magnetic elements of the beam line in the cyclotron vault have been precisely readjusted to within ±0.1 mm some adjustments turned out to deviate by up to 1 mm. The bending magnets had to be disassembled to get access to the magnetic reference marks on the pole faces. Now adjustment targets are mounted on top of the magnetic elements in the cyclotron vault to facilitate routine checks and the future modifications of the beam handling system (see chapter 7.5).

5. The new microprocessor controlled emittance measuring device has been installed at the cyclotron in the shut down time and meanwhile undergone first in-beam tests (see also chapter 7.4).

6. The strength factors of the quadrupole magnets along the line to the spectrograph BIG KARL have been determined more accurately by using the cyclotron beam producing different focus conditions at the various viewing screens and the according TRANSPORT calculations. The strength factors (in kG/A) are based on actual magnet current values provided by the data logging system (see chapter 7.3). The tuning of the beam line to the spectrograph BIG KARL has been improved a step further by this.

7. Specially deviced NMR-Gaussmeters, VICKSI type beam profile monitors and multipurpose beam probes (for viewer, stop and object plunger) as nearest as possible to the intermediate focus locations are in preparation to further facilitate the tuning of the beam line.

In close contact especially to our users from the universities in the state NRW intentional plans for the further improvement and extension of JULIC have been discussed. The goal is to achieve single turn extraction for improved beam quality with the light ions and to extend the energy range from now 22.5 down to approximately 5 MeV/A for the ions being available with ISIS (see also chapter 7.7) in the future. These plans are mainly basedon a completely new design of the RF-system with 3 decoupled resonators excited by 3 separately driven RF-amplifiers. This would allow the operation of the resonators with either 0 or 120^{o} phase shift at stabilities improved by at least one order of magnitude. In turn this is the presupposition for multiharmonic mode acceleration (necessary for the extension of the energy range) and for the single turn extraction. So far the external beam injection for the harmonic modes h = 2, 3 and 5 has been investigated in more detail (see chapter 7.6).

Prior to any realization of these plans comes the modernization of the beam line to the spectrograph BIG KARL. The ion optics for a modification of the double monochromator to produce a variable dispersion at lower level and as much as telescopic behaviour as possible has been worked out (see chapter 7.5).

Reference

1) L. Aldea, W. Bräutigam, R. Brings, C. Mayer-Böricke, J. Reich, P. Wucherer, Proc. 9th Int. Conf. on Cyclotrons and their Applications (Caen 1981) in press

7.2. Check of the Ion Optics of the Focussing Channel

L. Aldea, R. Brings, R. Fiedler, J. Reich, P. Wucherer

The exctraction[1,2] from the JULIC-cyclotron starts with a 20°-electrostatic deflector in the first part of a hill. In the following valley a totally screening compensated iron channel separates the extracted beam so effectively that the beam leaves the pole face at the end of the same valley. At this point a focussing channel is needed to compensate for the strongly defocussing and overfocussing action of the fringe field in the two planes, respectively. Fig. 1 shows a plan view of the channel (labels 1-4) and together with a pair of steering magnets (labels 5-6).

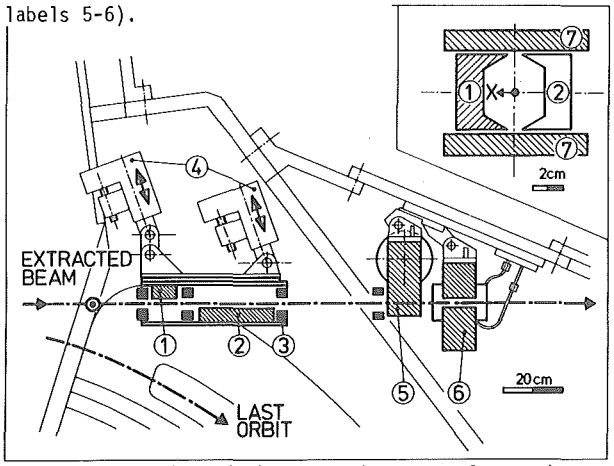

Figure 1: Plan view of the focussing channel together with a pair of steering magnets (for further explanation see text).

The channel had to be arranged inside the return section of the trim coil windings (label 7) where the vertical aperture is limited to 4.8 cm. It consists of a horizontally defocussing iron piece (1) followed by a focussing one (2). The cross section of the iron pieces (see insert of fig. 1) was the result of field measurements in a model. The design aim was to get a linearly variing magnetic field perpendicular to the nominal orbit in the channel for a wide range of valley fields (0.25 to 0.7 T). The scaling factor of the used model, however, was too large (7.3) and the iterative field measurements very cumbersome. The optical quality of the actual focussing channel was therefore doubtful.

To check the ion optics of the actual focussing channel half automated field measurements have been performed for different field settings and channel positions at the cyclotron. The readings of 3 Hall probes mounted on one support travelling along the axis of the channel were fed to the PDP11/34-computer at the cyclotron and after debugging and smoothening transferred to the central computer. By means of the orbit integration code SOTRM[3] an appropriate bundle of 30 particles around a reference trajectory were integrated through the smoothed field maps. The 30 particles represent the total phase space as it is known from external emittance measurements and theoretical aspects.[1]

The reference trajectory starts at point (◎) with the coordinates (x,α) measured against the channel axis (see fig. 1) in the horizontal plane. To find the reference trajectory for minimum distortion of the bundle a routine was coupled to the code SORTM to find the minimum of the function $(\bar{x}_{TOT} - \bar{x}_{LIN})/\bar{x}_{LIN}$ in the (x,α) space. $\bar{x}_T$ is the vector length corresponding to the bundle at the end of the field map as a result of the direct integration whereaus $\bar{x}_{LIN}$ refers to the vector length calculated from the linear transfer matrix, which in turn is evaluated at the same time by the code SORTM. Fig. 2 gives a representation of the described function in x and α for the two extreme field levels. They fall within 1 mm and 0.1 degrees onto the same location. Fig. 3 shows a typical bundle envelope. The envelopes for the other field levels are the same within less than 2 mm. The collimators inserted according to this investigation are shown as well. (The collimator in the middle only protects the channel in case of severe misalignments.) To avoid transmission losses the diameter of the first and third collimator has been made 3 mm larger than the mean taken from burned foil measurements in the past. To account for variations of the actual reference trajectory at the entrance of the channel in the operating range the focussing channel can be positionned in the horizontal plane (see label (4) in fig. 1).

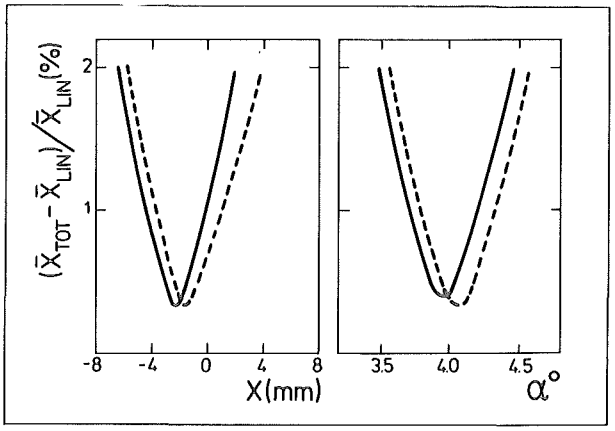

Figure 2: Representation of the minimum in the distortion of a bundle of rays after traversal of the focussing channel at - 0.70 T and ---- 0.26 T valley field (see text for further explanation).

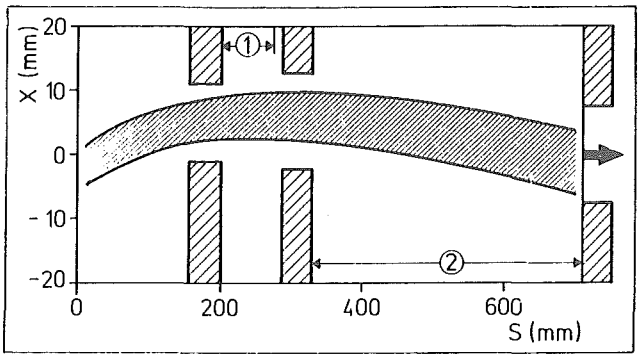

Figure 3: Horizontal envelope of a bundle of rays for an emittance $\varepsilon_x = \varepsilon_y = 6.4\ \pi$ mm·mrad at a valley field corresponding to 78 MeV deuterons together with the collimator set to minimize beam distortion.

This investigation shows that the optics of the focussing channel are sufficiently linear and vary only little with the magnetic field level as long as the reference trajectory is held within the presented limits by inserted collimators.

References

1) H. Thimmel, P. Wucherer, IEEE Trans. NS-16 (1969) 474
2) W. Bräutigam, R. Fiedler, W. Klein, U. Rindfleisch, P. Wucherer, IKP-Annual Report 1975, p. 245
3) E.R. Close, Nucl. Inst. and Meth. 89 (1970) 205

7.3. The Data Logging System at the Cyclotron

R. Brings, G. Schlienkamp

To improve the parameter setting and reproducibility at the cyclotron and the beam handling system a data logging system has been built up after the initialization of a PDP11/34 computer 2 years ago. The monitoring and check of parameters is based on the measurement of actual values.

The main component of the system (see block diagram given in figure 1) is a combination of an analogue multiplexer

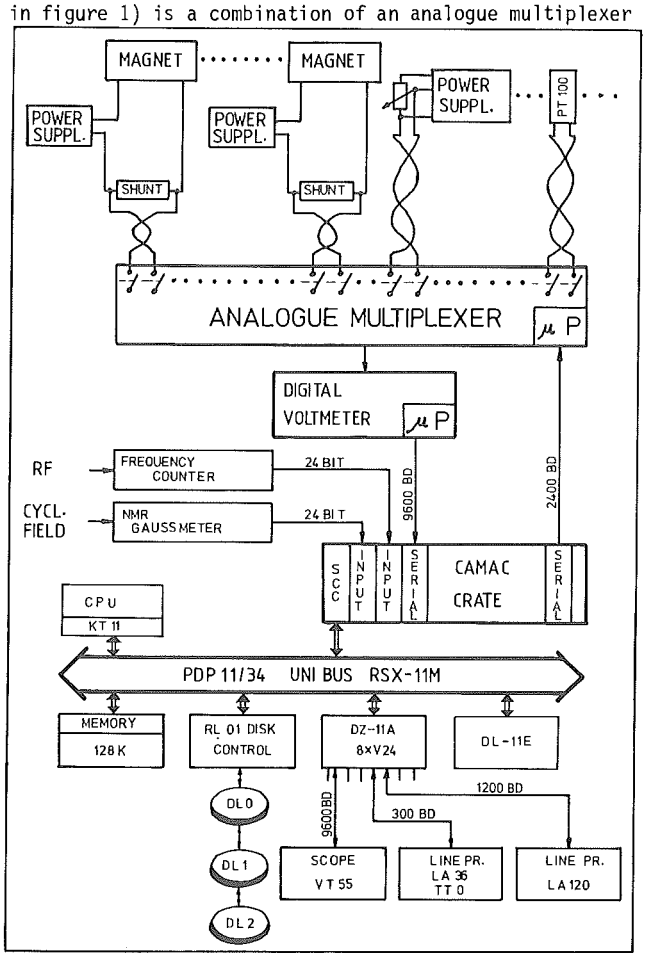

Figure 1: Block diagram of the data logging system at the cyclotron.

and a digital voltmeter (Fluke scanner 2204A and DVM 8502 with DC-option). In these devices microprocessors direct the different measurement cycles and their sequency, respectively. The Fluke system is controlled by the PDP11/34-computer at the cyclotron using the serial interface "RS 232" of the micro processors and serial asynchronous 8 bit-CAMAC-modules. Data from the Fluke system are received by a special inline CAMAC interrupt service routine written by our data aquisition group.

A total of 115 analogue signals are handled at present. They are derived from 70 shunts reading either trim coil or magnet currents (28 at the cyclotron, 42 at the beam handling system) potentiometers setting nominal values and from Pt 100-elements reading temperatures. The 70 shunts reading trim coil and magnet currents have been built, calibrated and installed to function independantly from the individual power supplies.

Among the digital signals the actual values of the cyclotron frequency and the cyclotron magnetic field (via NMR-gaussmeter) are red using a 24 bit parallel CAMAC input module.

The block diagram of figure 1 also gives the present hardware configuration of the PDP11/34-computer which runs under the control of the multi-user executive RSX-11M.

To have the full benifit of the data logging system much more further software work has to be done especially for parameter calculation and interpolation, parameter check and optimization (e.g. for the isochronous field[1]) as well as for a clearly arranged data protocol.

Reference

1) J. Linz, IKP-Annual Report 1977, Jül-Spez-15 (1978) 123

7.4. The New Emittance Measuring Device

R. Brings, P. Wucherer

The former emittance measuring device (EMD)[1] was not suited for computer control. The new EMD (see fig. 1 and fig. 2, section A) consists of a set of a slit (SL) and a

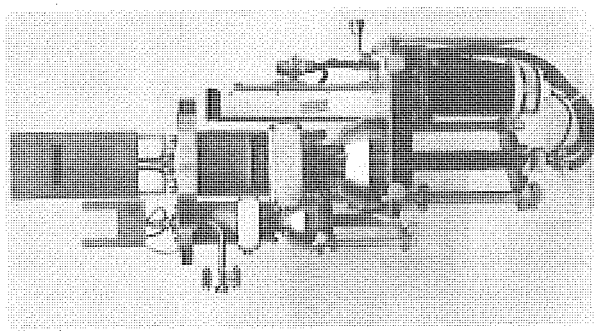

Figure 1: Slit and harp of the emittance measuring device (EMD).

harp made out of tungsten wires (PG) for the horizontal (x) and the vertical (y) plane. The drift between the corresponding slit and grid locations amounts to 2.4 m. Each harp carries 13 tungsten wires of 0.5 mm diameter. The slits are 1 mm wide. In the horizontal harp (PGX) the wires are 1.2 mm apart from each other while for the vertical harp (PGY) the wire separation is 2.4 mm. To minimize cross talking the wires are arranged at the corners of an equilateral triangle. The harps can be set to intermediate positions, which can be chosen nx0.2 mm (n=1,2,3,4) apart from each other, in case a higher resolution than given by the wire distance is required. The slits (SL) and the harps (PG) are moved by 1.8^{o}-stepping motors.

To complete measuring cycle consisting of the positionning of the selected system x or y, the start of the autoranging beam current amplifiers and the integrators, the switching of the analogue multiplexer, the read out of the 12 bit ADC as well as the storage of the measured data into the RAM is controlled and handled by a microprocessor (8085, see fig. 2, section B). The I/U-converter for the beam current signals on the harps can be switched to 4 different ranges (up to 1 nA, 10 nA, 100 nA and 1000 nA). To keep the signal cables as short as possible all measuring and control electronics is located underneath the beam line at the cyclotron exit.

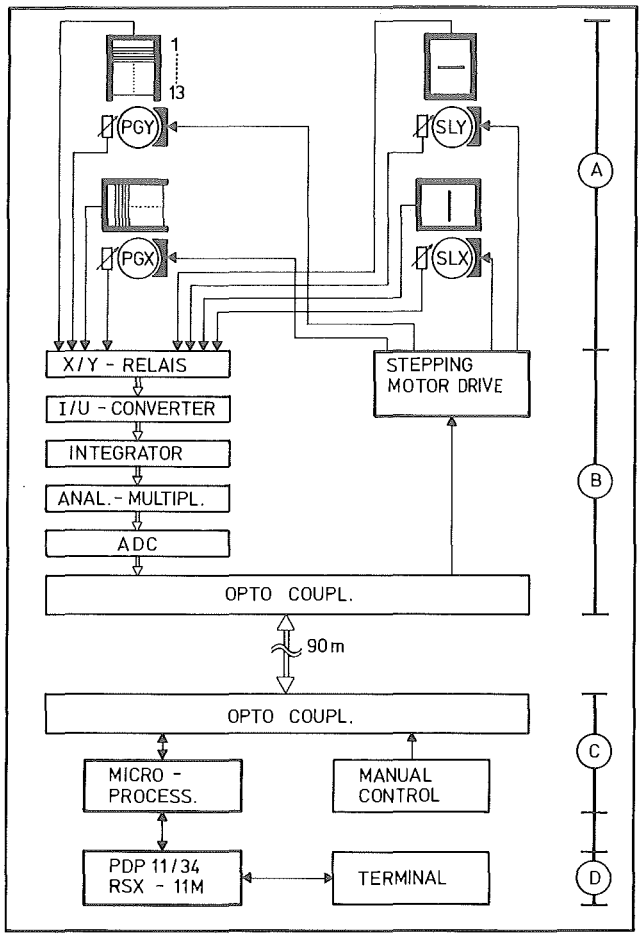

Figure 2: Block diagram of the EMD hardware (A) slits and harps with driving mechanism (B) analogue electronics and stepping motor drives (C) microprocessor and mannual control (D) data evaluation and display.

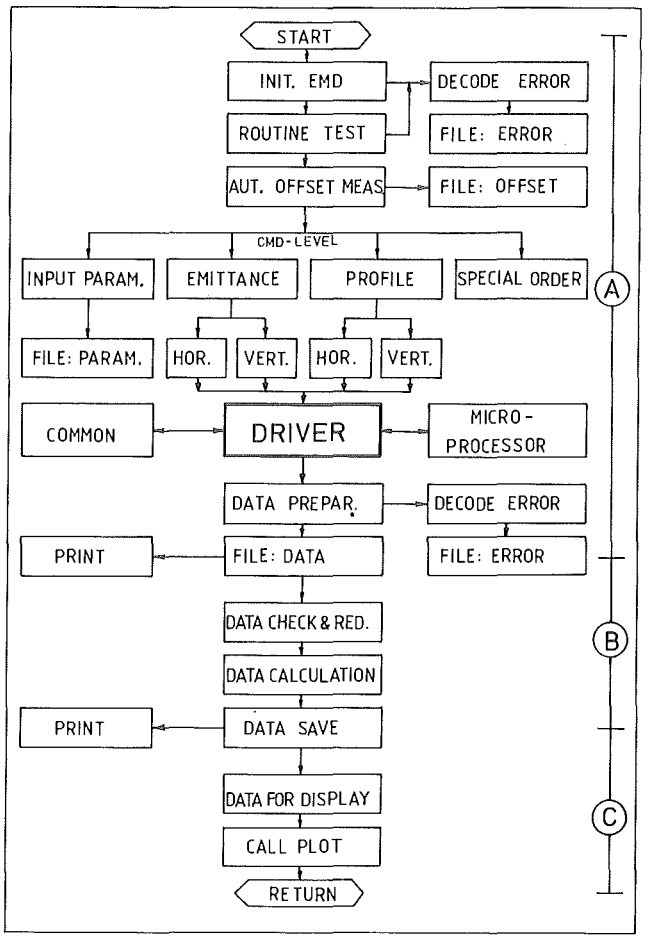

Figure 3: Block diagram of the EMD software (A) control software (B) data evaluation software (C) data display software.

The devices for remote control (see fig. 2, section C) are installed in the cyclotron control room. Between the two locations only digital signals are transmitted in a safe way by opto couplers. The microprocessor is connected serially to the PDP11/34-computer which is used for the remote control as well as the evaluation and the display of the measured data. There is only a simple mannual control for fault events available.

The system as it is described above was manufactured by NTG Gelnhausen[2] according to our specifications. The system has undergone extensive acceptance tests which brought about hard- and software modifications. The system has been installed at the cyclotron in 1981 during the last shut down time. The electronics had to be adjusted and has undergone trouble shooting in great detail. First test measurements with beam have been performed by the end of the year.

Parallel to this the basis software was performed on the PDP11/34 which runs with the multiuser system RSX-11M/V3.1 . For the data transfer to the micro processor therefore a high priority privileged subtask in assembler[3] had to be installed by our software group. Data and status informations are stored in a memory common. An overlay structured FORTRAN task uses this front end driver (fig. 3, sect. A). This task is suitable to generate test data, to manipulate the rough data and for trouble shooting. A first user version of this task allows for the selection of prepared input data sets. Initialyzing, check, measurement, data transfer, preparation and storage on a disk are performed automatically. First data sets have already been measured but no emittance has been evaluated and displayed so far because the according software (see fig. 3, sect. B and C) is not yet ready.

References

1) J. Bojowald, H. Borsch, W. Kuhlmann, A. Retz, Proc. 6th Int. Cycl. Conf. (Vancouver, 1972) p. 401

2) GSI-PB-3-74

3) J. Siefert, B. Siefert, IKP-Annual Report 1980, KFA, Jül-Spez-99 (1981) 166

7.5. On the Modification of the Double Monochromator

J. Reich

The design of the present Jülich double monochromator[1] (see fig. 1, upper part) was completed in 1967. The design aim at that time was to achieve a very high momentum resolving power characterized by the quotient of momentum dispersion/magnification D/M to be more than 30 cm/% at unity magnification. This was achieved by incorporating radially defocusing quadrupole singlets AQ1,2 within the inlet and outlet slits DS1,2, respectively, into the design. The system is pointsymetric with respect to the intermediate slit IS, the location of a horizontal cross over in the dispersive mode of operation. For the single achromatic mode of operation between the slits AS1,2 the beam is focused onto slit AS1. The double monochromator came into operation at the beginning of 1972.

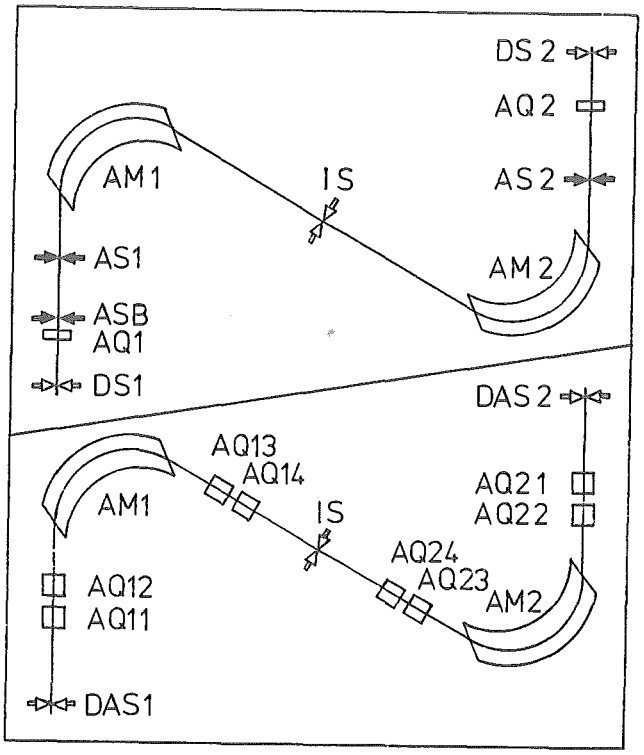

Figure 1: Lay out of the present (above) and a modified double monochromator system (below); AM analysing magnets; AQ quadrupole magnets; IS intermediate slit; DS dispersive slit; AS achromatic slits; ASB slit for modified achromatic mode; DAS dispersive and achromatic slit.

The essential features of the spectrograph BIG KARL[2] were worked out in 1972. His D/M-value was designed to be 20 cm/% momentum with a dispersion of 17 cm/%. The matching design between the spectrograph and the cyclotron[3] was finalized in 1975 and considered a single achromatic mode at a low D/M-value of 11 cm/% momentum (with inlet slit ASB, see fig. 1) besides the high dispersive mode for high transmission between cyclotron and spectrograph. It was in 1976 that it was noticed that the spectrograph BIG KARL had the built in feature of a variable dispersion. Since the first operation of BIG KARL at the beginning of 1979 this feature turned out to be most valuable for the different experiments in the spectrum between high resolution and large momentum range requirements.

To discuss the present situation and future modifications, we have to know that in first order ion optics a transfer matrix R_{ij} of an ion optical system transforms the coordinates of an incoming trajectory denoted o into the coordinates of the corresponding outgoing trajectory denoted 1 in the following way

$$\begin{pmatrix} x \\ \theta \\ y \\ \phi \\ \ell \\ \delta \end{pmatrix}_1 = R_{ij} \begin{pmatrix} x \\ \theta \\ y \\ \phi \\ \ell \\ \delta \end{pmatrix}_o \qquad (1)$$

x, θ and y, φ are the spatial coordinates of a trajectory. ℓ represents the longitudinal and $\delta = \Delta p/p$ the momentum deviation of the corresponding particle with respect to the reference particle.

If we now consider the transfer matrices for the present dispersive and single achromatic modes in the positions (1) and (3) of table 1, respectively, same drawbacks become evident. There are many off-diagonal element which are non zero (besides the coefficient $R_{16} = D$ as desired in the dispersive mode). This fact transfers more non avoidable fluctuations of the cyclotron beam than in case they are zero. Since any coefficient R_{ij} and its derivative shows up in the formulas for the second and higher order aberration coefficients[4] this might result in more second and even higher order effects, especially if the system is not tuned as perfect as possible to first and second order as it happens in real life. Especially the non zero angular dispersion R_{26} causes a change of the horizontal beam envelope in the subsequent system with any change of the momentum. For the main matching requirement the dispersion at the target must be

$$D_B = -(D/M)_S \qquad (2)$$

where B denotes for beam line and S for spectrograph. $(D/M)_S$ is variable typically between 0 and 20 cm/%. To cope with this situation there are only 3 constant $(D/M)_B$-values available from the double monochromator 0, 11 and 32 cm/% where only the last value is connected with a clear momentum analysis by slits. Referring to equation (2) this means that the subsequent beam line has to supply a magnification variable in a wide range at the target. This has turned out to be cumbersome with respect to beam line tuning and also disadvantageous since the size and divergence of the monochromatic beam changes at the target.

Clearly, the design aim for a modification of the double monochromator should be to supply a variable (D/M)-value with a clear momentum analysis by slits and a transfer matrix which has all unwanted off diagonal elements as zero or as small as possible and the diagonal elements staying constant and unity. The latter would mean that the ion optics of any subsequent system between double monochromator and target have not to be changed in case of dispersion matching with different dispersions at the target.

	MODE	TRANSFER MATRIX						BEAM SIZE
1	DISPERSIVE DS1→DS2 PRESENT	1.05312 13.42805 0.00000 -0.00002 -20.10275 0.0	-0.00010 0.94833 0.00000 -0.00000 -3.02924 0.0	-0.00000 0.00000 -0.83079 16.23738 -0.00001 0.0	-0.00000 -0.00000 -0.01076 -0.99340 0.00000 0.0	0.0 0.0 0.0 0.0 1.00000 0.0	-31.92091 -216.12692 0.00001 0.00008 52.33487 1.00000	0.168 CM 12.141 MR 0.154 CM 4.566 MR 38.582 CM 0.005 PC
2	DISPERSIVE DAS1→DAS2 MODIFIED	1.00000 -0.00000 -0.00000 -0.00001 0.00000 0.0	0.00000 1.00000 0.00000 -0.00000 -1.45405 0.0	-0.00000 0.00001 -1.00000 -0.00008 -0.00000 0.0	-0.00000 -0.00000 0.00000 -1.00000 0.00000 0.0	0.0 0.0 0.0 0.0 1.00000 0.0	-14.54050 0.00002 0.00002 0.00009 -2.99886 1.00000	0.088 CM 12.732 MR 0.180 CM 3.531 MR 18.513 CM 0.005 PC
3	ACHROMATIC AS1→AS2 PRESENT	-0.97784 11.58220 0.00000 -0.00001 -11.26133 0.0	0.00000 -1.02267 -0.00000 0.00000 0.00945 0.0	-0.00000 -0.00000 -0.21489 -2.78434 -0.00000 0.0	0.00000 -0.00000 0.34525 -0.18008 0.00000 0.0	0.0 0.0 0.0 0.0 1.00000 0.0	-0.09236 -114.07195 -0.00001 0.00009 52.33487 1.00000	0.159 CM 9.631 MR 0.680 CM 0.971 MR 4.331 CM 0.075 PC
4	ACHROMATIC DAS1→DAS2 MODIFIED	1.00003 27.82735 0.00001 0.00002 -0.00003 0.0	0.00000 1.00003 0.00000 0.00000 -0.00000 0.0	0.00000 0.00001 -1.00000 0.00000 -0.00000 0.0	-0.00000 -0.00000 -0.00000 -1.00000 -0.00000 0.0	0.0 0.0 0.0 0.0 1.00000 0.0	-0.00002 -0.00027 0.00000 -0.00003 -2.99882 1.00000	0.050 CM 12.808 MR 0.180 CM 3.531 MR 0.225 CM 0.075 PC

Table 1: Transfer matrices and half beam size for the present and a modified double monochromator working in dispersive and achromatic mode.

To come to a much more favourable solution, which requires minimum effort, in each half of the double monochromator any component has been arranged completely mirror symmetric with respect to the center of the bending magnet AM (see fig. 1, lower part). 2 quadrupole doublets have been incorporated. The location of the optical axis for the incoming and outgoing beam of the double monochromator was left unchanged. With only two quadrupole parameters being varied (AQ11 = AQ14 = AQ24 = AQ21 and AQ12 = AQ13 = AQ23 = AQ22) the solutions for a dispersive and a double achromatic mode as displayed in position (2) and (4) of table 1 have been worked out using the code TRANSPORT[5]. At least 3 other not as favourable dispersive or achromatic solutions using other optical mode combinations in half the system have been found for again 2 free parameters. They could be used to check out the ion optics of the system with the beam. Starting with the ideal solution in the dispersive case, which delivers a very convenient (D/M)-value of 14.9 cm/% momentum, the (D/M)-value can be varied between 13 and 26 cm/% by releasing 3 parameters: AQ11=AQ21, AQ13 = AQ23 and AQ14=AQ24. In the described range of D/M-values the nondesired off diagonal elements stay at very reasonably low values. The vertical beam size is below 24 mm in the magnets AM for all above discussed cases.

With respect to a hardware solution the calculation already used the parameters of the air cooled quadrupole doublets most abundant at the cyclotron which turned out to be almost sufficient. 3 doublets of this type are found for instance in the beam line between the double monochromator and the spectrograph which should be interchanged by larger aperture doublets to enhance the transmitted momentum bin.

References

1) J. Reich, C. Mayer-Böricke, S. Martin, K.L. Brown, F.E. Johnson, Proc. 6th Int. Cycl. Conf. (Vancouver, 1972) p. 401

2) A. Abdel-Gawad, A. Hardt, S. Martin, J. Reich, K.L. Brown, K. Halbach, Proc. of the 5th Int. Conf. on Magnet Technology (Rome, 1975) p.

3) J. Reich, S. Martin, D. Protić, G. Riepe, Proc. 7th Int. Conf. on Cyclotrons and their Applications (Zürich, 1975) p. 235

4) K.L. Brown, Proc. of the 3rd Int. Conf. on Magnet Technology (Hamburg, 1970) p. 348

5) K.L. Brown, D.C. Carey, Ch. Iselin, F. Rothacker, Report CERN 80-04, March 1980

7.6. Design of a RF-Center Region for Multiharmonic Mode Operation

L. Aldea, J. Reich, P. Wucherer

Our users developed a strong demand for energies outside the present operating range of 22.5 to 45 MeV/A. Especially, an extension from 22.5 down to 6 MeV/A is desired for nuclear spectroscopy experiments. This demand could in principle be met by providing a multiharmonic mode of operation at a somewhat extended frequency range. One solution to this, presently in discussion, would mean to decouple the three Dees, drive them separately and to provide a 120^{o} phase shift between every two Dees. The technical problems related to the multimode operation have not been investigated in detail so far. Nevertheless, the initial solutions to the necessary RF-center modification for h=5 and h=2 harmonic operation have been investigated. The h=5 mode is necessary to provide lower energies. At the same time it would extend the range of charge to mass ratios Q/A of ions, which can be accelerated, from 1/3 at present down to 1/6, a most favourable circumstance for the acceleration of heavier ions as in progress with the project ISIS[1]. The h=2 mode would push the H^{+} and $^{3}He^{2+}$ beam energies towards the focusing or the bending limit, respectively. The focusing limit in the smooth approximation for ν_z=0 is E/A≈100 MeV/A, while the bending limit is given by $E/A=180(Q/A)^2$ MeV/A for JULIC.

The method of calculation and the fitting procedure were as already described[2,3] except that an appropriate 120^{o}-phase shift was applied between every two Dees. The basic philosophy in the design was to reach as early as possible nearly scaled orbits referring to the h=3 mode and to use the same inflector. Table 1 compares the essential parameters and results for the h=2,3 and 5 harmonic modes. The phase width $\Delta\phi_o$ at the inflector exit was held constant assuming constant efficiency of the beam line buncher system. The resulting starting phase ϕ_o for h=2 and h=5 is larger (particles start later) and therefore the bunching effect (phase compression) of the first gaps is weaker and consequently the phase width, $\Delta\phi$, after the 25th gap is larger.

Parameter	Type	h = 2	h = 3	h = 5
R_{out} (cm)	free	2.6	3.2	4.3
R_{in} (cm)	result	1.7	2.1	2.5
$\phi_o(^{o}RF)$	free	-74	-103	-95
$\Delta\phi_o(^{o}RF)$	fixed	40	40	40
$\Delta\phi(^{o}RF)$	result	32	10	20
Ac(cm)	result	0.04	0.03	0.05
Ai(cm)	result	0.27	0.26	0.32

Table 1: Essential parameters and results for different harmonic modes. R_{out} radius where beam leaves the inflector; R_{in} radius where beam enters the inflector (axis of vertical beam line); ϕ_o starting phase, $\Delta\phi_o$ starting phase width, $\Delta\phi$ resulting phase width after the 25th gap; Ac, Ai coherent and incoherent beam amplitude calculated for the 4th revolution.

Even allowing for bad centering in the fit the position (compare R_{out} in table 1) where the beam leaves the inflector could not be held constant for the different modes. Consequently, the location of the axis of the vertical beam line also changes (compare R_{in} in Table 1).

Figure 1 shows the beam envelopes in the median plane up to the 3rd gap for the three different harmonic modes.

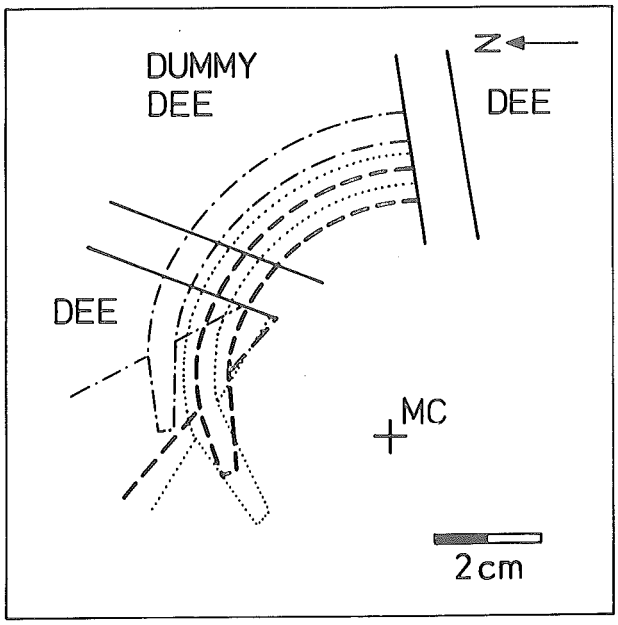

Figure 1: Beam envelopes up to the 3rd gap starting at the inflector exit together with the varying first gap geometry for different harmonic modes (..... h = 2, --- h = 3, -·- h = 5). MC = machine center.

Each beam envelope results from the calculation of 27 orbits starting with 3 different RF-phases at 9 different locations in the horizontal beam emittance (see ref. 3 for more details).

The figure demonstrates that with respect to the RF-center region only a kind of puller change would be necessary for a mode change, whereas a complete interchange of the yoke insert would be necessary for the beam line prior to inflection.

References

1) H. Beuscher, C. Mayer-Böricke, J. Reich, chapter 7.7. of this report, p.

2) L. Aldea, P. Wucherer, IKP Annual Report 1980, Jül-Spez-99 (1981) 156

3) L. Aldea, J. Reich, P. Wucherer, Proc. 9th Int. Conf. on Cyclotrons and their Applications (Caen 1981), in press

7.7. Status of ISIS

H. Beuscher, C. Mayer-Böricke and J. Reich

The project ISIS[1] (Injektion schwerer Ionen nach EZR-Stripping: Injection of heavy ions after ECR-stripping) was finally approved by the associates of KFA in November 1981 after a detailed project description[2] was turned in in spring. Therefore the superconducting magnet structure of the ECR-source[3] could be ordered in January 1982. The chosen bidder had worked out a precise study in close cooperation with the IKP which determined the final parameters of the magnet system.

A small and inexpensive ECR-plasma device for 2.45 GHz has been hooked up and has turned out already to be valuable to learn the techniques associated with microwaves, plasma formation, and beam extraction (see chapter 7.8).

For the beam handling and axial injection system[4] a special magnetic lense which shall substitute the einzel lense in front of the hyperboloid inflector has been designed (see chapter 7.9) as well as the different types of solenoids in the horizontal and vertical beam line. The insert carrying the vertical beam line is under mechanical design. A preliminary study of the beam behaviour in the strong fringe field of the ECR-source has been made.

For the design of the RF-center region[5] detailed numerical orbit calculations have been finalized (see chapter 7.10). They used electrical field distributions resulting from three dimensional relaxation calculations. The results ascertain the beam behaviour derived in an analytic orbit calculation procedure, especially the proper axial focussing, during the first gap transitions.

References

1) L. Aldea, R.K. Bhandari, H. Beuscher, H.G. Mathews, C. Mayer-Böricke, J. Reich, P. Wucherer, Frühjahrstagung der DPG, Sektion Kernphysik, Hamburg, März 1981

2) Erläuterungsbericht und Planungsunterlagen zum Projekt ISIS, März 1981

3) H. Beuscher, G.H. Mathews, C. Mayer-Böricke, J. Reich, Proc. 9th Int. Conf. on Cyclotrons and their Applications (Caen, 1981) in press

4) R.K. Bhandari, J. Reich, Proc. 9th Int. Conf. on Cyclotrons and their Applications (Caen, 1981) in press

5) L. Aldea, J. Reich, P. Wucherer, Proc. 9th Int. Conf. on Cyclotrons and their Applications (Caen, 1981) in press

7.8. An ECR-Plasma Device at 2.45 GHz for Test Purposes

H.-G. Mathews, H. Beuscher, R. Fiedler

Since the beginning of 1980 an ECR (Electron Cyclotron Resonance) source for fully stripped heavy ions for JULIC is under development. Parallel to the design and construction work for the ISIS ECR source[1] a small and fairly cheap version of an ECR source was set up during 1981. The reason for this PRE-ISIS-Source was to get some experience in microwave techniques, creation and diagnostics of an ECR-plasma, and the extraction of multiple charged ions from a plasma surface. In May 1981 the first ECR-plasma could be created in a magnetic mirror field of about 0.1 Tesla by microwave injection at 2.45 GHz. The installation of a permanent hexapole magnet between the two mirror coils completed the magnetic bottle structure for a hot ECR-plasma stage in July of the year. Fig. 1 shows a photo of the plasma confined by the B-minimum field between the hexapol bars in the center of the vacuum chamber.

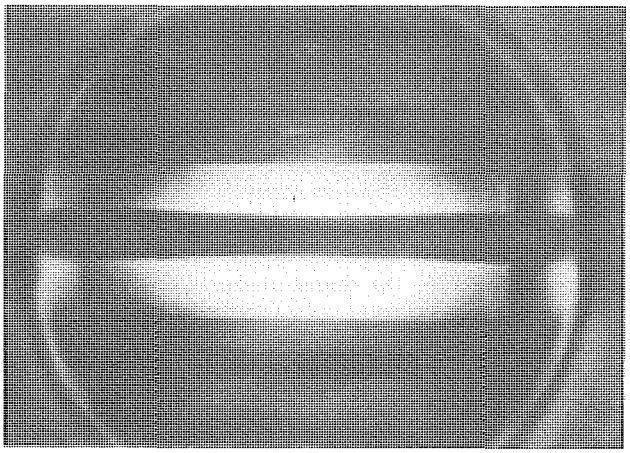

Figure 1: Photograph of the confined ECR-plasma partly masked by one of the hexapole bars.

A schematic drawing of the whole source is given in fig. 2 together with the magnetic field along the source axis (z-axis). The radial field shape of the permanent hexapole and the superimposed hexapole and mirror field at z=0 are also shown in fig. 2. The magnetic mirror field is generated by two solenoids made of watercooled copper pipes, normally run with a current density of 10-12 A mm^{-2}. The maximum field is about 1.3 kGauß. The mirror ratio is variable from 1.3 to 1.7 by changing the distance between the two coils. The hexapole magnet consists of six quadratic copper profiles filled with oxid ceramic magnet pieces of 10x10x5 mm size. Each hexapole bar has a cross section of 11x11 mm and a length of 15 cm. The inner diameter of the hexapole is 5 cm with a pole tip field of 1.36 kGauß. The hexapole is mounted inside the vacuum chamber of the source. Because of the good vacuum properties and heat stability of the magnet pieces there was no need for capsulating or extra cooling. The microwaves are

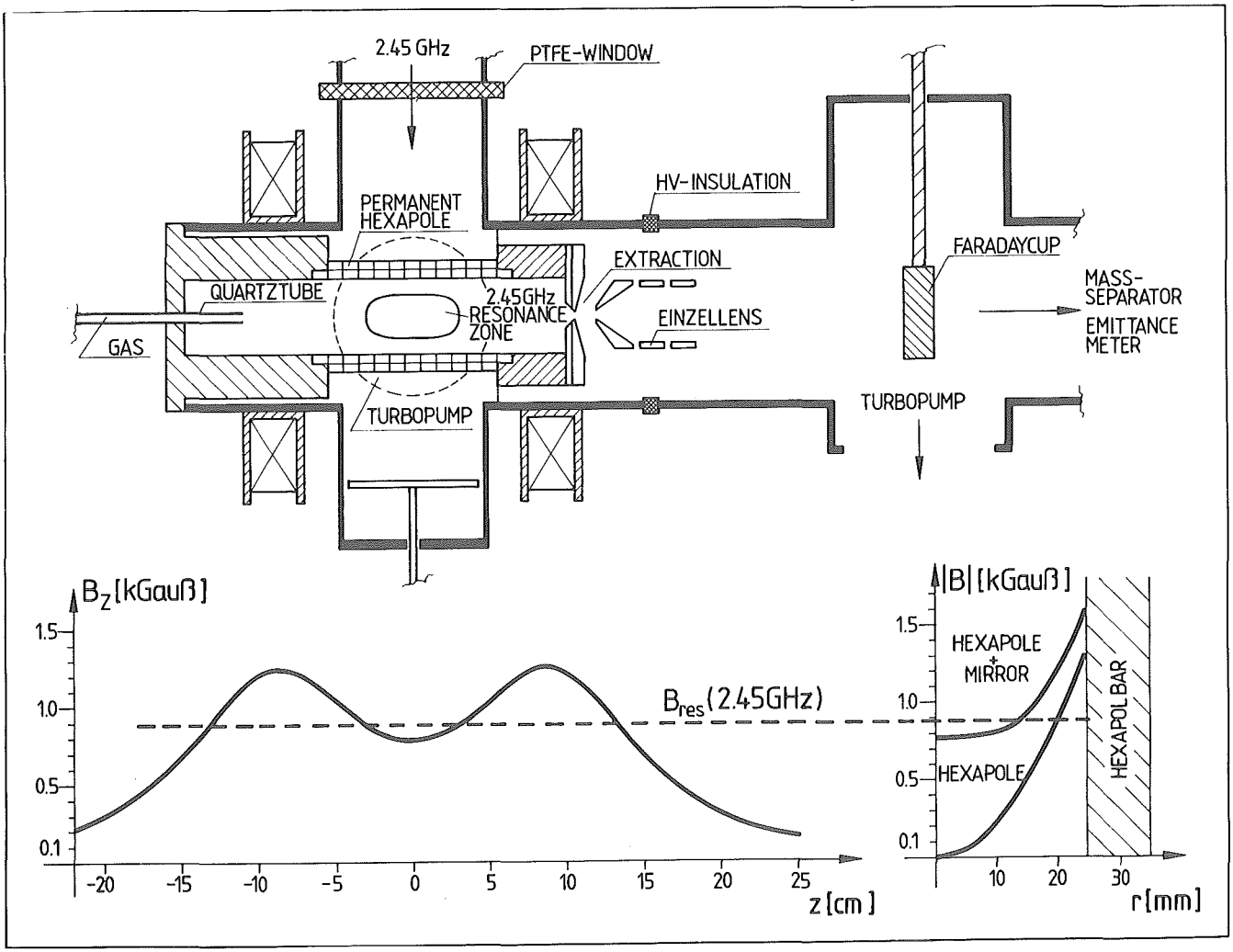

Figure 2: Schematic drawing of the source including the axial and radial magnetic field distribution.

injected through a PTFE-window in a direction perpendicular to the source axis. The microwave frequency is 2.45 GHz, being delivered by a 500 W magnetron; the corresponding magnetic field for ECR is 875 Gauß. The plasma chamber is pumped by a 360 l/s turbomolecular pump to some 10^{-6} Torr, while the region of the ion extraction system is pumped by another turbo pump having a pumping speed of 120 l/s. The gas flow into the source is typically between 3 and 10 cm^3 per hour. For ion extraction from the source, the plasma chamber can be put to 5 kV. The extraction system consists of two electrodes with Pierce geometry. The extraction bore is 6 mm in diameter. The beam leaving the source can either be measured on a faraday cup or - after momentum separation in a 45^0-dipole magnet - on a wire 2 mm in diameter at a distance of 1.34 m from the source exit.

Fig. 3 gives a typical spectrum of nitrogen ions at 4.3 kV extraction voltage. Charge states up to N^{5+} have

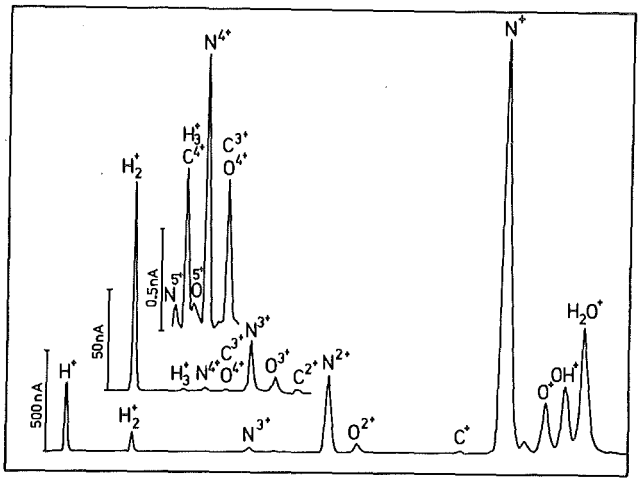

Figure 3: Spectrum of ions extracted from an N_2-ECR-plasma.

been observed. The transmission of the beam line has been measured for $^3He^+$ at 4.3 keV to be 15 %. Under the assumption of constant transmission for every mass and charge state, the ion charge states noted in table 1 have been

Z	1^+	2^+	3^+	4^+	5^+	6^+	7^+	8^+
^1H	30000	-	H_2^+: 170 µA		-	H_3^+: 14,5 µA		-
^2H	16400	-	-	-	-	-	-	-
^3He	61500	1300	-	-	-	-	-	-
^{14}N	13500	2500	160	12	0.8	-	-	-
^{40}Ar	8200	9800	3830	970	285	35	4	0.7

Table 1: Ion currents in nA extracted at 4.3 kV.

extracted with the given intensities at 4.3 kV extraction voltage.

The intensities for protons, deuterons, ^3He and α-particles encourage to use the device not only for test purposes but also as an external light ion source for the cyclotron after some further upgrading (i.e. better vacuum, bigger extraction hole, higher extraction voltage).

With a net power of 30-50 W and a vacuum pressure of about $8 \cdot 10^{-6}$ Torr the source works best for higher charge states. With increasing microwave power the plasma contracts and x-rays are emitted through the 4 mm steel walls of the vacuum chamber. Fig. 4 shows two x-ray-spectra measured with

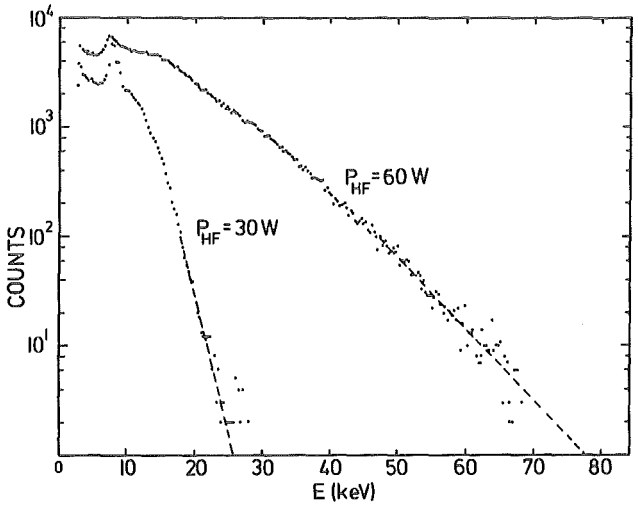

Figure 4: Two X-ray spectra emitted from the ECR-plasma for different microwave-power absorption. The spectra are not corrected for the detector efficiency and the absorption in the material in front of the detector.

a Si(Li)-detector through a 2 mm plastic window in the plasma chamber. As can be seen from the x-ray-spectra the energy of the plasma electrons strongly increases with the microwave power. But it has turned out, that the intensities of higher charge states decreased remarkably when increasing the microwave power much above 30 W in this case. The decrease is mainly due to the reduced ionization cross sections at high electron energies.

The emittance of the total nitrogen beam from the source was measured with a slit-wire system at 47 cm behind the extraction hole. With a total current of 45 µA 90 % of the ions were found within a phase space of $\varepsilon = 0.96 \pm 0.28\ \pi$ cm rad $eV^{1/2}$ (see fig. 5). Emittance

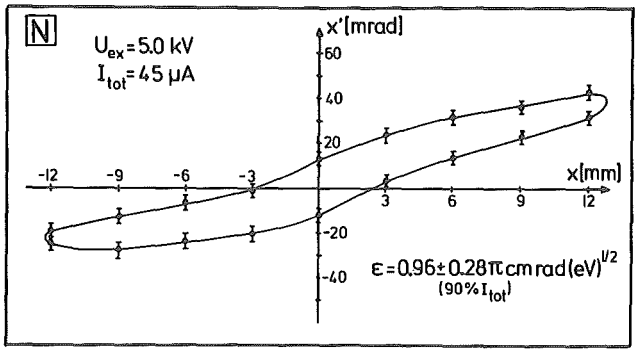

Figure 5: Emittance of the source.

measurements will be further continued with the different charge states after momentum separation.

In 1982 it is planned to test the source with double ECR frequency and magnetic field. An injector stage for the source is under construction.

Thanks to the Bonn cyclotron crew, i.e. K. Euler and H.D. Rosendaal for their support concerning the emittance meter and dipole magnet.

Reference

1) H. Beuscher, H.-G. Mathews, J. Reich, IKP-Annual Report 1980, Jül-Spez-99 (1981) 152

7.9. Design of a Magnetic Lens for ISIS

R.K. Bhandari

The axial injection system[1] for the project ISIS at JULIC utilizes a hyperboloid type inflector[2] in order to inflect the ions into the median plane of the cyclotron. If the trajectories are traced back from the exit of the inflector for $\nu_r = 1$ and an emittance of $160 \cdot \pi$ mm mrad it is seen that a divergent beam emerges out with a divergence of, as much as, $\sim$ 100 mrad. In order to accommodate such a beam in the axial hole it is evident that a strongly focussing lens should be placed as close as possible to the inflector. It turns out that this lens has to be a compact device. Therefore, we have chosen to use a spherical lens. The electrostatic einzel lenses, specially at this location, should be avoided because of their expected unstable operation due to penning discharge. We have, hence, decided to use a magnetic 'electron type' lens. The magnetic lenses introduce rotation of the beam which, however, can be taken care of easily[1]. Their operation is much more reliable.

Figure 1 shows the sketch of a usual symmetrical magnetic lens. A lens in the axial hole of the cyclotron should be

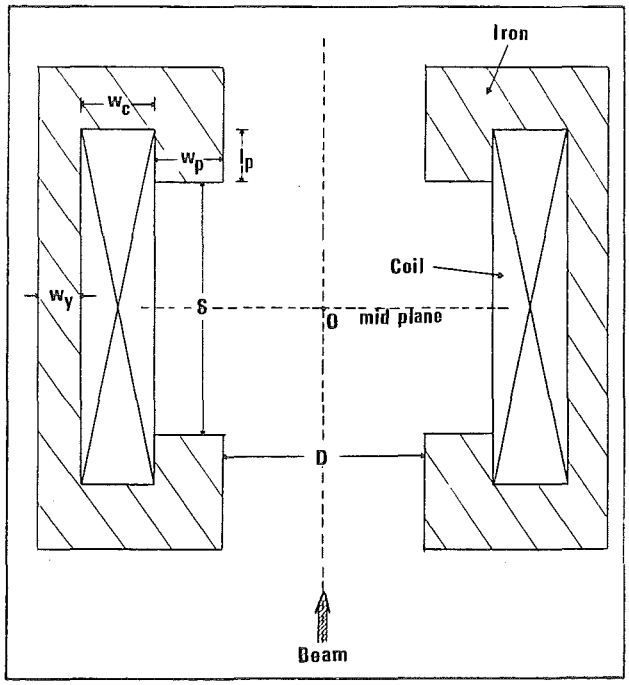

Figure 1: Sketch of the magnetic lens.

made very compact in the lateral direction in order to keep sufficient space for off-centering as it is requested by the center region design[3] and control and services connections etc. The bore size should be kept maximum in order to accommodate the beam which has a diameter of $\sim$ 4 cm in this region as well as for maximum pumping speed. The number of ampere-turns should be minimized and induction level in the iron must remain below the saturation level. For low spherical and chromatic aberration coefficients, the S/D ratio (fig. 1) is required to be large[4]. At the same time the lens cannot be made very large longitudinally as it has been pointed out already.

The design procedure has been worked out using Glaser and unsaturated symmetrical lens formulations[4]. Empirical formulae[5] have also been used. Keeping in mind the requirements and considerations mentioned in the above paragraph, POISSON code[6] has been used to work out an optimum design. The demand for a large S/D-ratio could not be realized. The detailed procedure and some examples are presented in an internal report[7]. For the optimum solution the parameters of the lens are: S=D=6 cm, ω_p=2 cm, ω_y=1.1 cm, ℓ_p=1.62 cm. The maximum field is $\sim$ 5.4 kGaus for 32,000 A-turns corresponding to a current density of 23.7 A/mm^2 in the directly water-cooled copper conductor (power dissipation $\sim$ 5.7 kW). At this excitation level the lens has a focal length of $\sim$ 16.5 cm for a 15 keV deuteron beam (taking into account possible future improvements of the cyclotron with higher injection energies than 9 keV).

Further investigations are necessary concerning the abberation errors. A modification of the pole face geometry[8] seems to solve this aperture problem.

References

1) R.K. Bhandari, J. Reich, Proc. 9th Int. Conf. on Cyclotrons and their Applications (Caen, 1981) in press

2) R.W. Müller, Nucl. Instr. & Meth. 54 (1967) 29

3) L. Aldea, J. Reich, P. Wucherer, Proc. 9th Int. Conf. on Cyclotrons and their Applications (Caen, 1981) in press

4) A.B. Al-Kareh and J.C. J El-Kareh, Electron Beam Lenses and Optics, Academic Press 1970

5) C. Fert and P. Durandeau, Focussing of Charged Particles, Vol. 1, Ed. A Septier, Academic Press 1967, Ch. 2.3

6) R. Holsinger, POISSON Group Programs - User's Guide, CERN, April 1975

7) R.K. Bhandari, IKP, KFA, Internal Report ISIS 4/82

8) O.C. Dermois, KVI, Rijksuniversiteit Groningen (Netherlands) private communication

7.10. Check of the h=3 RF-Center Region Design by Numerical Calculation

L. Aldea, P. Wucherer

An optimized design of the center region for external injection, which is a substantial part of the project design of ISIS[1-3], has already been presented[3,4]. In this design an analytical solution of the horizontal particle motion in the median plane has been used. For these calculations the electrical fields have to be assumed to be homogenous within the accelerating gaps and the axial focusing is only guaranteed by the restriction to slightly positive phases after the second gap (in the center of each gap). Therefore, for the first two gaps more accurate calculations are necessary. They can only be obtained by numerical integration of the orbits using realistic electrical fields.

In our case these fields were calculated by the three-dimensional relaxation code RESEKT. This code has been linked to the orbit integration code RUKU but the elaborate input of the complicated JULIC dee geometry excludes a self-optimizing procedure[3,4]. To overcome this the puller geometry had to be modified. In a few steps the finally resulting field form was close to the one which originally was anticipated. Fig. 1 shows the dee

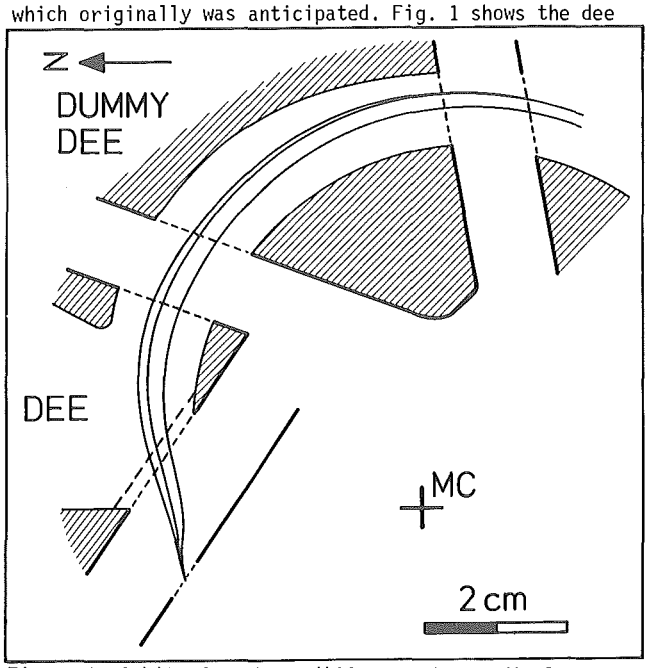

Figure 1: Orbits for three different phases displayed in the region of the first three accelerating gaps.

geometry and the orbits of 3 particles starting from the center of the horizontal emittance at three different starting phases in the region of the first three gaps. In the first gap the electrical field component perpendicular to the velocity vector in the horizontal plane is very strong. This results in a most valuable strong phase compression effect for a large emittance[3,4]. But inside the dee (puller) this component has to be zero to match the former calculations. The most effektive optimization step was therefore to avoid this component using an oper puller (see fig. 1) with an entrance and exit window instead of a solid piece with an appropriate channel for the beam.

Only for the first 3 gaps it is necessary to calculate the electric fields numerically. For gap number 3 and the higher gap numbers a gaussian distribution across the gap was used which proved to agree sufficiently well with the numerical calculations already at gap number 3.

The axial motion was integrated with three dimensional fields in the first two gaps obtained from the relaxation calculation. For the other gaps the z-distribution was develloped linearily as a function of z. Because of the strong axial focussing in the center region a vertical emittance corresponding to a rather large $\nu_z = 1/2$ was tried, which resulted in starting parameters of $z_{omax} = \pm 0.22$ cm and $z'_{omax} = \pm 73$ mrad for $\varepsilon_z = \pi \cdot 160$ mm mrad. The existing aperture of the dees and the dummy dees of ± 1.15 cm was not changed to avoid technical complications. The exit window of the inflector will be 0.5×0.5 cm^2 and the entrance height of the puller was chosen to be $\Delta_z = \pm 0.87$ cm. These geometrical parameters are sketched in figure 2 (upper part).

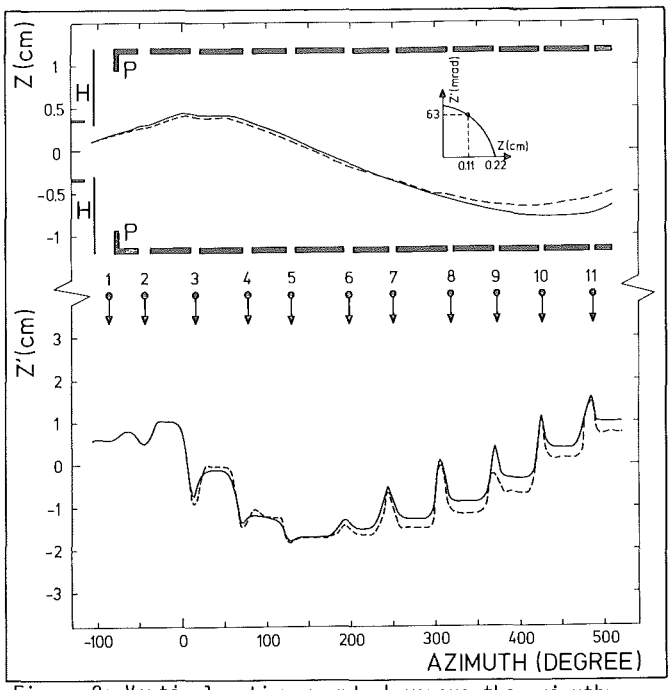

Figure 2: Vertical motion z and z' versus the azimuth; —— motion for a starting phase $\phi_0 = -85^o$, ----- for $\phi_0 = 125^o$, H - hyperboloid inflector, P-puller. The labels 1 to 11 refer to the centers of the gaps.

In the upper part of fig. 2 the aperture of the deflection plates of the hyperboloid inflector is given together with the accelerating gaps as well. Besides this geometrical discription of the accelerating structure the upper part of fig. 1 displays the vertical (z) motion for a particle with the same spatial starting coordinates but the two extreme starting phases. Spatially the particle starts in the center of the horizontal emittance and on the circumference of the vertical emittance (see inlet if fig. 2, upper part) for the worst case $z_0 = 0.11$ cm an $z'_0 = 63$ mrad. The vertical amplitude z keeps small in the first gaps but enlarges during the first two revolutions. A smaller ν_z describing the vertical emittance resulting in a smaller maximum divergence z'_{omax} will reduce the vertical amplitude during the first revolutions. The injection beam line can be tuned for any ν_z-value[2]

describing the vertical emittance at the exit of the hyperboloid inflector.

The lower part of fig. 2 shows the product of the vertical angle of the same above described particle and the instantaneous radius of curvature denoted as z' in cm. It clearly displays the action of the gaps, i.e. vertically focussing (z'-slope negative) and defocussing (z'-slope positive) at the gap entrance and exit, respectively. Because of the strong phase compression right at the beginning the phase dispersion of the vertical motion is very small and hardly to be seen in the upper and lower part of fig. 2. This fact excludes vertical slits for phase selection.

The main result of this investigation undertaken for the h=3 harmonic mode of acceleration: Essential beam losses due to the vertical motion in the cyclotron center region are not expected. But the antipated vertical emittance of $\varepsilon_z = \pi \cdot 160$ mm mrad at 5 keV/A is near to the acceptance of the center region with the present dee and dummy dee gap heights.

References

1) H. Beuscher, H.G. Mathews, C. Mayer-Böricke, J. Reich, Proc. 9th Int. Conf. on Cyclotrons and their Applications (Caen, 1981) in press
2) R.K. Bhandari, J. Reich, Proc. 9th Int. Conf. on Cyclotrons and their Applications (Caen, 1981) in press
3) L. Aldea, J. Reich, P. Wucherer, Proc. 9th Int. Conf. on Cyclotrons and their Applications (Caen, 1981) in press
4) L. Aldea, P. Wucherer, IKP-Annual Report 1980, JÜl-Spez.-99 (Februar 1981) 156

8. BIG KARL

8.1. The Magnet Spectrometer BIG KARL

G.P.A. Berg, U. Hacker, W. Huerlimann, I. Katayama M. Koehler**, S.A. Martin, J. Meissburger, J.G.M. Roemer, M. Rogge, T. Sagefka, O.W.B. Schult, B. Styczen***, J. Tain*

Spectrometer Operation:

The Spectrometer BIG KARL has been used during the last period to perform different experiments studying

- the spin flip reaction to 1+ states in 48Ca and 58Ni,
- the reaction 209Bi (d, 3He) 208 Pb at 45 MeV,
- the inelastic alpha scattering at very forward angles to study giant resonances in 208Pb,
- the (p,t)-reaction on 143, 145Nd and 208Pb,
- the (p,d)-reaction on 109Ag, 143Nd, 208Pb, and 151Eu,
- the electron capture process using the reaction ($3He^{++}$,$3He^{+}$) at 68 and 130 MeV,
- the reaction 62Ni (d,3He) to investigate the structure of 61Ni,
- the 144Sm(3He,d) 145Eu reaction,
- the in-beam alpha radioactivity of actinides for alpha energies above 5 MeV.

The data acquisition system MEMPHIS (Modular Experiment Multiparameter Puls Height Instrumentation System) in connection with a VAX-11/780 computer is in full operation now. Recent experiments are done using 6 ADC's and event rates of up to 20 000 events/sec (64bit/event).

Spectrometer Development:

Two types of window free gas jet targets have been developed to perform the electron capture experiments using a target thickness of less than 1 microgram per cm^2.

A septum magnet based on permanent magnets has been designed (see fig.2). It is planned to use such a magnet for bending the primary beam out of the scattering chamber.

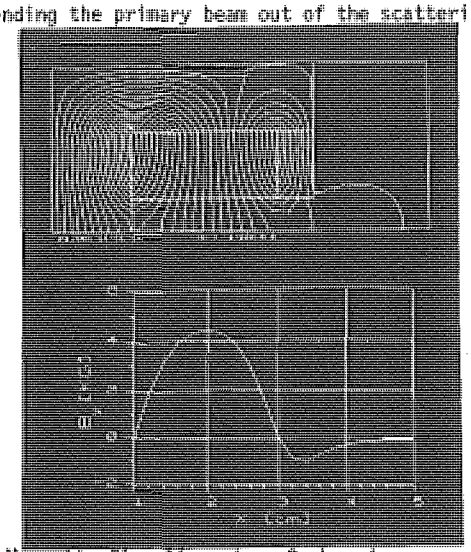

Fig.2: Magnetic flux lines in a C-shaped permanent magnet (RCO) and the magnetic field in the midplane of the septum magnet

A new gas control system was built. It allows to use the MWPC (Multi Wire Proportional Chamber) at constant gas pressures between 50 and 2000 mbar with a constant gas flow of about 36 l/h. The variable gas pressure allows to optimize the separation of the energy loss signals for different particle species in order to improve the particle identification at the focal plane of the spectrometer.

The new program BKARLO has been established to calculate the energy losses inside spectrometer and detectors and the light output of the plastic scintillators. An absolute scale of particle identification signals from the plastics is available. The use of the scintillator has been extended for timing up to a resolution of 0.6nsec.

Spectrograph Optimization Procedures:

In order to optimize the resolution and the solid angle of BIG KARL, the experimental ray-tracing method (1) has been improved with the help of a new interactive program "MATRIX". MATRIX determines the TRANSPORT matrix elements (i.e. aberrations) of the spectrograph of the desired order and optimizes the corresponding multipole strengthes which have to be generated by the H_t correction windings (2).

Furthermore, MATRIX allows to use for ray-tracing different lines of a reaction which shortens the optimization time and guarantees a constant resolution along the focal plane without the need to change magnetic fields.

As an example Fig.1 shows the second order aberration T122, which was minimized by using the H_t windings of dipole D1.

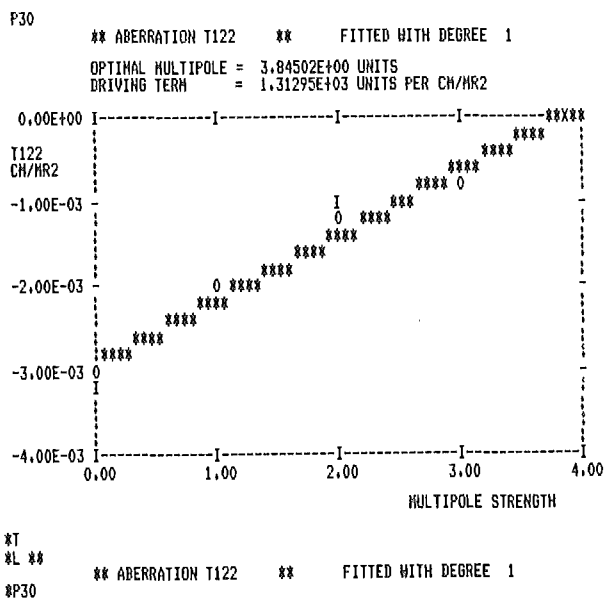

Fig.1: Second order aberration $T122=(x/\theta^2)$ as a function of the sextupole strength in dipole D1. Circles denote the experimental ray-tracing values which are fitted by a theoretical function (***) to determine the optimal sextupole strength (X).

Design Study for a Synchrotron with E-cooling:

A synchrotron has been designed which uses JULIC as injector. The synchrotron should boost the JULIC particle energies from 45 MeV/A up to 500 MeV/A. The synchrotron can run with a frequency between 0.1 and 10 Hz. It is plannedto use electron cooling and an internal target as well as an external beam with an emittance of less than 0.1 mm*mrad.

References:

(1) Annual Report 1979, p. 146

(2) Juel Report No. 1329 (1976), Juel Spez Report No. 104 (1981)

*Permanent address: RCNP, Osaka University, Japan

**Zentrallabor für Elektronik, KFA

***Permanent address: Jagiellonian University Cracow, Poland

8.2. Reduction of Background and Improvement of Resolution by Use of Time and Angle Information of Particles detected in BIG KARL

P. Decowski, C. Mayer-Böricke, H.P. Morsch, M. Rogge, L. Zemło

An attempt was made to improve the quality of spectra obtained in the focal plane of the Big Karl magnetic spectrograph. For this purpose correlations between the line shape and background in the spectrograph detection system on one side and various cyclotron and beam parameters on the other, were investigated. The reduction of background caused by scattering inside the spectrograph and the beam halo is very essential in inelastic scattering measurements at angles below 4 degrees[1].

The contribution of scattering from the walls may be reduced by rejection of particles passing the focal plane outside the normal angular range. For this purpose a simple position sensitive detector of resistive single wire type[2] was installed about 60 cm behind the Multiwire Proportional counter. In a first version a resolution of 6 mm was obtained. Improvement of performance is expected by changes of its geometry allowing for the use of more uniform and stronger electric fields.

The background particles from beam halo have a very different time of flight from the cyclotron to the end of the spectrograph as compared to "real" particles (see fig. 1).

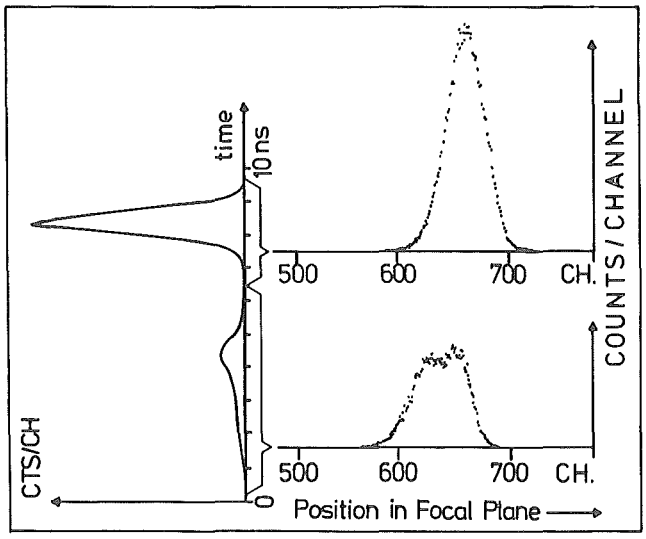

Figure 1: Dependence of the line shape in the focal plane of the Big Karl spectrograph on the time-of-flight. The dispersion of the magnet was 600 channels per percent energy.

Timing start signals were taken from both sides of a plastic scintillator[3] with a time resolution of about 0.6 nsec FWHM after reduction to the middle of the scintillator. The stop signals were derived from the zero-crossing of the RF of the cyclotron. An example for time spectra is given in Fig. 1 for ^{3}He particles of 68 MeV corresponding to a RF period of 46.8 nsec.

References

1) See contribution 1.12. in this report (H.P. Morsch et al.)

2) The detector was designed by A. Hardt, KFA Jülich and R.T. Kouzes, Princeton University

3) G.P.A. Berg, A. Hardt, W. Hürlimann, S.A. Martin, J. Meißburger, A. Retz and O.W.B. Schult, Annual Report 1979, IKP, KFA Jülich, Jül-Spez-72 (1980) 145

9. DETECTORS, TARGETS, SPECTROMETERS

9.1. Semiconductor Detectors

A. Hamacher, T. Künster, E. Lawin, H. Metz, K. Nicoll, D. Protić, G. Riepe

Like in the last years various detector systems were kept available for charged particle spectroscopy and particle discrimination in nuclear reaction experiments (IKP and visiting groups), among them 7 large cryostats for the 100 cm scattering chamber. They were equipped with side-entry Ge(Li) or HPGe detectors made by the detector laboratory. This routine work, consisting in checking detector parameters (also those of commercial Si ΔE detectors) and in regenerating or replacing radiation damaged detectors, could be reduced to some extent as compared to preceding years, since many experiments had been performed by the use of the magnet spectrometer.

For a special set-up a side-entry detector with a ΔE-E configuration in a single Ge(Li) and a HPGe diode was fabricated by cutting grooves into one contact side.

Two large area planar HPGe detectors, one of which a transmission type, with sensitive areas of 1400 mm^2 and thicknesses of 11 and 13 mm were prepared to be used as the two last detectors of a particle telescope, operated at 210 K.

For the use in a crystal spectrometer two planar HPGe detectors were made, one of which to serve as a monitor.

The existing cryostat designed for a multi-detector telescope was equipped with sets of one Si (400 μm thick) and several HPGe transmission type detectors and used for two experiments at HMI Berlin[1] and IPN Orsay[2]. For the first experiment 7 HPGe detectors with altogether 80 mm of Ge were mounted, for the second only 3 HPGe detectors with altogether 29 mm of Ge. In both cases an active collimator[3] made from HPGe with a central area of 6 mm diameter and a thickness of 2.3 mm was used to eliminate the effects of slit scattering.

While most of the essential problems concerned with the production of ion-implanted n^+-contacts in HPGe sustaining high electrical fields seem to have been solved, one still remains: The probability of obtaining a high quality contact decreases with increasing area. Since this effect seems to be due to incomplete cleaning prior to implantation, a plasma cleaning system (O_2 + CF_4) was installed inside a clean bench, which will be connected to the target chamber of the implantation system.

In connection with the development of various digitally position-sensitive detectors, problems concerned with the grooves between the stripes were investigated.

A simple procedure of masking resulted from an aluminium pattern obtained by evaporation through a grid of thin wires (≥ 50 μm). The investigation of photo-engraving techniques for masking was started. Ion-etching (Ar ion-source) combined with weak etching solutions have proven to be very reliable in realizing a depth of the groove needed for separation of adjacent contacts. It was found that the groove has to be etched much deeper than predicted from the doping profile.

Valuable information about the charge collection below a groove could be obtained by scanning across the groove with a collimated α-source.

A prototype of a XY position-sensitive HPGe detector with 8 stripes (each 1.6 mm wide with a spacing of 0.1 mm) on either side, with a thickness of 15 mm, is almost finished.

Detectors with position-sensitive structures, made according to these techniques, have found much interest (also by industrial companies) in various fields. A 4 mm thick Si(Li) detector, of which the ion-implanted entrance contact was divided into two halves, is now in use at the University of Bonn. To be used for a high energy physics experiment at CERN a side-entry HPGe detector is under construction in cooperation with a group of the INFN Milano and the TH Aachen. The thickness of this detector in beam-direction will be 4 mm, and one contact will be divided into 40 stripes of 50 μm width parallel to the entrance face.

Various types of Ge or Si detectors - among them many commercial ones - were regenerated or repaired.

Several improvements of the equipment could be achieved, like a larger vacuum chamber inside the magnet of the implantation system, to reduce the contribution of neutralized ions. A second cryostat for a multi-detector telescope (up to 100 mm Ge) is under construction. Additional computer programs have been obtained for automatically testing of detectors.

Guests from Brazil and China were trained in detector technology.

References

1) See contribution (Machner et al.) in this report
2) See contribution (Machner et al.) in this report
3) To be published in Proceedings of the 1981 International Symposium on Nuclear Radiation Detectors, March 81, Tokyo, Japan

9.2. Target Laboratory

J. Pfeiffer, G. Riepe

For the use in experiments (IKP and visiting groups) at the cyclotron, at the research reactor, and at niversity laboratories about 230 targets (with and without backing) were prepared from 32 different elements by the following techniques: vacuum deposition, rolling (mostly after reduction or melting) and eletrolytic plating. The thicknesses were ranging from 5 $\mu g/cm^2$ to 10 mg/cm^2, and the areas were between 30 to 500 mm^2.

A high percentage of these targets, especially those of large area and minor thickness, were prepared for experiments at the magnet spectrometer (BIG KARL).

9.3. Testproduction of an ^{26}Al-Target

L. Buchmann, H. Baumeister*, H.J. Probst and C. Rolfs**

Recent developments in the field of nuclear astrophysics made it desirable[1] to obtain an ^{26}Al target for measurement of the ^{26}Al destroying reaction $^{26}Al(p,\gamma)^{27}Si$. As ^{26}As is an astrophysically short living isotope ($T_{1/2} = 7.16 \times 10^5 y$), it must be produced artificially by a nuclear reaction. After the production, ^{26}Al must be separated from the target element. Hence, the target element should not be natural aluminium. For this and other reasons, the $^{26}Mg(p,n)^{26}Al$ reaction has been chosen for the production of ^{26}Al. For a minimum production of several μg ^{26}Al, a thick ^{26}Mg target had to be bombarded with high proton currents over a long running period without significant deterioration. The preparation of such a thick ^{26}Mg target (1.8 mm thick) is described elsewhere[2].

For optimal activation conditions as well as for interim storage of the target in an argon atmosphere, a special activation chamber (fig. 1) was constructed, where the

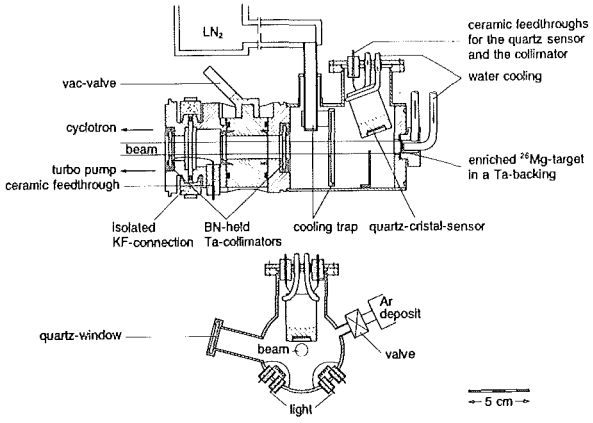

Fig. 1: Activation chamber for the production of ^{26}Al via the reaction $^{26}Mg(p,n)^{26}Al$.

target is directly watercooled. After the activation, the chamber was closed and filled with argon. The quartz-oscillator, the lamps and the window (fig. 1) were used to control the target during the course of activation.

The activation was carried out in July 1981 over a period of 5 days and at the position Bk1 of the Jülich cyclotron beam system with a proton energy of 25 MeV and a beam current of 20 μA on target. The main radioactivity was found to be ^{22}Na from the target and ^{56}Co from the target chamber (6 mC after two weeks, 2.5 mC after three months). The target chamber was transported to Münster in October 1981, the ^{26}Al was separated and could be transformed onto a Tantal-backing. The observed production yield of 20 ng ^{26}Al which is less than expected due to some technical problems is a sufficient basis for a new production planned in 1982.

References

1) R.A. Ward and W.A. Fowler, Astrophys. J. 238 (1980) 266

2) L. Buchmann and H. Baumeister, Jahresberichte 1979 und 1980, Institut für Kernphysik, Münster

*Institut für Kernphysik, Universität Münster

9.4. Measurement of Perturbed Angular Correlations at JOSEF

W. Borgs, J. Chatzipetros[+], *H. Lawin and K. Sistemich*

The gas-filled fission product separator JOSEF provides strong radioactive sources of neutron-rich nuclei far from stability. By measuring perturbed angular correlations[1,2] the magnetic moments of excited states can be determined. Applying the magnetic field of a conventional electromagnet (3 T) the g-factor of the first excited 2^+-state in ^{100}Zr was measured[3]. Based on the experience of this experiment an improved set-up was designed. The use of a superconducting split-coil magnet producing a much higher field should extend the possibility of measurements.

Fig. 1 gives an overall view of the apparatus. The separated fission products are transferred by an air-jet to a tape transport system irradiating a spot of 10 mm diameter. The tape is operated discontinuously and transports the implanted products to the counting position between the pole tips of the magnet, where the angular γ,γ-correlation is measured for 'field up' and 'field down' direction.

The new tape transport device was constructed based on a system which is in use[4]. An endless tape is applied. It covers the transport distance of 17 cm within a shortest transport time of 0.1 s. The acceleration, deacceleration and positioning of the tape is achieved by means of a mechanical drive using a Malteser cross gear.

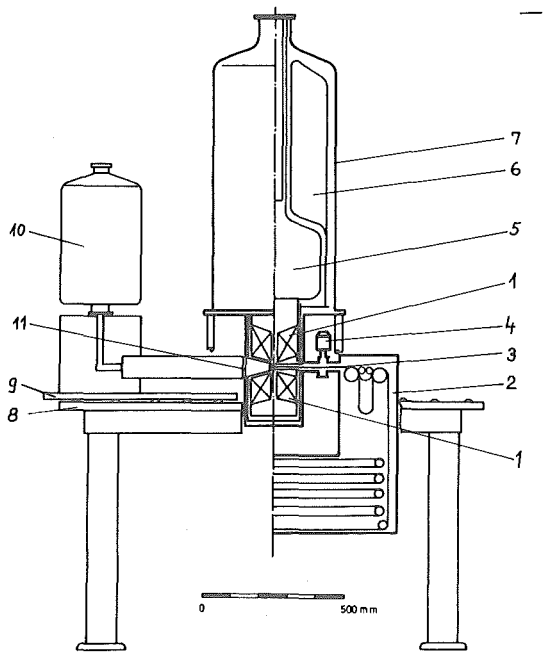

Fig. 1: Set-up for perturbed angular correlation measurements at JOSEF

The two halves of the split-coil magnet are assembled on a stainless steel form which is an integral part of the cryostat liquid helium vessel. Supports to withstand the compressive stresses are arranged such that maximum solid angles for radiation detection are achieved. Two equal sectors of 105^o (see fig. 2) give access to the sample in the median plane. By superconducting coils from NbTi a field of 6.5 T is produced. It can be increased by using iron pole pieces installed in the magnet bore above and below the midplane. The field homogeneity is at least 1.5 % in a sphere of 10 mm diameter.

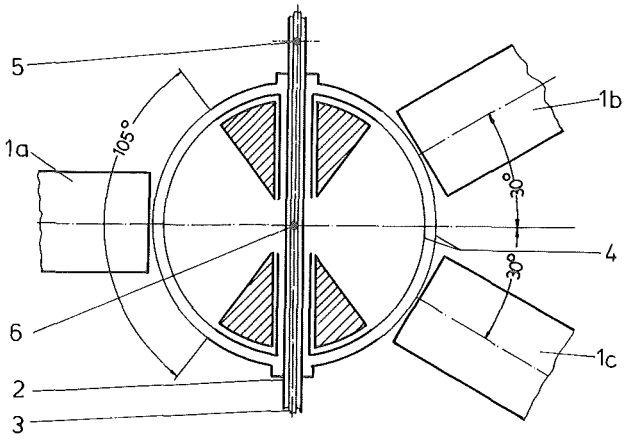

Fig. 2: Horizontal cut through the centre showing source-detector geometry

The cryostat is a conventional low temperature dewar with 77^o K and 4^o K shields. The channel for the moving tape in the midplane of the magnet is affixed to the outer cryostat jacket. It contains as temperature shielding multiple layers of aluminized mylar sheets (super-insulation).

An adjustable support for the apparatus was designed such that the transmission of vibrations into the cryostat system is minimized.

[+] Engineering and Workshop Centre of the KFA

References

1) E. Karlsson, E. Matthias, K. Siegbahn: Perturbed Angular Correlations North-Holland Publishing Company (1964)

2) H. v. Krugten, B. v. Nooijen: Angular Correlations in Nuclear Disintegration, Rotterdam University Press (1971)

3) A. Wolf, B. Battistuzzi, K. Kawade, H. Lawin and K. Sistemich, Phys. Lett. 97B, 2 (1980) 195

4) J. Eidens, E. Roeckl and P. Armbruster, Nucl. Phys. A141 (1970) 289

9.5. Superconducting Solenoid

A. Ercan, I. Katayama, M. Zupancic, A. Retz, U. Rindfleisch, Y. Nagai, P. Kleinheinz

The magnetic electron spectrometer have been widely used for in beam studies of nuclear structure. Superconducting magnetic lenses combined with high resolution Si-Li detectors present a modern tool to measure the medium to high energy conversion electrons. We have started the preparations for in beam installation of such a NbTi superconducting solenoid[+], which can produce up to 2 Tesla axial magnetic field having alternative field profiles as shown in fig. 1. The field calculations has been performed by using the program code LASL[1].

The magnetic field measurements using the calibrated Hall-probes have been carried out.

Different shapes of magnetic field are needed for different modes of operation: lens mode and transporter mode. In order to set up the buffle system for the lens mode, the electron trajectories in different type of magnetic field configurations have been computed by using the modified program code TURTLE[2]. Some results are shown in fig. 2.

An elementary but important step for the operation of magnet is the cooling the system down to 4.2° K. To optimize the required time and Helium consumption, several cooling procedures have been tried. One typical example is shown in fig. 3, where one can see it needs about

[+] Production of Cyrogenic Company

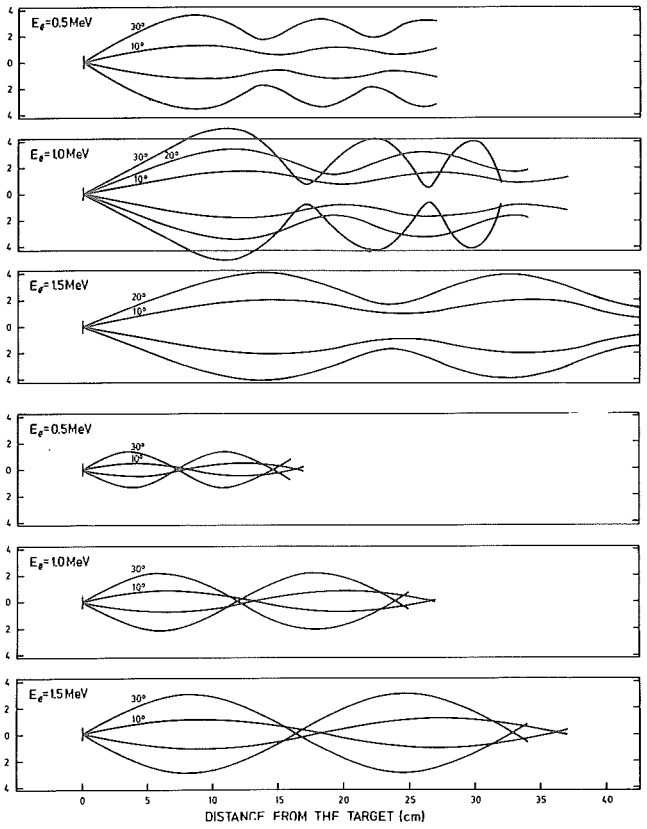

Fig. 2: Electron paths projected on (r,z) plane for different electron energies and for different take off angles: The upper 3 in the field (B) and the lower 3 in the field (C) of fig. 1.

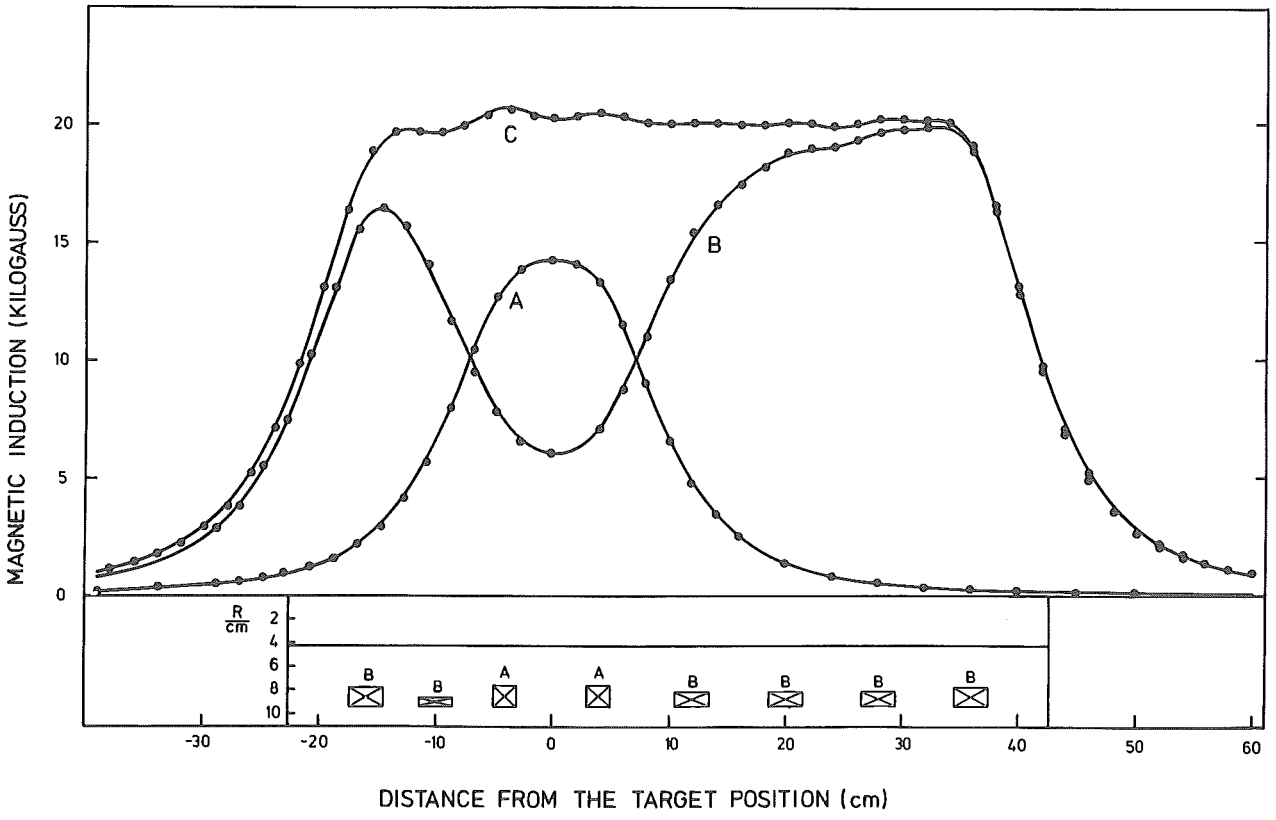

Fig. 1: Calculated and measured magnetic field shapes at 62 Amp spectrometer current, A) field produced only by 2 inner coils, B) field produced only by 6 outer coils, C) total axial field when all coils are energized.

6 hours time and 30 liters Helium for one cooling down (fig. 3). The solenoid system will be installed in the beam line (E) quite near future.

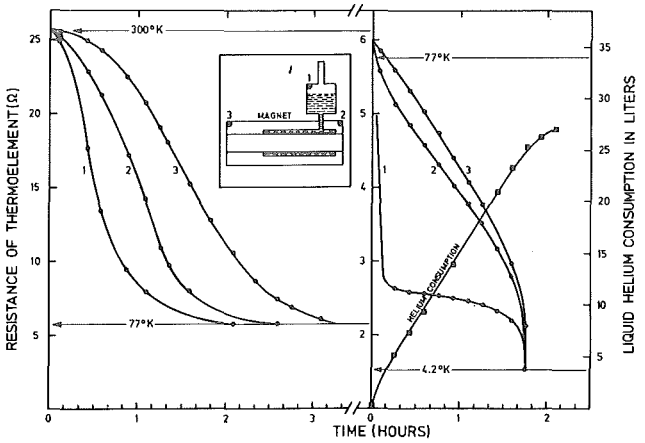

Fig. 3: Cool down procedure of the magnet from the room temperature to the 4.2°K. Left side presents measured temperatures during the liquid Nitrogen transfer and the right side during the Helium transfer. The numbers 1, 2 and 3 on the curves refer to the temperature measuring points in the solenoid as shown schematically in the small picture upper left.

References

1) R.F. Holsinger, private communication (1976)
2) K.L. Brown and Ch. Iselin, CERN 74-2 (1974)

9.6. A New Spectrograph for Experiments with Low Energy Pions at TRIUMF

*S. A. Martin, C. A. Wiedner**, PISCAT Group TRIUMF***

The M13 beam line at TRIUMF the Canadian Meson Factory in Vancouver features high fluxes of low energy pions. With the momentum slits at the dispersive intermediate focus (momentum acceptance $\delta p/p = \pm 7\%$) fully open the following intensities are obtained at the end of the ∿ 10m beam line [double achromatic focus]:

P_π [MeV/c]	$\frac{N_{\pi^+}}{\text{Int. of proton beam}}$	$\frac{N_{\pi^-}}{\text{Int. of proton beam}}$	[cts/Coul]
40	120	28	
70	4500	1000	
100	30000	5000	

The spot however due to aberrations extends over ± 1 - 1.5 cm (in both directions). Employing a hodoscope of scintillators (width 7mm) a momentum resolution of dp/p≈ 0.6% may be obtained.

Presently a Browne-Buechner spectrometer is used for experiments; its acceptance has been increased by a factor 4 by inserting a narrow Q-singlet to 2-4msr. The narrow dipole gap of 2 cm severely limits the acceptance.

Therefore a new layout has been anticipated, which should feature

- solid angle of at least 20 msr for object spots >1 cm^2
- momentum resolution dp/p < 0.2%
- momentum acceptance of ± 20%
- minimum overall length because of the π-decay.

At the same time existing magnets had to be used to save costs and enable experiments soonest possible. The moderate resolution requirement allows provision of two MWPC-s in front and behind the dipole (dx=.5mm FWHM d= 2mg/cm^2).

Minimum system length, together with maximum D/M and transmission requires optimum usage of the dipole magnet:

Axially: Phase space matching - i.e. a parallel beam - at the centre of the magnet.

Radially: The x/θ function should be maximum inside the dipole, hence symmetric.

Both criteria are readily fulfilled with 2 Q-singlets in front of the circular dipole magnet-the former 60 cm diameter lab magnet of the IKP Jülich.
Tab. 1 contains the most important specifications of this design in comparison to other planned instruments.
The figure of merit is defined as

$F.M. = \Omega \cdot \eta \frac{D}{M}$, where Ω[msr] stands for the solid angle, η for the pion survival in the spectrometer and $\frac{D}{M} = p/dp\ 2x_0$ is the first order momentum resolving power.

The new spectrometer is scheduled for experiments in spring 1982.
Fig. 1 shows a layout, Fig. 2 the instrument during the assembling in Dec. 1981.

Table 1

COMPARISON OF SPECTROMETERS

	QD (BB50-TRIUMF)	CLAMSHELL LAMPF	SIN-KA LEP Spectro	QQD This design
Ω(msr)	2-4	40	30	22.4
Target size x*y[cm^2]	1*1	2.8*1	10*3	> 1*1
Acceptance θ/φ[mrd]	±12/±50		±50/±100	±70/±80
Length [m]	1.8	1.7	5.5	2.43
η(50 MeV)	.778	.82	.466	.71
D[cm/%]	1.19	1.23	2.7	1.04
M_{radial}	.92	.54	.54	.52
D/M*10^2 [cm]	1.58	2.3	5.	2.
Momentum Acceptance	±9%	±15%	-15% +20%	±20%
Ang. Range	+60°-130°			+15°-149°
Figure of Merit	2.46(+2)	75.4	46.6	31.8

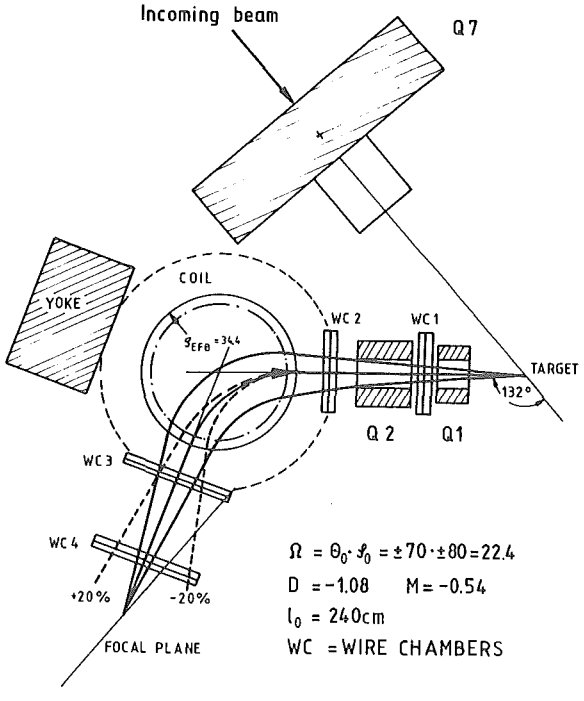

Fig. 1: Layout of the QQD - PISCAT - Spectrometer

* MPI, Heidelberg
**TRIUMF, Vancouver, Kanada

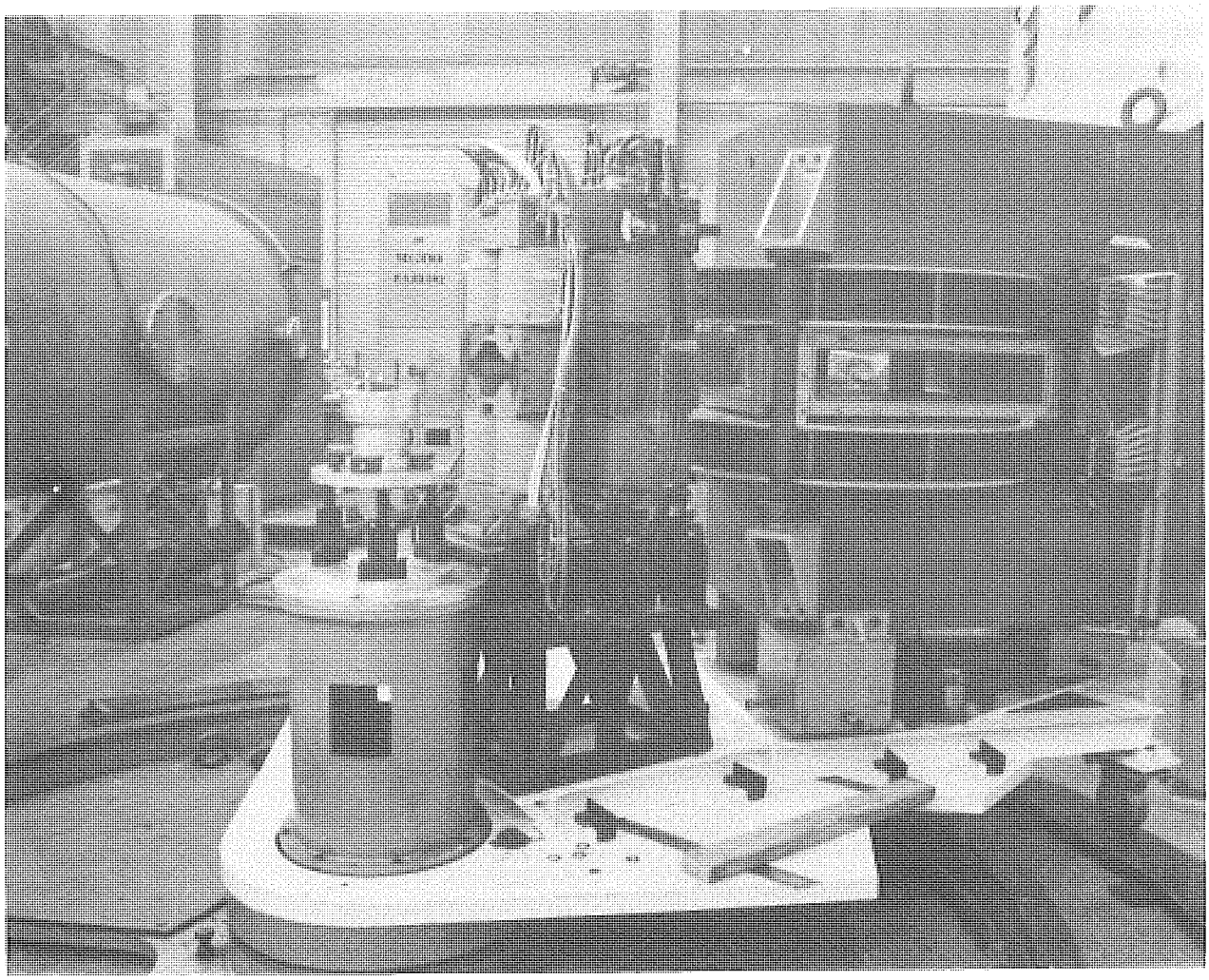

Fig. 2: Assembly of the QQD at TRIUMF

10. HP 9835 Software Developments

E. Brökel

The efficiency of a computer depends on the available software on it. So I implemented on our desk-top-computer configuration[1] a few basis programs. First there was a program installed for using the digitizer HP 9864. The digitized data can be written either on the internal cartridge tape or on the cartridge tape on the HP 2648 terminal. The cartridge tape on the terminal can be accessed by TSS, so one has the data available on the IBM central computer system.

As next two plot programs were installed for creating graphs, one in linear coordinate systems, the other in semi logarithmic coordinate systems on the HP 9872 plotter. The input for these programs may be received from either the keyboard, the internal cartridge tape or the cartridge tape on the terminal. So the user can generate his data to be plotted by the central computer and store them on the cartridge tape on the terminal. This cartridge tape will then be read by the plot program and the data on it plotted on the HP 9872 plotter.

For final polishing of the graphs an additional program was installed. With this,one is able to write text on any location in the graph.

All the installed programs described above are written for interactive use. So one will be prompted when the programs need input from the keyboard.

References

1) E. Brökel, Jül-Spez-99, Februar 1981, p. 167.

11. Electronic Division

H. Labus, J. Bojowald

The following devices partly announced in the annual report 1980 have been revised or set into operation.

1. A 14-fold analogue FAN-OUT-amplifier for complex nuclear reaction experiments within a 3/12-NIM-Module. Each stage has 3 outputs with individual gain adjust in the range from 0.1 to 1.0. Output impedance is 50 ohm. The range is 0V to±10V without load or 0V to± 5V at 50 ohm loads. The circuit is designed with OP-AMP's HA-2525 buffered with NH-0002.
(G. Lürken, K. Winkler)

2. The long time integrator and the T/ΔT amplifier (patent granted) specially developed for the requirements of the solar group of the IKP were redesigned to fit each on a Single Europe Board. Now'Test Units For Collector Testing and Solar Radiation Data Taking' are equipped by licensees with these boards in a very economic way. Within this job the long time integrater was extended by a DAC for plotter outputs and the T/ΔT amplifiers by a switch selectable digital output.
(H. Diesburg, H. Labus)

3. Also for the solar group collector data taking systems were equipped with lightning protection. Several fluid flow measuring devices were adapted for calorimetric measurements. An Aqua-Metro-Calorimeter serial output was changed to meet the standard V24 serial communication as used by the HP-9825 data acquisition system.
(K. Kruck)

4. Again difficult and time consuming maintenance and repair work was spent to the BIG-KARL-power-supplies. Reliability could be improved by optimizing the ignition points of the SCR's and the monitoring system e.g. current limits, earth fault and amplifier override detection.
(K. Kruck)

5. The scattering chamber F was equipped with high torque 24V DC-motors. The existing electronic controls for the old synchronons motors were modified and interfaced to the servo amplifiers of the DC-motors.
(N. Dolfus, K. Winkler)

6. The high voltage square wave pulse generator to switch the inner conductor of the fission product guide of the separator JOSEF from -30KV to +10KV was protected by filters against flash-over pulses between inner and outer conductor of the guide which occasionally destroyed the trigger stages of the 4PR250C-te trodes. Reliability was further improved by various isolating and shielding techniques. Now the instrument works without any fail since one half year.
(G. Lürken, H. Labus)

7. About 140 repair and maintenance jobs of NIM- and CAMAC-modules, TV-cameras and monitors, power supplies of all categories, electronically controlled scattering chambers and beams slits and a great variety of special instruments from our own or external production were performed.
(N. Dolfus, H. Diesburg, G. Brittner, K. Winkler, W. Ernst)

8. The disturbances on line and expecially ground potentials in the control room of the nuclear experiments due to ground loops and wrong wired line filters could be reduced to about 0.1 of the former levels. Now great distances between main amplifiers and ADC's can be tolerated.
(K. Kruck, J. Bojowald)

Main activities are now concentrated to the following subjects:

1. The redesign of the bent crystal spectrometer is continued. The circuits for collimator and crystal rotation motor controls, the piezo driver and band counter of the interferrometer are ready for lay out on Single Europe Boards. These will be interconnected with Siemens SMP-80 microcomputer boards. The software is being prepared on our new INTEL-DS246-software development system. The mechanic adusting devices of the phototransistors as well as the optical projections at the output of the spectrometer are also improved.
(H. Labus, N. Dolfus, G. Lürken)

2. For monitoring complex multiparameter nuclear reaction experiments a multiple coincidence simulator is developed. It has 16 outputs each driving positive and negative tailpulses into the testinputs of preamplifiers. Risetime is <10nsec, falltime is 100μsec, amplitudes are independendly adjustable in the range from 0 to 2.0V at 50ohm loads, crosstalk between outputs is $<10^{-4}$. The 16 pulsdrivers are controlled by a Siemens SKC-85 Single Board Computer in such a way that a predefined (in RAM or ROM) series of different coincident puls groups, each group having between 1 and 16 members, is passed through on consecutive external TTL trigger signals.
(H. Labus, G. Lürken)

12. Radiation protection

H. J. Probst

In 1981 the activity of the radiation protection group was strongly determined by the high internal beam currents used in the dispersive cyclotron mode. These currents causes:

a) Significantly high contaminations of the components of the vakuum chamber. The tungsten septum is shown by γ-spectroscopic analyses of wipe probes to be the origin of the contaminations. This septum is not only strongly activated but also considerably heated by the high beam currents, resulting in a partial evaporation and condensation on cooled machine components.
b) Increase of the man-rem-dose essentially produced during the working on the activated machine elements. In 1981 the total value for the institute is ≈19 rem. But no person exceeds 1.5 rem.

The high radiation fields in the cyclotron vault also necessitate measurement of the dose rate in the cyclotron control room. For an internal deuteron beam of about 30μA and an energy of 78 MeV the mean neutron equivalent dose rate at the working place is about 12μrem/h. Moreover an increase of the γ-dose rate of about 15μr/h was measured. Taking into account the beam time schedule, the cyclotron availability and the working time, no operator obtains more than 20 mrem per year based on the radiation in the control room additionally.

In order to be able to estimate the time between shut down and begin of the labour the knowledge of the decrease of the γ-dose rate in the cyclotron vault is important. Although many irradiation parameters influence the process, a qualitative prediction should at least be possible using the curves in fig. 1

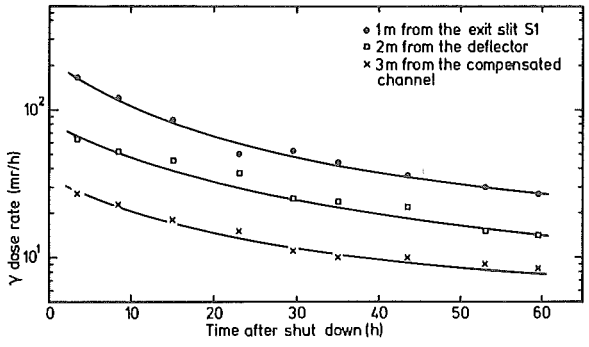

Fig.1: The time dependence of the γ-dose rate in the cyclotron vault after shut down (measured at different locations)

Finally it should be mentioned, that the shielding wall around BIG KARL is completed and the efficiency of the shielding is verified: so that all the required construction conditions concerning the radiation protection are fulfilled.

13. Design and Mechanical Workshop

W. Briell, D. Groß, K.H. Ramacher, A. Retz, U. Rindfleisch, H. Schwan

Apart from maintenance and servicing the cyclotron, beam-line and scattering chamber experiments most of the manpower of design and mechanical workshop went into the growing experimental activities at the magnet spectrometer BIG KARL.

Several special targets (e.g. gas-jet target) and detector systems (e.g. single-wire detector) have been built and came into operation.

In order to improve beam-line optimization for the magnet spectrometer experiments all beam-line magnets have been adjusted and equipped with external adjusting marks (see fig. 1).

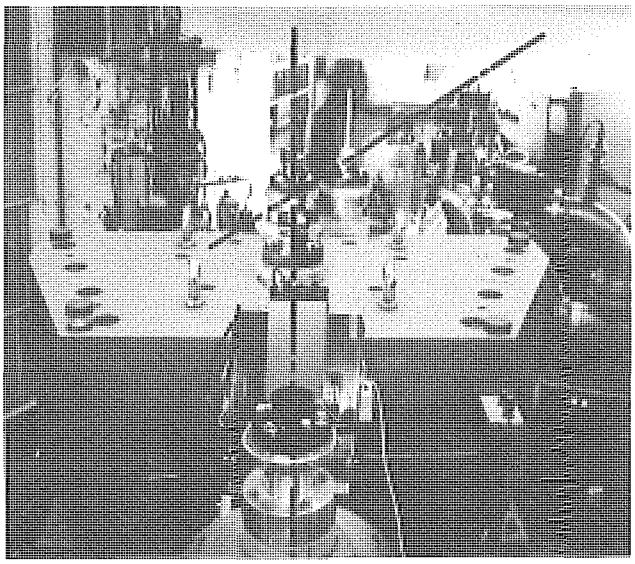

Figure 1

The new system of marks allows in the future an easy check of the mechanical adjustment of all beam-line components relative to cyclotron and building. The optical telescopes second-theodolite Th2 and the leveling instrument Ni1 from Zeiss and the optical "plumb-line" supplied by the company Kern have proven to work very satisfactorily.

A flexible tube level for large distances with an accuracy of 0.02 mm has been developed and works very successfully.

Solenoid Electron Spectrometer

For "in beam" measurements of conversion electrons a solenoid electron spectrometer has been designed and is under construction (fig. 2). The supraconducting solenoid system of 8 coils is designed to detect in particular low energy conversion electrons using the recoil-shaddow method.

For the detection and (momentum) energy analysis two Si(Li)-detectors will be used in order to allow e-e coincidence measurements. The solenoid is designed for magnetic fields up to 2 Tesla.

Because of the variable beam deviation the complete set-up is mounted on an vertical adjustable support and is equipped with additional bending magnets in front and behind the solenoid. The movable vacuum parts are connected on both sides by double-bellows. Cryogenic pumps and liquid nitrogen baffles guarantee the neccessary vacuum conditions.

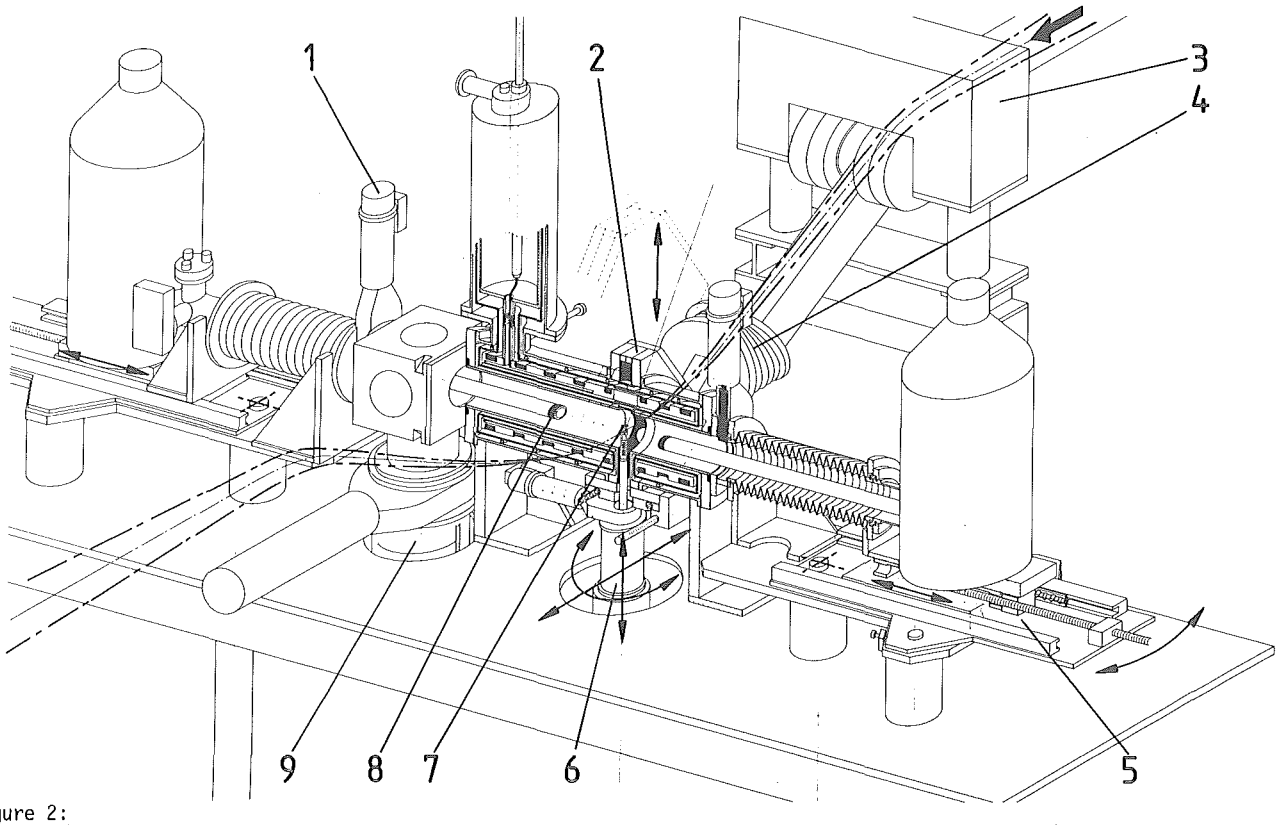

Figure 2:

1) vacuum valve
2) solenoid
3) bending magnet
4) bellows
5) detector mount
6) vacuum look
7) target
8) Si-detector
9) cryopump

V. SCIENTIFIC ADVISORY COUNCIL OF THE INSTITUTE OF NUCLEAR PHYSICS

Prof. Dr. K. Alder	University of Basel
Prof. Dr. R. Bock	GSI Darmstadt
Prof. Dr. G.E. Brown	Dept. of Phys. SUNY at Stony Brook
Prof. Dr. P.G. Hansen	University of Aarhus
Prof. Dr. T. Mayer-Kuckuk	University of Bonn
Prof. Dr. R. Santo (Chairman)	University of Münster
Prof. Dr. R. Sizmann	University of München
Prof. Dr. H.J. Specht	University of Heidelberg
Prof. Dr. H. Vonach	Österreichische Akademie der Wissenschaften, Wien
Prof. Dr. H.A. Weidenmüller	MPI für Kernphysik, Heidelberg
Prof. Dr. L.E. Feinendegen	KFA Jülich

VI. EXTERNAL COMMITTEE FOR GUEST EXPERIMENTS

Prof. Dr. R. Bock	GSI Darmstadt
Prof. Dr. R. Santo	University of Münster
Prof. Dr. P. von Brentano	University of Köln

VII. PERSONNEL

Institute for Nuclear Physics:

Dr. C. Mayer-Böricke	Director of the Institute for Nuclear Physics (Experiment I) Professor of Physics at University of Bonn
Dr. O. Schult	Director of the Institute for Nuclear Physics (Experimente II) Managing director of the Institute for the year 1981 Professor of Physics at University of Köln
Dr. J. Speth	Acting Director of the Institute for Nuclear Physics (Theory) Professor of Physics at University of Bonn

Scientific Staff:

Dr. L. Aldea (Cy)
until Dec. 21, 1981

Dr. G. Baur (Th)

DP U. Bechstedt (E1)

Dr. G. Berg (E2)

Dr. H. Beuscher (E1)

R.K. Bhandari (Cy)
until Oct. 16, 1981
(BARC, Calcutta/India)

Dr. B. Bochev (E1)
until Dec. 8, 1981
(Bulgarian Academy
of Sciences, Sofia/
Bulgarien)

T. Bocheva (E1)
until Aug. 31, 1981
(Bulgarian Academy
of Sciences, Sofia,
Bulgarien)

DP J. Bojowald (Ec)

Dr. G. Borchert (E2)

DP O. Bousshid (E1)
until Aug. 31, 1981

DI W. Bräutigam (Cy)

DP G. Co' (Th)

DP C. Conci (Th)

Dr. P. Decowski (E1)
since June 15, 1981
(Warsaw University,
Warsaw/Poland)

DP H. Dermawan (Th)

Dr. A. Djaloeis (E1)

Dipl. W. Ebke (E2)

DP A. Ercan (E2)

Prof. K. Göke (Th)
(Prof. at the
Univ. of Bonn)

Dr. S. Gopal (E1)
until June 2, 1981
(Univ. of Mysore,
Mysore/Indien)

Dr. F. Grümmer (Th)

DP R. de Haro (Th)

Prof. J. Hill (E2)
until Aug. 31, 1981
(Iowa State Univ., USA)

DP B. Hoffmann (Th)

Dr. Hürlimann (E2)

Dr. P. Jahn (E1)

Dr. R. Julin (E2)
since March 1, 1981

Dr. J. Katayama (E2)
(Osaka Univ./Japan)

Dr. P. Kleinheinz (E2)

Dr. V. Klemt (Th)

D. H.R. Koch (E2)

Dr. S. Krewald (Th)

Dr. H. Labus (Ec)

DP M. Lach (E2)
since Feb. 1, 1981

Dr. R.M. Lieder (E1)
(Privat Dozent at the
Univ. of Bonn)

Dr. H. Machner (E1)

Dr. S. Martin (Ms)

Dr. H.G. Mathews (E1)

Dipl. H. Mattheß (E2)

Prof. Dr. C. Mayer-Böricke (E1)
(Prof. at the Univ. of Bonn)

Dr. J. Meißburger (Ms)

Dr. H.P. Morsch (E1)

Dr. M. Müller-Veggian (E1)

DP K. Nakayama (Th)

Dr. A. Neskakis (E1)
(Univ. of Crete,
Iraklion/Greece)

Dr. W. Oelert (E1)

Dr. F. Osterfeld (Th)

Dipl. B. Poos (E2)
until Sept. 30, 1981

DI R. Posorski (E2)

DP H.J. Probst (Rp)

Prof. Dr. P. Prokofjev (E2)
until May 1, 1981
(Nucl. Research Center,
Riga/UdSSR)

DP D. Protić (Dt)

Prof. Dr. N.G. Puttaswamy (E1)
until June 21, 1981
(Bangalore Univ., Bangalore/
Indien)

DP J. Reich (Cy)

Dr. G. Riepe (Dt)

DP J. Römer (Ms)
since March 1, 1981

Dr. M. Rogge (E1)

DP T. Rose (E2)
since Apr. 1, 1981

DP B. Rubio (E2)
since July 6, 1981

DI B. Sack (E2)

Prof. Dr. O. Schult (E2)
(Prof. at the Univ.
of Cologne)

Dr. H. Selič (E2)
until May 31, 1981

Dr. H. Seyfarth (E2)

Dr. K. Shizuma (E2)

DP J. Siefert (Da)
until June 30, 1981

Dr. K. Sistemich (E2)
(Privat Dozent at the
Univ. of Cologne)

DP F. Soramel (E2)

Prof. Dr. J. Speth (Th)
(Prof. at the Univ.
of Bonn)

Dr. H.J. Stein (E2)

Dr. B. Styczen (E2)
until Aug. 27, 1981
(Jagellonian Univ. Cracow/
Poland)

Dr. J. Styczen (E2)
until Aug. 27, 1981
(Institute of Nuclear
Phys., Cracow/Poland)

Dr. T. Suzuki (Th)

DP J. Tain (E2)
since July 6, 1981

Dr. H. Talarek (E2)

DP Y. Tokunaga (E2)

Dr. P. Turek (E1)

Dr. R. Wagner (E2)

Dr. P. Wucherer (Cy)

Dr. L. Zemlo (E1)
since Sept. 15, 1981
(Institute of Nuclear
Research, Warsaw/Poland)

Dr. M. Zupancic (E2)
since Oct. 8, 1981

Research visitors
(for one week to six
months):

Prof. N.L. Balazs (Th)
from June 19 to July 31, 1981
(SUNY at Stony Brook,
Stony Brook, USA)

Dr. Bodek (E2)
from June 1 to July 31, 1981
(Univ. of Cracow/Poland)

Prof. V.R. Brown (Th)
from Sept. 21 to Dec. 18, 1981
(Lawrence Livermore
Laboratory, Livermore/USA)

Prof. Dr. A. Budzanowski (E1)
from June 15 to Aug. 14, 1981
(Institute of Nuclear Physics,
Cracow/Poland)

Dr. P. Decowski (E1)
from Oct. 20, 1980 to Jan. 19,
1981 (Warsaw Univ./Poland)

Prof. J.S. Dehesa (Th)
from July 1 to Oct. 31, 1981
(Univ. de Granada/Spain)

DP P. Drumm (E1)
from June 22 to July 21, 1981
(Univ. of Birmingham, England)

Research visitors
(for one week to six months):

Prof. L. Jarczyk (E2)
from June 1 to July 31, 1981
(Univ. of Cracow/Poland)

Dr. S. Lunardi (E2)
from Dec. 8 to Dec. 12, 1981
(INFN Padua/Italy)

Prof. V.A. Madsen (Th)
from July 24 to Sept. 9, 1981
(Oregon State Univ., Corvallis/USA)

Prof. Dr. A. Marinov (E1)
from Sept. 1 to Nov. 30, 1981
(The Hebrew Univ. of Jerusalem, Jerusalem/Israel)

Prof. H.A. Mavromatis (Th)
from June 15 to Sept. 14, 1981
(American Univ., Beirut/Libanon)

Dr. T. Morek (E1)
from May 18 to Aug. 18, 1981
(Warsaw Univ., Warsaw/Poland)

Dr. S. Pesič (E1)
from June 7 to June 12, 1981
(Boris Kidrič Institute, Belgrad)

Dr. H. Reinhardt (Th)
from March 15 to Apr. 5, 1981
(ZfK Rossendorf, Dresden, DDR)

Priv. Doz. Dr. K.W. Schmid (Th)
from June 29 to July 11, 1981
and Oct. 27 to Nov. 7, 1981
(Univ. Tübingen)

Dr. R. Shyam (Th)
from March 15 to Apr. 5, 1981
(Daresbury Lab., Warrington, England)

Dr. M. Sommermann (Th)
from Apr. 15 to May 14, 1981
(SUNY at Stony Brook, Stony Brook/USA)

Prof. A. Strzalkowski (E2)
from June 1 to July 31, 1981
(Univ. of Cracow/Poland)

Dr. J. Wambach (Th)
from March 23 to May 31, 1981
(SUNY at Stony Brook, Stony Brook/USA)

Prof. S. Yates (E2)
from July 1 to Dec. 31, 1981
(Univ. of Kentucky)

Dr. D. Zawischa (Th)
until March 31, 1981
(Univ. of Hannover)

Technical and administrative staff:

J. Anhalt (E2)
K. Barth (Ec)
H.G. Böge (Cy)
W. Borgs (E2)
H. Borsch (Cy)
W. Briêll (Cd)
R. Brings (Cy)
G. Brittner (Ec)
E. Brökel (Th)
U. Burck (Ad)
J. But (Ws)
H. Diesburg (Ec)
A. Dohmen (Ad)
N. Dolfus (Ec)
F. Drees (Cy)
R. Enge (Ws)
P. Engels (Cy)
M. Erkens (Ad)
since Sept. 1, 1981
W.R. Ermer (E2)
W. Ernst (Ec)
R. Fiedler (Cy)
N. Gad (Cy)
J. Geremeck (Cd)
until July 31, 1981
G. Göbbels (Ws)
A. Golik (Ws)
E. Gollnick (E2)
E. Griesen (Ad)
since Oct. 10, 1981
D. Groß (Cd)
M. Habrichs (Cd)
from May 4 to Oct. 31, 1981
U. Hacker (Ms)
H. Hadamek (Ws)
M. Heese (Ad)
H. Heinrichs (Cy)
K. Hieble (Cy)
H. Hintzen (Rp)
W. Hoffmeister (Cy)
K. Hütten (Ws)
H.M. Jäger (E1)
I. Jannakos (Cy)
H. Jansen (Ms)
since Sept. 1, 1981
H.J. Jansen (Ws)
R. Janssen (Ad)
A. Jeglorz (E2)
M. Karnadi (Da)
H. Klapperich (Ws)
M. Köhnen (E2)
K. Krafft (Rp)
R. Krewel (Ms)
K.P. Kruck (Ec)
T. Künster (Dt)
E. Lawin (Dt)
H. Lengerke (Ad)
until July 31, 1981
G. Lürken (Ec)
H. Majd-Moghaddam (Ms)
since Oct. 15, 1981
H. Mauel (Da)
H. Metz (Dt)
H. Meuser (Ws)
A. Müller (Cy)
R. Nellen (Da)
K. Nicoll (Dt)
J. Pfeiffer (Dt)
J. Pitzen (Ms)
H.W. Pohl (E1)
K.H. Ramacher (Cd)
A. Retz (Cd)
U. Rindfleisch (Ws)
N. Rotert (Cy)
T. Sagefka (Ms)
H. Sauer (Ad)
M. Scherer (Ad)
G. Schlienkamp (Cy)
P. Schmidt (E2)
Jos. Schmitz (Ws)
Jürg. Schmitz (Cy)
F.-J. Schopen (Ws)
from Jan. 29 to July 31, 1981
R. Schröer (E2)
F. Schultheiß (Ws)
H. Schwan (Ws)
R. Seidemann (E2)
B. Siefert (Da)
until June 30, 1981
H. Sieling (Ad)
M.L. Stehr (Ad)
until June 30, 1981
J. Strehl (Ws)
H. Velten (Ec)
from Jan. 23 to July 31, 1981
K.P. Wieder (E2)
W. Wilms (Cy)
G.-C. Winger (Ad)
from June 24 to Sept. 9, 1981
K. Winkler (Ec)
J. Wolanski (Ws)

(E1) Institute for Experimental Nuclear Physics I
(E2) Institute for Experimental Nuclear Physics II
(Th) Institute for Theoretical Nuclear Physics

(Ad) Administration
(Cd) Construction and Design
(Cy) Cyclotron Laboratory
(Da) Data Acquisition Group
(Dt) Detector and Target Laboratory
(Ec) Electronics
(Ms) Magnetic Spectrograph 'Big Karl'
(Rp) Radiation Protection
(Ws) Mechanical Workshop

VIII. PUBLICATIONS

IKP-100181
Anhalt, J., Maßmeyer, K., Stein, H.J.
Teststation für Solarkollektoren in Brasilien.
BMFT-Forschungsbericht BMFT-FB-T 81-224, Dezember 1981.
2o.6o.1

IKP-100281
Baba, C.V.K., Bjørnholm, S., Christensen, O., Herskind, B., Lieder, R.M., Pedersen, J., Sletten, G., Folkmann, F., Simon, R.S.
Non-collective properties of the continuum γ rays feeding two high-spin isomers in ^{152}Er.
Physica Scripta 24 (1981) S. 290-293.
2o.1o.o

IKP-100381
Babiński, B., Gocławski, M. Jaskóła, M., Kucharski, M., Zemło, L.
Multi-elemental analysis of lubricating oil.
Nucl. Instr. & Meth. 181 (1981) S. 523-525.
2o.o6.o

IKP-100481
Baur, G.
Survey of fragmentation processes in nucleus-nucleus collisions.
Proc. Daresbury Study Weekend "Topics of Heavy Ion Reactions", Daresbury, 4.-5.10.1980, Hrsg. A.K. Dhar, J.S. Lilley, M.A. Nagarajan, Daresbury Laboratory (1981) S. 38-46.
2o.8o.o

IKP-100581
Baur, G., Shyam, R., Rösel, F., Trautmann, D.
Projectile fragmentation and stripping to unbound states: An important reaction mechanism for peripheral nucleus-nucleus collisions.
Helvetica Physica Acta 53 (1980) S. 506-529.
2o.8o.o

IKP-100681
Baur, G., Hoffmann, B., Rösel, F., Trautmann, D., Shyam, R.
A review of fragmentation processes in nucleus-nucleus collisions.
Proc. XIX Int. Winter Meeting on Nuclear Physics, Bormio, Italien, 26.-31.1.1981, Hrsg. I. Iori (Ricerca Scientifica ed Educazione Permanente, Milano) S. 598-605.
2o.8o.o

IKP-100781
Betigeri, M.G., Chung, W., Djaloeis, A., Oelert, W., Turek, P.
The reactions ^{50,52}Cr(d,^{6}Li)^{46,48}Ti at E_d = 65 MeV.
Nucl. Phys. A363 (1981) S. 35-44.
2o.o6.o

IKP-100881
Blomqvist, J., Kleinheinz, P., Broda, R., Daly, P.J.
Atomic masses above ^{146}Gd derived from a shell model analysis of high spin states.
Proc. 4th Int. Conf. on Nuclei far from Stability, Helsingør, Dänemark, 7.-13.6.1981, CERN 81-09, 20.7.1981, S. 545-546.
2o.1o.o

IKP-100981
Borchert, G.L., Schult, O.W.B., Speth, J., Hansen, P.G., Jonson, B., Ravn, H., McGrory, J.B.
Study of the charge radii of the stable lead isotopes.
Proc. 4th Int. Conf. on Nuclei far from Stability, Helsingør, Dänemark, 7.-13.6.1981, CERN 81-09, 2o.7.1981, S. 56-61.
2o.1o.o + 2o.8o.o

IKP-101081
Borchert, G.L., Hansen, P.G., Ravn, H.L., Schult, O.W.B.
Study of higher order effects on the energies of K X-ray transitions.
Proc. Vth Int. Conf. on Hyperfine Interactions, Berlin, 21.-25.7.1980, Hrsg. G. Kaindl, H. Haas (North-Holland Publ. Comp., Amsterdam, 1981) S. 1119-1122.
2o.1o.o

IKP-101181
Bousshid, O.
Messung von ^{197}Au(,xnyp)-Anregungsfunktionen für 15 MeV ≤ E_τ ≤ 135 MeV und Analyse im Rahmen des Hybridmodells.
Jül-Spez-98, Januar 1981, ISSN 0343-7639.
2o.o6.o

IKP-101281
Brown, G.E., Speth, J., Wambach, J.
Energy dependence of the coupling potentials in (p,n) reactions.
Phys. Rev. Lett. 46 (1981) S. 1057-1061.
2o.8o.o

IKP-101381
Carter, J., Clarkson, R.G., Frahn, W.E., Hnizdo, V., Osterfeld, F., Richter, A., Sellschop, J.P.F.
Excitation of the lowest 1$^-$ state in ^{18}O by scattering from ^{16}O.
S.-Afr. J. Phys. 4 No. 1 (1981) S. 13-15.
2o.8o.o

IKP-101481
Decowski, P., Morsch, H.P., Benenson, W.
Low-lying isoscalar dipole excitations in ^{208}Pb.
Phys. Lett. 101B (1981) S. 147-150.
2o.o6.o

IKP-101581
Dickhoff, W.H., Faessler, A., Meyer-ter-Vehn, J., Müther, H.
Pion condensation and realistic interactions.
Phys. Rev. C23 (1981) S. 1154-1173
2o.8o.o

IKP-101681
Djaloeis, A., Gopal, S.
High energy helion scattering: A model-independent analysis.
Nucl. Phys. A356 (1981) S. 97-113.
2o.o6.o

IKP-101781
Faessler, A., Izumoto, T., Krewald, S., Sartor, R.
A complex effective force for heavy-ion collisions.
Nucl. Phys. A359 (1981) S. 509-536.
2o.8o.o

IKP-101881
Gill, R.L., Chrien, R.E., Shmid, M., Gowdy, G. M., Liou, H.-I., Brenner, D.S., Wohn, F.K., Sistemich, K., Yamamoto, H., Chung, C., Walters, W.B.
Band structure in ^{148}Ce from the decay of mass separated ^{148}La.
Proc. 4th Int. Conf. on Nuclei far from Stability, Helsingør, Dänemark, 7.-13.6.1981, CERN 81-09, 20.7.1981, S. 569-575.
2o.65.o

IKP-101981
Goeke, K., Reinhard, P.-G., Rowe, D.J.
A study of collective paths in the time-dependent Hartree-Fock approach to large amplitude collective nuclear motion.
Nucl. Phys. A359 (1981) S. 408-430.
2o.8o.o

IKP-102081
Gopal, S., Djaloeis, A., Bojowald, J., Bousshid, O., Oelert, W., Puttaswamy, N.G., Turek, P., Mayer-Böricke, C.
Broad structure in t spectra from (^{3}He,t) reactions at $E_{^{3}He}$ = 130 MeV; its angle and target-mass dependence.
Phys. Rev. C23 (1981) S. 2459-2462.
2o.o6.o

IKP-102181
Gowdy, G.M., Chrien, R.E., Chu, Y.Y., Gill, R. L., Liou, H.-I., Shmid, M., Stelts, M.L., Sistemich, K., Wohn, F.K., Yamamoto, H., Brenner, D.S., Yeh, T.R., Meyer, R.A., Chung, C., Walters, W.B., Petry, R.F.
Levels in ^{146}Ce and the N = 88 isotones.
Proc. 4th Int. Conf. on Nuclei far from Stability, Helsingør, Dänemark, 7.-13.6.1981, CERN 81-09, 20.7.1981, S. 562-568.
2o.65.o

IKP-102281
Haenni, D.R., Beuscher, H., Bochev, B., Kutsarova, T., Morek, T., Müller-Veggian, M., Neskakis, A., Mayer-Böricke, C.
A new 5.0 ns isomer in ^{144}Eu.
Nucl. Phys. A365 (1981) S. 229-236.
2o.1o.o

IKP-102381
Hill, J.C., Koch, H.R., Shizuma, K.
First observation of the decay of the neutron rich nucleus ^{36}P.
Proc. 4th Int. Conf. on Nuclei far from Stability, Helsingør, Dänemark, 7.-13.6.1981, CERN 81-09, 20.7.1981, S. 372-375.
2o.65.o

IKP-102481
Hill, J.C., Shizuma, K., Lawin, H., Shaanan, M., Selic, H.A., Sistemich, K.
Extension of the systematics for even-even Zr isotopes to A = 102.
Proc. 4th Int. Conf. on Nuclei far from Stability, Helsingør, Dänemark, 7.-13.6.1981, CERN 81-09, 20.7.1981, S. 443-446.
2o.65.o

IKP-102581
Hoffmann, B.
Coulombdissoziation bei nichtrelativistischen und relativistischen Energien.
Jül-Spez-131 (1981)
2o.8o.o

IKP-102681
Hornshoj, P., Zelazny, Z., Jaskóła, M. Zemło, L., Celler, A., Szerypo, J.
The K-shell ionisation of $_{90}$Th by protons and alpha particles.
J. Phys. B (GB) 14 (1981) S. 2391-2398.
2o.o6.o

IKP-102781
Izumoto, T., Krewald, S., Faessler, A.
Nuclear matter approach to the heavy-ion optical potential. (II). Imaginary part.
Nucl. Phys. A357 (1981) S. 471-487.

IKP-102881
Kawade, K., Battistuzzi, G., Lawin, H., Sistemich, K., Blomqvist, J.
Life-times of the 4^{+}_{1}-states in ^{134}Te and ^{136}Xe.
Z. Physik A298 (1980) S. 187-190.
2o.65.o

IKP-102981
Kawade, K., Battistuzzi, G., Lawin, H., Sistemich, K., Blomqvist, J.
A μs-isomer in ^{135}Te.
Z. Physik A298 (1980) S. 273-278.
2o.65.o

IKP-103081
Kleinfeller, J., Bisplinghoff, J., Ernst, J., Mayer-Kuckuk, T., Baur, G., Hoffmann, B., Shyam, R., Rösel, F., Trautmann, D.
Study of inclusive proton spectra from low energy deuteron reactions in terms of spectator break-up and Coulomb dissociation of the projectile.
Nucl. Phys. A370 (1981) S. 205-230.
2o.8o.o

IKP-103181
Kleinheinz, P., Styczen, J., Piiparinen, M., Kortelahti, M., Blomqvist, J.
The 2.57 MeV 19/2^{-} two-phonon octupole state in ^{147}Gd.
Proc. 4th Int. Conf. on Nuclei far from Stability, Helsingør, Dänemark, 7.-13.6.1981, CERN 81-09, 21.7.1981, S. 542-544.
2o.1o.o

IKP-103281
Kleinheinz, P.
Yrast octupole excitations in the ^{146}Gd region.
Physica Scripta 24 (1981) S. 236-242.
2o.1o.o

IKP-103381
Klemt, V.
A new method for a consistent description of the structure of even-even and even-odd nuclei.
Proc. 4th Int. Conf. on Nuclei far from Stability, Helsingør, Dänemark, 7.-13.6.1981, CERN 81-09, 21.7.1981, S. 530-531.
2o.8o.o

IKP-103481
Knöpfle, K.T., Riedesel, H., Schindler, K., Wagner, G.J., Mayer-Böricke, C., Oelert, W., Rogge, M., Turek, P.
Threshold effects in the decay of the isoscalar giant quadrupole resonances in ^{58,62}Ni.
J. Phys. G7 (1981) S. L99-L103.
2o.o6.o

IKP-103581
Knöpfle, K.T., Riedesel, H., Schindler, K., Wagner, G.J., Mayer-Böricke, C., Oelert, W., Rogge, M., Turek, P.
Direct decays of the isoscalar giant quadrupole resonance in ^{28}Si.
Phys. Rev. Lett. 46 (1981) S. 1372-1375.
2o.o6.o

IKP-103681
Koch, H.R., Grüter, J.W.
Short interval meteorological data for computational methods.
Report EUR 7307 en MF, 1981.
2o.6o.1

IKP-103781
Krewald, S.
Magnetic resonances and the spin dependence of the particle-hole force.
Lecture Notes in Physics, Vol. 137, Hrsg. H. Arenhövel, A.M. Saruis (Springer-Verlag, 1981), S. 31-41.
2o.8o.o

IKP-103881
Krewald, S.
No precritical phenomena in nuclei?
Proc. Int. Workshop IX on Gross Properties of Nuclei and Nuclear Excitations, Hirschegg, 19.-24.1.1981, Hrsg. H. Feldmeier, TH Darmstadt (1981)
2o.8o.o

IKP-103981
Krewald, S., Djaloeis, A., Gopal, S.
Empirical constraints on the ^{16}O+^{40}Ca optical potential.
Phys. Rev. C24 (1981) S. 966-970.
2o.6o.o + 2o.8o.o

IKP-104081
Krewald, S., Osterfeld, F., Speth, J., Brown, G.E.
Nuclear structure effects connected with charge-exchange resonances.
Phys. Rev. Lett. 46 (1981) S. 103-106.
2o.8o.o

IKP-104181
Lee, S.Y., Osterfeld, F., Tam, K., Kuo, T.T.S.
General properties of energy independent nuclear optical model potentials.
Phys. Rev. C24 (1981) S. 329-334.
2o.8o.o

IKP-104281
Li Chu-Hsia, Klemt, V.
Distribution of single-particle strengths in the ^{208}Pb±1 nuclei.
Nucl. Phys. A364 (1981) S. 93-104.
2o.8o.o

IKP-104381
Lieder, R.M.
Physikalische Methoden in der Paläoklimatologie.
Physik in unserer Zeit 12 (1981) S. 68-77.
2o.1o.o

IKP-104481
Lieder, R.M., Bochev, B., Kutsarova, T., Beuscher, H., Haenni, D.R., Morek, T., Müller-Veggian, M., Neskakis, A., Mayer-Böricke, C., Didelez, J.P.
Study of α-induced non-equilibrium reactions with particle-γ coincidences.
Physica Scripta 24 (1981) S. 123-129.
2o.1o.o

IKP-104581
Lund, T., Randt, R., Molzahn, D., Tress, G., Vater, P., Marinov, A.
Search for spontaneous fission emitters in Atlantis II (Part II).
Z. Physik A - Atoms and Nuclei 300 (1981) S. 285-288
2o.o6.o

IKP-104681
Machner, H.
Break-up studies with loosely bound projectiles.
Proc. Int. Workshop IX on Gross Properties of Nuclei and Nuclear Excitations, Hirschegg, 19.-24.1.1981, Hrsg. H. Feldmeier, TH Darmstadt (1981) S. 61-64.
2o.o6.o

IKP-104781
Machner, H.
On the validity of pre-equilibrium model assumptions.
Z. Physik A - Atoms and Nuclei 302 (1981) S. 125-132.
2o.o6.o

IKP-104881
Nagai, Y., Styczen, J., Piiparinen, M., Kleinheinz, P., Bazzacco, D., v. Brentano, P., Zell, K.O., Blomqvist, J.
Proton single-particle states above Z=64.
Phys. Rev. Lett. 47 (1981) S. 1259-1262
2o.1o.o

IKP-104981
Osterfeld, F., Madsen, V.A.
Nuclear structure approach to the Coulomb correction of the imaginary nucleon-nucleus optical potential.
Phys. Rev. C24 (1981) S. 2468-2474.
2o.8o.o

IKP-105081
Osterfeld, F., Krewald, S., Dermawan, H., Speth, J.
Pionic, ΔL=1-charge-exchange modes in heavy mass nuclei.
Phys. Lett. 105B (1981) S. 257-262.
2o.8o.o

IKP-105181
Osterfeld, F., Suzuki, T., Speth, J.
No evidence for precritical phenomena of pion condensation in A=48-nuclei.
Phys. Lett. 99B (1981) S. 75-79.
2o.8o.o

IKP-105281
Osterfeld, F., Wambach, J., Madsen, V.A.
Antisymmetrized, microscopic calculation for the ^{40}Ca(n,n) optical potential.
Phys. Rev. C23 (1981) S. 179-193.
2o.8o.o

IKP-105381
Paić, G., Antolković, B., Djaloeis, A., Bojowald, J., Mayer-Böricke, C.
Continuous spectra of protons and deuterons from the α+α interaction in the incident energy interval 110-172 MeV.
Phys. Rev. C24 (1981) S. 841-848.
2o.o6.o

IKP-105481
Piiparinen, M., Pengo, R., Nagai, Y., Hammaren, E., Kleinheinz, P., Roy, N., Carlen, L., Ryde, H., Lindblad, Th., Johnson, A., Hjorth, S.A., Blomqvist, J.
High spin shell model excitations in ^{149}Gd.
Z. Physik A - Atoms and Nuclei 300 (1981) S. 133-142.
2o.1o.o

IKP-105581
Piiparinen, M., Broda, R., Nagai, Y., Kleinheinz, P.
The 235 ns 9^+ isomer in $^{148}_{63}Eu_{85}$.
Z. Physik A - Atoms and Nuclei 301 (1981) S. 231-235.
2o.1o.o

IKP-105681
Rösel, F., Trautmann, D., Baur, G.
Coulomb-Ionisation innerer Schalen bei asymmetrischen Systemen.
2. Arbeitsbericht der Arbeitsgruppe "Energiereiche atomare Stöße", Gesamthochschule Kassel, Hrsg. J. Eichler, B. Fricke, R. Hippler, D. Kolb, H.O. Lutz, P. Mokler (1981) S. 122-123.
2o.8o.o

IKP-105781
Rullhusen,P., Mückenheim, W., Smend, F., Schumacher, M., Berg, G.P.A., Mork, K., Kissel Lynn.
Test of vacuum polarization by precise investigation of Delbrück scattering.
Phys. Rev. C23 (1981) S. 1375-1383
2o.o6.o

IKP-105881
Sartor, R., Faessler, A., Khadkikar, S.B., Krewald, S.
Folding computation of the ^{16}O+^{16}O optical potential with a complex effective force.
Nucl. Phys. A359 (1981) S. 467-476.
2o.8o.o

IKP-105981
Shizuma, K., Hashimoto, E., Yoshizawa, Y., Kino, T.
Temperature dependence of the positron annihilation radiation spectra for Aluminium by means of Doppler broadening measurement.
J. Phys. F: Metal Phys. 11 (1981) S. 2461-2473.
2o.65.o

IKP-106081
Shyam, R., Baur, G., Rösel, F., Trautmann, D.
Break-up calculations for light projectile E = 10-40 MeV/nucleon.
Proc. Daresbury Study Weekend "Topics in Heavy Ion Reactions", Daresbury, England, 4.-5.10. 1980, Hrsg. A.K. Dhar, J.S. Lilley, M.A. Nagarajan, Daresbury (1981) S. 68-72.
2o.8o.o

IKP-106181
Speth, J., Suzuki, T.
Spin-isospin modes and high momentum transfer electron scattering.
Nucl. Phys. A358 (1981) S. 139c-152c.
2o.8o.o

IKP-106281
Speth, J., van der Woude, A.
Giant resonances in nuclei.
Reports on Progress in Physics 44 (1981) S. 719-786.
2o.8o.o

IKP-106381
Suzuki, T.
Path integral and classical dynamics of many body systems.
Proc. Int. School on Critical Phenomena in heavy ion physics, Poiana Brasov, Rumänien, 25.8.-10.9.1980, Hrsg. A.A. Raduta, G. Stratan, Bucharest, Rumänien, S. 994-997.
2o.8o.o

IKP-106481
Suzuki, T.
Time-dependent Hartree-Fock and superposition principle: Semiclassical method in phase space representation.
Proc. Workshop on Semiclassical Methods in Nuclear Physics, Grenoble, Frankreich, 18.-20. 3.1981, Hrsg. P. Schuck, Ph. Quentin, ILL Grenoble (1981) 9 S.
2o.8o.o

IKP-106581
Suzuki, T., Fuyuki, M., Matsuyanagi, K.
Dynamical interplay of pairing and quadrupole modes in transitional nuclei. III.
Prog. Theor. Phys. 65 (1981) S. 1667-1683
2o.8o.o

IKP-106681
Suzuki, T., Osterfeld, F., Speth, J.
Critical analysis of precritical phenomena of pion condensation in finite nuclei.
Proc. Int. School of Critical Phenomena in Heavy Ion Physics, Poiana Brasov, Rumänien, 25.8.-10.9.1980, Hrsg. A.A. Raduta, G. Stratan, Bucharest, Rumänien, S. 1087-1092.
2o.8o.o

IKP-106781
Suzuki, T., Krewald, S., Speth, J.
Experimental signatures of the Δ(1236)-hole quenching mechanism in pionic states.
Phys. Lett. 107B (1981) S. 9-13.
2o.8o.o

IKP-106881
Suzuki, T., Osterfeld, F., Speth, J.
Critical analysis of a precritical phenomenon in connection with pion condensation.
Phys. Lett. 100B (1981) S. 443-447.
2o.8o.o

IKP-106981
Schmid, K.W., Grümmer, F.
Microscopic description of nuclear excitations in deformed light and heavy nuclei.
Proc. Nucl. Phys. Workshop, Trieste, Italien, 5.-30.10.1981.
2o.8o.o

IKP-107081
Schröer, R., Ungeheuer, J.
Verfahren zur Bestimmung der effektiven Wärmekapazität thermischer Flachkollektoren.
Jül-Spez-93, Dezember 1980.
2o.6o.1

IKP-107181
Schussler, F., Blachot, J., Monnand, E., Pinston, J.A., Lawin, H., Sistemich, K., Kawade, K., Heyde, K., Sau, J.
Level scheme of ^{131}Sb.
Proc. 4th Int. Conf. on Nuclei far from Stability, Helsingør, Dänemark, 7.-13.6.1981, CERN 81-09, 20.7.1981, S. 532-535.
2o.65.o

IKP-107281
Schussler, F., Pfeiffer, B., Lawin, H., Monnand, E., Münzel, J., Pinston, J.A., Sistemich, K.
Nuclear spectroscopy of neutron rich A = 147 nuclei.
Proc. 4th Int. Conf. on Nuclei far from Stability, Helsingør, Dänemark, 7.-13.6.1981, CERN 81-09, 20.7.1981, S. 589-591.
2o.65.o

IKP-107381
Stein, H.J.
Solare Meßtechnik.
Jahresbericht 1980/81 der KFA Jülich, ISSN 0341-8790, S. 49-58.
2o.6o.1

IKP-107481
Stein, H.J.
Why do we need collector testing?
Proc. Egyptian-German Workshop onSolar Collectors, Cairo, Ägypten, 31.1.-2.2.1981, S. 1-22.
2o.6o.1

IKP-107581
Styczen, J., Kleinheinz, P., Piiparinen, M., Blomqvist, J.
The N = 82 gap in ^{146}Gd from β-decay studies of Tb isotopes.
Proc. 4th Int. Conf. on Nuclei far from Stability, Helsingør, Dänemark, 7.-13.6.1981, CERN 81-09, 20.7.1981, S. 548-550.
2o.1o.o

IKP-107681
Tam, K.C., Müther, H., Sommermann, Kuo, T.T.S., Faessler, A.
A folded diagram microscopic calculation of nuclear Coulomb displacement energies.
Nucl, Phys. A361 (1981) S. 412-434.
2o.8o.o

IKP-107781
Thirumala Rao, B.V., Broda, R., Günther, C., Kleinrahm, A., Ogawa, M.
The $(\nu i^{-1}_{13/2}\pi h_{9/2})10^-$ isomer and other high-spin states in ^{202}Bi.
Nucl. Phys. A362 (1981) S. 71-85.
2o.1o.o

IKP-107881
Urbano, J.N., Goeke, K., Reinhard, P.-G.
Dynamical and quantum mechanical corrections to heavy-ion optical potentials.
Nucl. Phys. A370 (1981) S. 329-348.
2o.8o.o

IKP-107981
Walters, W.B., Chung, C., Brenner, D.S., Gill, R.L., Shmid, M., Chrien, R.E., Liou, H.-I., Gowdy, G., Stelts, M.L., Chu, Y.Y., Wohn, F.K., Sistemich, K., Yamamoto, H.
Angular correlations and coincidence studies of excited 0^+ and other levels in the transitional Ce nuclides ^{142}Ce, ^{144}Ce, ^{146}Ce and ^{148}Ce.
Proc. 4th Int. Conf. on Nuclei far from Stability, Helsingør, Dänemark, 7.-13.6.1981, CERN 81-09, 20.7.1981, S. 557-561.
2o.65.o

IKP-108081
Wiktor, S., Mayer-Böricke, C., Kiss, A., Rogge, M., Turek, P., Dabrowski, H.
Elastic scattering of 120, 145 and 172.5 MeV α-particles by ^{12}C, ^{24}Mg and ^{27}Al and optical model analysis.
Acta Physica Polonica B12, No. 5 (1981) S. 491-503.
2o.o6.o

IKP-108181
Wolf, A., Battistuzzi, G., Kawade, K., Lawin, H., Sistemich, K.
Magnetic moment of the first excited 2^+ state in ^{100}Zr.
Phys. Lett. 97B (1980) S. 195-196.
2o.65.o

IX. CONFERENCE CONTRIBUTIONS, TALKS

IKP-200181
Aldea, L., Reich, J., Wucherer, P.
The modified center region for the project ISIS at JULIC.
Ninth Int. Conf. on Cyclotrons and their Applications, Caen, Frankreich, 7.-10.9.1981.
2o.3o.o

IKP-200281
Aldea, L., Bräutigam, W., Brings, B., Mayer-Böricke, C., Reich, J., Wucherer, P.
Status of JULIC.
Ninth Int. Conf. on Cyclotrons and their Applications, Caen, Frankreich, 7.-10.9.1981, Poster Session.
2o.3o.o

IKP-200381
Aldea, L., Beuscher, H., Bhandari, R.K., Mathews, H.-G., Mayer-Böricke, C., Reich, J., Wucherer, P.
Status of ISIS.
18th European Cyclotron Progress Meeting, Louvain-la-Neuve, Belgien, 25.-28.3.1981, Poster Session.
2o.3o.o

IKP-200481
Aldea, L., Reich, J., Wucherer, P.
Modification of the central region for axial beam injection at JULIC.
Frühjahrstagung der DPG, Sektion A: Kernphysik, Hamburg, 23.-27.3.1981.
2o.3o.o

IKP-200581
Aldea, L., Bhandari, R.K., Beuscher, H., Mathews, H.-G., Mayer-Böricke, C., Reich, J., Wucherer, P.
The project ISIS at JULIC.
Frühjahrstagung der DPG, Sektion A: Kernphysik, Hamburg, 23.-27.3.1981.
2o.3o.o

IKP-200681
Anhalt, J.
Technical aspects of testing solar collectors.
Universität Sao Paulo, Brasilien, Mai 1981.
2o.6o.1

IKP-200781
Anhalt, J.
Performance of linear concentraging collectors under Brasilian climatic conditions.
Postervortrag, Solar Worls Forum, Brighton, Großbritannien, 23.-28.8.1981.
2o.6o.1

IKP-200871
Baur, G.
Ist unsere Materie stabil?
Universität Bonn, 21.12.1981.
2o.8o.o

IKP-200981
Baur, G.
Der Zerfall des Protons und Neutrino-Oszillationen.
IKP, KFA Jülich, 7.12.1981.
2o.8o.o

IKP-201081
Baur, G.
Inclusive breakup processes and semiclassical methods.
Workshop on Direct Reactions in Nuclear Physics, Bad Honnef, 5.-9.10.1981.
2o.8o.o

IKP-201181
Baur, G.
A review of fragmentation processes in nucleus-nucleus collisions.
XIX Int. Winter Meeting on Nuclear Physics, Bormio, Italien, 26.-31.1.1981.
2o.8o.o

IKP-201281
Berg, G.P.A., Hürlimann, W., Katayama, I., Martin, S.A., Meißburger, J., Römer, J., Seyfarth, H., Styczen, B.
Nuclear spectroscopy of ^{108}Ag using the (p,d) transfer reaction in comparison to neutron capture investigations.
4th Int. Symp. on Neutron Capture Gamma-Ray Spectroscopy and Related Topics, Grenoble, Frankreich, 7.-11.9.1981.
2o.o6.o

IKP-201381
Berg, G.P.A., Decowski, P., Katayama, I., Martin, S.A., Meißburger, J., Morsch, H.P., Rogge, M., Styczen, B., Turek, P.
Search for isoscalar 1^+ excitations in ^{208}Pb.
Frühjahrstagung der DPG, Sektion A: Kernphysik, Hamburg, 23.-27.3.1981.
2o.o6.o

IKP-201481
Berg, G.P.A., Gaul, G., Hürlimann, W., Katayama, I., Martin S.A., Meißburger, J., Römer, J., Santo, R., Sondermann, G., Styczen, B., Osterfeld, F.
Strong 1^+ excitation in $^{48}Ca(p,p')$ scattering at E_p = 44.4 MeV.
Workshop on Direct Reactions in Nuclear Physics, Bad Honnef, 5.-9.10.1981.
2o.o6.o + 2o.8o.o

IKP-201581
Berg, G.P.A., Hürlimann, W., Katayama, I., Martin, S.A., Meißburger, J., Römer, J., Seyfarth, H., Styczen, B.
Nuclear spectroscopy of ^{108}Ag using the (p,d) transfer reaction in comparison to neutron capture investigations.
Workshop on Direct Reactions in Nuclear Physics, Bad Honnef, 5.-9.10.1981.
2o.o6.o

IKP-201681
Berg, G.P.A., Hürlimann, W., Katayama, I., Martin, S.A., Meißburger, J., Römer, J., Seyfarth, H., Styczen, B.
High resolution spectroscopy study of $^{109}Ag(p,d)^{108}Ag$.
Workshop on Direct Reactions in Nuclear Physics, Bad Honnef, 5.-9.10.1981.
2o.o6.o

IKP-201781
Berg, G.P.A., Hürlimann, W., Katayama, I., Martin, S.A., Meißburger, J., Römer, J., Styczen, B., Osterfeld, F., Gaul, G., Santo, R., Sondermann, G.
Spin excitation in the f-p shell with inelastic proton scattering.
Workshop on Direct Reactions in Nuclear Physics, Bad Honnef, 5.-9.10.1981.
2o.o6.o + 2o.8o.o

IKP-201881
Berg, G.P.A., Decowski, P., Katayama, I., Martin, S.A., Meißburger, J., Morsch, H.P., Rogge, M., Styczen, B., Turek, P.
Search for isoscalar 1^+ excitations in ^{208}Pb.
Frühjahrstagung der DPG, Sektion A: Kernphysik, Hamburg, 23.-27.3.1981.
2o.o6.o

IKP-201981
Beuscher, H., Mathews, H.-G., Mayer-Böricke, C., Reich, J.
The ECR-source for the project ISIS at JULIC.
Ninth Int. Conf. on Cyclotrons and their Applications, Caen, Frankreich, 7.-10.9.1981, Poster Session.
2o.3o.o

IKP-202081
Bhandari, R.K., Reich, J.
The beam handling and axial injection system for the project ISIS at JULIC.
Ninth Int. Conf. on Cyclotrons and their Applications, Caen, Frankreich, 7.-10.9.1981.
2o.3o.o

IKP-202181
Bochev, B., Didelez, J.P., Kutsarova, T., Lieder, R.M., Mayer-Böricke, C., Morek, T., Müller-Veggian, M., Neskakis, A.
Mechanism of α-induced non-equilibrium reactions from particle-γ coincidence studies.
Frühjahrstagung der DPG, Sektion A: Kernphysik, Hamburg, 23.-27.3.1981.
2o.1o.o

IKP-202281
Bojowald, J., Borchert, G.L., Labus, H., Schult, O.W.B., Siefert, B., Siefert, J., Wieder, K.P.
Ein Kristallspektrometer für on-line Experimente am Jülicher Isochronzyklotron.
Frühjahrstagung der DPG, Sektion A: Kernphysik, Hamburg, 23.-27.3.1981.
2o.1o.o

IKP-202381
Borchert, G.L., Schult, O.W.B., Speth, J., Hansen, P.G., Jonson, B., Ravn, H., McGrory, J.B.
Isotope shifts of K X-rays of Lead.
Second Int. Conf. on Precision Measurement and Fundamental Constants, National Bureau of Standards, Gaithersburg, Maryland, USA, 8.-12.6.1981.
2o.1o.o + 2o.8o.o

IKP-202481
Borchert, G.L., Schult, O.W.B., Speth, J., Hansen, P.G., Jonson, B., Ravn, H., McGrory, J.B.
Isotope shifts of K X-rays of Lead.
4th Int. Conf. on Nuclei far from Stability, Book of Abstracts, S. 8, Helsingør 1981, Hrsg. Physics Institute, The University of Aarhus, Dänemark.
2o.1o.o + 2o.8o.o

IKP-202581
Borchert, G.L., Hansen, P.G., Jonson, B., Ravn, H.L., Schult, O.W.B.
Mechanism for energy shifts in atomic K X-ray spectra.
European Conf. on Atomic Physics, Heidelberg 1981, Book of Abstracts S. 282, Hrsg. J. Kowalski, G. zu Putlitz, H.G. Weber, Publ. E.P.S. Vol. 5A, Part 1.
2o.1o.o

IKP-202681
Borchert, G.L.
Higher order effects on the energy of K x-rays.
Oak Ridge National Laboratory, Oak Ridge, Tenn., USA, 16.6.1981.
2o.1o.o

IKP-202781
Borchert, G.L., Schult, O.W.B., Speth, J., Hansen, P.G., McGrory, J.B., Jonson, B., Ravn, H.L.
Isotope shifts of K X-rays of Lead.
Frühjahrstagung der DPG, Sektion A: Kernphysik, Hamburg, 23.-27.3.1981.
2o.1o.o + 2o.8o.o

IKP-202881
Bräutigam, W., Aldea, L., Mayer-Böricke, C., Reich, J., Wucherer, P.
Status of JULIC.
18th European Cyclotron Progress Meeting, Louvain-la-Neuve, Belgien, 25.-28.3.1981, Poster Session.
2o.3o.o

IKP-202981
Brown, V.R.
Selected topics in nucleon charge-exchange reactions: Multistep effects and isospin considerations.
IKP, KFA Jülich, 17.12.1981.
2o.8o.o

IKP-203081
Cheifetz, E., Selic, H.A., Wilhelmy, J.B.
Studies of the most neutron rich isotopes from primary fission processes.
Frühjahrstagung der DPG, Sektion A: Kernphysik, Hamburg, 23.-27.3.1981.
2o.65.o

IKP-203181
Chung, C., Walters, W.B., Wohn, F.K., Sistemich, K., Yamamoto, H., Hill, J.C., Brenner, D., Chu, Y.Y., Gowdy, G.M., Shmid, M., Gill, R.L., Liou, H.I., Stelts, M.L., Chrien, R.E.
Study of the decay of even-mass, neutron-rich Ba isotopes.
Bull. Am. Phys. Soc. 26 (1981) S. 552.
2o.65.o

IKP-203281
Conci, C., Klemt, V.
RPA calculations for ^{132}Sn with effective forces including meson exchange potentials.
Frühjahrstagung der DPG, Sektion A: Kernphysik, Hamburg, 23.-27.3.1981.
2o.8o.o

IKP-203381
Decowski, P., Morsch, H.P.
Excitation of giant dipole resonances in hadron scattering.
Frühjahrstagung der DPG, Sektion A: Kernphysik, Hamburg, 23.-27.3.1981.
2o.o6.o

IKP-203481
Decowski, P.
Dipole compressional modes in nuclei.
KVI Groningen, Niederlande, 6.1.1981.
2o.o6.o

IKP-203581
Decowski, P.
New giant resonances.
Universität Bonn, 8.1.1981.
2o.o6.o

IKP-203681
Dermawan, H., Krewald, S., Osterfeld, F., Speth, J.
Higher charge exchange resonances in nuclei.
Frühjahrstagung der DPG, Sektion A: Kernphysik, Hamburg, 23.-27.3.1981.
2o.8o.o

IKP-203781
Dermawan, H., Osterfeld, F., Madsen, V.A.
Nuclear structure approach to the microscopic calculation of the imaginary alpha-nucleus optical potential.
Frühjahrstagung der DPG, Sektion A: Kernphysik, Hamburg, 23.-27.3.1981.
2o.8o.o

IKP-203881
Djaloeis, A., Gopal, S., Bojowald, J., Mayer-Böricke, C., Oelert, W., Puttaswamy, N.G., Turek, P.
Study of (τ,d) reaction on ^{27}Al and ^{28}Si at E_τ = 130 MeV.
Frühjahrstagung der DPG, Sektion A: Kernphysik, Hamburg, 23.-27.3.1981.
2o.o6.o

IKP-203981
Drumm, P.
Recent results from Birmingham on breakup reactions.
IKP, KFA Jülich, 26.6.1981.
2o.o6.o

IKP-204081
Eversheim, P.D., Hinterberger, F., von Rossen, P., Römer, J.
Suche nach der T = 5/2 Analogresonanz zum Grundzustand von ^{23}F in ^{23}Na(T = 1/2).
Frühjahrstagung der DPG, Sektion A: Kernphysik, Hamburg, 23.-27.3.1981.
2o.o6.o

IKP-204181
Fretwurst, E., Lindström, G., von Reden, K.F., Riech, V., Vlachodimitropoulos, P., Kolalis, R., Zarubin, P., Berg, G., Martin, S., Meißburger, J., Oelert, W., Blok, H.P., van Hienen, J.F.A.
High precision proton scattering experiments on the even isotopes of Palladium, techniques, results and optical model analysis.
Hamburg-Tage in Leningrad, Oktober 1981.
2o.o6.o

IKP-204281
Fretwurst, E., von Geramb, H.V., Jakiel, J., Lindström, G., von Reden, K.F., Riech, V., Vlachodimitropoulus, P., Berg, G., Martin, S., Meißburger, J., Oelert, W., Kolalis, R., Zarubin, P.
Präzisionsexperimente zur elastischen und inelastischen Protonenstreuung an Pd-Kernen.
Frühjahrstagung der DPG, Sektion A: Kernphysik, Hamburg, 23.-27.3.1981.
2o.o6.o

IKP-204381
Gill, R.L., Shmid, M., Chrien, R.E., Gowdy, G. M., Liou, H., Stelts, M.L., Brenner, D.S., Sistemich, K., Yamamoto, H., Wohn, F.K., Chung, C., Walters, W.B., Petry, R.F.
Band structures in ^{148}Ce.
Bull. Am. Phys. Soc. 26 (1981) S. 553.
2o.65.o

IKP-204481
Goeke, K.
Microscopic theory of large amplitude nuclear collective motion.
Silverjubilee Symp. at Bhabha Atomic Research Centre, Bombay, Indien, 31.12.1981.
2o.8o.o

IKP-204581
Goeke, K.
Mikroskopische Beschreibung von kollektiven Eigenschaften der Kerne.
DPG-Sommerschule für Physik 1981, Bad Honnef, 7.-18.9.1981.
2o.8o.o

IKP-204681
Goeke, K.
Mikroskopische Theorie kollektiver Bewegungen (Schwerionenreaktionen, Fusion).
Zentralinstitut für Kernforschung Rossendorf, Dresden, DDR, 2.9.1981.
2o.8o.o

IKP-204781
Goeke, K.
Consistent microscopic theory of subbarrier fusion processes.
Universität Tübingen, 18.5.1981.
2o.8o.o

IKP-204881
Goeke, K.
Theoretische Bestimmung des besten kollektiven Weges in Fusion und Kernspaltung.
Expertentreffen für Kernphysik, Schleching, 4.-13.3.1981.
2o.8o.o

IKP-204981
Gopal,S., Djaloeis, A., Bojowald, J., Bousshid, O., Mayer-Böricke, C., Oelert, W., Puttaswamy, N.G., Turek, P.
Broad structure in t-spectra from (τ,t) reactions at E_τ = 130 MeV; its angle and target mass dependence.
Frühjahrstagung der DPG, Sektion A: Kernphysik, Hamburg, 23.-27.3.1981.
2o.o6.o

IKP-205081
Gowdy, G.M., Chrien, R.E., Chu, Y.Y., Gill, R. L., Liou, H.I., Shmid, M., Stelts, M.L., Brenner, D.S., Yeh, T., Sistemich, K., Wohn, F.K., Yamamoto, H., Chung, C., Walters, W.B., Petry, R.F., Meyer, R.A.
Study of the decay of low-spin ^{148}Pr to levels in ^{148}Nd.
Bull. Am. Phys. Soc. 26 (1981) S. 552.
2o.65.o

IKP-205181
Grabmayr, P., Knöpfle, K.T., Mayer-Böricke, C., Riedesel, H., Rogge, M., Schindler, K., Sükösd, C., Turek, P., Wagner, G.J.
Charged particle decay of giant resonances in ^{15}N and ^{18}O.
Frühjahrstagung der DPG, Sektion A: Kernphysik, Hamburg, 23.-27.3.1981.
2o.o6.o

IKP-205281
Grümmer, F., Goeke, K., Reinhard, P.-G.
ATDHF calculations for low energy fusion.
Frühjahrstagung der DPG, Sektion A: Kernphysik, Hamburg, 23.-27.3.1981.
2o.8o.o

IKP-205381
Grümmer, F., Schmid, K.W., Faessler, A.
Angular momentum projection of two quasiparticle states.
Frühjahrstagung der DPG, Sektion A: Kernphysik, Hamburg, 23.-27.3.1981.
2o.8o.o

IKP-205481
Grümmer, F., Schmid, K.W., Faessler, A.
Moments and transitions in the $i_{13/2}$ model.
Frühjahrstagung der DPG, Sektion A: Kernphysik, Hamburg, 23.-27.3.1981.
2o.8o.o

IKP-205581
de Haro, R.
High multipolarity giant resonances and higher nuclear compression modes.
Nucl. Phys. Workshop, Trieste, Italien, 19.10. 1981.
2o.8o.o

IKP-205681
de Haro, R., Krewald, S., Speth, J.
Can we find concentrated strength of high multipolarity giant resonances?
Frühjahrstagung der DPG, Sektion A: Kernphysik, Hamburg, 23.-27.3.1981.
2o.8o.o

IKP-205681
Hill, J.C., Wohn, F.K., Mercier, M., Smith, A.R.
Study of one nucleon removal reaction with relativistic heavy ions.
Frühjahrstagung der DPG, Sektion A: Kernphysik, Hamburg, 23.-27.3.1981.
2o.65.o

IKP-205781
Hill, J.C., Shizuma, K., Lawin, H., Shaanan, M. L., Sistemich, K.
Decay of ^{102}Y to levels of ^{102}Zr.
Tagung der Sektion Kernphysik der American Phys. Society, Asilomar, Calif., USA.
2o.65.o

IKP-205881
Hoffmann, B., Baur, G.
Sind Prozesse höherer Ordnung zur Beschreibung von Aufbruchsreaktionen notwendig?
Frühjahrstagung der DPG, Sektion A: Kernphysik, Hamburg, 23.-27.3.1981.
2o.8o.o

IKP-205981
Hoyler, F., Rohwer, T., Staudt, G., Klapdor, H.V., Turek, P., Martin, S.
Dreiteilchentransfer an ^{26}Mg und ^{27}Al.
Frühjahrstagung der DPG, Sektion A: Kernphysik, Hamburg, 23.-27.3.1981.
2o.o6.o

IKP-206081
Julin, R., Kantele, J., Luontama, M., Passoja, A., Kleinheinz, P., Blomqvist, J.
The first excited 0^+ state in the doubly closed ^{146}Gd nucleus.
Frühjahrstagung der DPG, Sektion A: Kernphysik, Hamburg, 23.-27.3.1981.
2o.1o.o

IKP-206181
Kawade, K., Battistuzzi, G., Lawin, H., Sistemich, K., Blomqvist, J.
A µs-isomer in ^{135}Te.
Frühjahrstagung der DPG, Sektion A: Kernphysik, Hamburg, 23.-27.3.1981.
2o.65.o

IKP-206281
Kleinheinz, P.
Octupole excitations in the ^{146}Gd region and the single particle gaps at N = 82 and Z = 64.
Lawrence Livermore Lab., Livermore, Calif., USA, 30.6.1981.
2o.1o.o

IKP-206381
Kleinheinz, P.
New results on ^{146}Gd and its neighbours.
4th Int. Conf. on Nuclei far from Stability, Helsingør, Dänemark, Juni 1981.
2o.1o.o

IKP-206481
Kleinheinz, P., Broda, R., Daly, P.J., Lunardi, S., Nagai, Y., Piiparinen, M., Styczen, J., Backe, H., Blomqvist, J.
High spin shell model states and octupole yrast excitations in nuclei above ^{146}Gd.
Frühjahrstagung der DPG, Sektion A: Kernphysik, Hamburg, 23.-27.3.1981.
2o.1o.o

IKP-206581
Kleinheinz, P.
Schalenmodellspektroskopie im Gebiet von ^{146}Gd.
Universität Göttingen, 9.11.1981.
2o.1o.o

IKP-206681
Kleinheinz, P.
Kernstruktur in der ^{146}Gd Region.
Universität Bonn, 12.11.1981.
2o.1o.o

IKP-206781
Klemt, V.
On a selfconsistent treatment of even-even and even-odd nuclei.
TU München, 13.1.1981.
2o.8o.o

IKP-206881
Klemt, V.
On the consistent treatment of even-even and even-odd nuclei.
Frühjahrstagung der DPG, Sektion A: Kernphysik, Hamburg, 23.-27.3.1981.
2o.8o.o

IKP-206981
Knöpfle, K.T., Mayer-Böricke, C., Oelert, W., Riedesel, H., Rogge, M., Schmidt, H.R., Wagner, G.J.
Isoscalar transition rates in ^{14,15}N and ^{17,18}O.
Frühjahrstagung der DPG, Sektion A: Kernphysik, Hamburg, 23.-27.3.1981.
2o.o6.o

IKP-207081
Knöpfle, K.T., Mayer-Böricke, C., Riedesel, H., Rogge, M., Schindler, K., Sükösd, C., Turek, P., Wagner, G.J.
Decay properties of the isoscalar giant quadrupole resonance in ^{20,22}Ne.
Frühjahrstagung der DPG, Sektion A: Kernphysik, Hamburg, 23.-27.3.1981.
2o.o6.o

IKP-207181
Koch, H.R.
Sensitivity analysis of the useful energy output for solar converters with respect to quality and completeness of meteorological data sets.
EC Solar Energy R+D Programme, Project F Review Meeting, Brüssel, Belgien, 20.11.1981.
2o.6o.1

IKP-207281
Krewald, S., Djaloeis, A., Gopal, S.
Empirical constraints on the heavy ion optical potential.
Frühjahrstagung der DPG, Sektion A: Kernphysik, Hamburg, 23.-27.3.1981.
2o.o6.o + 2o.8o.o

IKP-207381
Krewald, S.
Mesonic degrees of freedom in the atomic nucleus.
Gesamthochschule-Universität Siegen, 16.11.1981.
2o.8o.o

IKP-207481
Krewald, S.
Does the Δ_{33}-resonance reduce the Gamow-Teller sum-rule strength?
Indiana Cyclotron Facility, Bloomington, Ind., USA, 12.6.1981.
2o.8o.o

IKP-207581
Krewald, S.
The role of subnucleonic degrees of freedom in low-energy nuclear physics.
Univ. of New Hampshire, Durham, N.H., USA, 22.6.1981.
2o.8o.o

IKP-207681
Krewald, S.
Spin-isospin modes in atomic nuclei.
Int. Workshop IX on Gross Properties of Nuclei and Nuclear Excitations, Hirschegg, 19.-24.1. 1981.
2o.8o.o

IKP-207781
Krewald, S.
Mesonische Freiheitsgrade im Atomkern.
Expertentreffen für Kernphysik, Schleching, 4.-13.3.1981.
2o.8o.o

IKP-207881
Kuo, T.T.S., Osterfeld, F., Lee, S.Y.
Theory of energy independent optical model potentials.
Frühjahrstagung der DPG, Sektion A: Kernphysik, Hamburg, 23.-27.3.1981.
2o.8o.o

IKP-207981
Lieder, R.M.
Experimental study of side bands in Os nuclei around A = 182.
Nucl. Phys. Workshop, Trieste, Italien, 12.1O. 1981.
2o.1o.o

IKP-208081
Lieder, R.M.
New trends in nuclear spectroscopy.
Vth Int. School on Nuclear Physics, Neutron Physics and Nuclear Energy, Varna, Bulgarien, 7.1O.1981.
2o.1o.o

IKP-208181
Lieder, R.M.
Study of non-equilibrium reactions.
Vth Int. School on Nuclear Physics, Neutron Physics and Nuclear Energy, Varna, Bulgarien, 7.1O.1981.
2o.1o.o

IKP-208281
Lieder, R.M.
Study of the depopulation mechanism in non-equilibrium reactions.
Gordon Research Conf. on Nucl. Chemistry, New London, N.H., USA, 19.6.1981.
2o.1o.o

IKP-208381
Lieder, R.M.
Band crossings and blocking in ^{182}Os.
Workshop on Nucl. Structure at High spin, Risø, Dänemark, 18.5.1981.
2o.1o.o

IKP-208481
Lieder, R.M.
Band crossings in ^{182}Os.
Niels Bohr Institute, Kopenhagen, Dänemark, 13.4.1981.
2o.1o.o

IKP-208581
Lieder, R.M.
Mechanism of α-induced non-equilibrium reactions from particle-γ coincidence studies.
Institut de Physique Nucléaire, Université de Paris, Orsay, Frankreich, 26.1.1981.
2o.1o.o

IKP-208681
Machner, H.
Break-up studies with loosely bound projectiles.
Frühjahrstagung der DPG, Sektion A: Kernphysik, Hamburg, 23.-27.3.1981.
2o.o6.o

IKP-208781
Machner, H.
Pre-Equilibrium Emission komplexer Teilchen.
Universität Bremen, 11.11.1981.
2o.o6.o

IKP-208881
Martin, S.
Bericht über die Strahlqualität von Hochstrom LINACS.
NRW-Beschleunigerseminar, Jülich, 3.11.1981.
2o.o6.o

IKP-208981
Martin, S.
Eigenschaften von Protonenstrahlen aus Synchrotrons mit e-Kühlern.
Universität Bonn, 19.12.1981.
2o.o6.o

IKP-209081
Martin, S.
Recent experiment at the Jülich BIG KARL.
Indiana Cyclotron Facility, Bloomington, Ind., USA, 12.1O.1981.
2o.o6.o

IKP-2o9181
Martin, S.
Recent experiment at the Jülich BIG KARL.
Michigan State University, East Lansing, Mich., USA, 9.1O.1981.
2o.o6.o

IKP-209281
Mayer-Böricke, C.
Nuclear research at the Jülich isochronous cyclotron JULIC with light-particle-beams up to 18O MeV.
National Centre for Radiation Research and Technology, Cairo, Ägypten, 25.1O.1981.
2o.3o.o

IKP-209381
Morsch, H.P., Rogge, M., Turek, P., Sükösd, C., Mayer-Böricke, C., Decowski, P.
Investigation of new isoscalar resonances in heavy nuclei.
Frühjahrstagung der DPG, Sektion A: Kernphysik, Hamburg, 23.-27.3.1981.
2o.o6.o

IKP-209481
Morsch, H.P.
Introduction into the folding approach and application to light and heavy ion scattering.
Universität Grenoble, Frankreich, 19.-22.5.1981.
2o.o6.o

IKP-209581
Morsch, H.P.
Investigation of new isoscalar giant resonances.
Workshop on Direct Reactions in Nuclear Physics, Bad Honnef, 5.-9.1O.1981.
2o.o6.o

IKP-209681
Morsch, H.P.
Excitation and fission decay of isoscalar giant resonances.
Int. Symp. on Fission and Related Collective Phenomena and Properties of Heavy Nuclei, Bad Honnef, 26.-29.1O.1981.
2o.o6.o

IKP-209781
Morsch, H.P.
Dynamische Aspekte in der Anregung von Riesenresonanzen in Leicht- und Schwerionenstreuung.
AGF Workshop über Schwerionenreaktionen um 2O MeV/Nukleon, HMI Berlin, 7.-8.5.1981.
2o.o6.o

IKP-209881
Morsch, H.P., Rogge, M., Sükösd, C., Machner, H., David, P., Debrus, J., Janssen, H., Schulze, J.
Giant resonances observed in α-induced fission of ^{238}U.
Frühjahrstagung der DPG, Sektion A: Kernphysik, Hamburg, 23.-27.3.1981.
2o.o6.o

IKP-209981
Morsch, H.P.
Study of compressional modes of nuclear excitation.
Oak Ridge National Lab., Oak Ridge, Tenn., USA, 22.6.1981.
2o.o6.o

IKP-210081
Morsch, H.P.
Compressional modes of nuclear excitation.
Texas A&M University, College Station, Texas, USA, 24.6.1981.
2o.o6.o

IKP-210181
Morsch, H.P.
New giant resonances.
Michigan State University, East Lansing, Mich., USA, 1.7.1981.
2o.o6.o

IKP-210281
Morsch, H.P.
Compressional modes of nuclear excitation.
SUNY at Stony Brook, Stony Brook, N.Y., USA, 3.7.1981.
2o.o6.o

IKP-210381
Oelert, W., Djaloeis, A., Mayer-Böricke, C., Turek, P.
Questions on the reaction mechanism in alpha-transfer reactions.
Frühjahrstagung der DPG, Sektion A: Kernphysik, Hamburg, 23.-27.3.1981.
2o.o6.o

IKP-210481
Osterfeld, F.
Vorschläge zur Physik mit einer hochenergetischen, energievariablen Hadronenmaschine.
NRW-Beschleunigerseminar, Jülich, 24.11.1981.
2o.8o.o

IKP-210581
Osterfeld, F.
Mikroskopische optische Potentiale für Nukleon-Kern- und Alpha-Kern-Streuung.
Universität München, 17.12.1981.
2o.8o.o

IKP-210681
Osterfeld, F.
The effect of the Δ-isobar in Gamow-Teller resonances.
Workshop on Nucleon-Nucleon Interactions, Santa Barbara, Ca., USA, 16.-20.8.1981.
2o.8o.o

IKP-210781
Osterfeld, F.
Microscopic analysis of Gamow-Teller resonances including Δ-degrees of freedom explicitly.
Gordon Research Conf. on Nucl. Structure in Physics, Plymouth, N.H., USA, 10.-14.8.1981.
2o.8o.o

IKP-210881
Osterfeld, F.
Microscopic calculation of the imaginary optical potential for nucleon-nucleus and α-nucleus scattering.
Workshop on Direct Reactions in Nuclear Physics, Bad Honnef, 5.-9.10.1981.
2o.8o.o

IKP-210981
Osterfeld, F.
Microscopic analysis of Gamow-Teller resonances.
Workshop on Direct Reactions in Nuclear Physics, Bad Honnef, 5.-9.10.1981.
2o.8o.o

IKP-211081
Osterfeld, F.
Microscopic nucleon-nucleus optical potentials.
Michigan State University, East Lansing, Mich., USA, 14.1.1981.
2o.8o.o

IKP-211181
Pfeiffer, B., Münzel, J., Schussler, F., Monnand, E., Pinston, J.A., Lawin, H., Sistemich, K.
The level schemes of neutron rich nuclei in mass chain A = 147.
Frühjahrstagung der DPG, Sektion A: Kernphysik, Hamburg, 23.-27.3.1981.
2o.65.o

IKP-211281
Posorski, R.
Experimental experience with standards for solar collector testing.
Solar World Forum, Brighton, Großbritannien, 23.-28.8.1981, Postervortrag.
2o.6o.1

IKP-211381
Prokofjev, P.T., Soramel, F., Styczen, J., Ercan, A., Karnadi, M., Kleinheinz, P.
Rotational bands in the doubly odd $^{152}_{89}Eu_{63}$ nucleus.
Frühjahrstagung der DPG, Sektion A: Kernphysik, Hamburg, 23.-27.3.1981.
2o.1o.o

IKP-211481
Puttaswamy, N.G., Oelert, W., Djaloeis, A., Mayer-Böricke, C., Turek, P.
Proton hole states in $^{53,55,57}Mn$.
Frühjahrstagung der DPG, Sektion A: Kernphysik, Hamburg, 23.-27.3.1981.
2o.o6.o

IKP-211581
Rullhusen, P., Mückenheim, W., Smend, F., Schumacher, M., Berg, G.P.A., Mork, K., Kissel, L.
Test of vacuum polarization by precise investigations of Delbrück scattering.
Europen Conf. on Atomic Physics, Heidelberg, 6.-10.4.1981.
2o.o6.o

IKP-211681
Sartor, R., Faessler, A., Khadkikar, S.B., Krewald, S.
Folding computation of the $^{16}O+^{16}O$ optical potential with a complex effective force.
Frühjahrstagung der DPG, Sektion A: Kernphysik, Hamburg, 23.-27.3.1981.
2o.8o.o

IKP-211781
Seyfarth, H.
Nuclear physics research at KFA Jülich.
Boris Kidric Institute of Nuclear Sciences, Vinca/Belgrad, Jugoslawien, 29.1.1981.
2o.1o.o

IKP-211881
Seyfarth, H.
Search for the two-photon decay of a new light penetrating particle - axion? - at a nuclear reactor.
4th Int. Symp. on Neutron Capture Gamma-Ray Spectroscopy and Related Topics, Grenoble, Frankreich, 7.-11.9.1981.
2o.1o.o

IKP-211981
Seyfarth, H.
Nuclear spectroscopy of ^{108}Ag using the (p,d) transfer reaction in comparison to neutron capture investigations.
4th Int. Symp. on Neutron Capture Gamma-Ray Spectroscopy and Related Topics, Grenoble, Frankreich, 7.-11.9.1981.
2o.o6.o

IKP-212081
Shaanan, M., Hill, J.C., Lawin, H., Selic, H. A., Shizuma, K., Sistemich, K.
The energy spectrum of the delayed neutrons from the decay of ^{85}As.
Frühjahrstagung der DPG, Sektion A: Kernphysik, Hamburg, 23.-27.3.1981.
2o.65.o

IKP-212181
Sistemich, K., Kawade, K., Battistuzzi, G., Lauppe, W.-D., Lawin, H., Blomqvist, J.
Shell structures at ^{132}Sn.
Bull. Am. Phys. Soc. 26 (1981) S. 551.
2o.65.o

IKP-212281
Sistemich, K., Kawade, K., Battistuzzi, G., Lauppe, W.-D., Lawin, H., Blomqvist, J.
Shell structures at $^{132}_{50}Sn_{82}$.
Bull. Am. Phys. Soc. 26 (1981) S. 550.
2o.65.o

IKP-212381
Sistemich, K.
Magnetic moments in fission.
Iowa State University, Ames, Iowa, USA, 12.5.1981.
2o.65.o

IKP-212481
Sistemich, K.
Der Physiker in staatlichen Großforschungseinrichtungen.
Regionalverband Hessen, Mittelrhein, Saar der Deutschen Physikalischen Gesellschaft, 31.10.1981.
2o.65.o

IKP-212581
Sistemich, K.
Spektroskopie am Spaltproduktseparator TRISTAN/BNL.
Universität Mainz, 5.11.1981.
2o.65.o

IKP-212681
Sistemich, K.
Shell structure at medium-mass nuclei.
Universität Gent, Belgien, 9.11.1981.
2o.65.o

IKP-212781
Soramel, F., Styczen, J., Ercan, A., Prokofjev, P., Kleinheinz, P.
A $T_{1/2}$ = 45 ns high spin isomer in the doubly odd $^{150}_{63}Eu_{87}$ nucleus.
Frühjahrstagung der DPG, Sektion A: Kernphysik, Hamburg, 23.-27.3.1981.
2o.1o.o

IKP-212881
Speth, J.
Spin-Isospin-Moden in Kernen.
Universität Mainz, 16.12.1981.
2o.8o.o

IKP-212981
Speth, J.
Spin-Isospin-Moden in Kernen.
GSI Darmstadt, 8.12.1981.
2o.8o.o

IKP-213081
Speth, J.
Spin-Isospin-Moden in Kernen.
TU und Universität München, 4.12.1981.
2o.8o.o

IKP-213181
Speth, J.
The nonlocality of nuclear forces in the spin-isospin channel.
University of Illinois, Urbana, Ill., USA, 12.11.1981.
2o.8o.o

IKP-213281
Speth, J.
Spin-isospin modes in nuclei.
University of Illinois, Urbana, Ill., USA, 11.11.1981.
2o.8o.o

IKP-213381
Speth, J.
Giant spin-isospin modes in nuclei.
SUNY at Stony Brook, Stony Brook, N.Y., USA, 5.11.1981.
2o.8o.o

IKP-213481
Speth, J.
Spin-isospin modes in nuclei.
Int. Symp. on Nuclear Fission and Related Collective Phenomena and Properties of Heavy Nuclei, Bad Honnef, 27.10.1981.
2o.8o.o

IKP-213581
Speth, J.
Resumé talk on giant resonances.
Nucl. Phys. Workshop, Trieste, Italien, 15.-19.10.1981.
2o.8o.o

IKP-213681
Speth, J.
Does the Δ33-isobar account for the missing Gamow-Teller strength?
IX Int. Conf. on High Energy Physics and Nuclear Structure, Versailles, Frankreich, 6.-10.7.1981.
2o.8o.o

IKP-213781
Speth, J.
Spin-Isospin-Moden in Kernen.
Universität Köln, 5.6.1981.
2o.8o.o

IKP-213881
Speth, J.
Ladungsaustauschresonanzen.
AGF Workshop über Schwerionenreaktionen um 20 MeV/Nukleon, HMI Berlin, 7.-8.5.1981.
2o.8o.o

IKP-213981
Speth, J., Zawischa, D.
Gamow-Teller resonances in nonspherical nuclei.
Frühjahrstagung der DPG, Sektion A: Kernphysik, Hamburg, 23.-27.3.1981.
2o.8o.o

IKP-214081
Speth, J.
Spin-isospin modes in nuclei.
Workshop on Quantum Liquids, Santa Barbara, Ca., USA, 23.-27.3.1981.
2o.8o.o

IKP-214181
Speth, J.
Dynamical theory of collective states.
Oak Ridge National Lab., Oak Ridge, Tenn., USA, 19.3.1981.
2o.8o.o

IKP-214281
Speth, J.
Nuclear structure aspects connected with (p,n) reactions.
(p,n) Workshop, Oak Ridge National Lab., Oak Ridge, Tenn., USA, 18.3.1981.
2o.8o.o

IKP-214381
Speth, J.
New aspects on magnetic properties of nuclei.
Oak Ridge National Lab., Oak Ridge, Tenn., USA, 12.3.1981.
2o.8o.o

IKP-214481
Speth, J.
Precritical phenomena in nuclei.
Informal Study Meeting, Louvain-la-Neuve, Belgien, 25.-26.2.1981.
2o.8o.o

IKP-214581
Speth, J.
Spin-Isospin Resonanzen im Kern.
HMI Berlin, 16.2.1981.
2o.8o.o

IKP-214681
Speth, J.
Spin-isospin resonances in nuclei.
Universität Tübingen, 13.2.1981.
2o.8o.o

IKP-214781
Speth, J.
Collective spin-isospin resonances in nuclei.
Universität Hamburg, 12.1.1981.
2o.8o.o

IKP-214881
Suzuki, T., de Haro, R., Krewald, S., Speth, J., Osterfeld, F., Wambach, J.
Structure of spin-isospin modes and their excitation via electron and hadron scattering.
Frühjahrstagung der DPG, Sektion A: Kernphysik, Hamburg, 23.-27.3.1981.
2o.8o.o

IKP-214981
Suzuki, T.
Time-dependent Hartree-Fock and superposition principle: Semiclassical method in phase space representation.
Workshop on Semiclassical Methods in Nuclear Physics, Grenoble, Frankreich, 18.-20.3.1981.
2o.8o.o

IKP-215081
Suzuki, T.
Quantum mechanical superposition of TDHF paths in a collision of schematic nuclei.
Frühjahrstagung der DPG, Sektion A: Kernphysik, Hamburg, 23.-27.3.1981.
2o.8o.o

IKP-215181
Schult, O.
Summary Talk: 4th Int. Symp. on Neutron-Capture Gamma-Ray Spectroscopy and Related Topics, Grenoble, Frankreich, 7.-11.9.1981.
2o.1o.o

IKP-215281
Schult, O.
Über die Messung sehr kleiner K-Röntgenenergieverschiebungen.
GSI Darmstadt, 6.1.1981.
2o.1o.o

IKP-215381
Stein, H.J.
Why do we need collector testing?
Egyptian-German Workshop on Solar Collectors, Cairo, Ägypten, 31.1.-2.2.1981.
2o.6o.1

IKP-215481
Stein, H.J.
Sonnenenergie - Technik und Potential für die Bundesrepublik.
Universität Hamburg, 2.7.1981.
2o.6o.1

IKP-215581
Styczen, J., Nagai, Y., Piiparinen, M., Kleinheinz, P., Bazzacco, D., von Brentano, P., Blomqvist, J.
Single particle energies for protons above Z=64 from $^{147}_{82}Tb_{65}$.
Frühjahrstagung der DPG, Sektion A: Kernphysik, Hamburg, 23.-27.3.1981.
2o.1o.o

IKP-215681
Styczen, J.
Proton single particle states in ^{147}Tb.
Universität Krakau, Polen, 23.4.1981.
2o.1o.o

IKP-215781
Talarek, H.D.
IEA round-robin testing of solar collectors.
Second Int. Symp. on Non-Conventional Energy, Trieste, Italien, 14.7.-6.8.1981.
2o.6o.1

IKP-215881
Talarek, H.D.
Pyranometry in solar energy research and development: A technique of radiation measurements to be developed.
Second Int. Symp. on Non-Conventional Energy, Trieste, Italien, 14.7.-6.8.1981.
2o.6o.1

IKP-215981
Talarek, H.D.
IEA round-robin testing of solar collectors.
Solar World Forum, Brighton, Großbritannien, 23.-28.8.1981, Postervortrag.
2o.6o.1

IKP-216081
Talarek, H.D.
Messungen an einer Warmwasseranlage.
Oberseminar: Nutzung solarer Energie und verwandte Fragen, TU München, 27.11.1981.
2o.6o.1

IKP-216181
Talarek, H.D.
Solarenergieforschung in der KFA Jülich.
Seminar über Energiefragen, Universität Köln, 11.12.1981.
2o.6o.1

IKP-216281
Tokunaga, Y., Börner, H.G., Seyfarth, H., Barreau, G., Schreckenbach, K., Faust, H., Brissot, R., Hofmeyr, Ch., Weinreich, R., Schult, O.W.B.
Study of low spin states in $^{75,77}Se$ populated in slow neutron capture.
4th Int. Symp. on Neutron Capture Gamma-Ray Spectroscopy and Related Topics, Grenoble, Frankreich, 7.-11.9.1981.
2o.1o.o

IKP-216381
Udagawa, T.
Breakup-fusion approach to deeply inelastic scatterings.
Universität München, 28.5.1981.
2o.8o.o

IKP-216481
Udagawa, T.
Breakup-fusion approach to deeply inelastic scatterings.
MPI Heidelberg, 1.6.1981.
2o.8o.o

IKP-216581
Udagawa, T.
Breakup-fusion approach to deeply inelastic scatterings.
HMI Berlin, 16.6.1981.
2o.8o.o

IKP-216681
Udagawa, T.
Breakup-fusion approach to deeply inelastic scatterings.
KVI Groningen, Niederlande, 6.7.1981.
2o.8o.o

IKP-216781
Walters, W.B., Chung, C., Brenner, D.S., Clark, U., Gill, R.L. Shmid, M., Chrien, R.E., Liou, H.I., Petry, R.F., Sistemich, K., Yamamoto, H., Wohn, F.K.
Decay of ^{144}La to levels of ^{144}Ce.
Asilomar Meeting of the American Physical Society, Asilomar, Ca., USA, 28.-30.10.1981.
2o.65.o

IKP-216881
Walters, W.B., Chung, C., Wohn, F.K., Sistemich, K., Yamamoto, H., Brenner, D., Gill, R.L., Shmid, M., Liou, H.I., Stelts, M.L., Gowdy, G. M., Chu, Y.Y., Chrien, R.E.
Angular correlation studies of the low-lying O^+ states in transitional $^{142-146}$Ce nuclides.
Bull. Am. Phys. Soc. 26 (1981) S. 552.
2o.65.o

IKP-216981
Wambach, J., Hulthage, I.
Magnetic moments of nonstrange baryons in the Chiral bag model.
Frühjahrstagung der DPG, Sektion A: Kernphysik, Hamburg, 23.-27.3.1981.
2o.8o.o

IKP-217081
Wambach, J., Jackson, A.D., Speth, J.
Isoscalar 1^+-state in ^{208}Pb and the stability of the spin part of the ph-interaction.
Frühjahrstagung der DPG, Sektion A: Kernphysik, Hamburg, 23.-27.3.1981.
2o.8o.o

IKP-217181
Wohn, F.K., Hill, J.C., Sistemich, K., Yamamoto, H., Brenner, D.S., Gowdy, G.M., Gill, R.L., Shmid, M., Chrien, R.E., Liou, H., Stelts, M.L., Walters, W.B., Chung, C., Meyer, R.A.
Decay of the low-spin isomer of ^{146}La to ^{146}Ce.
Bull. Am. Phys. Soc. 26 (1981) S. 552.
2o.65.o

IKP-217281
Yamamoto, H., Wohn, F.K., Sistemich, K., Walters, W.B., Chung, C., Gill, R.L., Shmid, M., Gowdy, G.M., Liou, H., Chrien, R.E., Stelts, M.L., Brenner, D.S., Petry, R.F.
Low-lying levels in the N=85 isotone ^{141}Ba.
Bull. Am. Phys. Soc. 26 (1981) S. 551.
2o.65.o

IKP-217381
C. Mayer-Böricke
Nuclear Research at the Jülich Isochronous Cyclotron with light particle beams up to 180 MeV.
Invited lecture, University of Mysore, Mysore, India, Dec. 22, 1981
2o.o6.o

IKP-217481
C. Mayer-Böricke
Nuclear Physics Research Programme at the Jülich Cyclotron.
Invited lecture, Bangalore University, Bangalore, India, Dec. 23, 1981
2o.o6.o

IKP-217581
C. Mayer-Böricke
Recent advances in giant resonance research using hadronic particles.
Invited lecture, Bangalore University, Bangalore, India, Dec. 24, 1981
2o.o6.o

IKP-217681
C. Mayer-Böricke
Recent advances in nuclear giant resonance studies by hadronic scattering.
Invited talk at the 'Silver Jubilee Physics Symposium', BARC, Bombay, India, Dec. 29, 1981
2o.o6.o

PATENTE

IKP-300181
Labus, H.
Meßgerät für die praktisch simultane ΔT,T-Messung.
DE: 29 10 608.9-52(29.7.81); US: 4,294.115(13.10.81)
20.60.1

X. INTERNAL REPORTS

IKP-500181
Aldea, L., Beuscher, H., Bhandari, R.K., Bräutigam, W., Mathews, H.-G., Mayer-Böricke, C., Reich, J., Wucherer, P.
Projektbeschreibung ISIS - Injektion schwerer Ionen nach ECR-Stripping in das Jülicher Isochronzyklotron zur Beschleunigung schwerer Ionen zwischen 22.5 und 45 MeV/Nukleon.
Interner Bericht, IKP, Januar 1981.

IKP-500281
Anhalt, J., Maßmeyer, K., Stein, H.J.
Teststation für Solarkollektoren in Brasilien.
Interner Bericht IKP-IB-3/79, September 1981.

IKP-500381
Bundschuh, V., Dittrich, A., Grüter, J.W., Kleemann, M., Meliß, M., Pohlmann, D., Stein, H.J., Wagner, H.J.
Mustersolarhäuser - Untersuchung der wissenschaftlichen Zielsetzung und Durchführbarkeit eines Forschungs- und Entwicklungsprojekts.
Abschlußbericht, BMFT-FB ET 4244A, April 1981.

IKP-500481
Grümmer, F., Mayer-Böricke, C., Schult, O., Seyfarth, H., Speth, J., Turek, P.
Annual Report 1980.
Jül-Spez-99, Februar 1981.

IKP-500581
Grüter, J.W.
Solarnet - Ein Datenerfassungs- und Kommunikationssystem für Experimente der Solarenergieanwendung bei der KFA.
Interner Bericht IKP/STE-IB-6/81.

IKP-500681
Kusdogan, B.
Projektierung eines solarzellengespeisten Pumpenantriebssystems zur Umwälzung des flüssigen Wärmeträgers in einer Sonnenkollektoranlage.
Diplomarbeit, Fachhochschule Aachen, Abt. Jülich, März 1981.

IKP-500781
Müller, G., Berg, G.P.A., Hardt, A., Kelleter, H.J., Martin, S.A., Meißburger, J., Retz, A.
Aufbau eines Plastikszintillationszählers für den Magnetspektrographen "BIG KARL" am Jülicher Zyklotron "JULIC".
Jül-Spez-81.

IKP-500881
Poos, B.
Wärmeübergänge am Absorberelement.
Diplomarbeit, RWTH Aachen, Oktober 1981.

IKP-500981
Stein, H.J.
Why do we need collector testing?
Interner Bericht IKP-IB-1/81.

IKP-501081
Talarek, H.D.
Annual Progress Report Task III, Performance Testing of Solar Collectors.
IEA Internal Report, Januar 1981.

IKP-501181
Wagner, R.
Aspekte der Kurzzeitspeicherung von Wärmeenergie aus Solarstrahlung mit Hilfe von Adsorptions-Trocknungsmitteln.
Interner Bericht IKP-IB-4/81.

INDEX TO AUTHORS